Methodology for Design and Operation of Active Building-Integrated Thermal Energy Storage Systems

Yuxiang Chen

A Thesis

In the Department

of

Building, Civil and Environmental Engineering

Presented in Partial Fulfillment of the Requirements

for the Degree of

Doctor of Philosophy (Building Engineering) at

Concordia University

Montréal, Québec, Canada

September 2013

©Yuxiang Chen, 2013

CONCORDIA UNIVERSITY
SCHOOL OF GRADUATE STUDIES

This is to certify that the thesis prepared

By: Yuxiang Chen

Entitled: Methodology for Design and Operation of Building-Integrated Thermal Energy Storage System

and submitted in partial fulfillment of the requirements for the degree of

Doctor of Philosophy (Building Engineering)

complies with the regulations of the University and meets the accepted standards with respect to originality and quality.

Signed by the final examining committee:

Dr. W. Ghaly — Chair

Dr. M. Bernier — External Examiner

Dr. S. Williamson — External to Program

Dr. L. Tirca — Examiner

Dr. R. Zmeureanu — Examiner

Dr. A. Athienitis & Dr. K. Galal — Thesis Supervisor

Approved by

Chair of Department or Graduate Program Director

Dean of Faculty

Abstract

Methodology for Design and Operation of Building-Integrated Thermal Energy Storage System

Yuxiang Chen, Ph.D.

Concordia University, 2013

Thermal energy storage (TES) systems that are part of the building fabric and are exposed to room air can be described as building-integrated thermal energy storage (BITES) systems. BITES systems with appropriate space conditioning strategies can significantly improve the thermal performance of buildings. The present study focuses on active BITES systems, which embody controllable internal charge/discharge system. Thermal energy can be stored and released in an appropriate manner to control zone temperature for improved comfort and energy performance.

To assist the design and control analysis of active BITES systems, methodologies are first developed for three numerical modeling approaches: time domain lumped-parameter finite difference model, frequency domain analytical model and regression model. The regression model is demonstrated for the charge control of active BITES cooling using outdoor cool air. A frequency domain methodology is presented with guidelines for the design and operation of active BITES systems that facilitate primary space conditioning with low operating energy, relatively flat power demand, and improved thermal comfort. Three key factors considered by the methodology are as follows: sufficient thermal coupling between the BITES systems and their thermal zones, integration of design and operation, and integration of thermal and structural designs. A heuristic approach based on building physics

is suggested for establishing a near-optimal room air temperature set-profile. Dynamic response of active systems derived from their frequency domain transfer functions are used to enhance the set-profile. Using the set-profile and corresponding space conditioning load profile as inputs, the charge and discharge rates for the active BITES can be predicted over a desired time horizon. A bounding-condition-based design approach is presented. Finally, a procedure for the integration of structural and thermal designs is demonstrated with focus on ventilated BITES systems using standard structural components and their variations. The methodology and guidelines are general and applicable to different BITES systems and different buildings with different thermal and structural loads.

Acknowledgements

This work could not have been accomplished without the support and help of many people and institutions, for which I am very grateful.

I am especially grateful to my co-supervisor Dr. A. K. Athienitis for conveying his enthusiasm for and profound knowledge of high-performance buildings. His effort on guiding me through the writing of this thesis is invaluable. Dr. K. E. Galal, my co-supervisor, have been extremely thoughtful and supportive. Without their insightful knowledge on thermal and structural aspects of advanced buildings, this interdisciplinary research work would not be possible. Dr. Athienitis and Dr. Galal have been mentoring me since my undergraduate studies. I am full of gratitude for their continuous guidance, encouragement and trust over the years.

While realizing that the following list must be incomplete, I would like to thank in no particular order:

- My close friends and colleagues, Costas Kapsis, Liam O'Brien, Leanne Robinson, Eleni Mouriki, Yichao Chen, Jose Candanedo, Jose-Daniel Candelario, Sam Yip, Diane Bastien, Jason Gkountis, Dimitris Ladas, Tingting Yang, Edvinas Bigaila, Caroline Hachem and their significant others, for the important moments we shared, their encouragement, and all kinds of help;
- Sam Yip for carefully proofreading the manuscript and giving me helpful writing suggestions;
- Josef Ayoub, Lyne Dee, Jacques Payer, and Dr. Jiwu Rao for their administrative assistance;

- Gabriel Miclette, his mother Monique Daoust, his little daughter Rose, and his wife Amy Vanelslande for their tremendous moral support and lovely home feeling;
- My wife Yuqing Guan for her love, good food, understanding and patience.

Finally, I sincerely want to thank my mother, Zhuanying Liang, my father, Junfa Chen, and my sister, Minhua Chen, for their endless love and continuous financial support. I would like to dedicate this work to them.

The work is funded by Postgraduate Scholarship from Natural Sciences and Engineering Research Council (NSERC) of Canada, the NSERC Smart Net-zero Energy Buildings Strategic Research Network (SNEBRN, previously SBRN), and Graduate Student Support Program from the Faculty of Engineering and Computer Science of Concordia University, Montreal, Canada.

You are against strong wind only because you are up high on a mountain.

高山才有劲风

Table of Contents

List of Figures xi

List of Tables xviii

Preface xix

CHAPTER 1 INTRODUCTION ..... - 1 -

1.1. Problem identification and significance ..... - 4 -

1.2. Potential of active building-integrated thermal energy storage ..... - 12 -

1.3. Objectives and scope ..... - 27 -

CHAPTER 2 LITERATURE REVIEW OF BITES ..... - 32 -

Section 2.1 Building-Integrated Thermal Energy Storage (BITES) – State of the Art, Part I: Literature and Technology Survey ..... - 33 -

2.1.1. Introduction ..... - 33 -

2.1.2. State of the art of BITES ..... - 42 -

2.1.3. Concepts and technologies associated with BITES ..... - 53 -

2.1.4. Conclusion ..... - 58 -

Section 2.2 Building-Integrated Thermal Energy Storage (BITES) – State of the Art: Part II, Evaluation and Comparison ..... - 61 -

2.2.1. Introduction ..... - 61 -

2.2.2. Evaluations ..... - 62 -

2.2.3. Comparisons ..... - 67 -

2.2.4. Design and operation considerations ..... - 77 -

2.2.5. Conclusion ..... - 91 -

CHAPTER 3 NUMERICAL MODELING ..... - 94 -

Section 3.1 Thermal performance and charge control methodology of a ventilated concrete slab (VCS) using outdoor air for active cooling ..... - 95 -

3.1.1. Introduction ..... - 96 -

3.1.2. Numerical model and verification ..... - 98 -

3.1.3. VCS thermal performance ..... - 105 -

3.1.4. Charge control and sizing methodology ..... - 110 -

3.1.5. Discussion ..... - 114 -

3.1.6. Conclusion ..... - 117 -

Section 3.2 Frequency domain and finite difference modeling of ventilated concrete slabs and comparison with field measurements: Part 1, modeling methodology ..... - 120 -

3.2.1. Introduction ..... - 121 -

3.2.2. Modeling Methodology ..... - 124 -

3.2.3. Conclusion ..... - 140 -

Section 3.3 Frequency domain and finite difference modeling of ventilated concrete slabs and comparison with field measurements: Part 2, application ..... - 142 -

3.3.1. Introduction ..... - 143 -

3.3.2. Model development ..... - 144 -

3.3.3. Simulations and comparison results ..... - 150 -

3.3.4. Discussion ..... - 160 -

3.3.5. Conclusion ..... - 162 -

CHAPTER 4 DESIGN OF PREDICTIVE CONTROL STRATEGIES FOR ACTIVE BITES SYSTEMS USING FREQUENCY DOMAIN MODEL ..... - 163 -

4.1. Introduction ..... - 164 -

4.2. Methodology ..... - 165 -

4.3. Applications ..... - 174 -

4.4. Discussion ..... - 197 -

4.5. Conclusion ..... - 201 -

CHAPTER 5 DESIGN AND OPERATION METHODOLOGY FOR ACTIVE BUILDING-INTEGRATED THERMAL ENERGY STORAGE SYSTEMS AND APPLICATIONS USING STANDARD STRUCTURAL COMPONENTS ..... - 203 -

5.1. Introduction ..... - 204 -

5.2. Scope ..... - 205 -

5.3. Integrating design and operation ..... - 205 -

5.4. Integrating structural and thermal functions ..... - 231 -

5.5. Other application considerations ..... - 242 -

5.6. Conclusion ..... - 243 -

CHAPTER 6 CONCLUSION ..... - 245 -

Future studies ..... - 249 -

REFERENCES ..... - 250 -

APPENDICES ..... - 261 -

NOMENCLATURES ..... - 284 -

List of Figures

FIG. 1.1: SCHEMATIC OF DEMAND AND GENERATION PROFILE FOR CANADIAN NEAR NET-ZERO ENERGY HOUSE (COLD SUNNY DAY) (COURTESY OF A. ATHIENITIS AND C. HACHEM, SOURCE DATA: DOIRON ET AL (2011)) ..... - 2 -

FIG. 1.2: NET-ZERO ENERGY SOLAR HOME CONCEPT (IEA-SHC 2008) ..... - 3 -

FIG. 1.3: PROFILES OF OUTDOOR TEMPERATURE AND ELECTRIC SPACE HEATING POWER DEMAND OF TWO BUNGALOW HOUSES. (THE PLOTTED VALUES OF POWER DEMAND ARE 1/10 OF THE ACTUAL VALUES. SOURCE DATA ARE PROVIDED BY DR. J. MILLETTE FROM ENERGY TECHNOLOGY LABORATORY OF HYDRO QUEBEC.) ..... - 6 -

FIG. 1.4: ÉCOTERRA DEMONSTRATION HOUSE, NOVEMBER 2007 (THE PHOTOVOLTAIC SYSTEM MADE UP OF AMORPHOUS SILICON LAMINATE PANELS ATTACHED TO METAL ROOF IS ON THE UPPER ROOF SECTION). ..... - 7 -

FIG. 1.5: SCHEMATIC OF THE INTEGRATED ENERGY SYSTEM AND LOCATIONS OF THERMAL MASS (CHEN ET AL. 2010A). ..... - 8 -

FIG. 1.6: TEMPERATURE AND SOLAR RADIATION PROFILES ON TWO WINTER DAYS (FEB. 25TH AND 26TH) - 10 -

FIG. 1.7: SCHEMATICS OF TYPICAL ACTIVE BITES CROSS SECTIONS (CHEN ET AL. 2013A). ..... - 13 -

FIG. 1.8: CONCEPTUAL SCHEMATICS OF ACTIVE BITES SYSTEMS AND THEIR THERMAL COUPLING WITH THE INTERIOR ("INDOOR MASS" INCLUDES ROOM AIR, WALLBOARDS, AND FURNITURE; CNV: CONVECTION; ADV: ADVECTION; LR: LONG-WAVE RADIATION; HRV: HEAT RECOVERY VENTILATOR) - 14 -

FIG. 1.9: CONCEPTS OF PASSIVE MEASURES, AND PRE-CONDITIONING (TYPICAL TEMPERATURE PROFILES OF A ZONE WITH DIFFERENT LEVELS OF BITES APPLICATIONS AND HIGH SOLAR/INTERNAL HEAT GAINS) ..... - 17 -

FIG. 1.10: VCS IN ÉCOTERRA: (A) BEFORE HOUSE WAS OCCUPIED; (B) OCCUPIED ..... - 19 -

FIG. 1.11: SCHEMATIC OF PASSIVE MEASURES AND PRE-CONDITIONING CONCEPTS (Prm IS THE HEAT GAIN/LOSS OF THE ROOM; PB_rm IS THE THERMAL OUTPUT FROM THE BITES TO THE ROOM; Psc IS THE THERMAL ENERGY INJECTION RATE TO THE BITES) ..... - 25 -

FIG. 1.12: SCHEMATICS OF THE CROSS SECTIONS OF TWO REINFORCED CONCRETE SLABS ..... - 26 -

FIG. 1.13: SCHEMATIC OF A HYDRONIC SLAB IN PRACTICE (ZHAI ET AL. 2009) (INSULATION IS PLACED BELOW THE PIPES TO DIRECT HEAT FLOW UPWARD) ..... - 27 -

FIG. 1.14: CONCEPTUAL SCHEMATIC OF THE DIFFERENT ACTIVE BITES SYSTEMS: (A) VENTILATED SYSTEMS; (B) HYDRONIC SYSTEMS (VMBW: VENTILATED MASONRY BLOCK WALL; VCS: VENTILATED CONCRETE SLAB) ..... - 28 -

FIG. 2.1: CONCEPTUAL SCHEMATICS OF WORKING MECHANISMS OF COMMON AIR-BASED SYSTEMS LISTED IN TABLE 2.1 (CV: CONVECTIVE HEAT TRANSFER; IR: INFRARED RADIATION) ..... - 41 -

FIG. 2.2: SCHEMATICS OF THE FUNCTIONING OF AN “INTERIOR CLOSED-LOOP” VENTILATED CONCRETE SLAB (FIG. 2.1-C) (CHEN ET AL. 2010A, CHEN ET AL. 2010B)..... - 41 -

FIG. 2.3: TERMODECK ILLUSTRATION (SOURCE: SWEDISH INTERNATIONAL PRESS BUREAU. WWW.PUBLICITET.COM) ..... - 52 -

FIG. 3.1: SCHEMATIC OF BIPV/T SYSTEM AND THERMAL MASS (DIRECT GAIN SYSTEM IN MAIN LIVING AREA AND VCS IN BASEMENT). ..... - 98 -

FIG. 3.2: SCHEMATIC OF THE 9-LAYER 3D DISCRETIZATION OF THE VCS. ..... - 100 -

FIG. 3.3: MEASURED TEMPERATURE PROFILES OF SITE TEST ON JULY 16TH (FAMILY ROOM IS ON TOP OF BASEMENT) ..... - 103 -

FIG. 3.4: MEASURED TEMPERATURE PROFILES AND SIMULATED OUTLET AIR TEMPERATURE PROFILE (JULY 16TH) ..... - 104 -

FIG. 3.5: MEASURED TEMPERATURE PROFILES AT DIFFERENT LOCATIONS IN THE MIDDLE LAYER (“TC-2” IN FIG. A2.1(B)) (JULY 16TH)..... - 106 -

FIG. 3.6: SIMULATED VCS TOP SURFACE TEMPERATURE DISTRIBUTIONS AT THE END OF THE COOLING PERIOD FOR AUGUST 10TH ..... - 108 -

FIG. 3.7: PREDICTED THERMAL ENERGY TRANSFERRED FROM AIR TO SLAB FOR AUGUST 10TH INITIAL CONDITIONS. (INITIAL SLAB AND SOIL TEMPERATURES WERE 21.8 AND 15.0°C (71.2 AND 59.0°F), RESPECTIVELY. (A) 1.35 M/S (265 FPM) CONSTANT AIR VELOCITY WITH DIFFERENT INLET AIR TEMPERATURES; (B) 16°C (60.8°F) CONSTANT INLET AIR TEMPERATURE WITH DIFFERENT AIR VELOCITIES)..... - 109 -

FIG. 3.8: SCHEMATICS OF A VCS-B ("-B" INDICATES THE AIR CHANNELS AT THE BOTTOM OF THE CONCRETE SLAB), ITS EQUIVALENT CROSS SECTION, AND ONE-DIMENSIONAL THERMAL NETWORK AFTER TRANSFORMATION (THERE IS NO NEED FOR "INTERNAL NODES" IN FR THERMAL NETWORK) - 126 -

FIG. 3.9: A DIFFERENTIAL LENGTH OF AN AIR CHANNEL BOUNDED BY 2 SURFACES ($B = 2$; ONE SURFACE CONTAINS THE TOP, FRONT, AND BACK SURFACES; THE OTHER ONE IS THE BOTTOM SURFACE, WHICH IS IN A DIFFERENT COLOR). ..... - 127 -

FIG. 3.10: SCHEMATIC OF AN ASSEMBLY CONSISTING OF N LAYERS, AND THE LABELING OF ITS EXCITATIONS AND ITS INDICES. ..... - 132 -

FIG. 3.11: TRANSFORMATION OF THERMAL NETWORK (NODE 0 IS THE OUTERMOST NODE OF ASSEMBLY $1 \leftarrow sc1$, WHILE NODE l IS THE OUTERMOST NODE OF ASSEMBLY $scN \leftarrow N$. HEAT SOURCE NODE sc IS IN-BETWEEN THE TWO ASSEMBLIES) ..... - 134 -

FIG. 3.12: SCHEMATICS OF TWO TYPES OF VCS ..... - 143 -

FIG. 3.13: EQUIVALENT CROSS SECTIONS, ONE-DIMENSIONAL THERMAL NETWORKS AND SPATIAL DISCRETIZATION OF THE TWO KINDS OF VCS (FIG. 3.12) AFTER TRANSFORMATION (THERE ARE NO INTERNAL GRID NODES FOR FR THERMAL NETWORKS)..... - 145 -

FIG. 3.14: EXCITATION PROFILES (A SUNNY DAY IS FOLLOWED BY A CLOUDY DAY; ROOM AIR TEMPERATURE IS CONTROLLED BY A SPACE HEATING SYSTEM AND OPTIMIZED FOR PASSIVE SOLAR HEATING) ..... - 147 -

FIG. 3.15: THERMAL NETWORK OF A VCS-C SYSTEM ..... - 149 -

FIG. 3.16: TEMPERATURE AND HEAT FLUX PROFILES FOR VCS-B IN A TWO-DAY DESIGN PERIOD (FIG. 3.14) (8-LAYER LPFD MODEL, TIME STEP OF 60 SECONDS, AND EFFECTIVE SLAB THICKNESS OF 0.15 M)..... - 153 -

FIG. 3.17: 8-LAYER LPFD MODEL VS. FR MODEL FOR VCS-B (TIME STEP OF 60 SECONDS, EFFECTIVE SLAB THICKNESS OF 0.2 M. OTHER INFORMATION IS IN TABLE 3.4) ..... - 155 -

FIG. 3.18: MEASURED EXCITATION PROFILES ..... - 156 -

FIG. 3.19: MEASURED AND SIMULATED RESPONSE PROFILES FOR VCS-B (2-LAYER LPFD MODEL; TIME STEP OF 180 SECONDS; EQUIVALENT SLAB THICKNESS OF 0.15 M) ..... - 156 -

FIG. 3.20: 3-LAYER LPFD MODEL VS. FR MODEL FOR VCS-C (TIME STEP OF HALF AN HOUR, EQUIVALENT SLAB THICKNESS OF 0.2 M) ..... - 159 -

FIG. 3.21: FR MODEL AND 3-LAYER LPFD MODEL FOR VCS-C UNDER HIGH ABSORBED SOLAR RADIATION (TIME STEP OF HALF AN HOUR, EQUIVALENT SLAB THICKNESS OF 0.2 M) ..... - 160 -

FIG. 4.1: PREDICTIVE CONTROL STRATEGY FLOWCHART ..... - 166 -

FIG. 4.2: WEATHER CONDITIONS AND ROOM AIR TEMPERATURE SET PROFILE DURING A TWO-DAY SPACE HEATING PERIOD (SUNNY DAY FOLLOWED BY CLOUDY DAY) ..... - 169 -

FIG. 4.3: DFS REPRESENTED ROOM AIR TEMPERATURE SET-PROFILE AND CORRESPONDING ENERGY PROFILES ..... - 172 -

FIG. 4.4: THERMAL NETWORK OF AN ACTIVE BITES FLOOR WITH ITS CROSS SECTION TRANSFORMED- 173 -

FIG. 4.5: SCHEMATIC OF AN N-LAYER ASSEMBLY, AND ITS EXCITATIONS (SAME AS FIG. 3.10) ..... - 173 -

FIG. 4.6: SIMPLIFIED THERMAL NETWORK OF A ROOM WITH A CLOSED-LOOP BITES SYSTEM SITTING ON SOIL (FIG. 4.4) ..... - 175 -

FIG. 4.7: COMPARISON OF SET AND SIMULATED ROOM AIR TEMPERATURES AND BITES THERMAL OUTPUTS (CLOSED-LOOP) ..... - 179 -

FIG. 4.8: SIMULATED THERMAL PERFORMANCE BASED ON PREDICTED THERMAL ENERGY INJECTION RATES (CLOSED-LOOP BITES) ..... - 180 -

FIG. 4.9: COMPARISONS OF (A) SET AND SIMULATED ROOM AIR TEMPERATURES AND (B) BITES THERMAL OUTPUT AFTER SMOOTHING THERMAL ENERGY INJECTION RATES (CLOSED-LOOP) ..... - 182 -

FIG. 4.10: SIMULATED ROOM AIR TEMPERATURES AND BITES THERMAL OUTPUT AFTER SMOOTHING THERMAL ENERGY INJECTION RATES WITH AN ALTERED ROOM AIR TEMPERATURE SET-PROFILE (CLOSED-LOOP) ..... - 183 -

FIG. 4.11: WEATHER CONDITIONS AND SIMULATED ROOM AIR AND BITES TEMPERATURES BASED ON SMOOTHED THERMAL ENERGY INJECTION RATES (CLOSED-LOOP; SMOOTHED INJECTION; COOLING DOMINATED) ..... - 184 -

FIG. 4.12: THERMAL NETWORK OF AN OPEN-LOOP BITES SYSTEM SITTING ON SOIL ..... - 185 -

FIG. 4.13: SCHEMATIC OF ENERGY FLOWS AND VARIABLES FOR THE OPEN-LOOP SYSTEM SHOWN IN FIG. 1.8-B ..... - 185 -

FIG. 4.14: COMPARISON OF SET AND SIMULATED ROOM AIR TEMPERATURES AND BITES THERMAL OUTPUT (OPEN-LOOP; FLOW RATE OF 3 ACH; HEATING DOMINATED) ..... - 191 -

FIG. 4.15: SIMULATED THERMAL OUTPUT BASED ON PREDICTED THERMAL ENERGY INJECTION RATE AT AHU (OPEN-LOOP; SMOOTHED INJECTION; FLOW RATE OF 3 ACH; HEATING DOMINATED) ..... - 192 -

FIG. 4.16: SIMULATED THERMAL RESPONSES AFTER INJECTION SMOOTHING (OPEN-LOOP; FLOW RATE OF 3 ACH; HEATING DOMINATED) ..... - 193 -

FIG. 4.17: COMPARISON OF SET AND SIMULATED ROOM AIR TEMPERATURES AND BITES THERMAL OUTPUT (OPEN-LOOP WITH SIMPLIFIED MODEL; FLOW RATE OF 3 ACH (78 L/S OR 26L/S PER AIR PATH); SMOOTHED INJECTION; HEATING DOMINATED) ..... - 196 -

FIG. 4.18: COMPARISON OF SIMULATED THERMAL PERFORMANCE OF A CLOSED-LOOP (CL) AND AN OPEN-LOOP (OL) SYSTEMS (SMOOTHED INJECTION; COOLING DOMINATED) ..... - 198 -

FIG. 5.1: THERMAL ATTRIBUTES (TES: THERMAL ENERGY STORAGE) ..... - 207 -

FIG. 5.2: CONCEPTUAL SCHEMATIC OF DYNAMIC RESPONSE (ATHIENITIS AND SANTAMOURIS 2000) - 209 -

FIG. 5.3: (A) TRANSFORMED CROSS SECTION AND (B) THERMAL NETWORK OF AN OPEN-LOOP BITES SLAB AND ITS ASSOCIATED ROOM ..... - 210 -

FIG. 5.4: DYNAMIC RESPONSE OF AN OPEN-LOOP BITES SLAB AND ITS ASSOCIATED ROOM FOR 1 CYCLE PER DAY EXCITATIONS (LEFT Y-AXIS IS TIME LAG IN HOURS; RIGHT Y-AXIS IS THE MAGNITUDE OF TRANSFER FUNCTIONS (UNIT LESS); X-AXIS IF EQUIVALENT CONCRETE THICKNESS IN METERS) - 216 -

FIG. 5.5: WEATHER CONDITIONS AND ROOM AIR TEMPERATURE SET-PROFILE DURING A TWO-DAY SPACE HEATING PERIOD (ROUND DOTS: PIVOTS, TL: TIME LAG) ..... - 219 -

FIG. 5.6: THERMAL ENERGY INJECTION RATES AT THE AIR HANDLING UNIT (AHU) AND CORRESPONDING ROOM AIR AND BITES TEMPERATURES: (A) TEMPERATURE PROFILES; (B) HEAT FLUX PROFILES (OPEN-LOOP SYSTEM) ..... - 220 -

FIG. 5.7: ACTIVE BITES SYSTEMS DESIGN PROCEDURE ..... - 231 -

FIG. 5.8: A VENTILATED BITES SYSTEM (SOURCE: PTY LTD, WWW.HOLLOWCORE.COM.AU) ..... - 232 -

FIG. 5.9: A TYPICAL CONCRETE MASONRY BLOCK ..... - 235 -

FIG. 5.10: SCHEMATIC OF CREATING CONNECTION BETWEEN HOLLOW CORES (AIR CHANNELS) ..... - 237 -

FIG. 5.11: POTENTIAL APPROACH FOR INCREASING STORAGE CAPACITY: (A) REDUCE VOID SPACE; (B) ADD THICKER PLASTERING OR ADDITIONAL THERMAL STORAGE PANELS; (C) INCREASE FACE SHELL THICKNESS ..... - 237 -

FIG. 5.12: SCHEMATIC OF A CONNECTION BETWEEN A HOLLOW CORE SLAB AND A MASONRY BLOCK WALL ..... - 240 -

FIG. 5.13: NETWORK OF DESIGN ELEMENTS FOR STRUCTURAL AND THERMAL FUNCTIONS 241

FIGURES IN APPENDIX

FIG. A1.1: VERTICAL CROSS SECTION OF THE COMPOSITE TROMBE WALL (SHEN ET AL. 2007) ..... - 266 -

FIG. A1.2: SCHEMATIC OF THE EVAPORATIVE COOLING SYSTEM (KRUGER ET AL. 2010). ..... - 270 -

FIG. A2.1: PLAN VIEW, LONGITUDINAL CROSS SECTION (A), AND TRAVERSAL CROSS SECTION (B) OF VCS WITH MONITORING POINTS INDICATED ..... - 272 -

FIG. A5.1: THERMAL NETWORK FOR HEAT FLOW DIVISION CONCEPT (NODE 0 IS THE OUTERMOST NODE OF ASSEMBLY $1 \leftarrow SC1$, WHILE NODE L IS THE OUTERMOST NODE OF ASSEMBLY $SCN \leftarrow N$. SOURCE NODE SC IS IN-BETWEEN THE TWO ASSEMBLIES) ..... - 276 -

FIG. A6.1: DYNAMIC RESPONSE OF AN OPEN-LOOP BITES SLAB AND ITS ASSOCIATED ROOM FOR 1 CYCLE PER DAY EXCITATIONS (FLOW RATE OF 0.3 ACH) ..... - 280 -

FIG. A8.1: SIMULATED TEMPERATURES OF THE WALL ASSEMBLY (FR: FREQUENCY RESPONSE; FD: FINITE DIFFERENCE) ..... - 281 -

FIG. A8.2: THERMAL NETWORK AND SCHEMATIC OF A CONCRETE WALL WITH EXTERIOR INSULATION - 282 -

FIG. A8.3: BOUNDARY CONDITIONS ..... - 282 -

List of Tables

TABLE 1.1: ENERGY CONSUMPTION FOR SPACE THERMAL CONDITIONING ..... - 1 -

TABLE 2.1: APPLICATIONS OF CHARGE/DISCHARGE COMBINATIONS ..... - 40 -

TABLE 2.2: HEATING/COOLING CAPACITY OF HYDRONIC BITES SYSTEMS ..... - 71 -

TABLE 2.3: OPERATION (I.E. FAN OR PUMP) ENERGY CONSUMPTION ..... - 75 -

TABLE 3.1 COMPARISON OF OUTPUTS UNDER DIFFERENT CONFIGURATIONS ..... - 101 -

TABLE 3.2 MEASURED AND SIMULATED TEMPERATURE VALUES FOR JULY 16TH,°C (°F) ..... - 103 -

TABLE 3.3 THERMAL ENERGY SHARES BASED ON SIMULATIONS [16°C (60.8°F) AIR AT 200 L/S (424 CFM) FOR 6 HRS] KWH (MBTU) ..... - 105 -

TABLE 3.4: COMPARISON OF VCS-B MODELS WITH EXCITATION PROFILES AND INTERIOR TEMPERATURE FROM FIG. 3.14. ..... - 152 -

TABLE 4.1: KEY PARAMETERS OF THE ROOM THERMAL MODEL ..... - 171 -

TABLE 4.2: SAMPLE RESULTS USING SIMPLIFIED MODEL (AFTER SOURCE INPUT SMOOTHING TREATMENT) ..... - 196 -

TABLE 5.1: THERMAL ATTRIBUTES RELATED DIMENSIONS OF STANDARD HOLLOW CORE SLABS (CPCI 2010) AND THEIR VARIATIONS ..... - 234 -

TABLE 5.2: THERMAL ATTRIBUTE RELATED DIMENSIONS OF STANDARD CONCRETE MASONRY BLOCKS (CSA 2004, DRYSDALE 1999) AND THEIR VARIATIONS ..... - 236 -

Preface

This is a manuscripts-based dissertation, containing four manuscripts ready to be submitted for review, and three published or in-press journal papers. The three published or in press papers compose the three sections of Chapter 3.

For ease of reading and to avoid repetition, these manuscripts have been modified from their originals, mainly reducing their introductions. Equations variables are independent in each manuscript, and may be different between manuscripts. The numbering of equations, tables, and figures includes the numbers of the chapters they belong to. All the appendices, nomenclatures, and references from different chapters and sections (i.e. manuscripts) are moved to the end of this thesis and combined. Note that, the numbering of the subsections restarts in each section/chapter (i.e. paper) in the body of the text, not as being continuous in the table of content.

Chapter 1 Introduction

Research indicates that space thermal conditioning (i.e. space heating and cooling) accounts for a large percentage of energy consumption (Table 1.1) and peak electricity demand (Fig. 1.1). The energy consumption for space conditioning of buildings in residential sector accounts for more than 55% of the sector's total energy consumption for Canada and United States (US) (Table 1.1). For European Union (EU) countries, the space heating energy consumption of residential buildings was about 150 kWh/m^2 in 2005 (EEA 2011). As shown in Table 1.1, the space conditioning energy consumption of commercial/institutional buildings is even higher than that of residential buildings.

Table 1.1: Energy consumption for space thermal conditioning

Conditioning type	Sector	Canada*	United States**
		Energy intensity, kWh/m^2 (percentage of sector's energy consumption, %)	Energy intensity, kWh/m^2 (percentage of sector's energy consumption, %)
Heating	Residential	146 (62.8)	69 (48.2)
	Commercial/ Institutional	230 (47.8)	87 (24)
Cooling	Residential	3.6 (1.6)	10 (7.2)
	Commercial/ Institutional	22 (4.6)	32 (8.9)

*year 2008 (OEE 2011); **year 2005, source: (EERE 2007, 2011).

Besides reducing energy consumption, decreasing peak power demand for space conditioning is also important. Fig. 1.1 shows a monitored demand and generation profiles of a Canadian low-energy solar house on a cold sunny day. The demand profile also

represents the typical demand profile of residential buildings. As can be seen peak electricity demand (negative) is caused by space heating in the early morning. Thermal energy storage (TES) could be used to reduce this peak through collected solar gains from previous sunny day(s) if available or pre-heating using off-peak utility power. Lowering the peak power demands of individual buildings may enable designers to reduce the capacities of the selected mechanical systems if taken into account at the design stage. A collective effort of many buildings will reduce the peak electricity demand from communities, thus reducing the need to add new capacity for power generation and transmission infrastructure.

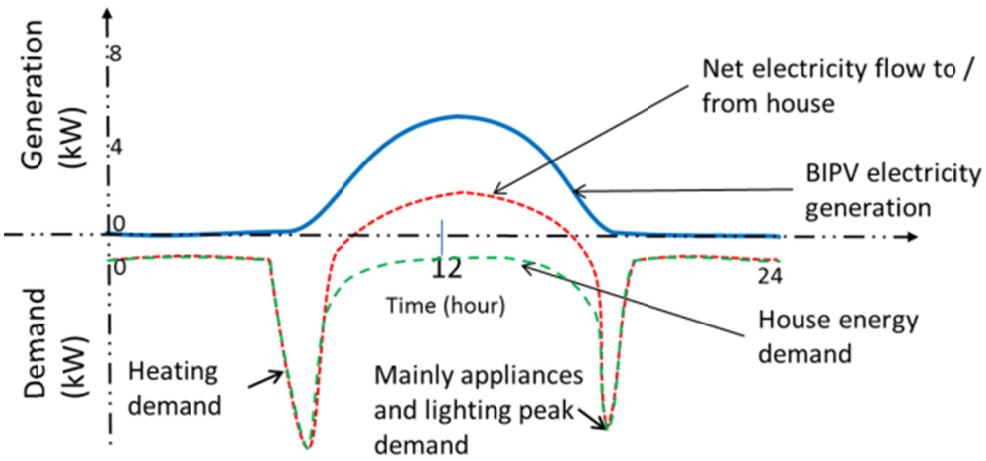

Fig. 1.1: Schematic of demand and generation profile for Canadian near net-zero energy house (cold sunny day) (courtesy of A. Athienitis and C. Hachem, source data: Doiron et al (2011))

European Environment Agency (EEA) (2008) stated that there is a great potential in reducing the energy consumption and peak power demand in heating/cooling in buildings. Various research and development (R&D) activities worldwide are demonstrating the potentials, such as the EQuilibrium demonstration project in Canada (CMHC 2006), and international research project Net-Zero Energy Solar Buildings (IEA-SHC 2008).

Net-zero energy buildings are now becoming possible through optimal combinations of renewable energy technologies and energy efficiency measures (IEA-SHC 2008). The net-zero energy balance may be achieved through a combination of passive and active technologies, building-integrated photovoltaic systems, thermal energy storage, heat pumps, and energy efficiency measures to reduce energy consumption for lighting appliances as shown in Fig. 1.2. PHEV may possibly be used as an electricity storage/backup device. One should keep in mind that reducing energy consumption and peak power demand should not compromise thermal comfort. High performance buildings should provide enhanced thermal comfort.

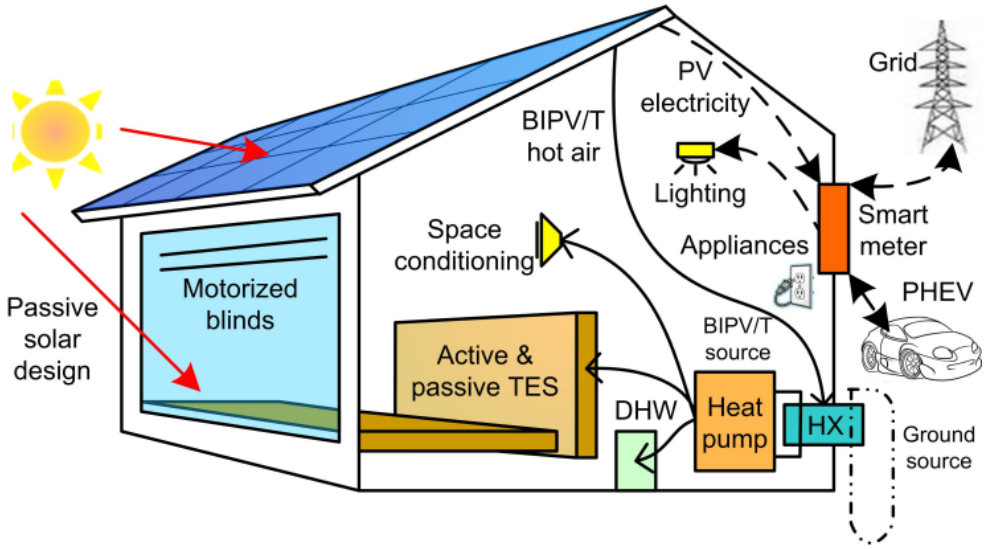

Fig. 1.2: Net-zero energy solar home concept (IEA-SHC 2008)

While reductions of energy consumption and peak power demand of buildings are important, thermal comfort is another major concern of building owners and occupants. Thermal comfort has a significant impact on the health and productivity of occupants (ASHRAE 2004a). The comfort range of indoor temperature for normally dressed people is relatively narrow (from 21 to 26 ºC) (ASHRAE 2009f) as compared to the annual variation of outdoor

temperature, especially in cold climate regions. Even though, this range can be relaxed at night and through adaptive thermal comfort approaches (ASHRAE 2004a), especially for cooling situations, the temperature difference between outdoor and indoor desired conditions is still considerable. The air temperature distribution, mean radiant temperature, interior surface temperatures, and air movement are among the primary factors affecting thermal comfort (ASHRAE 2009f).

This thesis aims to develop energy-efficient and cost-effective methods to reduce the energy consumption and peak power demand for space conditioning without sacrificing thermal comfort in buildings. The study begins with a discussion of the current situation of energy consumption and power demand for space conditioning of residential buildings.

1. Problem identification and significance

An analysis of the energy performance of two average houses is presented first to identify the representative energy performance of average residential buildings. After that, the case study of a state-of-the-art low energy solar house shows how energy-efficient approaches can be adopted in residential buildings to significantly improve their energy performance. It also helps identify research needs. The author participated in the modeling, design, and assessment of the monitored performance of the solar house. The work serves as the preliminary work of the present research.

1.1. Average houses

The space heating power demand of average lightweight houses that adopt instantaneous (on-demand) space heating (e.g. electric), almost linearly follows the temperature difference between interior and exterior. Fig. 1.3 shows the electric space heating power demands of

two bungalow houses (one-story detached houses) located in the suburban area of Montréal, Québec, Canada. They have gross floor areas of around 110 m^2.

These two houses did not significantly use solar thermal energy, passively or actively, for space heating. On sunny winter days, solar radiation somehow reduced the space heating load, but the contribution was insignificant. Their electric space heating peak power demands reached 10 and 8 kW, respectively. Their average electric energy consumptions were about 119 kWh/m^2 in 1994 and 98 kWh/m^2 in 1995. For comparison, the average values in residential sector in the same region (Québec, Canada) were about 189, 180, and 156 kWh/m^2 for year 1994, 1995, and 2008, respectively (OEE 2011). These two houses have less space heating energy consumption than the average of the region. The main reasons are that they are constructed complying with a higher insulation standard, and located at the south part of the region. The higher regional value also indicates that houses in this cold climate region normally don't use energy efficient approaches to reduce their space heating energy consumption.

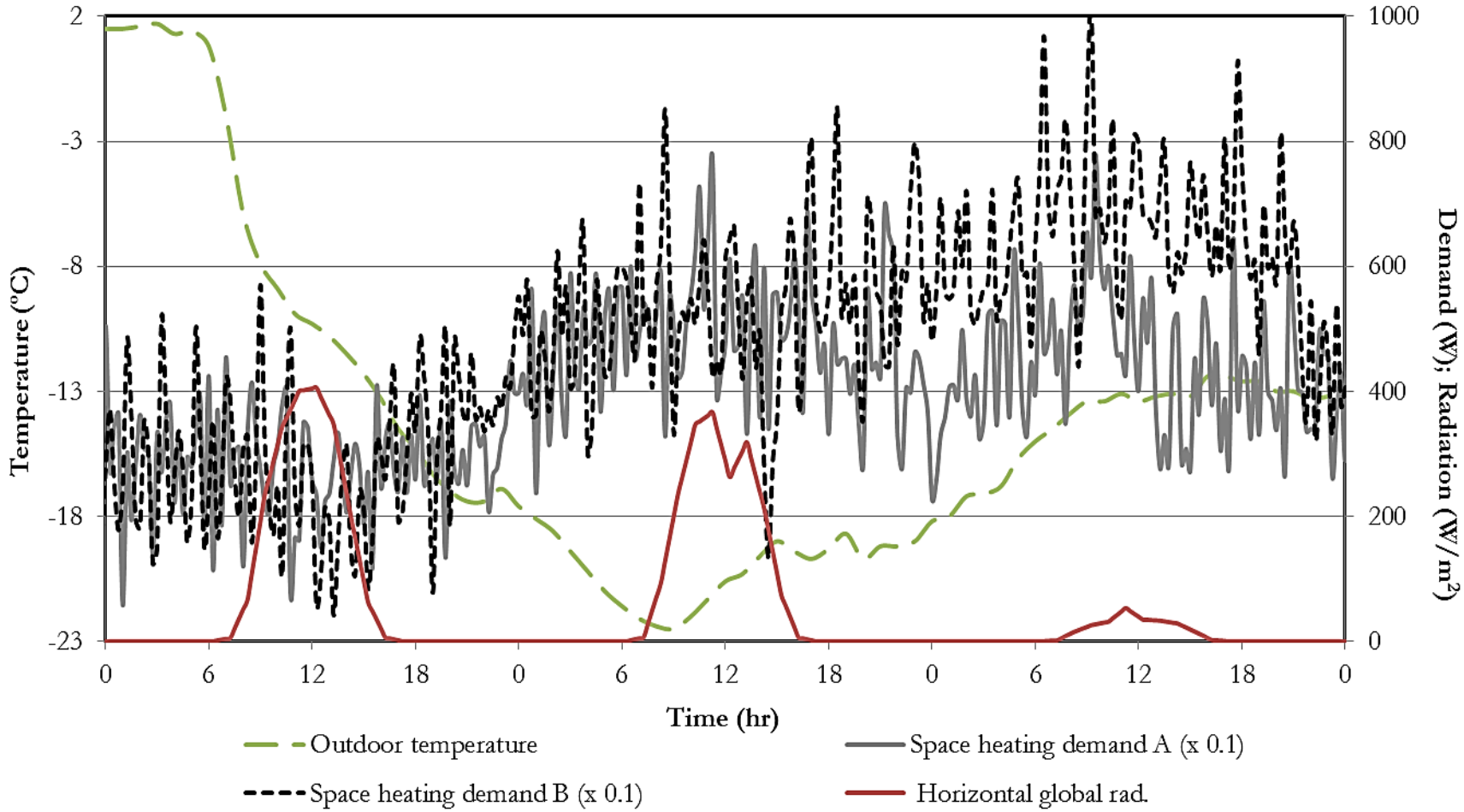

Fig. 1.3: Profiles of outdoor temperature and electric space heating power demand of two bungalow houses. (The plotted values of power demand are 1/10 of the actual values. Source data are provided by Dr. J. Millette from Energy Technology Laboratory of Hydro Quebec.)

1.2. Low-energy solar house - ÉcoTerra™

Fig. 1.4: ÉcoTerra demonstration house, November 2007 (the photovoltaic system made up of amorphous Silicon laminate panels attached to metal roof is on the upper roof section).

ÉcoTerra (Fig. 1.4), a low-energy solar house, is an EQuilibrium demonstration house (CMHC 2006). Its energy design and energy performance monitoring and analysis were led by Dr. A. Athienitis from Concordia University. Chen et al. (2010a, 2010b) described the modeling, design, and preliminary energy performance assessment of the house and its building-integrated photovoltaic/thermal (BIPV/T) system thermally coupled with a ventilated concrete slab (VCS). Doiron et al. (2011) provided a detailed energy analysis of the house. ÉcoTerra currently serves as an important case study in the International Energy Agency (IEA), Solar Heating and Cooling Task 40 "Net-Zero Energy Solar Buildings" project (IEA-SHC 2008). Since August 2009 the house is occupied and its control system has been custom designed and implemented with input from the Concordia research team. Measured data from the occupied period provide important occupant behavior data related to thermal comfort – an important aspect of this research.

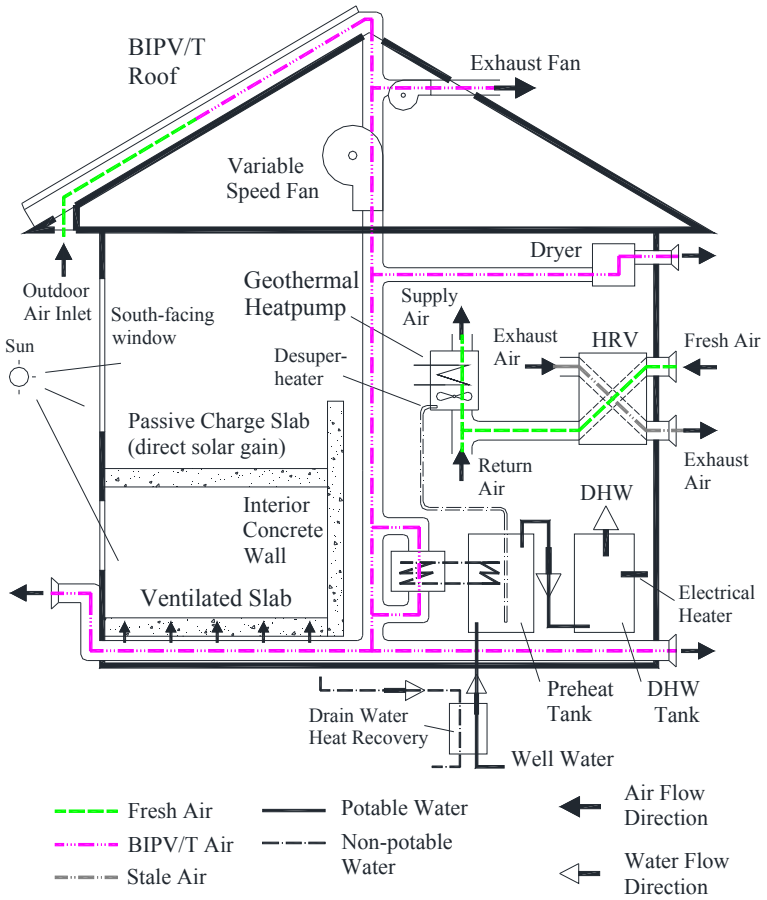

Fig. 1.5: Schematic of the integrated energy system and locations of thermal mass (Chen et al. 2010a).

ÉcoTerra is a two-storey detached house with gross floor area of 240 m^2 including a heated basement. It was prefabricated in a factory in seven modules and assembled on site in 2007 in Eastman, Québec, Canada. This house had a design goal of near net-zero annual energy consumption. Energy efficient devices and several practical solar technologies are adopted to help reach this goal. An air-based open-loop BIPV/T system produces electricity and collects heat simultaneously. Building-integrated thermal energy storage (BITES) is utilized in passive and active forms (Fig. 1.5). Relatively large south facing triple-glazed windows (equivalent to about 9% of floor area) and distributed thermal mass in the direct gain zone are employed to collect and store passive solar thermal gain. The primary heating and

cooling is provided by a 3-ton (10.5 kW) two-stage water-to-air ground source heat pump (GSHP). A forced-air system is adopted for space conditioning and ventilation with a heat recovery ventilator to reduce heat loss due to ventilation.

The BITES system, VCS, stores part of the collected thermal energy from the BIPV/T system. The thermal energy stored in the thermal mass is released passively through the top surface of the mass into the room. It is an active charge and passive discharge TES system. This VCS has a floor area of 30 m^2 and a storage volume of about 5 m^3. For every degree Celsius temperature change, it can store or release almost 3 kWh of thermal energy. For heat storage application, Chen et al. (2010b) showed that the VCS can store 9 to 12 kWh of thermal energy with 30 to 35 ºC inlet air at 200 L/s flowing through the system for roughly 6 hours. It can store thermal energy during a series of clear sunny days without overheating the slab surface or the living space. This research shows that coupling the VCS with the BIPV/T system is a viable method to enhance the utilization of solar thermal energy.

Fig. 1.6 shows the temperature profiles of ÉcoTerra on winter days. Space heating was not needed during a sunny daytime and the following evening. The space heating power demand was about 2.7 kW, by using a GSHP with an average COP of 3.8 (Doiron et al. 2011). For year 2010, the mechanical space heating load was about 42 kWh/m^2, and the energy consumption of the GSHP was about 11 kWh/m^2 (Doiron et al. 2011). The space heating energy consumption is dramatically reduced as compared to regional average value. The heating power demand was also greatly reduced due to the application of the GSHP. Without the GSHP, it would have been about 10.5 kW. Long-term monitored data show that the peak power demands of space heating and the whole house typically occurred in the evenings of overcast days or in the cold mornings.

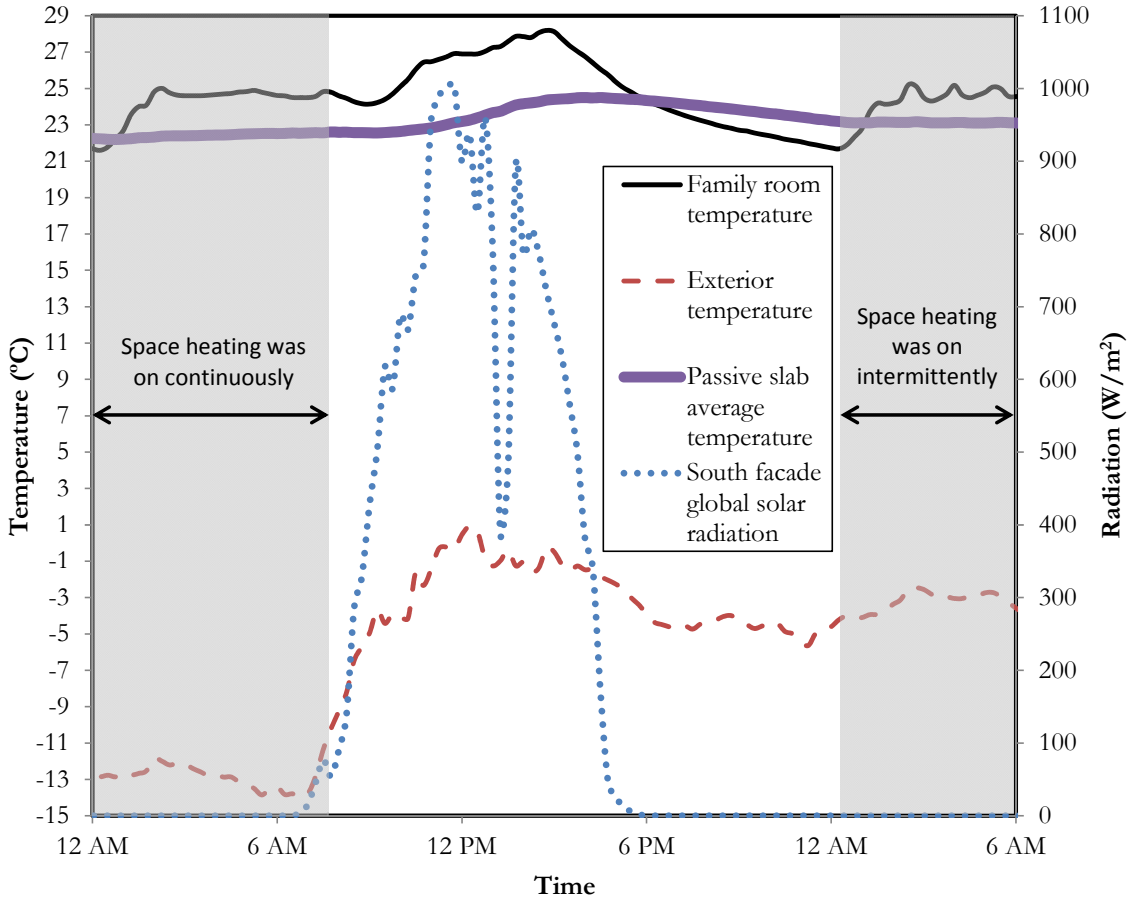

Fig. 1.6: Temperature and solar radiation profiles on two winter days (Feb. 25th and 26th)

Long-term monitored data also show that space overheating took place during the afternoons of sunny days with mild outdoor temperatures (higher than 0 °C). For example, space overheating occurred (higher than 28 °C) during the daytime on Feb. 25th of 2009 (Fig. 1.6), which was sunny with mild outdoor temperature. The space overheating would have been avoided if the thermal coupling between the BITES systems (VCS and passive concrete mass) and the rest of the room (i.e. the room air and other interior surfaces) was stronger and hence excess heat can be transferred to the BITES systems. The stored heat could be used to reduce the space heating load for the following morning. Also, the space overheating

could have been avoided if the heating set-point (24.5 ºC) at the night of Feb. 24th was reduced.

1.3. Discussion

The energy performance investigation of the average houses and ÉcoTerra provides some important findings as discussed below. These findings are also applicable to other types of buildings (e.g. office, commercial or institutional).

- The energy consumption for space conditioning and thermal comfort of residential buildings have potential high improvements:
    - Utilization of solar thermal energy (e.g. passive and active solar heating) can significantly reduce the space heating energy consumption effectively;
    - Large and continual fluctuations in room temperature can be avoided by more effectively coupling thermal storage mass to room air
- The energy and thermal performance of the low-energy house can be further improved through means such as
    - Better TES design for storing more renewable energy (e.g. passive solar gain, from BIPV/T or solar air heating system) or excess heat gain for later use;
    - Space conditioning peak power demand can be reduced if TES systems can store more energy and release it at the desired time of the day (e.g. mornings and evenings).

In these potential improvements, TES plays an essential role – a thermal repository for the re-allocation and amplitude reduction of demand and supply. Hasnain (1998a, b) stated that properly designed and controlled TES can result in significant savings in the energy consumption, initial cost, and operation and maintenance costs.

2. Potential of active building-integrated thermal energy storage

Building fabric (i.e. structural skeleton, envelope, and interior partitions) constitutes a significant portion of the building's thermal capacity. Braun (2003) stated that the thermal capacity of a typical concrete building is in the order of 0.1 kWh/m^2/K in gross floor area. Antonopoulos and Koronaki (1998, 1999) estimated that the effective thermal capacitance of buildings ranges from 0.06 to 0.18 kWh/m^2/K. Concrete and masonry as common building construction materials have their own advantages of being ideal TES materials such as long term chemical and physical stability, and fire resistance. These findings indicate that concrete and masonry building fabric have high potential in being TES systems, and are available to be used for TES practices in a wide range of existing and new buildings. In this thesis, TES system that use building fabric (e.g. masonry block walls and concrete slabs) to store thermal energy and release it directly to their thermal zones to facilitate space conditioning are defined as building-integrated thermal energy storage (BITES) systems.

2.1. Active BITES

BITES systems are considered active if they embody controllable internal charge/discharge system, such as hydronic, air-based (i.e. ventilated) or electric systems (Fig. 1.7). Note that each system shown in Fig. 1.7 can be a floor, wall, or roof; insulation is optional and can be placed on the other sides of the tube to direct heat flow in the opposite direction. Internal charge/discharge systems engage more storage mass and heat exchange area. Hence, active systems are able to store and release more thermal energy at desired time and rate. Furthermore, active systems can have higher efficiency in storing and releasing thermal energy. For example, chiller-assisted slab pre-cooling saves overall operation energy

consumption, and increases the amount of energy can be stored due to lower temperature input.

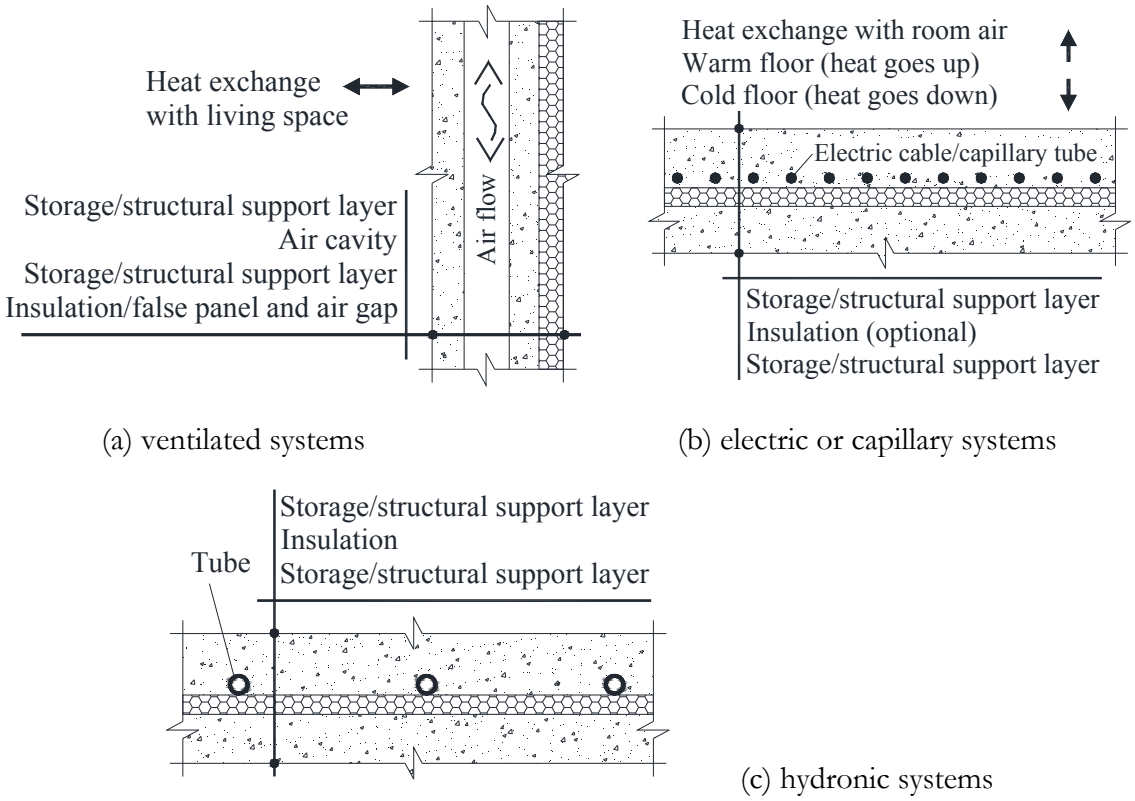

Fig. 1.7: Schematics of typical active BITES cross sections (Chen et al. 2013a).

Active BITES systems can be categorized into open-loop and closed-loop systems. Hydronic systems are always closed-loop since the heat transfer liquid circulates in a closed loop. In the case of air-based systems, there are various open-loop and closed-loop configurations. Open-loop air systems can have the outdoor air heated or cooled and then entering the living space (have ventilation and heat transfer functions) or just perform a heat transfer function as in the ÉcoTerra house. The VCS adopted in the ÉcoTerra house (Fig. 1.5) is an exterior open-loop but room interior closed-loop system – air passes through the slab to charge/discharge the slab, but does not enter the conditioned space.

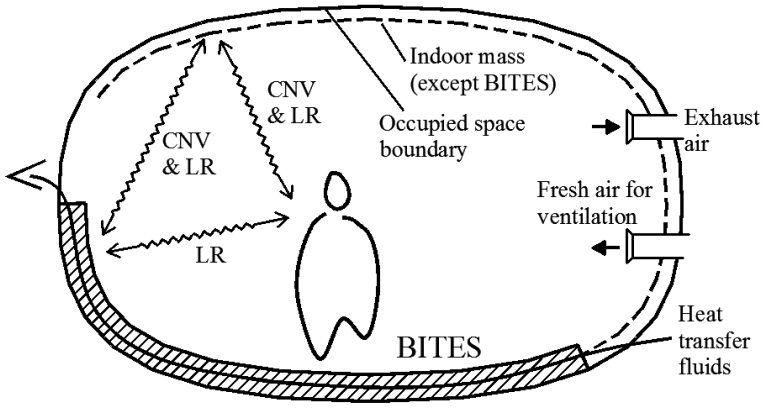

(a) Closed-loop to room interior (heat transfer fluids can be either liquids or air. In latter case, air does not pass from the BITES into the zone but the loop can be open to the exterior as in ÉcoTerra)

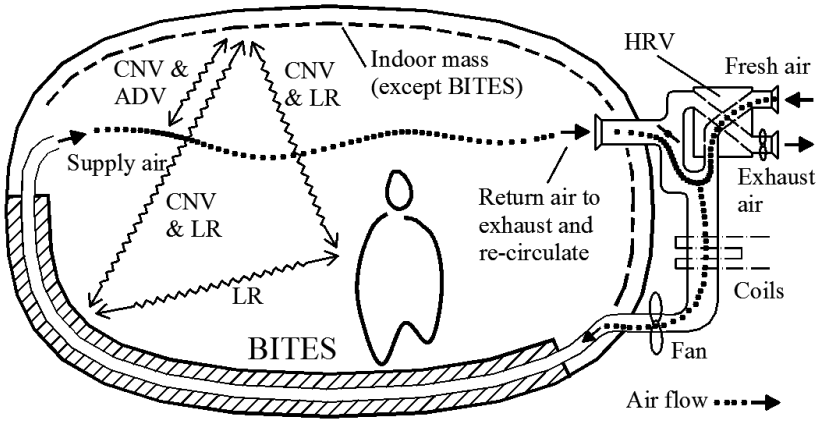

(b) Open-loop to room interior (air passes from BITES into the zone)

Fig. 1.8: Conceptual schematics of active BITES systems and their thermal coupling with the interior ("indoor mass" includes room air, wallboards, and furniture; CNV: convection; ADV: advection; LR: long-wave radiation; HRV: heat recovery ventilator)

For the rest of this thesis, "open-loop" or "closed-loop" only refers to room interior open-loop or closed-loop, since thermal interaction between the active BITES systems and the living space is the focus of this thesis. Closed-loop systems (Fig. 1.8-a) can be liquid- or air-

based. The heat transfer fluid is only for BITES charging/discharging, not interacting directly with room air. Open-loop systems (Fig. 1.8-b) will only be air-based. The air flow enters the room after passing through the BITES. Another possible open-loop configuration is that room air returns to air handling units (AHU) via BITES systems, but this configuration is not the focus of this thesis. In Fig. 1.8, the active BITES systems can be located in the ceiling, floor, or walls.

BITES systems have direct thermal coupling with their thermal zones as shown in Fig. 1.8. The thermal output from the BITES system to its thermal zone is through convection and long-wave radiation on the exposed surface of the BITES system, neglecting conduction at edges. For the open-loop configuration (Fig. 1.8-b), an additional path for the thermal output – advection – is available, implying a stronger thermal coupling and a higher rate in extracting the stored thermal energy.

With active BITES systems (e.g. hydronic or ventilated systems), primary direct space conditioning can be provided through the BITES in a distributed manner – the room side surface of the BITES systems serve as radiant heating/cooling panels. Inard et al. (1998) stated that distributed heat sources result in better thermal comfort over localized heat sources. Radiant heating generally results in improved comfort (ASHRAE 2011). With radiant floor heating, it is possible to achieve relatively uniform air space temperature in the vertical direction (ASHRAE 2008). Comfort levels offered by radiant heating/cooling can be better than that of other conditioning systems because thermal sensations of occupants are satisfied directly and air motion in the space is at normal ventilation levels for air quality.

2.2. Operation logic

The diurnal pattern of outdoor thermal conditions is roughly sinusoidal, and the heat gain/loss of well-designed buildings fluctuates about its neutral axis for a considerable time of a year. For example, in a cooling season, outdoor temperature is high during daytime, but night time temperature is usually lower than the upper limit of indoor comfort temperature range. The coolness during the night time can be stored and used to compensate the heat gain during the daytime.

Before supplying mechanical space conditioning, **passive measures with possible fan assistance** should be applied to flatten varying space conditioning demand due to fluctuating internal heat gain and exterior temperature, and take advantage of freely available energy. Passive measures (e.g. passive solar design) are based on the passive thermal dynamics of buildings. They can be enhanced with local air re-circulation in an open-loop configuration (Fig. 1.8-b). In Fig. 1.9-a, heating is needed during the night time, while cooling is during the daytime. Applying passive measures with possible fan assistance, the excess heat can be stored with BITES system and released during the daytime to reduce/avoid space cooling (Fig. 1.9-b).

For average houses with low thermal mass, their space conditioning demands are usually in phase with weather conditions and follow common occupancy schedules. For example, major residential units turn on their space heating between 7 and 8 o'clock in a cold winter morning. On a community scale, infrastructure peak power load occurs when the power demand of individual unit (households, offices) takes place together. Space conditioning demand can be made less dependent on weather conditions by using thermal storage buffering (part of passive measures).

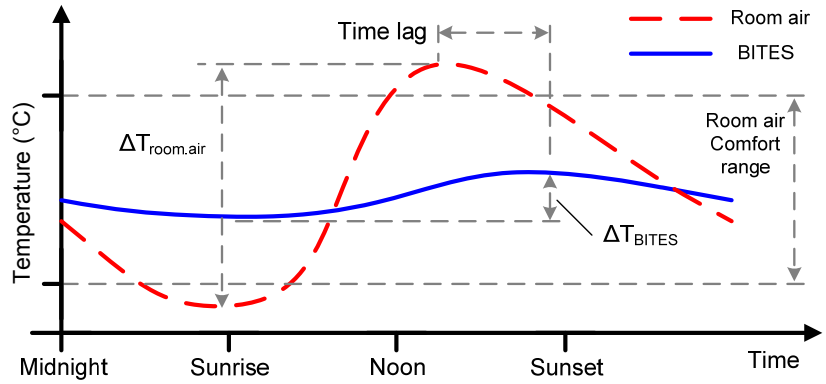

(a) Typical response with a low thermal storage BITES or weak interior thermal coupling in the presence of high interior solar or internal gains

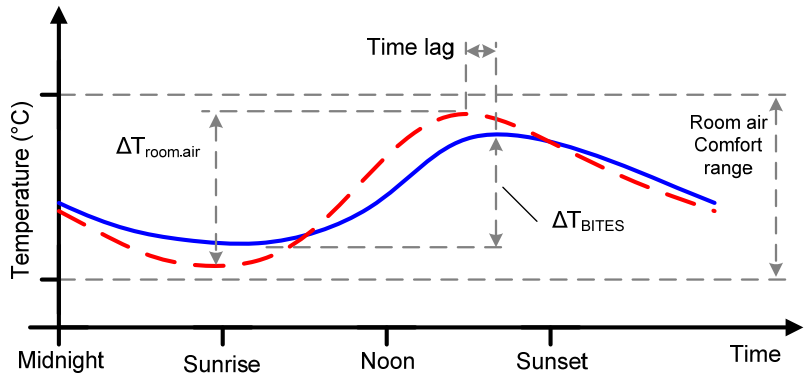

(b) Passive measures: strong thermal coupling between passive BITES and the thermal zone

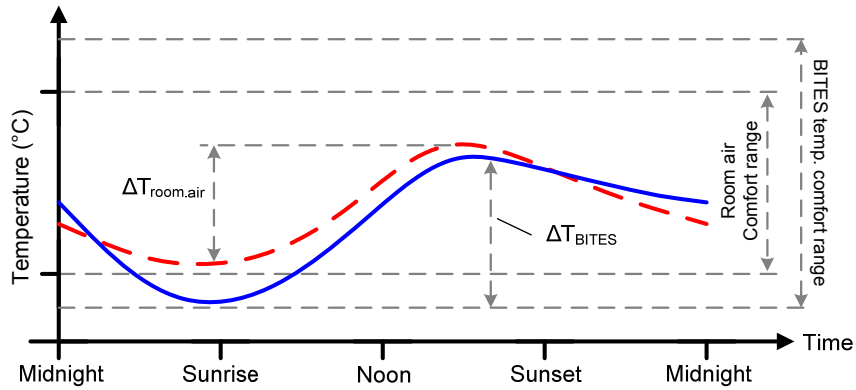

(c) Passive measures with possible fan assistance and pre-conditioning: active BITES systems and strong thermal coupling

Fig. 1.9: Concepts of passive measures, and pre-conditioning (typical temperature profiles of a zone with different levels of BITES applications and high solar/internal heat gains)

Furthermore, individual power demands can be shifted and reduced if auxiliary thermal energy is stored ahead of forecasted weather, and then used later - **pre-conditioning**. For the example shown in Fig. 1.9-c, chillers can be operated before the peak space cooling period, which normally has better operating conditions. Natural ventilation can be used instead if conditions permit. The provided coolness can be stored in active BITES systems and released later during on-peak periods.

Space conditioning demand should be first flattened as much as possible with passive measures, and then, if necessary, satisfied with the storage of auxiliary thermal energy during off-peak periods and/or renewable energy. Pre-conditioning shifts part of the demand forward, and buffering delays part of the demand. With both of them, the power demand for space conditioning can be significantly flattened. To take full advantage of active BITES, designers should adopt predictive control strategies in conjunction with enhanced passive response within the allowable comfort range.

2.3. Key design elements

Active BITES applications need to address three key elements: **thermal coupling with their zones**, **integrated design and operation**, and **integration of structural and thermal functions.** These elements are inter-related.

2.3.1. Thermal coupling

Sufficient thermal coupling between the BITES systems and their thermal zones should be provided in order to enable BITES systems to absorb and release thermal energy from and to the zone effectively, especially when primary space conditioning is supplied through BITES systems.

On the room side surface, the thermal coupling is mainly due to natural convection and long-wave radiative heat exchange between the exposed surface of the BITES system and the rest of the room. There is also direct solar radiation absorption by the surfaces of the BITES systems. These heat exchanges may be weakened by coverings such as furniture, carpet or wooden flooring (Fig. 1.10).

(a) (b)

Fig. 1.10: VCS in ÉcoTerra: (a) before house was occupied; (b) occupied

Previously presented Fig. 1.9 also graphically compares the typical dynamic thermal responses of a room with different BITES systems and different thermal coupling levels between the BITES and the thermal zone. In situation (a), there exists a low thermal storage BITES or weak interior thermal coupling in the room. Hence, the BITES has low effectiveness in moderating the room temperature fluctuation. The fluctuation of the room air temperature is large while the temperature of the BITES barely changes. Space cooling will be needed during daytime and possibly heating for night time.

In situation (b), the passive BITES is thermally coupled with the rest of the room. The time lag between the peak temperatures of the room air and the BITES system will be shortened.

The temperature amplitude of the room air will be significantly reduced, while the temperature amplitude of the BITES system will be increased. The temperature of the room air will follow closely that of the BITES system. The contribution of the BITES to the room air temperature amplitude reduction is significant. The coolness accumulated in the BITES during the night time is able to keep the room cool during the daytime.

In a zone with high passive solar gains during a sunny cold day, if strong thermal coupling is not present the room air temperature will increase significantly and often exceed the upper thermal comfort limit. This situation is also sometimes observed in ÉcoTerra (Fig. 1.6). For the conditions shown in Fig. 1.6, the living room was overheated during the sunny day even when the outdoor temperature was below 0ºC. The room temperature exceeded 27ºC for several hours due to the passive solar gains even though no significant space heating was used. During the following night, the room temperature dropped much quicker than the slab temperature, indicating the weak thermal coupling between the room air and the passive concrete slab.

Fig. 1.9-a reflects the situation shown in Fig. 1.6. If there is a stronger thermal coupling between the room and the BITES system (Fig. 1.9-b), excess thermal energy will be effectively stored and daytime space overheating will be avoided. Room temperature peak is shifted later. During the night time, the stored thermal energy will be released from the BITES system to the room air. Room temperature could falls within comfort zone without auxiliary space heating or cooling. This is the passive measures concept presented earlier.

In situation (c) (Fig. 1.9-c), active BITES system is adopted and strong thermal coupling with its thermal zone exists. The temperature of the active BITES system leads the room air temperature proactively, instead of following. The temperature amplitude of the BITES can

be larger than that of the room air. Near the sunrise hour, in contrast to (a) and (b), there is no significant time lag between the temperature responses of room and the BITES due to the active charge/discharge in the BITES system.

Increasing the thermal coupling can also reduce the temperature difference between the BITES and its thermal zone. This reduction has significant benefits. The operation temperature of the BITES systems can be lower for space heating and higher for cooling. This will reduce the operation energy consumption and the initial costs of the mechanical equipment and service systems (by downsizing them). It also creates a wide set of solutions in the choice of energy sources (e.g. renewable and recovered waste heat).

2.3.2. Integrated design and operation

BITES systems can be categorized into passive and active systems. Active systems embody charge/discharge systems to actively charge and/or discharge thermal energy. Hydronic radiant floor with significant storage mass is a common example of an active closed-loop BITES system. For passive BITES systems, control is normally external to the system, such as control of the transmitted solar radiation (through motorized shading) and night time building pre-cooling. For active BITES systems, operation has to be taken into account during the design stages.

Key challenges for proper operation of active BITES systems include the following:

(1) Due to the relatively strong thermal coupling between the BITES system and the rest of the room, the operative temperature (sense of occupants) will be significantly influenced by the exposed BITES surface temperature and the possible advective thermal output of the BITES (e.g. the supply air from the BITES in Fig. 1.8). The BITES temperature has to be controlled in the thermal comfort range well;

(2) High thermal inertia of BITES systems. This means slow response and significant amount of thermal energy is needed to regulate the BITES temperature. High power intensity and precise schedule are needed for fast regulation without high overshoot. The dynamic response of indoor objects (e.g. furniture and wallboards) also need to be considered;

(3) Improving building energy performance through use of active BITES systems.

- Pre-conditioning of BITES and indoor mass to utilize off-peak energy and reduce peak power demand.
- Efficient utilization of renewable energy. This requires storing energy as much as allowed with respect to energy availability (e.g. night time for relatively cooler air) and other constraints (e.g. room temperature).
- Allowing room temperature to float with exterior weather conditions to utilize the thermal zone as thermal collector and thermal storage (e.g. passive solar heating or night time free cooling). For example, room temperature is allowed during sunny daytime to rise up to the upper comfort limit to capture useful passive solar heat gain.

The first two factors are the main challenges for control because the active BITES systems have to provide good thermal comfort as their first priority; while optimizing the energy performance of the active BITES in a whole building context.

Using passive measures with possible fan assistance, excess thermal energy from a thermal zone can be transferred to its BITES, and released back to the zone when needed. In this process, the temperatures of the active BITES system and its thermal zone swing within allowable thermal comfort limits. The time period for the swing should suit that of the

thermal load – ideally the zone temperature reaches its peak at the time or after when the thermal load switches from cooling to heating. The design of the active BITES system should provide a suitable dynamic response that matches the time period required. For example in passive solar design, an active BITES system should be able to absorb significant portion of the transmitted solar heat gain and release it back to the room after a suitable time to avoid space overheating. Thermal coupling between the BITES system and the thermal zone is also critical in these storage and release processes. It can be enhanced with open-loop design (e.g. local re-circulation of room air through BITES systems (Fig. 1.8-b)).

Pre-conditioning takes advantage of available ambient renewable and/or off-peak purchased energy. These two kinds of energy can be used to pre-heat or pre-cool the BITES and its zone to reduce purchased energy consumption. Proper active BITES design will enable sufficient charge/discharge capacity to store desirable energy within a limited time.

Fig. 1.11 demonstrates the passive measures and pre-conditioning of an active BITES system and its thermal zone during a shoulder season period – it is sunny and cool during daytime but heating may be needed during night time. Through optimizing passive measures with possible fan assistance, the BITES system keeps the room cool during the daytime by absorbing the excess heat from the room, but warms the room during the night time by releasing previously absorbed heat. However, passive measures with possible fan assistance alone are not sufficient, and some auxiliary heat injection to the BITES system is required during the night time in order to keep the room temperature within comfort range. With pre-conditioning operation (action "6"), heat is injected to the BITES system and consequently to the room (action "3") during the daytime. Consequently, the temperatures of the room and the BITES systems are raised (action "1" and "2"). Thus, the thermal

energy originally needed for the night time is reduced (action "5"). Heat injection for actions "3" and "6" can be accomplished with solar thermal collectors or heat pump.

Ideal operations should make use of active BITES systems to reduce space heating/cooling through storage and buffering, and to store useful thermal energy during favorable periods (e.g. ambient renewable energy) and release it in the following unfavorable periods. Also, peak power demand reduction should also be addressed. These objectives require energy-conserving operation strategies and predictive control. The acceptable range of thermal comfort offers flexibility but also imposes limits on operating strategies.

The design and operation of an active BITES system are interrelated, but the operation leads the design. This is mainly because the BITES has become part of a service system that supplies primary space conditioning. The operations aim to maintain room air temperature within comfort zone in a low cost manner, by managing the thermal energy input with respect to source choice (e.g. ambient renewable energy vs. purchased energy) and scheduling (e.g. on-peak purchased energy vs. off-peak). To accomplish the desired operations, a suitable design is needed. On the other hand, operations have to adapt to the allowable design and attain potential benefits. In some cases, designs may be limited by other building parameters. For example, the maximum amount of thermal mass may be limited by the allowable structural load.

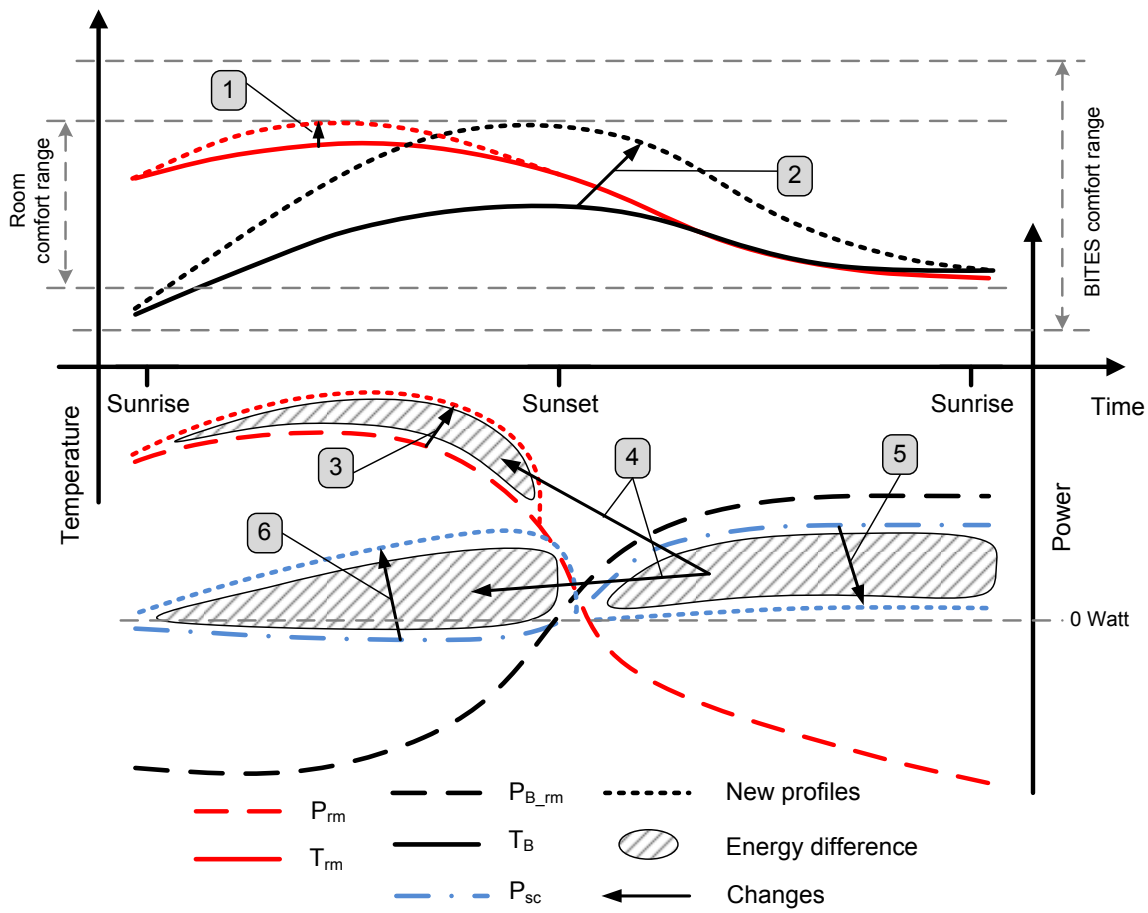

1. Room temperature increases within comfort range due to action "6";
2. BITES becomes warmer due to action "6";
3. More heat gain into the zone;
4. Auxiliary thermal energy is stored ahead for predicted heating load;
5. Use of auxiliary energy is avoided due to action "4";
6. BITES pre-heating operation.

Fig. 1.11: Schematic of passive measures and pre-conditioning concepts (P_{rm} is the heat gain/loss of the room; P_{B_rm} is the thermal output from the BITES to the room; P_{sc} is the thermal energy injection rate to the BITES)

2.3.3. Integration of structural and thermal designs

In using the structural components for TES, the structural and thermal functions are related to the material's thermo-physical and mechanical properties, and the geometry of the

components. In the example of a reinforced concrete slab, if the property of the material is given, the flexural strength will be influenced by the thickness of the slab and the placement of the reinforcement. Its TES capacity per unit surface area is determined by the net cross-section area, but its thermal admittance (Chapter 5 and Section A4 in Appendix) is related to the geometry of the cross section (e.g. D-1 and D-2 in Fig. 1.12). Fig. 1.12 shows the conceptual cross sections of two reinforced concrete slabs. Assuming the thickness of the slab (a) equals to that of slab (b), and the amount of the reinforcement and their placement depths are the same for these two cross sections, the flexural strengths of both for positive moment (i.e. downward loads) are about the same since the tensile strength is mainly provided by the reinforcement. However, slab (b) has lighter dead load than slab (a), and more effective use of material. Another important observation is that the TES capacity of slab (a) is higher than that of slab (b) since its cross-sectional area is larger; however, the TES function of slab (a) may not be as effective as that of slab (b) since slab (b) has higher thermal coupling due to larger cross-sectional Biot number and larger surface area per unit floor area. That means slab (a) is able to store and release more thermal energy than slab (b) in a long duration, but slab (b) will store and release more thermal energy within a short term (e.g. one day). Short term storage capacity is actually more important in peak load reduction.

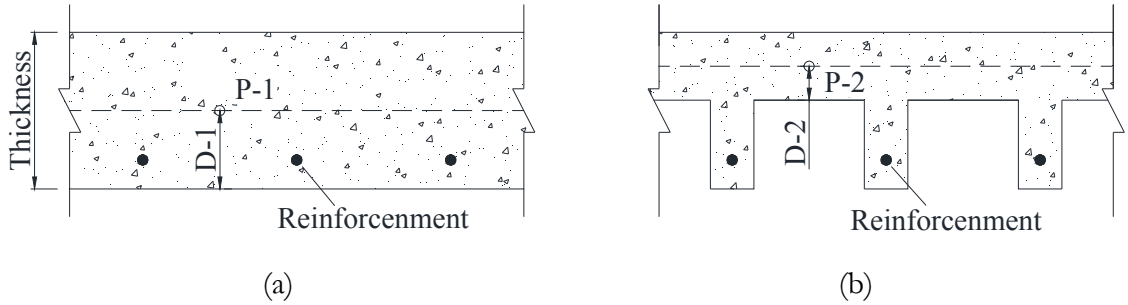

Fig. 1.12: Schematics of the cross sections of two reinforced concrete slabs

In current practices, the structural and TES functions are not well integrated. Often the use of storage mass is an afterthought and leads to additional structural loads, waste of material, and extra cost. For example, common design of hydronic slabs for radiant space conditioning is shown in Fig. 1.13. Extra non-structural concrete (just "thermal storage mass") is placed on top of the structure. This design increases the structural load, occupies extra room space, and initial construction cost. In light-weight buildings, such as wood-frame structure, passive concrete slab is placed on top of the wood-truss supported wooden floor. The wooden floor reduces the surface heat transfer coefficient of the bottom surface of the concrete. In these practices, the structural functions are completely separated from the TES function, thus leading to increased costs. This is due to a disconnection that exists between structural and thermal design of buildings and which needs to be addressed.

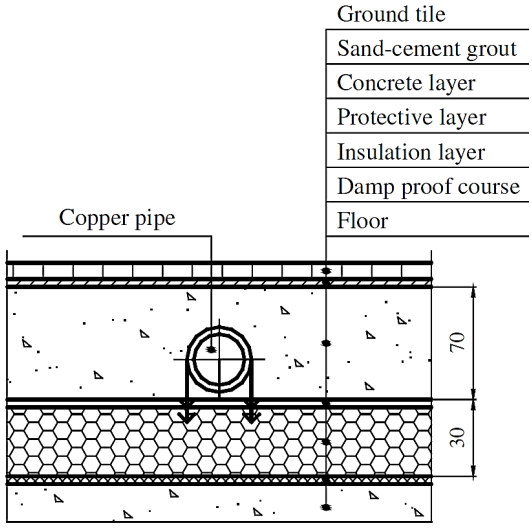

Fig. 1.13: Schematic of a hydronic slab in practice (Zhai et al. 2009) (insulation is placed below the pipes to direct heat flow upward)

2.4. Objectives and scope

The main objective of the present work is to develop a methodology and guidelines for the design and operation of active BITES systems that facilitate primary space conditioning with

low operating energy, relatively flat power demand, and improved thermal comfort. The three key factors considered by the methodology are as follows: sufficient thermal coupling between the BITES systems and their thermal zone, integration of design and operation, and integration of thermal and structural designs. The methodology and guidelines are general and applicable to different BITES systems and different buildings with different thermal and structural loads.

The research will focus on active BITES systems. Fig. 1.14 shows the concepts of ventilated (air-based) (Fig. 1.14-a) and hydronic (Fig. 1.14-b) systems. Working fluids (air or water) condition the wall, floor or ceiling, which in turn condition the zone through radiation and convection. Air-based systems with open-loop configuration also have advective thermal output in addition to heat transfer from the BITES room surface. In these figures, the configurations are conceptual; not all the components will be integrated into one configuration. For example, either the slabs or the walls, or both of them can be used as active BITES. The return grill and supply diffuser in Fig. 1.14-a can be at other locations.

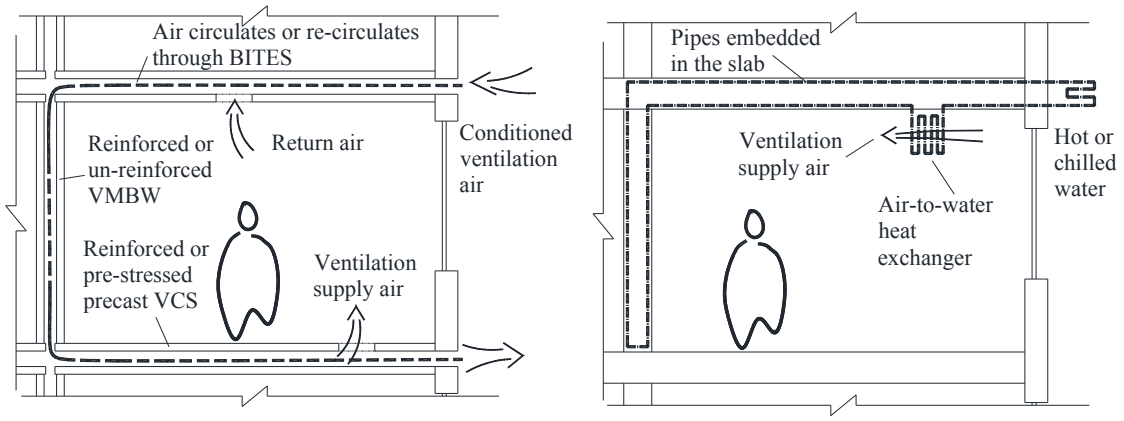

(a) (b)

Fig. 1.14: Conceptual schematic of the different active BITES systems: (a) ventilated systems; (b) hydronic systems (VMBW: ventilated masonry block wall; VCS: ventilated concrete slab)

By using ventilated systems, wires, pipes, and ducts of service systems can possibly be arranged in a space-efficient way. For example, the hollow cores or corrugated void space of the concrete slabs and masonry block wall cells can be used as ducts for ventilation air. Wires and pipes can also be incorporated. By eliminating the conventional space required for service systems, the floor-to-floor height can be reduced and additional floors may be possible over the permitted building height.

Concerns about potential air contamination from using concrete building fabric as air ducts have been raised by building designers and occupants. The risk of contamination is minimal considering that the materials for concrete slabs or masonry blocks walls are inorganic. Oswald and Sedlbauer (1995) suggested hygienic maintenance on interior open-loop systems. The main measure is to limit the relative humidity of channel air flow from being higher than 65%. Furthermore, it has been more than 30 years since concrete slabs were first used as air ducts in practice (Anderson et al. 1979). No literature, to the author's knowledge, has been reported on air contamination issue.

Chapter 2 "Literature review of BITES" consists of two sections. The first section, Section 2.1 "Building-Integrated Thermal Energy Storage (BITES) – State of the Art, Part I: Literature and Technology Survey" presents different technologies, building-integration approaches, and case studies. It discusses the advantages of BITES systems relative to isolated TES systems. Based on the first section, Section 2.2 "Building-Integrated Thermal Energy Storage (BITES) – State of the Art: Part II, Evaluation and Comparison" presents a quantitative comparison the thermal and energy performance of different types of BITES systems. Discussions on other important design and operation aspects are also provided,

such as improvement measures for active thermal coupling with thermal zone. Chapter 2 covers both passive and active BITES.

To assist the thermal analysis and control of active BITES systems, modeling techniques and guidelines for active BITES systems are presented in Chapter 3 "Numerical Modeling". In Section 3.1 "Thermal performance and charge control methodology of a ventilated concrete slab (VCS) using outdoor air", an explicit finite difference thermal model was developed for a VCS adopted in a low energy solar house, and verified with full scale measurements from the house. Based on the finite difference model, a simple regression model is also developed for the predictive control of active cooling using outdoor air. To advance the thermal model for integrated design and predictive control, modeling techniques for lumped-parameter explicit finite difference approach in time domain and analytical approach in frequency domain are presented in Section 3.2 "Frequency domain and finite difference modeling of ventilated concrete slabs and comparison with field measurements: Part 1, modeling methodology". The applications of the modeling techniques are presented in Section 3.3 "Frequency domain and finite difference modeling of ventilated concrete slabs and comparison with field measurements: Part 2, application".

Chapter 4 "Design of predictive control strategies for active BITES systems using frequency domain model" presents a design methodology for predictive control of active BITES systems using frequency domain modeling. This methodology applies the modeling methodology and techniques developed in Chapter 3 on closed-loop and open-loop systems. Using desired room air temperature and corresponding space conditioning load as inputs, the thermal energy injection rates can be predicted over a desired prediction horizon with

the frequency domain models. Frequency domain models also provide insights for BITES design through study of key frequency domain transfer functions.

Based on the findings from Chapter 4, Chapter 5 "Design and operation methodology for active building-integrated thermal energy storage systems and applications using standard structural components" develops a methodology to integrate the design and operation using frequency domain modeling. This chapter addresses the three key requirement of active BITES system – low energy consumption, relatively flat power demand profile, and good thermal comfort, as well as the three influencing parameters for comprehensive design of BITES systems – thermal coupling, integrated design and operation, and integration of structural and thermal designs.

Chapter 6 "Conclusion" summarizes the research findings, key contributions and proposes future work.

Chapter 2 Literature review of BITES

This chapter comprises 2 manuscripts ready for submission. Each of the manuscripts makes up one section of this chapter. Section 2.1 provides a literature review and technology survey, and Section 2.2 provides the valuation and comparison of different BITES systems based on the findings from Section 2.1.

Section 2.1 Building-Integrated Thermal Energy Storage (BITES) – State of the Art, Part I: Literature and Technology Survey

Section Abstract

This first paper (section) in a series of two presents a review of building-integrated thermal energy storage (BITES) systems - TES systems that use building fabric (e.g. masonry block walls and concrete slabs) to store thermal energy and release it directly to their zones to facilitate space conditioning. The review presents different technologies, building-integration approaches, and case studies. There are numerous applications of different types of BITES systems, such as passive systems (e.g. massive solid walls and slabs in passive solar heating and natural ventilation), active-charge/passive-release systems (e.g. hydronic radiant heating concrete slabs), active-charge/release systems (e.g. open-loop ventilated concrete slabs), and their combinations. BITES systems have been applied in buildings in different climates with different functions. The literature and technology survey shows that, on top of the generally known TES benefits, BITES systems have additional advantages such as improved thermal comfort, utilization of ambient renewable energy, cost and space savings and further reduction of capacities of service systems.

1. Introduction

Research and development (R&D) activities have indicated that effective TES systems can significantly improve the thermal and energy performance of buildings. The improvements include enhanced thermal comfort by reducing temperature fluctuation, shifting and

decreasing peak power demands, higher efficiency and smaller required capacity of auxiliary heating/cooling mechanical equipment, and offsetting the mismatch of energy supply/availability and demand (ASHRAE 2007b, Dincer 2002, Hadorn 2005, Howard and Fraker 1990). The benefits of reducing loads and demands become more distinct when using renewable thermal energy sources. For example, coolness from night time outdoor air can be accumulated in TES systems to offset the heat gain in the coming daytime. In active and passive solar heating applications, sufficient amounts of solar heat can be collected and stored during daytime, and used during night time.

The main task of thermal energy storage (TES) applications in buildings is to improve buildings' thermal energy logistics. Common outdoor sources of thermal energy are solar thermal energy, geothermal, ground water, and ambient air. Internal heat gain (appliances and human bodies), heat and coolness from auxiliary space conditioning systems are common indoor sources. Thermal energy is mainly stored for space heating/pre-heating, cooling/pre-cooling, and occasionally for facilitating ventilation (Gan 1998). There are two main types of common storage mechanisms for TES – sensible and latent heat storage. Other mechanisms include mechanical, thermo-chemical, and sorption (Hadorn 2005, Hariri and Ward 1988, Sharma et al. 2009).

In building applications, rocks, concrete, masonry, and water are commonly used for sensible heat storage. The volumetric heat capacity (sometimes referred to as heat storage density) of water is about 1.2 $kWh/m^3/K$ at room temperature; that for common masonry and normal weight concrete are close to each other, and range from 0.4 to 0.7 $kWh/m^3/K$ (Doran 1992). The major advantages of sensible heat storage are its low cost, robustness and durability. However, the disadvantages, such as heat loss and low volumetric heat capacity,

are also obvious. For latent heat storage, ice is commonly used. Other phase-change materials (PCM) are currently attracting significant R&D attention. The latent heat (i.e. heat of fusion) of PCM reported in literature ranges from about 0.028 to 0.083 kWh/kg (100 to 300 kJ/kg) (Hadorn 2005, Hauer et al. 2004, Sharma et al. 2009). Generally within practical operation temperature range for space conditioning, the volumetric heat capacity of PCM is about 6 to 17 kWh/m^3/K – five to 14 times more than that of sensible storage materials, such as water and concrete (Sharma et al. 2009). High volumetric heat capacity is one of the advantages of PCM. Another advantage is that the phase-transition temperatures can be designed. Certain PCM have phase-transition temperatures within comfortable room temperature range, and are suitable to be integrated into occupied space for TES purposes (Sharma et al. 2009, Zhu et al. 2009b). The limitations in using PCM include low heat transfer rate inside the PCM, high cost of production, fire-safety issues, and long term chemical instability (Dincer 2002, Zhu et al. 2009b). See subsection 3.1 "Applications of PCM" for more discussion.

Recently, TES by sorption and thermo-chemical reactions has attracted noticeable research interest. N'Tsoukpoe et al. (2009) provided a clarification on the confusing terminologies related to sorption and thermo-chemical TES. Sorption and thermo-chemical TES use reversible physico-chemical phenomena. Thermal energy can be stored with negligible loss (Kato 2005) since thermal energy is not kept in sensible or latent form but as a chemical potential. Among the potential material candidates, magnesium sulphate heptahydrate (MgSO4.7H2O) is one of the most appropriate for building applications due to its high energy density, solar thermal collector compatible storage temperature (around 85°C), and availability of chemical reaction components (Hadorn 2005, N'Tsoukpoe et al. 2009). It has an energy density of 2.8 GJ/m^3 (780 kWh/m^3), which is one order of magnitude larger than

that of sensible heat storage using water with a 60°C temperature change. The advantages of using sorption and thermo-chemical technologies for TES is mainly due to its high volumetric thermal capacity with negligible sensible heat loss, and minimum material waste (Masruroh et al. 2006). However, sorption and thermo-chemical TES face problems in preservation, such as leakage and high vacuum requirement, as well as with complex technologies in reaction acceleration and heat extraction (Demir et al. 2008, N'Tsoukpoe et al. 2009). Other than TES functions, sorption and thermo-chemical technologies can be also used in heat pump applications (often referred as chemical heat pump) to provide space cooling and heating in a more energy efficient way (Demir et al. 2008, Wongsuwan et al. 2001). Even though TES applications using PCM and sorption and thermo-chemical reactions face serious technical and economic challenges, these two TES approaches have obvious potential for further development leading to practical applications.

Concrete and masonry, as common building construction materials, have their own advantages as good TES material candidates. Even though they have only about a quarter to a half of the volumetric heat capacity of water, and even less as compared to PCM in their phase-transition temperatures, concrete and masonry have long term chemical and physical stability, which means low operation and maintenance costs. Due to their inherent structural functionality and the availability of raw materials, concrete and masonry are among the world's most widely used building materials. This means there are already TES systems in existing and new buildings available for use.

Building fabric (i.e. the structural skeleton, partitions, and architectural envelope) accounts for a significant portion of a building's thermal capacity. Braun (2003) stated that the thermal capacity of a typical concrete building is in the order of 0.1 $kWh/K/m^2$ gross floor area.

Antonopoulos and Koronaki (1998, 1999) estimated that the effective thermal capacitance (i.e. taking the building as one lumped capacitance) of buildings ranges from 0.06 to 0.18 $kWh/m^2/K$ (0.2 to 0.6 $MJ/m^2/K$), and about 78% of it is attributed to building structure and envelope, 14% to partitions, and 7% to furnishings. These findings indicate that the building fabric is a valuable candidate for TES.

In the literature, there have been several reviews conducted on general TES applications in buildings. Hariri and Ward (1988) reviewed TES applications for space thermal conditioning in the 1980s. The fundamentals, general requirements, and drawbacks of different systems and material for sensible heat storage in solid/liquid and latent heat storage were presented in their review. Rock bed and pebble bed storage systems were extensively discussed. Hasnain (1998a, b) reviewed the materials and technologies of TES systems in the 1990s and before, with a brief discussion on using building fabric for TES. The researcher's case studies indicated that properly designed and controlled TES can result in significant savings in the energy consumption, initial cost, and operation and maintenance costs. Dincer and Dost (1996) conducted a survey on TES materials and technologies in solar thermal applications. The researchers discussed the application ranges of different TES materials and systems. Dincer (2002) provided fundamental information about the advantages, design criteria, application ranges and evaluation of different TES systems. Nielsen et al. (2003) presented a detailed report on the state of the art of TES systems with focus on seasonal underground thermal energy storage (UTES). The researchers also described the interactions between TES and other design issues for high-performance buildings, such as indoor environment quality, building-integrated energy systems, and integrated design. The present study focuses on R&D activities related to using building fabric for TES to directly facilitate space conditioning. Space conditioning in this study refers to space heating and cooling.

Humidifying or dehumidifying is not included. Relevant technologies and building-integration approaches will be presented and discussed.

1.1. Building-integrated thermal energy storage

In the literature, the concept of using building fabric for TES has been referred to as fabric energy storage (Winwood et al. 1997a), fabric thermal storage (Braham 2000) or building mass thermal storage (ASHRAE 2007b). When building fabric is used for TES, naturally, it will affect the thermal behavior of the room since it is not thermally isolated from the room. Its stored heat will be passively or actively released directly to the room. In this study, TES systems that use the building fabric (e.g. masonry block walls and concrete slabs) to store thermal energy and release it directly to their zones to facilitate space conditioning are defined as building-integrated thermal energy storage (BITES) systems. The building fabric used for BITES is not thermally isolated from room air. The add-on TES systems, such as ice storage, hot water tanks and PCM in containers, are not considered BITES systems.

Howard and Fraker (1990) presented a study on BITES systems for houses in the 1970s and early 1980s; they covered background knowledge and criteria for successful applications. Applications using air as the heat transfer fluid were studied by Bansal and Shail (1999) and Winwood et al. (1997a), and were briefly presented by Fraisse et al. (2006). Examples are air-core systems (Howard 1999), ventilated concrete slabs (VCS) (Chen et al. 2010b), and other systems with natural or mechanical ventilation (ASHRAE 2007b). Ventilated (or air-based) BITES systems employ the hollow cores of the building components as integral ductwork and heat transfer surface area to exchange thermal energy with the air passing through the cores. Examples are hypocaust (Fort 2000), and ventilated slab (Braham 2000, Chen et al. 2010a, Chen et al. 2010b). The designation of thermally active (or thermo-active) building

systems (TABS) (Henze et al. 2008, Lehmann et al. 2005) was introduced in recent R&D activities on hydronic systems with massive floors. In these systems, the floor is actively conditioned (or so called thermally activated) by the heat-transfer water circulating in the pipes, which are embedded in the floor. TABS floors are considered hydronic BITES slabs in the present study.

1.2. Charge/discharge and active/passive systems

There are passive and active charging or discharging mechanisms in the operations of BITES systems. Charge is normally equivalent to discharge since heating is negative cooling. In cases when only heating or cooling BITES systems are being discussed, charge and discharge can be differentiated in terms of operation. All BITES systems undergo passive charge/discharge by conductive, convective and long-wave radiative heat exchange with their environment. The charge/discharge is considered active if its mechanisms involve mechanical devices. Otherwise, the charge/discharge is passive. Active charge/discharge implies that the TES systems undergo both active and passive charge/discharge. In passive scenarios, the storage materials are in direct contact with thermal sources such as direct solar radiation or cool air. Heat transfer media (air, radiation) are driven by natural forces (e.g. wind or buoyancy). Thermal energy is charged into the TES systems without mechanical devices. In active scenarios, mechanical devices are employed to facilitate heat transfer between the BITES systems and the indoor environment. Heat transfer media are driven by mechanical devices to circulate between the thermal sources and the BITES systems.

BITES systems are considered active when they embody controllable internal charge/discharge systems, such as a hydronic, ventilated (or air-based and air-core), electric, or capillary system. Otherwise, the TES systems are passive systems. Systems with air flow in

the air channels or liquid media (normally water) circulating in pipes due to buoyancy effect (i.e. thermosiphon phenomenon) are considered passive systems. For a building using mechanical ventilation for night time pre-cooling, the whole building is an active BITES system, comprised of many passive BITES systems. On the other hand, if the ventilation is natural, the building by itself is a passive BITES system.

Table 2.1: Applications of charge/discharge combinations

Combinations	**Main applications**
Passive charge and discharge (Fig. 2.1-(a))	Massive wall or slab in the direct gain zone in passive solar design (2.1.1, 2.2.1); night time whole building cooling/pre-cooling by natural ventilation (A1.1); roof slab, solar pond, porous roof (A1.3); exterior solid walls (2.1.1); classic Trombe wall and its variations (A1.2), Barra-Costantini system (2.2.3).
Passive charge and active discharge (Fig. 2.1-(b))	Rare in applications. Trombe wall equipped with fan circulating air (A1.2 in Appendix); solarium with TES systems and forced-air recirculation.
Active charge and passive discharge (Fig. 2.1-(c))	Pre-cooling solid concrete slab using night time mechanical ventilation (A1.1); hydronic slab (2.2.2); ventilated slab (2.2.3); hydronic or "interior closed-loop" ventilated wall (2.1.2); indirect evaporative roof pond with forced ventilation (A1.3); capillary tube mat or electric heating with TES systems (3.3, 3.4).
Active charge and discharge (Fig. 2.1-(d))	"Open-loop to room interior" (i.e. room air is supplied or returns through BITES systems) ventilated walls and slabs (2.1.2, 2.2.3).

Note: the numbers in parentheses are the heading number of subsections. Subsection names started with a "A" is in Appendix.

Combinations of active and passive charge/discharge mechanisms are commonly employed (Table 2.1). Fig. 2.1 illustrates the conceptual working mechanisms and generic locations of

major air-based systems (see subsection 2 "State of the art of BITES"). Fig. 2.2 shows a practical application of an active charge and passive discharge system – an "interior closed-loop" ventilated concrete slab (Chen et al. 2010a, Chen et al. 2010b).

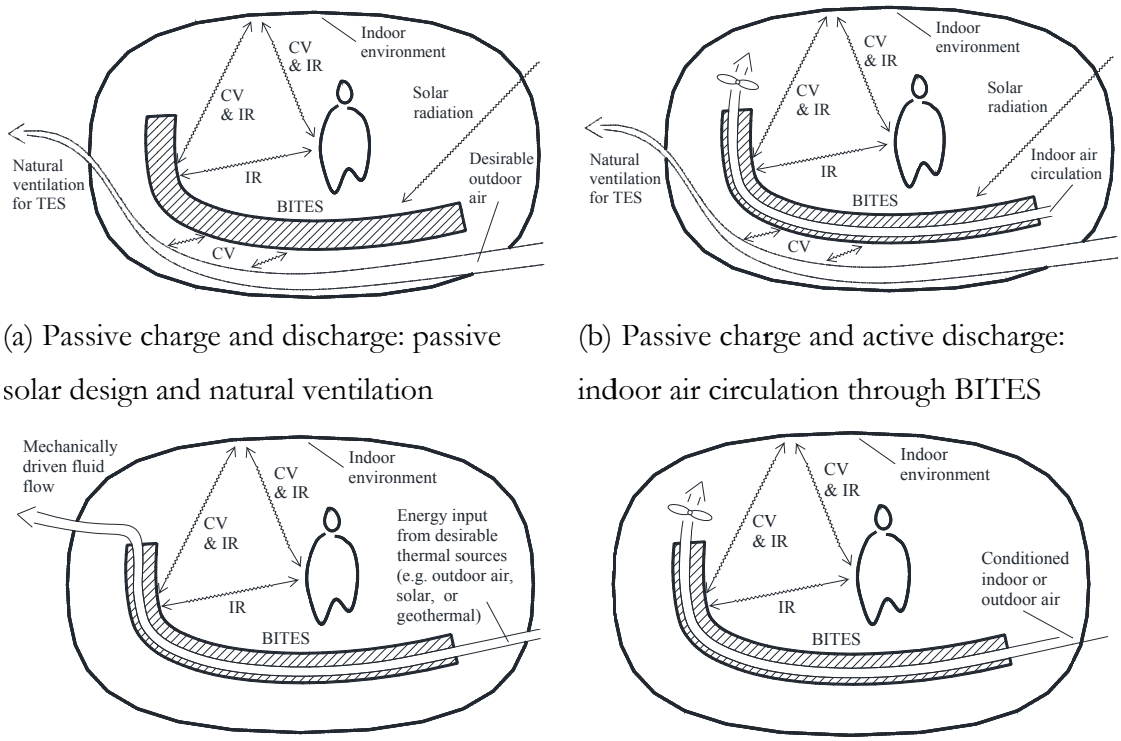

(a) Passive charge and discharge: passive solar design and natural ventilation

(b) Passive charge and active discharge: indoor air circulation through BITES

(c) Active charge and passive discharge: air passes through BITES systems ("interior closed-loop" systems)

(d) Active charge and discharge: ventilated BITES systems with air released directly into room ("open-loop" systems)

Fig. 2.1: Conceptual schematics of working mechanisms of common air-based systems listed in Table 2.1 (CV: convective heat transfer; IR: infrared radiation)

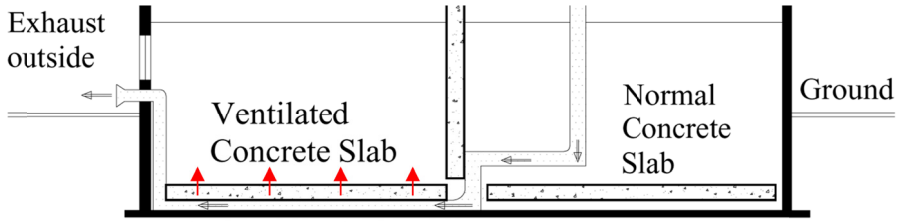

Fig. 2.2: Schematics of the functioning of an "interior closed-loop" ventilated concrete slab (Fig. 2.1-c) (Chen et al. 2010a, Chen et al. 2010b)

1.3. Objective and scope

High-performance buildings should have low life cycle energy consumption (e.g. construction and operation energy) and peak power demands. There exists another need: to improve the thermal comfort of buildings without sacrificing energy efficiency. Better understanding and utilization of BITES will help satisfy these three needs. The majority of previous reviews focused on add-on TES material and systems. Hence, there is a necessity to survey and review energy-efficient and cost-effective BITES technologies. To serve this necessity, this section (paper) reviews the state of the art on BITES systems: different technologies, integration approaches, and case studies on using building fabric for TES and space conditioning. Firstly, a review of different groups of BITES systems will be presented in subsection 2, "State of the art of BITES". After that, this study will present other general concepts and technologies that can be used in building components to enable or improve their TES functions in subsection 3, "Concepts and technologies associated with BITES". Comparisons and evaluation of the thermal and energy performance of different types of BITES systems, as well as general design and operation considerations will be presented in the companion paper, Part II (Section 2.2).

2. State of the art of BITES

The BITES systems presented in this subsection are categorized into four types according to their locations in the building fabric – whole building (see Appendix A1.1), wall type, floor/ceiling type, and roof type (see Appendix A1.3). For each type, passive systems will be presented first, followed by active systems.

2.1. Wall type

This subsection presents the R&D activities on BITES systems that use exterior building walls and interior partitions. The thermal properties of solid walls will be discussed first, followed by walls with internal air channels or embedded pipes for thermal energy transfer. Different types of Trombe walls, as a special group, will be reviewed independently in Appendix A1.2.

2.1.1. Solid walls

Solid walls are usually studied as passive TES systems. Committee 122 of the American Concrete Institute (ACI) (2002) presented a guide on the thermal performance of concrete and masonry envelope systems. The guide provided the thermal property data and design techniques that are useful in designing concrete and masonry building envelopes for energy code compliance. The guide also presented studies that analyzed the TES effect of concrete and masonry exterior walls on the thermal performance of buildings. It quantified the thermal lag effect induced by different kinds of concrete and masonry envelopes.

Zhu et al. (2009a) investigated the thermal performance of an insulated concrete wall using actual data in comparison to a conventional wood frame system in a desert climate. The insulated wall was precast with a 51-mm layer of extruded polystyrene board insulation in between a 102-mm interior layer of reinforced concrete and a 51-mm exterior layer of concrete. The monitored data showed that during transition seasons, less heat was transferred through the massive wall into the room during the warm daytimes while more heat was released inward during the cool night times, as compared to conventional wood-framed walls. However, this also resulted in a slightly higher cooling load on summer days. The simulated equivalent thermal resistance value of the mass walls under local climate

conditions are 6.98 $m^2 \cdot K/W$. Fallahi et al. (2010) carried out a numerical study on the effect on energy load by replacing the venetian blind slats, the inner glazing or the outer glazing with thermal storage materials, in double-skin facade applications. For mechanically ventilated configurations energy savings from 21% to 26% in summer and from 41% to 59% in winter respectively, are achievable in comparison with conventional designs. On the other hand, naturally ventilated double-skin facades combined with TES were not found to be energy efficient in winter due to stack effect and airflow rate increase within the air channel.

The BITES capacity of walls can be exploited by active approaches such as hydronic and ventilated charge/discharge systems. According to the literature, these active approaches are mainly applied on interior walls.

2.1.2. Hydronic and ventilated interior walls

For ventilated interior walls, Howard (1986) reviewed the generic hollow-core-masonry heat storage systems. Design considerations such as construction approaches, cost, efficiency and thermal comfort, were reviewed. The researcher also presented a case study on the application of a ventilated wall in a solar house together with a Trombe wall and sunspace. The warm air from the Trombe wall and sunspace was circulated into the ventilated wall with assistance from a fan. The monitored data showed that the house has good thermal performance. The ventilated wall heat storage system has been proven effective in storing and redistributing solar thermal energy collected by the solar systems. Howard and Fraker (1990) reviewed the principles of designing, analyzing and predicting the performance of ventilated TES systems that use concrete masonry units (CMU). Several successful built examples of passive solar residential buildings in the early 1980s using ventilated wall systems were also presented. Design guidelines for ventilated systems were also provided.

The main advantages of the ventilated masonry unit system are its simplicity, low cost, and improved year-around thermal comfort level.

Fort (2000) presented design guidelines for two kinds of BITES that can be integrated into solar air heating systems: murocaust - a massive wall with channels through which warmed air is circulated, and hypocaust - a massive slab with channels serving a similar function. The air circulation can be natural or forced convection, and can be open-loop or closed-loop. The thermal energy discharge can be passive by radiation or active by forced air. For various hypocaust types, Fort also provided their respective characteristics, such as specific heat storage capacity, time constant, phase delay, and recommended range of air velocity. Fraisse et al. (2006) studied, through simulations, the energy performance of a ventilated wall which is thermally coupled with solar air collectors in different configurations in a timber frame house. The researchers concluded that, when heat recovery ventilation (HRV) is adopted, a "closed-loop" system is better than an "open-loop" system (Fig. 2.1-(d)) with conditioned outdoor air) because it is more effective in energy storage and reduces the risk of unhealthy air pollution. Fraisse et al. (2010) conducted numerical investigations on the feasibility of improving summer comfort in wood-frame houses by using a ventilated internal double wall (VIDW). The researchers concluded that VIDW is more effective in lowering cooling consumption and improving thermal comfort than normal solid concrete walls, with the application of night time pre-cooling ventilation. High air velocity (1 – 1.5 m/s) in the air gap of the VIDW is necessary to create high convective heat transfer. The area ratio of VIDW to floor needs to be above 0.9 to cool the room effectively.

For hydronic BITES walls, Marmoret et al. (2000) experimentally investigated the thermal performance of a vertical wall (150 x 125 x 20 cm thick) under a heating mode of operation.

The wall is made of cellular clayey (lightweight) concrete, and has water pipes embedded in it. The influence on the wall thermal performance of different water flow rates and temperatures was evaluated over 24-hour cycles which included an 8-hour period of water circulation. It has been shown that a variation in the flow rate does not create significant fluctuations in the wall's thermal performance.

2.2. Slab type

The R&D reviews on floor and ceiling type of BITES systems are presented together as BITES slabs. Three types of BITES slabs will be discussed: passive, hydronic and ventilated slabs.

2.2.1. Passive slabs

The thermal behaviour of passive slabs in passive solar applications has been intensively studied in the literature. Some of the studies have been reviewed in other subsections (e.g. Appendix A1). Shaw et al. [1994] conducted an experimental study on the effective utilization of building structural mass as a room air temperature regulator. They concluded that false ceilings reduce the effectiveness of the thermal-mass effect of the concrete ceiling concrete slab, and result in higher peak air temperature. The cooling load can be reduced if pre-cooling of the slabs is employed. Recently, Athienitis and Santamouris (2002) applied transfer functions to study the thermal behaviour of passively charged concrete slabs in solar direct gain zones and their optimal thickness. The researchers concluded that a concrete slab thickness of more than 20 cm will not significantly reduce the slab surface temperature variation for avoiding space and slab surface overheating. This also means thicker slabs will not have a significant increase in their diurnal TES capacity. Chen et al.(2010a) presented the thermal performance of a 15-cm passive slab in the direct gain zone of a low-energy

detached house in a cold climate zone. The monitored data showed that the slab effectively prevented the overheating of the house year-round. Other than passive approaches, hydronic and ventilated slabs are used as active approaches.

2.2.2. Hydronic slabs

Hydronic BITES slabs can be actively conditioned with heat transfer liquid passing in the pipes embedded in the massive slabs (Fig. 1.7). The cooling or heating rate can be controlled so as to achieve the desired slab temperature. This manner is sometimes referred to as concrete core conditioning (Koschenz and Dorer 1999). Many R&D activities have been conducted to evaluate the effectiveness of using hydronic slab in facilitating space conditioning and pre-cooling/-heating. Some of them will be summarized here, and a few will be presented later in the subsection 3.2, "Solar direct".

In cooling applications, Feustel and Stetiu (1995) showed the advantages of radiant cooling by hydronic thermal distribution systems, as compared to the commonly used all-air systems. They reported the development, thermal comfort, and cooling performance of the hydronic systems. The peak-power requirement was also compared between hydronic systems and conventional all-air systems. Lehmann et al. (2007) conducted simulations on the achievable comfort and maximum total heat load of a typical office zone with carpet or raised access flooring using hydronic slabs. The researchers pointed out that these values are governed by the heat transfer rate to the building structure on the room side. Koschenz and Dorer (1999) developed a simplified model for the design of hydronic slabs. Henze et al. (2008) conducted a performance comparison between a hydronic TABS assisted with a variable air volume (VAV) system and a conventional VAV system for space cooling in a low energy office building. The study showed that VAV assisted TABS resulted in a higher cooling load than

the conventional VAV system, but the primary energy consumption was about 20% lower due to low-exergy cooling and heat recovery measures.

In heating applications, Hanibuchi and Hokoi (1998) conducted a full scale experimental study on the air temperature, air velocity, and heat loss in a room. The measurement indicated that the air temperature distribution is uniform in the vertical direction, except near the ceiling. Convective heat transfer accounted for about half of the heat exchange in the room. The thermal behavior and optimal control strategies of hydronic floor heating systems incorporated with massive slabs was studied by Athienitis and Chen (1993). After this study, Athienitis (1997) conducted theoretical studies on the thermal performance of this system when the floor mass was employed to store both auxiliary heat and direct passive solar gain in a passive solar building. The major objectives of the study were to determine satisfactory slab thickness and to develop efficient control strategies for saving energy and maintaining good thermal comfort. The study revealed the difficulty in sizing and controlling hydronic massive floors in the presence of direct solar gains, which often causes slab surface overheating. (See companion paper Part II (Section 2.2) for the recommendations of the control strategies from the above two studies.) Later, Athienitis and Chen (2000) employed a three-dimensional explicit finite difference model to study the effect of direct solar radiation on the floor temperature with different flooring covers. Their study showed that direct solar radiation will cause illuminated areas to have a significant higher temperature than the shaded areas (~8°C). This difference is increased with floor coverings such as carpets. The study also demonstrated that floor coverings will obstruct the TES function of a massive floor and result in high heating energy consumption.

There are several R&D activities conducted on charging hydronic floors with renewable thermal energy. Zhai et al. (2009) investigated, through monitored full scale data, the thermal performance of a hydronic floor being actively charged by solar thermal collectors in an institutional building. The collectors' area is 1/3 of the heating floor area. The researchers claimed that the efficiency of the system is about 40%. The researcher also concluded that the solar radiation has more distinct influence on the performance/efficiency of the system than the outdoor temperature. Pfafferott and Kalz (2007) presented an initial assessment of the energy performance of three new non-residential buildings, which adopted hydronic floor heat/cooling systems with the "concrete core temperature control" configuration. The heating/cooling thermal energy is from natural sinks such as the ground, ground water, and cool night air. The heating energy consumption (electricity for the water pump and ground source heat pump) ranged from 23.4 to 36 kWh/m^2/yr. Xu et al. (2010) presented a review of the technologies of thermally coupling the hydronic slab with low-grade energy sources (e.g. geothermal energy and favorable ambient air) for space conditioning. Four loop configurations were investigated: open system coupled with cooling towers; closed system coupled with chillers/heat pumps; open system using ground water; closed system coupled with ground heat exchangers. Significant reductions in energy consumption, peak power demand, and capacity of mechanical equipment were confirmed with on-site monitored data.

2.2.3. Ventilated slabs

In ventilated slabs, the hollow cores inside the massive slab allow air to pass through and exchange thermal energy with the surrounding slab mass. The BITES mechanism is similar to that of the hydronic BITES slabs; however, the system configurations are more flexible due to air being the working fluid. The stored thermal energy can be released to the room passively by natural convection and radiation through the slabs' exposed surfaces, or be

actively extracted by mechanical ventilation through the hollow cores. One of the earliest studies on ventilated slab was conducted by Short and Kutscher (1984) through steady state simulation. Howard (1986) and Howard and Fraker (1990) presented case studies on several successful practices. Buzzoni et al. (1998) presented their numerical modelling on a Barra-Costantini system – outdoor air circulated between the collector facade, the massive ceiling and the room air due to buoyancy effect. The researchers concluded that the Barra-Costantini system had better energy performance than the classic Trombe wall. Fort (2000) presented working mechanisms and design guidelines for ventilated slabs (referred to as hypocaust systems).

Chen et al. (2010b) presented their study on a ventilated concrete slab (VCS) (Fig. 2.2). Besides its building enclosure function as the basement slab, the VCS also serves as an active-charge/passive-discharge BITES system. Normal density concrete was poured on the corrugated steel decks. The underside channels of the steel decks were utilized as the air channels. The slab can be heated with warm air from a roof-mounted building-integrated photovoltaic/thermal system (BIPV/T) for heat storage, or cooled with night time cool outdoor air for coolness storage - combining the functions of a solar direct floor (see subsection "Solar direct") and free cooling. The stored thermal energy was released to the room passively from the top surface of the slab. The monitored data showed that the VCS can effectively and efficiently store the thermal energy from the air, and thermally coupling

the VCS with the BIPV/T system was a viable method to enhance the utilization of solar thermal energy.

There are several commercial ventilated BITES slabs, such as AIRFLOOR[1] (also referred to as hollow-core-screed system (Winwood et al. 1997a)) and TermoDeck™. The TermoDeck™ system was introduced by Anderson et al. (1979) (Fig. 2.3). Its applications focus on reducing cooling load in commercial buildings. TermoDeck utilizes the hollow cores within precast concrete floor slabs as ventilation ducts. Supply air is circulated through these ducts before being released into the room. During this process, the slab acts as a thermal energy reservoir and the air is tempered. In some applications, for example, during summer nights, outdoor cool air passes at low velocity through these ducts to extract the stored heat during daytime and to cool down the slabs to a desired temperature. In the daytime, the pre-cooled slabs condition the fresh air passing through their internal cores. The conditioned air then is released into the room underneath. The temperature of the room is also regulated by the thermal radiation of the slabs. The TermoDeck slab is an active charge and discharge BITES system. Anderson et al. (1979) presented a simplified empirical equation for calculating the required thermal storage capacity (J/K) in the TermoDeck application. It is equal to the cooling load (in watts or J/s) divided by the indoor air temperature rise rate of 0.125 K/hr.

---

1 Airfloor, Inc. www.airfloor.com

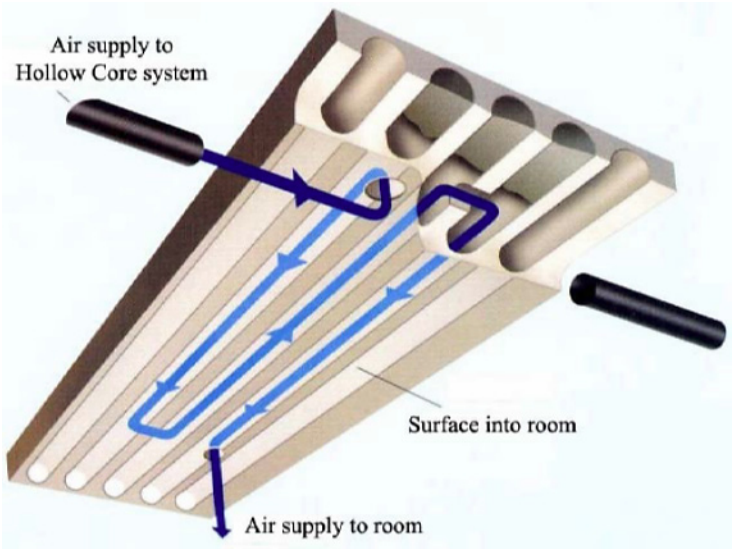

Fig. 2.3: TermoDeck illustration (source: Swedish International Press bureau)

Winwood et al. (1997a, b, c, d) presented their comprehensive study on advanced fabric energy storage (FES) – ventilated slabs. The first paper presented a literature survey of advanced FES systems with focus on the TermoDeck system. The theoretical analysis of the thermal performance of the whole building and the slab were presented in the second and third papers. A simplified multi-node slab model was incorporated into full-building simulations. The verification showed that whole-building simulations using this model produce accurate results as compared to experimental data. The last paper presented monitored results of the first UK building that has installed the TermoDeck system. The monitoring included the thermal performance and the energy consumption. The results showed that the TermoDeck system provided stable and comfortable thermal conditions throughout the whole year. Recommendations for improvements were made for future applications of a similar kind. Turner and Tovey (2006) conducted a case study on the energy performance and control strategies of the low-energy educational building ZICER, which adopts the TermoDeck system. The design details and monitored energy performance and thermal comfort of another TermoDeck building – the Elizabeth Fry building were

presented by Team-Probe (1998). The study showed that the building's heating energy consumption was only 1/5 of the average value, and its thermal comfort was at a good level.

Forced airflow through the internal hollow cores of TES systems enhances the convective heat transfer coefficient (CHTC) (Ren and Wright 1998) and utilizes a larger heat transfer area as compared to natural convection alone on outer surfaces. Consequently, the TES effectiveness is considerably increased – the heat exchange rate between the storage materials and the heat source is significantly increased, more storage materials become active, and more thermal energy can be stored or released. Barton et al. (2002) studied the effects of the bends and the numbers of the cores on the thermal performance of the TermoDeck. The studies on TermoDeck also show that mechanically facilitated heat transfer within the TES systems also helps in improving the control of TES (e.g. temperature and heat transfer rate) (Shaw et al. 1994, Winwood et al. 1997a).

More R&D activities on ventilated slabs will be presented in the later subsection 3.2, "Solar direct".

3. Concepts and technologies associated with BITES

BITES systems located in different parts of the building fabric have been presented in the previous subsection. This subsection will present other concepts and technologies that can be used on the building fabric to enable or improve its TES functions.

3.1. Applications of PCM

Many R&D activities have investigated the thermo-physical properties of PCM and their applications in BITES systems (Castellon et al. 2009, Nielsen et al. 2003, Sharma et al. 2009, Tyagi and Buddhi 2007, Zhou et al. 2008). Athienitis et al. (1997) presented an experimental

and theoretical study on the application of PCM gypsum boards in a passive solar building. The study showed that the PCM gypsum board was able to significantly reduce the wall surface temperature (by ~6°C) when the wall was receiving transmitted direct solar radiation. This improved the storage of solar gains without compromising thermal comfort. Zhang et al. (2006a, 2006b) and Lin et al. (Lin et al. 2005) investigated the thermal properties of the PCM they developed and its application and thermal performance in a prototype floor configuration, in which PCM plates are placed on top of an insulation layer and covered by wood flooring. The researchers pointed out that the wood flooring and the air layer between the wood flooring and the PCM plates reduced the effectiveness of the TES function of the PCM, as it obstructs the direct contact of the PCM with room air. Nagano et al. (2006) experimentally investigated the thermal performance of a floor displacement ventilation system incorporated with granular PCM. The results indicated a significant cooling energy saving.

Zhou et al. (2008) conducted a numerical study on the effects of the thermo-physical properties, plate thickness, and locations of shape-stabilized PCM (SSPCM) plates on the BITES functions of the PCM. The researchers stated that (1) the appropriate melting temperature was about 20°C and the heat of fusion should not be less than 90 kJ/kg; (2) it was the inner surface convection, rather than the internal conduction resistance of SSPCM, that limited the latent heat storage; (3) thin PCM plates with large areas were better than thick but small plates. Kuznik et al. (2009) experimentally investigated the thermal performance of a PCM copolymer composite wallboard in a full scale test room under three weather conditions: a summer day, a winter day, and a mid-season day. The researchers stated that the PCM material included in the walls significantly reduced the temperature fluctuation, decreased the chances of space overheating or overcooling, and enhanced the

natural convection mixing of the air preventing uncomfortable thermal stratifications. Thermal comfort was also enhanced by the radiative heat transfer between the wall surfaces and occupants.

Conclusively, the important advantages of using PCM in BITES systems are as follows. The phase-transition temperature range can be manipulated to be within the range of comfortable indoor temperatures. Hence, using PCM or adding PCM into the storage materials can significantly increase the volumetric thermal capacity of the BITES systems within this range of temperatures. Another advantage is based on the first one. The temperature of PCM will not considerably change in the process of storing/releasing thermal energy. This will enhance the heat transfer rates between the storage materials and the media (e.g. room air or heat transfer fluids) because of the relatively larger temperature difference. Due to the increased heat transfer rate, larger amounts of thermal energy can be stored/released in a given time. The space conditioning capacities of the BITES systems will be increased. The temperature swings both in the building fabric and room air can be reduced. These benefits will also promote the storage of renewable energy that is only available periodically in a limited time and/or of low-grade (i.e. solar energy, night time cool air).

R&D activities on PCM have demonstrated their potential to enhance TES functions and thermal coupling of BITES systems with their thermal zones. Incorporating PCM into building fabric, especially in light-mass buildings, will significantly improve the energy performance and thermal comfort of the buildings. However, practical applications are rare due to concerns about long term performance, chemical stability, health, and safety issues (Dincer 2002, Zhu et al. 2009b). Adding PCM into load bearing building components have

to further consider the combined structural characteristics of the new composite materials, such as the long-term compressive and flexural strengths. This is the main constraint in mixing PCM with structural materials. This is also the reason that main current practices use add-on PCM panels, or adding PCM material in non-load-bearing components like gypsum boards.

3.2. Solar direct

The concept of solar direct means that the collected solar thermal energy is directly stored in BITES systems, without being temporarily stored in isolated TES systems (e.g. water tanks). The process increases the energy efficiency by reducing the storage and transmission loss of otherwise useful energy, and saves the cost and space for mechanical equipment (e.g. pump, heat exchanger, and tanks).

The solar direct concept was reflected in many previously presented studies, such as the classic Trombe walls, the ventilated concrete slab studied by Chen et al. (2010a, 2010b), and the internal wall with air gap by Fraisse et al. (2006). In the study conducted by Short and Kutscher (1984), the ventilated slab was thermally coupled with a solar air collector. The study showed that the performance and the economics are better than that of active systems with rock bed storage. Letz (2005) presented the development and applications of solar direct floor (SDF) systems in France. The SDF system was introduced mainly to eliminate the storage tank in the solar hot water heating system. The SDF system was later combined with domestic hot water heating systems, and auxiliary boilers to increase the efficiency of space and water heating.

The direct thermal coupling between BITES systems and photovoltaic/thermal (PV/T) cogeneration systems (Bazilian et al. 2001) is a new and efficient trend. Fraisse et al. (2007)

investigated the energy performance of photovoltaic/thermal (PV/T) collectors that were thermally coupled with a SDF for space heating. The researchers stated that the operation temperature level of the SDF (about 35°C maximum at the inlet of the heating floor) favoured the operation temperature of the PV cells. Chen et al. (2010a, 2010b) proved that thermally coupling ventilated slabs to BIPV/T systems can significantly enhance the utilization of collected solar thermal energy and increase the electricity generation efficiency of the PV panels.

3.3. Capillary tube mat

Capillary tube mats are composed of small 2-mm-diameter polypropylene tubes. Warm/cool water can be passed through the tubes to transfer thermal energy to their attached building components (e.g. walls, ceilings) (Building Services 1993, Feustel and Stetiu 1995). Due to the small size of the tubes, the mat can be incorporated into the plaster of the walls or ceilings. The mat can be used on irregular curved surfaces due to the flexibility of the mat. The claimed cooling capacity can reach 80 W/m^2. This technology is useful in retrofit projects – the building fabric components of the existing building can be converted into active TES systems by incorporating capillary tube mats.

3.4. Electric heating systems

Electric heating cables, mats, membranes or panels can be embedded in the building fabric and supply space heating. Sun et al. (2008) presented their study on an electrical floor heating system using black carbon mortar blocks. This kind of block has proper conductivity, structural, and thermal properties for electrical slab heating. ASHRAE (2008) presented the design and installation of electrically heated floors and walls. As shown by ASHRAE (2008), the application of electric heating systems are limited by safety concerns and regulations. If

the local electric company offers time-of-use rates, using electric heating systems in conjunction with BITES can be beneficial, particularly if the operation time is controlled to be within the hours of low peak demand (and low energy price).

4. Conclusion

This section (paper) presented the state of the art on building-integrated thermal energy storage (BITES) systems that directly facilitate space conditioning, including the concepts, perspectives, technologies, research findings, and case studies. There are various ways to utilize building fabric for thermal energy storage (TES), such as passive or active systems, hydronic or air-based approaches. BITES systems can be effectively incorporated into all kinds of buildings to improve their thermal comfort and energy efficiency.

Other than the common advantages of TES systems, the literature and technology survey has shown that BITES systems have the following additional advantages:

- BITES design exploits the space conditioning potential of building fabric in an energy-efficient and cost-effective way. BITES design takes advantage of building fabric being a distributed form of TES in which it maximizes its contact area with room air as well as the surface-to-volume ratio. This advantage enhances the thermal coupling between the systems with the room air, and hence the effectiveness of the systems' TES and space conditioning functions. BITES design enhances or adds the TES function on top of the components' original building functions (e.g. structural and architectural) without excess construction and material cost. BITES design avoids occupying useful room space as is the case for add-on TES systems (e.g. ice containers, water tanks).

- BITES design enhances the building performance in several aspects. Storing and releasing thermal energy locally by BITES systems can reduce local demand and separate the task of ventilation for air quality from space conditioning. Hence the size of the service system lines (e.g. pipes and ducts) between central plants and local space can be reduced. More space can be saved in both floor area and storey height. It also reduces the energy consumption and size of the fans, as well as the noise from large air flow in conventional all-air systems.
- Further energy saving and peak power demand reduction could be achieved by the utilization of local low grade thermal energy (e.g. night time cool outdoor air). Hence, this further reduces the capacities of building mechanical systems, and the size of energy transportation infrastructure and power plants capacity in communities as a collective effect of many BITES systems.
- BITES design is able to provide better thermal comfort than conventional air-conditioning systems because of the minimization of air movement, surface temperature differences, room temperature fluctuations, and uniformity of indoor air temperature. With an evenly distributed radiant heating/cooling area, radiant temperature asymmetry can be minimized. Comfort may also be improved with enhanced radiative heat exchange between occupants and BITES systems.

For active BITES systems, thermal comfort, TES capacity, charge/discharge capacity, and space conditioning capacity are critical to their thermal performance. These aspects are interrelated and influenced by the operation. For example, the heat from heat-transferring fluids and direct solar gain will significantly affect the amount of thermal energy stored in the slab, the surface temperature, and the heat flux being released from the top surface

(Athienitis and Chen 2000). Dynamic thermal responses, integration of structural and thermal functions, and predictive control methodology are recommended for future studies. A comprehensive study on integrating design and operation is necessary in optimizing the overall thermal performance.

Evaluation, comparison, and discussion of the energy performance, thermal comfort, and other concerns of the different types of BITES systems and guidelines for selection will be presented in the companion paper part II (Section 2.2).

Section 2.2 Building-Integrated Thermal Energy Storage (BITES) – State of the Art: Part II, Evaluation and Comparison

Section Abstract

Based on the literature and technology survey on building-integrated thermal energy storage (BITES) systems presented in the companion paper Part I (Section 2.1), this study attempts to advance the understanding of different BITES systems to a more comprehensive, comparative, and quantitative level. This study first discusses and evaluates the current research and development activities on the different groups of BITES systems, highlighting their own advantages, limitations and challenges. After that, comparisons between the thermal and energy performances of the different types of BITES systems are provided, followed by pertinent discussions. One of the important findings from the present studies is that providing sufficient thermal coupling between the BITES systems and the room air is critical in achieving a successful application. Ideas for enhancement of thermal coupling are suggested in the last part of the section (paper), including discussion of other important design and operation aspects such as thermal comfort, charge and discharge control strategies, structural considerations, and selection of BITES system. This section (paper) also provides suggestions for future research needs.

1. Introduction

In the companion paper Part I (Section 2.1), a survey on the literature and technologies of building-integrated thermal energy storage (BITES) systems was presented, with emphasis

on the concepts and working mechanisms of the different BITES systems for thermal energy storage (TES) and space conditioning. The survey indicates that successful applications of BITES systems are sensitive to many factors, including climate conditions, building types, utility fee structure, occupant behaviour, operation strategies, thermal comfort, and quality and quantity of locally available sources (e.g. favourable ambient air, solar and geothermal energy) (Braun 2003, Xu et al. 2010). More quantitative and comparative information is needed for system selection and subsequent design and operation.

To serve this need, this study firstly presents the discussions and evaluations of each type of BITES system, highlighting their individual advantages, limitations and challenges in subsection 2, "Evaluations." After this, comparisons and quantification of thermal and energy performance between different BITES approaches are provided in subsection 3, "Comparisons." In subsection 4, "Design and operation considerations," the important design and operation considerations are suggested and corresponding studies from the literature are presented. The aforementioned content is based on the findings from paper Part I (Section 2.1), further literature review, and the opinions of the author.

2. Evaluations

In the companion paper part I (Section 2.1), BITES systems are categorized into four types according to their locations in the buildings, and presented. In this subsection, the discussion and summary for each type will be presented.

2.1. Whole building

Utilizing the overall mass of a building for passive solar design and night time building pre-cooling by natural ventilation can effectively improve the thermal and energy performance of buildings (see A1.1 in Appendix). In practices of pre-cooling the building's overall mass, reported investigations have shown that energy costs can be reduced by 10 to 50% under dynamic rates, and reduced by 10 to 35% for on-peak power demand (ASHRAE 2007b). Effective thermal use of building fabric requires proper architectural and engineering design, including (1) suitable amount of storage mass, and (2) effective thermal coupling between the storage mass and the room. For maximizing the thermal coupling, there are mainly two methods. The first approach is to maximize the exposure area of the building fabric. The second approach is to increase the heat exchange rate per unit exposed BITES surface area, such as increasing the ventilation flow rate during night time pre-cooling to increase the convective heat transfer coefficient, and avoiding the use of false ceilings and flooring materials with low thermal conductivity.

The most obvious advantage of using the whole building for TES is the ease of implementation (i.e. sole requirement of proper design as mentioned above) and low operation cost. Previous research and development (R&D) activities have provided abundant design and operation guidelines. The obvious drawbacks are the uncertainties in heat transfer rate, the amount of thermal energy stored, and the resulting operative temperature (i.e. the effective temperature based on air and radiant temperature (ASHRAE 2009f)). Recent research activities have targeted these problems. In cooling applications, the heat transfer rate and maximum indoor temperature without mechanical conditioning systems can be estimated based on empirical correlations from previous studies. The approximate amount

of thermal energy stored and the operative temperature can be obtained by temperature sensors embedded in the building fabric. Another potential drawback is that when thermally heavy buildings are over-heated or –cooled, their slow thermal response will cause problems in quick adjustment of the indoor temperature.

2.2. BITES walls

Because of exterior walls' direct exposure to solar radiation, and their relatively small solar incident angles during heating season, using exterior walls for direct solar thermal energy collection and storage has attracted a lot of research interest. Other than for winter space heating, the stored thermal energy can be used to facilitate natural ventilation for summer cooling. On the other hand, the utilization of exterior massive walls as BITES systems is subject to many other design constraints, such as undesirable heat loss/gain, air and water tightness, daylight harvesting, structural load bearing capacity, aesthetic appearance of the building, and outdoor view obstruction. Due to these constraints, recent successful practical applications are rarely reported, except for Trombe Walls.

Trombe wall systems have several advantages: simple configuration, high autonomy; and zero running cost (Yakubu 1996). There are also obvious disadvantages, mainly the aesthetic appearance – visible blackened wall behind clear glass for achieving high thermal absorption performance. Collective measure on the appearance is under study (Schuler et al. 2005). The majority of the conducted studies considered only the heating gain during sunny winter periods. Heat loss during non-sunny periods and annual energy performance were not considered. The undesirable heat gain in summer should be addressed (Chel et al. 2008, Ji et al. 2007a).

In the literature, there are concerns about the ventilation of the Trombe wall. Ventilation enhances the convection in the air gap, and hence tends to negate the storage effect of the wall and weaken the effectiveness of the air gap as thermal insulation (Balcomb et al. 1983). Negating the storage effect of the wall will increase the temperature fluctuation of the room because, during sunny times, the heat injection rate into the living room could be intensive (Ji et al. 2009). Another concern is reverse thermo-circulation, which happens when the air temperature in the air gap is lower than that of the room (Zalewski et al. 1997). There will be more undesirable heat loss from the room to the exterior through the Trombe wall as compared to the classic Trombe wall, which is not vented (Ji et al. 2008). Balcomb et al. (1983) claimed that in most cases, the unvented Trombe wall performs better than the vented. Other research activities (Chel et al. 2008, Ji et al. 2008, Zalewski et al. 1997) showed that control ventilation with motorized dampers will result in higher overall thermal performance. However, using motorized dampers increases costs for construction, maintenance, and operation. Furthermore, potential air leakage around the vents was overlooked in most of the theoretical studies.

Unlike exterior walls, interior walls (i.e. partitions) face much fewer design constraints for being BITES systems. Their first advantage is that the stored thermal energy won't be lost to the exterior. This is the main reason why the majority of BITES wall implementations use interior walls. Attention is needed for reducing energy consumption and loss of useful energy in delivering the thermal energy from remote thermal energy sources. These points are applicable to other types of BITES systems, such as roof and interior slabs.

Passive BITES walls, due to their stabilities of thermal behaviour and independence of maintenance and control, are widely deployed. However, their effective TES capacities are

highly influenced by the surface natural heat transfer rate (Akbari et al. 1986, 1987), and normally, the heat transfer rate is low. Recently, active walls are noticeably attracting R&D interests.

2.3. BITES slabs

Using concrete slabs for TES increases the effective thermal storage mass of the building, especially in passive solar design applications. The main advantages in terms of location, shape and quantity, are as follows:

- When a large window area is adopted in a passive solar design, a massive TES must be placed at the location of first incidence to absorb the transmitted solar radiation. If a large portion of the transmitted solar radiation is reflected and re-distributed instead of being absorbed, space over-heating can occur. Because the floor is often the location of first incidence, a massive floor in a medium dark color should be used (e.g. exposed concrete).

- In concrete structure buildings, the slab accounts for the largest portion of the structural mass. An abundant amount of thermal mass is already available for use. A large amount of energy can be stored for only a small variation in temperature.

- A concrete slab is in a distributed form and it is already, or can easily be, exposed to interior air. An example of this is a ceramic floor and an exposed ceiling (i.e. no suspended ceiling). This enables the concrete slab to absorb and release thermal energy directly and evenly into the indoor room. This also means the slab can be used for radiant floor heating or cooling.

- Indoor thermal discomfort is sometimes caused by the warm-head-and-cool-feet situation, due to vertical air temperature stratification (ASHRAE 2004a, 2009f). Maintaining heat storage at the floor level or using radiant floor heating can counteract the inevitable stratification tendency.

- Using concrete slabs for TES will not block the outdoor view of occupants. In some cases, Trombe walls are placed close to windows to absorb and store solar energy. In such cases, outdoor views and indoor room use are sacrificed.

By means of charging/discharging, thermal energy can be internally and actively charged into the slabs. This also leads to increasing the heat exchange area and rate between the heat transfer fluids and the storage mass. The control for storage amount and temperature becomes easier (see paper Part I (Section 2.1)). The thermal energy storage becomes more efficient and effective. Different kinds of ambient renewable energy, such as direct solar gain, night time cooling air, PV/T thermal energy, can be utilized as sources for TES.

Active slabs can regulate the room temperature by acting as heating/cooling panels, instead of being only thermal sinks like passive slabs. Radiant slab heating/cooling has shown advantages in both energy performance and thermal comfort (ASHRAE 2008, Feustel and Stetiu 1995, Inard et al. 1998). The main advantage is that the space heating/cooling effectiveness can be enhanced by radiative heat transfer and large exposed slab area.

3. Comparisons

In this subsection, the comparisons of the thermal and energy performance for different BITES systems and approaches will be presented, as well as discussion pertinent to each comparison.

3.1. General performance

Bansal and Shail (1999) studied four passive and active solar air heating techniques associated with hypocaust. The system with a solar chimney (i.e. solar air thermal collector) integrated on a south façade and storage in the ceiling (similar to the Barra-Costantini system described by Buzzoni et al. (1998)) provides the most solar heating output – the annual heating fuel ($J/K/m^2$) is the least.

Lucas et al. (2000) conducted a comparative and experimental analysis on the thermal performance of three passive systems (unvented classic Trombe wall, direct gain and sunspace) for various operations (e.g. with/without night/day movable thermal insulation and natural ventilation) and seasons. The researchers stated that the system of a sunspace associated with a massive wall gave the best results – least annual space conditioning load.

Three types of BITES slabs and their associated ventilation and energy storage strategies were investigated by Braham (2000) for low-energy UK buildings. The first type is natural ventilation in occupied space with exposed slab. The second type is natural ventilation through the hollow cores of the slabs. The third type is mechanical ventilation through the slab cores. The researcher reviewed independently published performance data and stated that the third type is superior to the other two in terms of thermal comfort, heating/cooling energy cost, mechanical equipment size and maintenance cost.

Baskin (2005) compared the energy performance and indoor thermal comfort conditions with a forced-air system and/or a hydronic floor system under different space cooling and heating modes. In the cooling tests, overall cooling energy consumption of the forced-air alone space cooling mode (C1) is three times that of C2 mode, which is C1 mode plus slab night time hydronic pre-cooling by heat pump. C2 mode was able to shift the peak cooling

loads to the evenings. Furthermore, C2 mode consumed only half the energy of C3 mode, which is C1 mode plus mechanical ventilation for night time house pre-cooling and partial slab pre-cooling. In other words, heat pump assisted slab pre-cooling is more energy efficient than pre-cooling with mechanical space ventilation. In C3 mode, the fan consumed a major portion of the energy. In heating tests, the hydronic floor heating mode is slightly better than the forced-air mode in terms of energy performance.

When building envelopes combine BITES and solar thermal collector functions, such as the Trombe walls and the BITES roof systems, the long-term net gain on thermal energy (i.e. the difference between the undesirable energy loss and useful energy gain) is of important consideration. Little literature has quantified the overall energy contribution of BITES roof systems as previously mentioned. For Trombe walls, Zrikem and Bilgen (1986) conducted a theoretical study, and stated 8 to 26% solar fraction (i.e. the portion of the overall space heating contributed by the collected solar thermal energy) in their Trombe wall model for a typical winter week in Montreal, Canada. Howard (1986) reported 19% solar fraction in a monitored solar house with Trombe wall, a sunspace, and an interior ventilated wall. Studies conducted by Ji et al. (2009, 2007a) showed that replacing the massive wall with a layer of insulation and shading curtain can improve the thermal efficiency of the Trombe walls. Furthermore, Ji et al.(2007b) proved that installing a fan to assist the thermo-circulation in the cavity can help extract more heat from a mass-less Trombe wall system. These studies show that the Trombe walls' energy efficiency is lower than that of a solar thermal collector, which is located on the exterior wall and conveys collected heat directly into the room.

The space conditioning capacities of different hydronic BITES systems are listed in Table 2.2. Capillary systems' (paper Part I (Section 2.1)) cooling capacity was reported to be up to

80 W/m^2 (Feustel and Stetiu 1995). Even though the space conditioning capacities were reported mainly for the hydronic floor/wall systems (see paper Part I), the values can be the benchmark reference for other hydronic and ventilated BITES systems. It is worth noting that the space conditioning capacity is affected by a system's dynamic response. For example, when heat is being supplied by a hydronic system, part of the heat will be absorbed by the storage mass, and hence the instantaneous space heating output will be less. Some reported values are obtained from steady-state simulations or experiments; therefore, the actual values will not be the same in real applications (transient states).

3.2. Active and passive charge/discharge

The advantages of passive systems, as compared to active approaches, are their reduction in operation energy consumption for charging/discharging the systems, and also simple construction, and little maintenance (Howard 1999).

The major shortcoming of passively storing/releasing thermal energy from or to the room (i.e. thermally coupling the BITES systems with room air through natural convection) is that the effectiveness of heat exchange is restricted by the systems' exposed surface area and low natural convective heat transfer coefficient (Shaw et al. 1994). The combined heat transfer (convective and radiative) between the BITES surface and the rest of room is about 6 to 9 W/m^2/K (about 5 W/m^2/K for radiation), depending on the heat flow direction and surface location (ASHRAE 2008). False ceilings and low-conductance flooring will further weaken the thermal coupling between the BITES systems and the rest of the room. Another drawback is that local passive systems cannot store thermal energy from remote sources (e.g. geothermal).

Table 2.2: heating/cooling capacity of hydronic BITES systems

Locations	Cooling (W/m^2)	Heating (W/m^2)	Notes		References
Floor	n/a	14	Constant room and floor temp. at 20.1 and 23.5°C, respectively. Capacity is calculated based on data provided in the paper.		(Hanibuchi and Hokoi 1998)
Ceiling	30 to 40	25 to 30	Ceiling temperature ranges from 21 to 25°C; Supply water temp. are 18-22°C for cooling and 27-29°C for heating		(Pfafferott and Kalz 2007)
Floor	30	n/a	Assisted with variable-air-volume system for space cooling		(Henze et al. 2008)
Floor	max. 32	n/a	Carpet on top of floor		(Lehmann et al. 2007)
	max. 39	n/a	Raised access floor on top		
Ceiling	25	n/a	24°C AUST*, and 21°C panel		(ASHRAE 2008)
	50	n/a	24°C AUST, and 18°C panel		
Wall/floor	n/a	33	21°C AUST, and 25°C panel		
Wall	n/a	Max. 85	Water at 42°C	Room air at 20°C; Water at 3 $L/min/m^2$	(Marmoret et al. 2000)
	n/a	Max. 20	Water at 25°C		
Slab	30 to 60	10 to 30	Values are based on experience for normal applications		(Hauser et al. 2000)
Slab	30 (80)	n/a	The value becomes 80 if transmitted solar radiation presents as constant heat fllux; supply water at 13°C; return temp. at 19°C.		(Simmonds et al. 2000)

*AUST: average un-conditioned surfaces temperature

Generally, active charge/discharge enables faster thermal energy storage/release rates as compared to passive charge/discharge due to higher fluid velocity and flow rate in the heat

transfer area (pipes, air channels, or interior space).For example, higher air velocity results in higher convective heat transfer coefficient (CHTC, either inside the air channels, or on the exposed surfaces), and hence higher heat exchange rate between the working fluid and the storage mass. A higher flow rate means larger amount of energy can be transported by the working fluid with a given fluid inlet temperature. Therefore more thermal energy can be stored/released if TES capacity allows. One example is night time cooling facilitated by mechanical ventilation stores more coolness than natural ventilation, which has a lower number of air changes per hour (ACH) (Santamouris et al. 2010). However, high CHTC is not always an advantage. In ventilated BITES systems, the intensified heat transfer process causes fast temperature drop of the air flow and consequently the temperature field on the exposed surface has a high gradient (Zukowski 2005). The monitored results from Chen et al. (2010b) also showed an un-even floor temperature distribution. Uneven temperature fields may reduce the thermal comfort level due to radiant temperature asymmetry (ASHRAE 2004a). Another advantage of active charge/discharge is that the heat transfer rate can be controlled by regulating the flow rate. Hence, the amount of thermal energy and the rate of charge/discharge can be controlled more easily than in passive systems.

Interior open-loop approaches for ventilated BITES systems enable advective heat exchange between the BITES systems' air flow and room air, improving the thermal coupling between them. Open-loop approaches can be used to compensate for the thermal coupling reduction due to false ceilings, low-conductive flooring, or furniture. Ventilation air being supplied through a BITES system is an example of the "open-loop" approach. "Open-loop" approaches with air entering the BITES system from the room before passing through the AHU, or local air recirculation bypassing the AHU has not been reported in any literature to the author's knowledge.

BITES systems can significantly reduce the thermal conditioning energy consumption of buildings. Active approaches exploit their potential by improving the thermal coupling between the BITES systems and the room air, but they are not necessary if the thermal function requirement can be met by passive approaches. The thermal coupling can also be improved by other means (see subsection 4.1 "Effective thermal coupling").

3.3. Hydronic and ventilated systems

Both hydronic and ventilated approaches enable the active charge/discharge of BITES systems – working fluids accelerate the transportation of thermal energy in or out of the systems. The advantages of active systems have been discussed in the previous subsection.

Among active systems, hydronic BITES systems permit substantial heat flow even for relatively small temperature differences between the mass and the working fluids. This, consequently, allows the use of low-grade (i.e. low-temperature) energy as direct cooling or heating sources, such as a geothermal source or recovered process heat (ASHRAE 2011, Xu et al. 2010). Another advantage of hydronic BITES systems is that cooling floors and walls are able to absorb and remove significant direct solar radiation striking them. A value of up to 50 W/m^2 of transmitted solar radiation was reported by Simmonds et al. (Simmonds et al. 2000). Ventilated systems with an "open-loop" (to the room interior) configuration can improve the thermal coupling between the BITES systems and room air. This is realized by releasing the thermal energy stored in the core of the BITES directly to the room air, in addition to the surface radiation and convection.

Some studies pointed out that the transportation efficiency and volumetric heat capacity of air is low in comparison with water (ASHRAE 2011), and tends to lose much of its heating/cooling potential by various distribution losses (e.g. air leakages, and thermal loss

due to large duct area) (Feustel and Stetiu 1995, Xu et al. 2010). If air is used as the medium instead of water, four times the mass or 3480 times the volume would be transported for removing the same amount of heat. For the case of removing intensive direct solar heat gain, changing the working fluid from air to water will result in up to 30% of energy savings at the fan motor (ASHRAE 2011). This saving could also be a gain in delivering intensive heat. On the other hand, ventilation for air quality requirements (e.g. fresh air and humidification or dehumidification) is always needed in occupied space. Constructing hydronic and ventilation systems in parallel would obviously increase the construction cost. Supply air can be conditioned to facilitate space conditioning to some extent. This will reduce the requirement of the thermal conditioning capacity of the BITES system. Additional space heating/cooling means may be eliminated if the space heating/cooling demand is minimized with a high performance envelope (Persson et al. 2006). Note that the main concept and advantage of BITES design is that space heating/cooling demand should be balanced locally by the TES. Remote transportation of intensive energy should be avoided.

Table 2.3 shows the reported energy consumption of fans or pumps of different space conditioning systems. The fan energy consumption in the TermoDeck system uses about twice the energy of the pumps in hydronic slabs, and saves about 15 to 25 % of fan energy as compared to a conventional all-air system. Some of the fan energy is attributed to night time ventilation for slab pre-cooling. The expected low fan energy consumption, in comparison to conventional all-air systems, is due to minimization of heating/cooling supply by ventilation air – the building has been pre-conditioned and there is a strong thermal coupling between the slabs and the room air. Note that buildings using hydronic BITES systems still have to spend energy on the ventilation fan. On the other hand, the study on hydronic systems by Deecke et al. (ASHRAE 2011) showed that significant electric energy

saving on pumps can be achieved by intermittent operation without reducing the room-side conditioning capacity – up to 70% of pump energy savings with a 25% duty cycle. Note that, for both hydronic and ventilated BITES systems, perimeter heating may be needed for buildings in cold climate areas due to the intensive space heating load; hence the operation energy consumption will be increased.

Table 2.3: Operation (i.e. fan or pump) energy consumption

System type	Building type, locations	Operation	Energy consumption (kWh/m^2/yr)	Note (references)
Hydronic radiant floor	40-storey office, Bonn, Germany	Pumping ground water	10 (pump)	n/a (Pfafferott and Kalz 2007)
Hydronic radiant floor	4-storey office, Aachen, Germany	Pumping ground water for heating	9.3 (pump)	25 kWh/m^2/yr for space heating using GSHP*(see below)
		Pumping ground water for cooling	14.3 (pump)	n/a (Pfafferott and Kalz 2007)
		Ventilation	12.7 (fan)	n/a (see above)
Termo-Deck	4-storey institutional, Norwich, UK	Ventilation and pre-cooling	16-18 (fan)	fan power is 5.3 W/m^2; zero cooling load (Braham 2000, Team-Probe 1998)
Termo-Deck	4-storey institutional, Norwich, UK	Ventilation and pre-cooling	19 (fan)	n/a (Turner and Tovey 2006)
All-air conditioned	Standard office, UK	Ventilation and space conditioning	22 (fan)	n/a (DETR 1998)

*GSHP: ground source heat pump

Radiant conditioning systems (e.g. hydronic slab, TermoDeck slabs) can reduce the first-cost in construction by reducing the capacities of mechanical equipment and distribution systems,

as well as by saving space. The spacing of piping embedded in the slab is normally about 100 to 300 mm (ASHRAE 2008). Feustel and Stetiu (1995) stated that hydronic radiant cooling systems can have lower first-cost, if specific cooling loads are above 55 W/m^2. It also reduces the energy consumption for thermal distribution (e.g. circulating water instead of air) and for space conditioning. The peak-power requirement for cooling can be reduced by about 28% in conditions specified in their study. Their case study showed that the yearly energy consumption in an office in Europe can be reduced from 141 kWh/m^2 with VAV systems to 131 kWh/m^2 with hydronic radiant cooling systems. In the case studies presented by Xu et al. (2010), the payback time for hydronic slabs ranges from 2 to 3 years.

For TermoDeck systems, TermoDeck Ltd[2] claims that the first-cost of fans, chillers and ducts used for TermoDeck in hot climates is about 40-50% of that for conventional all-air systems. TermoDeck systems can also result in a 45-50% reduction in required cooling capacity. The reduction of peak cooling demand can be as high as 70-90%. As compared to equally sized conventional buildings, TermoDeck projects in Europe have up to 50% lower energy consumption for total heating & cooling. In the Middle East, they have 30-50% lower energy consumption for cooling. There are obvious financial savings in using ventilated BITES slabs over hydronic BITES slabs – the elimination of ventilation ductwork and water pipes. This advantage will result in significant savings on construction cost (e.g. labour and material) and space for service systems.

---

2 www.termodeck.com

4. Design and operation considerations

Significant savings on energy consumption and utility cost resulting from the use of BITES systems have been demonstrated in all kinds of buildings in the literature, using simulations, controlled laboratory tests, and field demonstrations. Studies indicate that savings are sensitive to many factors, including utility rates, type of equipment, occupancy schedule, building construction, climate conditions, and control strategy. The most important factor for savings is probably the utility rate structure (Braun 2003). Other than savings, thermal comfort is another important consideration.

The important influencing factors for successful application of BITES systems include the following:

(1) Dynamic nature of buildings' space conditioning loads;

(2) Proper design of the BITES systems (e.g. thermo-physical characteristics of the storage mass, TES capacity, thermal coupling, and charge/discharge rate);

(3) Shapes and locations of systems relative to the bounding space, for thermal comfort purposes;

(4) Operation strategies (ASHRAE 2007b).

This subsection presents the design and operation considerations for general BITES systems, including the thermal coupling between the systems and the room air, thermal comfort, operating and control strategies, alternatives of thermal energy sources, over-storage issues, structural considerations, and guidelines for BITES system selection.

4.1. Effective thermal coupling

Thermal coupling refers to the heat exchange rate between the BITES systems and their zones.

$$q_{TC} = \sum U_i \cdot \Delta T_i \approx U_{TC} \cdot \Delta T_{avg} \tag{2.1}$$

where ΔT_{avg} is the average temperature difference between the BITES system and the room air. U_{TC} is the thermal coupling coefficient, the sum of the different advective, convective, conductive, and radiative heat transfer coefficients. Each of them is the product of heat transfer area and heat transfer coefficient. Except for ventilated systems with "open supply" configurations, U_{TC} includes the product of mass flow rate and the specific heat of the air. In this case, ΔT_i will be the temperature difference between the outlet air and the room air.

Based on the studies presented in the companion paper Part I (Section 2.1), this section (paper), and especially the findings of several studies (Akbari et al. 1986, 1987, Henze et al. 2008, Koschenz and Dorer 1999, Lehmann et al. 2007, Shaw et al. 1994), thermal coupling is critical to the exploitation of the space conditioning capacity of the BITES systems and the effective utilization of the storage mass. Low thermal coupling limits the potential of the BITES systems (see Table 2.2).

Problems due to insufficient thermal coupling have been shown in many practices. For example, in some passive solar heating design practices, excessive south glazing area and inadequate thermal coupling between the passive BITES systems and the rest of the room result in space overheating (Yakubu 1996). In radiant floor heating/cooling practices, relatively high thermal loads plus weak thermal coupling always cause surface temperature

overheating (Athienitis 1997) or overcooling. Overheating or overcooling problems are mainly due to a low combined heat transfer coefficient U_{TC} (i.e. radiation and natural convection) between the BITES exposed surface and rest of the room needs. This shortage needs compensation from a high temperature difference, ΔT. In other words, a high q_{TC} requirement with limited U_{TC} causes a high ΔT. Also, energy efficiency will be compromised due to high temperature operations. If space conditioning loads cannot be met by BITES systems alone, assisting conditioning systems, such as forced-air system assisted hydronic TABS (Henze et al. 2008) or perimeter auxiliary heating, are needed. Increasing the thermal coupling can reduce the requirements for auxiliary heating/cooling and the excessive ΔT between the systems and the room air. It also increases the amount of potentially useful thermal energy that can be stored in the systems. For example, excess solar gain can be stored in the BITES during the daytime and then used at night time.

There are cost-effective methods to enhance the thermal coupling, and hence maximize the contribution of the BITES systems. The CHTC between the room air and the surface of the systems can be increased by enhancing the air movement, with a ceiling fan, for example. Selecting surface materials with high short-wave absorptivity (e.g. dark surfaces) can enhance the storage of solar gain (Balcomb 1983). However, the idea of selecting radiative properties is not applicable for long-wave radiative heat transfer since most common non-metal construction materials have similar emissivity or absorptivity around 0.9 to 0.95 (Lindstrom et al. 1998). Roughening a surface will always tend to slightly increase its effective emittance and the CHTC in turbulent forced convection – air velocity greater than 0.3 m/s (Lindstrom et al. 1998). Applying PCM can maintain the temperatures of storage mass within a narrow range and hence provide a relatively larger temperature difference between the BITES

surfaces and the room air (i.e. ΔT) during the charge/discharge process (see paper Part I (Section 2.1) for more information on applications of PCM).

Sodha et al. (1992) found through simulations that passive systems with larger surface areas are more effective in reducing the temperature swing than those with larger thermal capacities. Removing false ceilings and low conductive flooring, and adopting curved ceiling surfaces can enlarge the exposed area of the BITES systems. However, Shaw (1994) showed that simply exposing the building structure to the workspace provides limited TES capacity and hence, underexploits the structural mass' ability to moderate room temperature. Ventilated systems with interior-open-loop configurations, such as local air circulation between the cores of the systems and the room air, can engage the core area for heat exchange and thermal storage, and hence significantly increase the thermal couple. They offers much better thermal coupling than those of conventional hydronic slab heating/cooling systems.

Naturally, BITES systems offer relatively good thermal coupling because of their large exposed area and the pre-conditioned surfaces, which offers a better ΔT. It is worth pointing out that the required level of thermal coupling depends on the thermal load characteristics of the occupied space.

4.2. Thermal comfort

BITES systems generally provide good thermal comfort based on the literature and technology survey presented in paper Part I (Section 2.1). The main reason is that BITES systems can provide radiant heating/cooling in a distributed manner. Inard et al. (1998) stated that distributed heat sources present better thermal comfort over localized heat sources. Radiant energy offers better perception of thermal comfort than convective energy

(ASHRAE 2011). Comfort levels offered by radiant heating/cooling can be better than those of other conditioning systems because thermal sensations of occupants are satisfied directly and air motion in the space is at normal ventilation levels. With radiant heating, it is possible to achieve relatively uniform air space temperature in the vertical direction (ASHRAE 2008).

Under radiant heating/cooling conditions, thermal discomfort can be caused by radiant temperature asymmetry. When an active BITES design is adopted in only some parts of the building components (i.e. only ceiling or walls), the interior surface temperatures of these components will not be the same as those of the other surfaces. Even within the same surface, an uneven temperature field could exist (Chen et al. 2010b). According to ASHRAE standard 55 (2004a), a warm ceiling is the most susceptible to cause thermal discomfort due to asymmetric radiation, while a warm wall is the least. Excessive asymmetric radiation will most likely happen in the winter in the perimeter zone of buildings with large glazing – cold window surface(s) with warm interior face(s) of BITES system(s).

Furthermore, thermal discomfort can also be caused by temperature variation with time, cyclic variations, drifts or ramps, or surface temperature overheating/cooling (ASHRAE 2004a). Even though these situations do not normally happen in high-mass buildings, the design and operation of active BITES systems still have to take these criteria into consideration.

Building occupants' reactions to thermal and visual comfort need to be considered in the design and operation of BITES systems. For example, under a direct solar gain scenario, occupants will close blinds to avoid glare and direct exposure to solar radiation. Excessive asymmetrical radiation will also cause the occupant to close the blind to reduce the coolness

from the cold window side. This action will affect the transmittance of the otherwise useful solar energy (thermal and daylight).

4.3. Operation and control strategies

The general objective of the various operation strategies of BITES systems is to provide energy-efficient and economical operations fulfilling thermal comfort requirements. An operation strategy defines the overall method of control for a BITES system to achieve its design intent. It provides the logic for determining when and what operating modes and control strategies are selected; meanwhile, various control strategies implement the specific operating modes (ASHRAE 2007b).

Night time set-up (cooling season) or set-back (heating season) operation strategies have traditionally been applied to the majority of buildings (ASHRAE 2007a). Set-up/set-back strategies reduce the overall energy consumption due to the reduced temperature difference between exterior and interior, but they increase the demand during occupied periods due to the warming up or cooling down of the buildings (ASHRAE 2007b), especially at the beginning of the occupied periods – the morning period for commercial and residential buildings and the evening period for residential buildings (Braun et al. 2001, Doiron et al. 2011). By taking advantage of the BITES systems, there are several operation strategies that can provide energy-efficient and economical thermal comfort, such as building pre-cooling or –heating. The total energy consumption in pre-cooling or -heating strategies may be slightly higher; however, due to increased utilization of renewable energy, the amount of purchased energy will be reduced, and also due to off-peak energy pricing, the cost for both energy and demand is reduced as well (Braun 2003, Henze et al. 2008). R&D activities show that the savings potential is sensitive to the utility fee structure, building thermal

characteristics, weather conditions, and occupancy schedule (Braun 2003, Morgan and Krarti 2007). Researchers also point out that operation strategies should recognize if the objective is an energy cost minimization or a demand cost minimization.

For passive BITES systems, the controls mainly concern the heat gain/loss, room temperature heating/cooling set-points, and the HVAC systems. Candanedo and Athienitis (2010) investigated a control method of modulating the effective transmittance of façades through motorized blinds to control the solar gain of the BITES systems. Night time building free cooling/pre-cooling using cool outdoor air has been common practice (see paper Part I (Section 2.1)). General correlations between the ventilation rate, thermal capacity, and the indoor temperature were provided in the literature (Santamouris et al. 2010, Shaviv et al. 2001). Pre-cooling of a whole building using the chillers with night time favourable air conditions and utility tariff has showed superiority over the night time set-up strategies in terms of savings on energy and demand costs. Braun (Braun 2003, Braun et al. 2001) stated that the "maximum discharge" strategy – the occupied space is pre-cooled to 20.6°C from 1 am until 10 am and room cooling set-point is kept at 25°C (i.e. the upper limit of thermal comfort) from 10 am to 5pm – results in the largest savings.

In buildings with active BITES systems, there are more considerations than in those with passive systems, and hence the operation and control strategies are more complicated, especially when primary space conditioning is supplied through the systems. In the study of Gwerder et al. (2008) on the heating/cooling applications with a hydronic BITES system, the researchers stated that "the specification of control algorithms is difficult because of thermal inertia of the system and because of the challenge to comply with comfort

requirements in different rooms with different gains and these rooms being connected to the same supply of hot water."

Some basic strategies that rely on simpler control routines have been presented in the literature. Simmonds (1994) stated that for space heating, the required heat input to the BITES is proportional to the supply and return water temperature difference. For cooling, due to the lower limit of the floor temperature regulated by thermal comfort, the input is determined by the internal loads and increases as the room temperature rises. Athienitis and Chen (1993) conducted an experimental and numerical study on the thermal performance of an electric BITES slab to develop optimal control strategies for operation costs reduction. The study showed that night time set-back set-point with a ramp change is preferable to a step change in saving energy, and proportional control results in less system cycling than on/off control. Later on, Athienitis (1997) proposed a control strategy of using a half-sinusoid set-point for room operative temperature. Therefore, the electric BITES system applied in a passive solar house can store both auxiliary heat and direct passive solar gain.

Olesen et al. (2006) introduced a diagram method for calculating the allowable heating gain on the room side and the required cooling capacity on the water side for hydronic BITES slabs. ASHRAE (2011) provides detailed discussions on the controls of embedded systems (mainly for hydronic slab heating and cooling), including the control concept, central and individual controls, locations of thermostat sensors, time response of the massive floor, and self-regulating effects. It is suggested that energy output control of a central system (e.g. chillers or boilers) should be based on the average temperature of the supply and return water, so that the energy output is correlated with the current building load. Intermittent operation of pumps will save significant pump energy consumption (ASHRAE 2011,

Lehmann et al. 2011). The duty cycle of the pumps or fans can be further shortened due to the storage effect of the TES function. Henze et al. (2008) presented their simple control strategies on a hydronic BITES slab assisted with a separate VAV (variable air volume) heating/cooling system. The supply air temperature is based on outdoor conditions, while the hydronic BITES slab handles the rest of the space conditioning load. In buildings that adopt ventilated BITES systems, the temperature of the storage mass should be used for heating/cooling supply air control, instead of the return air temperature, to avoid cycling between free-cooling and heating (Turner and Tovey 2006).

For more sophisticated control strategies (i.e. optimal control), accurate but simple thermal models are essential. In order to select and optimize control strategies, the specific thermal model of the building needs to be capable of representing the building thermal characteristics, HVAC equipment, utility fee structure, design weather conditions, BITES systems, operation strategies and schedules of occupancy, lighting and appliances (Armstrong et al. 2006a, Braun 2003). For existing buildings, inverse thermal models (sometimes referred to as thermal response, backwards, or data-driven models) trained with field-measured data can be used to evaluate different control strategies and improve the current one (Armstrong et al. 2006a, b, Braun et al. 2001). Gwerder et al. (2008) proposed the Unknown-But-Bounded (UBB) method for the control of hydronic BITES systems. The UBB method is a model-based integrated approach that takes into account the design of the building automation system, thermal comfort and the unknown-but-bounded external and internal gains. Instead of forecast weather information, the floating mean value of the outside air temperature over the last 24 hours is used in the control.

Model-based predictive (or anticipatory) control has attracted significant attention in recent research activities, especially in optimal control applications. Hartman (1988) stated that dynamic control, which consists of anticipatory and integrated controls, is essential in order to take the full advantage of the BITES systems. Kummert et al. (2000) presented their study on optimal heating control in a passive solar commercial building, and found that the energy savings are about 9%, while maintaining or improving thermal comfort. LeBreux et al. (2006) presented their study on using fuzzy logic and a feed-forward controller to control the heat storage and release of an interior hybrid thermal energy storage wall. The wall can store direct solar radiation and/or heat from an embedded electrical wire, ideally using off-peak electricity. Their analysis showed that, compared to a traditional electric baseboard heating system, the hybrid system and the applied control strategy reduced the electricity consumption for the winter season by 24%, and 94% of the electricity is consumed during off-peak hours. In their more recent study (LeBreux et al. 2009), the same research team showed that inaccurate weather forecasting (e.g. five-day forecast) may cause space overheating and increased electricity consumption, but not to an extensive degree. Candanedo and Athienitis (2010) investigated their anticipatory control strategies on a solar-optimized net-zero energy house. They reported that adjusting the position of the window blinds improves comfort, but also reduces the amount of energy that can be stored in the slab.

For active systems, the controls for both TES and space conditioning functions have to be considered simultaneously. They are generally more schedule-dependent than that of instantaneous conventional space conditioning systems (ASHRAE 2007b) due to the long "response time" (i.e. large thermal inertia) of the BITES systems. If good thermal coupling

between the BITES systems and their thermal zones exists, the "self-regulation" of the systems is able to ease the accuracy requirement of controls (ASHRAE 2007b).

General guidelines are necessary for the design of BITES systems and the selection of the control strategies at the preliminary design stages for new buildings, and for improving the control strategies for existing buildings. Since the design and operation of the systems are interrelated, the design and corresponding operation strategies of the systems should be considered simultaneously at the building design stage. Accurate yet simple thermal models are needed in fine-tuning the control strategies for both new and existing buildings. Without general guidelines, choosing control strategies by running random and excessive thermal simulations is unwise. Some design and operation guidelines are provided in ASHRAE (2007b), as well as in the aforementioned literature. The exact execution of sophisticated control strategies as intended may not always be realized (Doiron et al. 2011). Furthermore, ASHRAE (2007b) points out that the economic benefits of optimal but complicated strategies are not significant in comparison to basic and robust strategies that rely on simpler control routines.

4.4. Thermal energy acquirement

For BITES systems heating, the most common renewable energy is from solar radiation. The energy acquiring measures can be passive solar design, or connecting the BITES systems to solar thermal collectors. Using heat from photovoltaic/thermal cogeneration systems (Bazilian et al. 2001) is attracting lots of research interest (Chen et al. 2010a, Fraisse et al. 2007) because the benefit is two-fold: (1) it increases the electricity generation efficiency by lowing the PV temperature, and (2) it uses the otherwise wasted heat for space heating purposes. For BITES systems cooling, night time cooling/pre-cooling using outdoor

cool air by natural or mechanical ventilation with/without chillers and cooling towers is common. Coupling the systems with geothermal sources is being adopted (Xu et al. 2010).

By using low-grade renewable energy or recovered waste energy as thermal energy sources, the purchased energy consumption will be much less. Sometimes in order to draw the most advantage from renewable or recovered waste energy, BITES charging/discharging operations may need to be extended. For example, the operation of building pre-cooling using favourable outdoor air may last for the whole night. The overall heat lost/gain of the building is likely to be more than that from using set-up/set-back strategies, but the overall purchased energy will still be reduced and the trade-off of energy cost is viable, especially if a strong incentive of time-of-use utility rate structure exists. When available renewable thermal energy is not adequate for direct usage (e.g. air temperature is not low enough for efficient building cooling), using a heat pump (e.g. ground or air sources) is an energy-efficient way to upgrade the thermal energy (Braun et al. 2001, Candanedo and Athienitis 2010), especially when taking advantage of inexpensive off-peak energy pricing.

4.5. Over-storage

The possibility of over-storage of thermal energy (i.e. overheating or overcooling of BITES systems) should be carefully considered. Zhu et al. (2009a) reported that in a desert area, the accumulated heat in an internally insulated concrete wall (insulation is placed between two concrete layers) resulted in a continuous heat flow to the room at night time and hence caused a slight higher cooling load than lightweight construction. In the applications of PCM, over-storage may not be easily noticed because the heat storage/release during the phase transition will cause negligible temperature change. In conclusion, calculation, control, and

detection of the amount of thermal energy stored or to be stored need careful consideration, especially in active-charge BITES systems.

4.6. Structural considerations

When integrating the BITES functions with the building structural components, modifications to the original structural design may occur, such as changing the shapes (e.g. thickness, cross section geometry, and surface texture) and material properties (mainly due to the change of thermal properties) of the structural components (Athienitis et al. 1997, Braham 2000, Chen et al. 2010b). Priority given to structural performance should always be kept in mind. Excessive increase of height and weight, or weakening of the structural strength should be avoided. In some designs of hydronic floor heating/cooling systems, the massive slab, in which the water pipes are embedded, rests on the structural floor (wooden or concrete) (Candanedo and Athienitis 2010, Pfafferott et al. 2007, Zhai et al. 2009). These add-on kinds of massive slabs dramatically increase the structural load of the floor. Instead, the designs could use the mass of the structural floor by directly embedding the water pipes into the structural concrete slab.

There are several possibilities for integrating BITES functions into the structural components without compromising their structural performance. In timber-frame buildings, integration can be accomplished using concrete-timber composite structure (Persaud and Symons 2006). In concrete masonry block walls, the core voids are suitable as air channels for the heat transfer air and as the heat exchanging surface between the air and the blocks (Howard 1999, Howard 1986). Ventilated systems can also use the voids (i.e. air channels) of the pre-cast and pre-stressed slab as the ductwork and heat exchanging surface (see paper

Part I (Section 2.1)). The openings at the bottom surface near the ends of the slabs only slightly weaken the flexural strength of the slab.

BITES functions can also be integrated into non-structural components, such as non-load-bearing partition walls. Without structural requirements, these components' shapes, and physical and thermal properties can be altered with fewer constraints. See paper Part I (Section 2.1) for information on applications.

4.7. Selecting BITES systems

BITES design is flexible. BITES systems can use different components of the building fabric. The charge and discharge mechanisms can be combinations of active and passive measures, or even behave in a pulse manner (i.e. switch between active and passive). The systems can be open- or closed-loop, or even a combination of the two.

The selection of BITES system is sensitive to many factors, such as climate conditions, building types, the quality and quantity of locally available sources (e.g. favourable ambient air, geothermal energy), fee structure for energy from utilities, and occupant behaviour. For example, BITES systems in composite climates should be able to store heat and coolness. In desert areas, effective night time system cooling by ventilation is important. Ventilated systems can directly utilize night time outdoor cool air, or the hot air from solar air thermal collectors. On the other hand, hydronic systems can be connected with loops from boreholes, lakes, hydronic solar thermal collectors, or heat pumps with a compact water-to-water heat exchanger, which has a much smaller area and a higher efficiency than a water-to-air heat exchanger. Roof pond cooling systems are not suitable if water is rare or the local dominant weather is humid. Massive floors are needed in direct gain rooms. Some R&D activities point out that certain occupant behaviour may interfere with the thermal functions

of TES systems (Howard and Fraker 1990), such as putting large carpeting on top of hydronic floors and lowering the sunshade on a sunny winter day.

A properly designed and operated BITES system can reduce the building's space conditioning energy consumption and peak power demand. After building construction is complete, the BITES system performance has to be monitored in order to adjust the system to function at its maximum capacity and resulting best benefit (Turner and Tovey 2006, Winwood et al. 1997d).

5. Conclusion

This section (paper) evaluated and compared the thermal and energy performance of different BITES systems in current research and development activities, highlighting their advantages, limitations and challenges. Design and operation considerations for BITES systems such as energy sources, thermal comfort, and operation and control strategies, are also presented in this section (paper). These evaluations, comparisons, design and operation considerations can help with the selection and design of BITES systems in a building's preliminary design stage.

Passive systems are easy to implement and are reliable; on the other hand, active systems are more effective and have better control. Active discharge can improve the thermal coupling between the BITES systems and the room air. Active approaches are efficient in utilizing the building fabric for TES and direct space conditioning. The space conditioning capacity is significantly increased, especially in "open-loop" approaches. The space conditioning (i.e. heating/cooling) capacities of hydronic BITES systems from different studies are tabulated. The data can be used as benchmark values for other BITES systems. The comparisons on operation cost between these two approaches are also provided.

Available studies in the literature on the operating and control strategies of BITES systems are provided. The literature review shows that the design and corresponding operation strategies of the BITES systems should be considered simultaneously at the design stage. Accurate yet simple thermal models are needed for fine-tuning the control strategies for both new and existing buildings.

One of the most important considerations in design and operations is to provide sufficient thermal coupling between BITES systems and their thermal zones. It is critical to fulfilling the thermal functions of BITES systems, and affects the space conditioning operation energy consumption and the initial costs of mechanical equipment and service systems. Ideas and solutions for improvement are suggested.

BITES systems serve mainly three functions: thermal energy storage, space conditioning, and building skeleton. In the design and operation processes, all these functions need to be considered in an integrated manner. When primary space conditioning is provided through BITES systems, operation becomes critically important. In active systems, operations have to consider both optimal thermal energy storage and space conditioning output in order to achieve both high energy efficiency and thermal comfort.

Based on the state-of-the-art review and analysis, the following topics are recommended for future studies:

- Approaches for improving the thermal coupling, such as active discharges;
- Alternating the structure (form, location and material) to facilitate the TES and space conditioning functions of BITES systems (i.e. further integration of the structural and BITES functions);

- Approaches to effectively increase the thermal inertia of light-weight buildings, such as using concrete-timber composite structure (Persaud and Symons 2006);
- The cost-effectiveness and viability of pre-heating BITES systems;
- The integrated design and control approach for BITES systems.

Chapter 3 Numerical Modeling

This chapter comprises 3 journal papers, one is published, and the other two are in press. Each of the paper makes up one section of this chapter.

Section 3.1:

Chen, Y., A. K. Athienitis and K. Galal. 2012. Thermal Performance and Charge Control Strategy of a Ventilated Concrete Slab (VCS) with Active Cooling Using Outdoor Air. *ASHRAE Transactions,* 118(2): 556-568.

Section 3.2:

Chen, Y., A. Athienitis and K. Galal. 2013a. Frequency domain and finite difference modeling of ventilated concrete slabs and comparison with field measurements: Part 1, modeling methodology. *International Journal of Heat and Mass Transfer,* in press.

Section 3.3:

Chen, Y., A. Athienitis and K. Galal. 2013b. Frequency domain and finite difference modeling of ventilated concrete slabs and comparison with field measurements: Part 2, application. *International Journal of Heat and Mass Transfer,* in press.

Section 3.1 Thermal performance and charge control methodology of a ventilated concrete slab (VCS) using outdoor air for active cooling

Based a published paper:

Chen, Y., A. K. Athienitis and K. Galal. 2012. Thermal Performance and Charge Control Strategy of a Ventilated Concrete Slab (VCS) with Active Cooling Using Outdoor Air. ASHRAE Transactions, 118(2): 556-568.

Section abstract

This section (paper) presents full-scale measurements and simulation results of the thermal performance of a ventilated concrete slab (VCS) with active cooling using cool outdoor air. A methodology for the charge control and sizing of building-integrated thermal energy storage (BITES) systems that can be used for active slab cooling was developed. This VCS, which has a floor area of 30 m^2 (323 ft^2) and a storage volume of about 5 m^3 (177 ft^3), is located in a near net-zero energy solar house. It serves as an active-charge/passive-discharge thermal mass, as well as the basement slab – it is a BITES system. An on-site test under summer night time outdoor condition was performed and the dynamic temperature distribution of the slab was monitored. The measured data is used for the verification of a thermal model under cooling operation. The verified thermal model is then used to predict the thermal performance of the slab under different operating conditions. The simulation results show that under typical operating conditions – an initial average slab temperature of 21.8°C (71.2°F), and cool outdoor air at 16°C (60.8°F) with a flow rate of 200 L/s (424 CFM), which corresponds to 1.35 m/s (265 FPM) air velocity in the typical section -

roughly 6.3 kWh (21.5 MBTU) of heat (1.26 kWh per m^3 of concrete (4.3 MBTU/m^3)) can be extracted by the flowing air from the VCS in 6 hours. A 3-parameter (temperature and velocity of inlet air, and cooling duration) correlation is developed to approximate the thermal energy storage under different operating conditions. Similar correlation can be developed and used for design and control of such systems. The methodology for design and charge control presented in this section (paper) is applicable to other types of BITES systems in different types of buildings.

1. Introduction

Concrete slabs are common in the basements of Canadian houses. Utilization of basement slabs as active BITES systems with proper control can improve the thermal performance of the house; however, the thermal behavior of the slabs in heating and/or cooling applications have to be well understood and quantified in order to realize successful designs and operations. Furthermore, easy application of control is critical in promoting building-integrated thermal energy storage, especially for houses in terms of effort and cost. To serve these purposes, a prototype VCS was constructed in a demonstration house for in-depth study. The house was built under the Canadian EQuilibrium Housing demonstration competition, which started in 2006. The house is located near Eastman, Quebec, Canada. Detailed information on the house can be found in work by Chen et al. (2010a). Implementing TES is one of the techniques employed in this house to reduce annual space heating energy consumption and peak power demand.

The VCS is located in the basement of the house (Fig. 3.1). It serves as a TES system, as well as the basement slab – it is a building-integrated thermal energy storage (BITES) system. The VCS is a ribbed concrete slab with voids that act as air channels (Fig. A2.1 in Appendix) –

concrete is poured on top of standard steel decks. It has a floor area of 30 m^2 (323 ft^2) and a storage volume of about 5 m^3 (177 ft^3). Chen et al. (2010b) presented the design, construction, and monitoring of this VCS. The temperature distribution of the slab is being monitored since 2009. The locations of the thermocouples are shown in Fig. A2.1. The ductwork configuration in the house enables both active slab heating and cooling. When used in heating, the VCS stores heat recovered from a roof-mounted building-integrated photovoltaic/thermal (BIPV/T) system (Candanedo et al. 2010). At the BIPV/T system, outdoor air is drawn with a variable speed fan underneath the warm/hot PV panels which are amorphous laminates integrated into the metal roof. The air extracts the heat from the PV panels and then passes through the VCS as shown in Fig. 3.1 (see Chen et al. (2010a) for more details about the BIPV/T and VCS active heating operation). In the active slab cooling operation, which normally happens at night, cool outdoor air passes through the same path as the warm BIPV/T air. Better arrangement for shorter ductwork for the cooling air intake is possible in future similar applications. The stored heat or coolness is released passively to the basement space through the top surface of the VCS by radiation and natural convection. The VCS slab considered in this section (paper) is an active-charge/passive-discharge BITES system, meaning it is charged by the air passing through it, but the release of thermal energy is passive – through radiation and natural convection from its top surface.

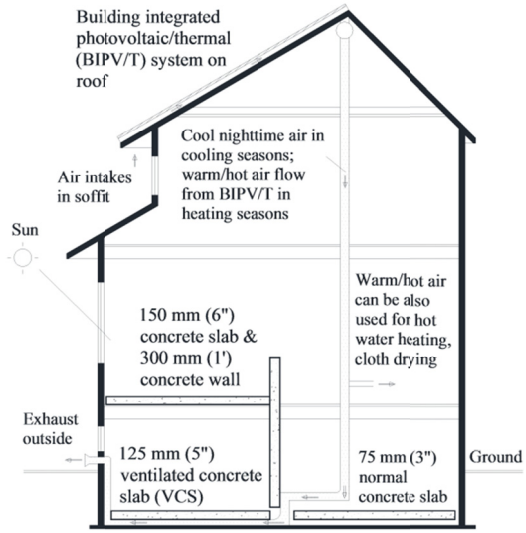

Fig. 3.1: Schematic of BIPV/T system and thermal mass (direct gain system in main living area and VCS in basement).

The site measurements and simulation for the thermal performance of the slab in the active slab heating operation mode were reported by Chen et al. (2010b). In this section (paper), the thermal performance of the active slab cooling is studied and the methodology for its sizing and charge control is presented.

2. Numerical model and verification

Concrete is used as the storage medium because it also has good structural properties for basement floors. The thermo-physical properties of concrete are assumed as follows: specific heat is 900 J/kg/K (0.215 BTU/lb/°F); density is 2300 kg/m^3 (144 lb/ft^3); conductivity is 1.9 W/m/K (1.1 BTU/hr/ft/°F). Small variations (of the order of ±10%) of the physical properties do not affect the slab's thermal behavior to a significant extent (Bilgen and Richard 2002). This statement is also verified by the preliminary design simulations for the VCS (Chen et al. 2010b).

A simplified three-dimensional, explicit finite difference thermal model was developed for the VCS. The 9-layer discretization scheme of the typical section of the VCS (not the manifold portions) is shown in Fig. 3.2. This discretization scheme is based on the typical pattern of temperature distribution on the cross section simulated with regular structured discretization (Chen et al. 2010b). Dense discretization at the top and bottom layers (i.e. Biot number smaller than 0.1) enhances the accuracy of the heat transfer modeling at the boundaries. The thickness of the control volumes is 2.4 mm (0.094 in.) at the top layer "Y-1". The corresponding Biot number (Kreith and Bohn 2001) is 0.015, assuming the surface combined convective and radiative heat transfer coefficient h_{cr} is 10 W/m^2/K (1.76 BTU/hr/ft^2/°F). In natural convection conditions, the value of h_{cr} is less than 10 W/m^2/K (1.76 BTU/hr/ft^2/°F) when the floor is less than 10°C (18°F) warmer than the room air (ASHRAE 2008, 2009d, Karadag and Akgobek 2008). It is even less in cool floor situations (i.e. when the floor cooler than the air). For the bottom layer "Y-9" (Fig. 3.2), the thickness is 2.7 mm (0.106 in.). It is 1/16 of the bottom width (38 mm (1.5 in.)) of the flute (the strut of the steel deck). Assuming h_{cr} equal to 15 W/m^2/K (2.64 BTU/hr/ft^2/°F) for the air channel, the calculated Biot number is about 0.02. From exterior layer to interior layer, the thickness of the layer increases with a scale factor of two. The calculation of effective conductance in Y direction between nodes with irregular shapes uses area-weighted equivalent distance.

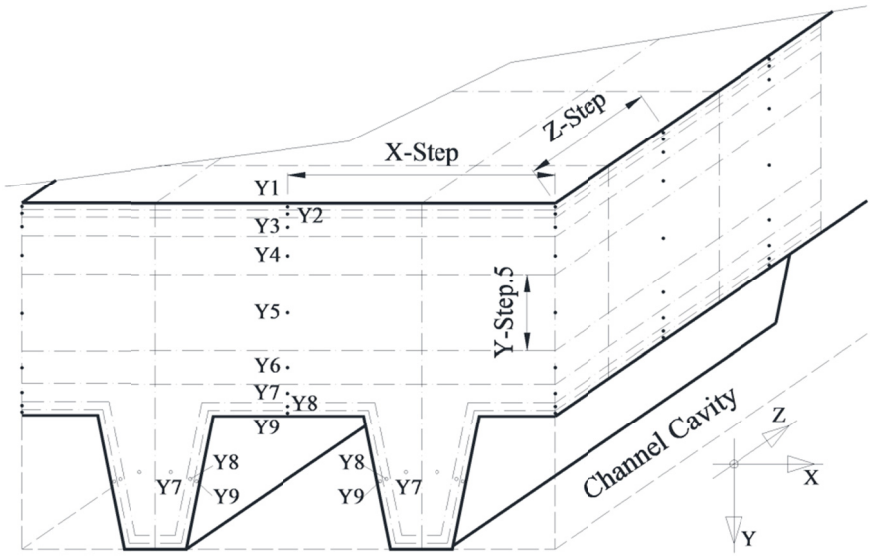

Fig. 3.2: Schematic of the 9-layer 3D discretization of the VCS.

The upwind differencing scheme method (Patankar 1980) is used for the calculation of the temperature of flowing air inside the channel, as shown in Eq. (3.1).

$$T_{air}^{i} = \frac{\dot{m}c_{p.air} \cdot T_{air}^{i-1} + \sum_j (T_{surface}^{j} \cdot U_c^j)}{\dot{m}c_{p.air} + \sum_j U_c^j} \tag{3.1}$$

where $\dot{m}c_{p.air}$ is the mass flow rate of the air. T_{air}^{i-1} is the temperature of the air in the previous control volume. U_c^j is the convective conductance between current air node and the surface in contact in direction j (i.e. either the bottom nodes of the slab or the ground). $T_{surface}^{j}$ is the surface temperature in direction j .

Eq. (3.2) developed by Chen et al. (2010b) is used as the correlation of the convective heat transfer coefficient (CHTC) inside the air channel for air velocities ranging from 0.67 to 1.68 m/s (132 and 330 FPM).

$$h_{c.vcs} = 3.94 \cdot V_{air} + 5.45 \ \ [\mathrm{W/m^2/K}] \qquad (V_{air} \text{is in m/s}) \tag{3.2}$$

In order to determine the adequate grid size of "Z-Step" in the Z direction (Fig. 3.2) and time step, three preliminary simulations were performed in which these two discretization parameters were varied while all other parameters and boundary conditions are kept the same. Table 3.1 compares the different outputs from these three simulations. It can be seen that, 300 mm (12 in.) for "Z-Step" and time step of 10 s is adequate to obtain a sufficiently converged accurate solution. 150 mm (6 in.) "X-Step" in X direction (i.e. the center-to-center distance of the channels) is used for all three simulations.

Table 3.1 Comparison of Outputs under Different Configurations

Model configuration		Thermal energy, kWh (MBTU)	
Z-Step, mm (inches)	Time step (s)	Recovered from air	Stored in VCS
150 (6)	6	-8.378 (-28.59)	-5.540 (-18.90)
300 (12)	6	-8.273 (-28.23)	-5.589 (-19.07)
300 (12)	10	-8.275 (-28.24)	-5.591 (-19.08)

Note: negative values in energy mean heat lost.

For the radiative heat transfer inside the air channels, it is assumed that the concrete nodes only exchange radiative heat with the insulation surrounding the same air control volume. This assumption is based on two factors. First, the length of the air control volume stream-wise is 300 mm (12 in.) in this discretization scheme (same length as the "Z-step"). This is four times the height of the air control volume (i.e. the height of the air channel). Second, the temperature difference between two adjacent concrete nodes or two adjacent insulation nodes is negligibly small.

The verification of the thermal model for active slab heating was previously performed by Chen et al. (2010b). The measured temperatures from site tests was compared with those from simulations that used the corresponding measured boundary conditions (i.e. the flow rate, the temperatures of the room air, the ground soil, and the inlet air) as inputs. This comparison indicated a good agreement between the measured and simulation results.

In this section (paper), site-measured thermal behavior of the slab in cooling mode is used to verify the thermal model. A site test of active slab cooling using outdoor cool air was carried out on July 15th and 16th, 2009. Cool outdoor air was drawn at night into the VCS at 200 L/s (424 CFM) for 7 hours - from 11:00pm of the 15th to 6:00 am of the 16th. The period between midnight and 6:00am is discussed below.

Fig. 3.3and Fig. 3.4 show the measured temperature profiles of the test. During the data sampling period, the forced-air ventilation system was continuously under fan mode (i.e. there was continuous air circulation between different floors without mechanical cooling). The measured variables (Fig. 3.3), such as the temperature and the flow rate of inlet air, soil temperatures underneath the slab insulation, and the room air temperature were used as the boundary conditions for the simulation. The measured soil temperatures based on nine-point monitoring setup (Fig. A2.1) were extrapolated and interpolated to obtain the soil temperatures under each of the bottom grid of the slab model (Chen et al. 2010b). These values are kept constant in the simulation. This is a reasonable approach as shown by the measured data in Fig. 3.3. Eq. (3.3) (Nu is the Nusselt number) (ASHRAE 2009d) is used in the model to calculate the natural convective heat transfer between the cool floor and the warmer space above.

$$Nu = 0.27 \cdot Ra^{1/4} \tag{3.3}$$

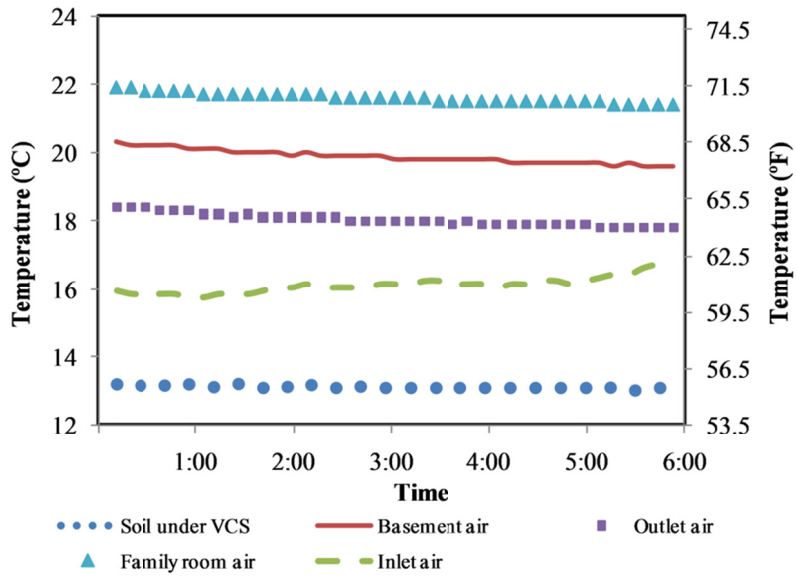

Fig. 3.3: Measured temperature profiles of site test on July 16th (family room is on top of basement)

The room temperature in the simulation was set 0.9°C (1.6°F) constantly higher than that of the varying slab top surface temperature (denoted as $\Delta T_{clg.rm.slab}$). It is based on the measured data shown in Fig. 3.4 – from 0.8°C (1.4°F) at the beginning of the on-site test to 1.0°C (1.8°F) at the end. The 0.9°C (1.6°F) average temperature difference between the surface and air was observed in other long-term data recorded as well. Measured data also indicate that the average slab surface temperature is typically about 0.5°C (0.9°F) lower than the room air temperature outside active slab cooling periods (denoted as $\Delta T_{off.rm.slab}$). These two just denoted variables are important and used for analysis in later subsections.

Table 3.2 Measured and Simulated Temperature Values for July 16th,°C (°F)

Data Source	Whole Slab Average Temperature	Slab Top Surface Average Temperature	Initial Room

	Beginning	End	Change	Beginning	End	Change	Temp.
Measurements	19.3	18.4	-0.9	19.5	18.6	-0.9	20.3
	(66.7)	(65.1)	(-1.6)	(67.1)	(65.5)	(-1.6)	(68.5)
Simulation	19.3	18.2	-1.1	19.5	18.5	-1.0	20.4
	(66.7)	(64.7)	(-2.0)	(67.1)	(65.3)	(-1.8)	(68.7)

Note: the accuracy of the measurement is ± 0.5°C (0.9°F).

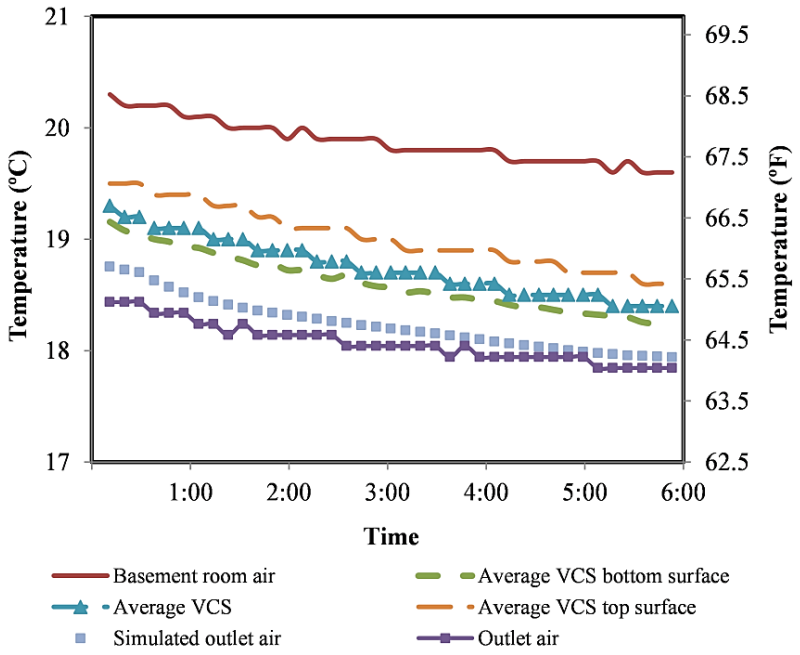

Fig. 3.4: Measured temperature profiles and simulated outlet air temperature profile (July 16th)

Table 3.2 tabulates the slab temperatures from the simulation and the measurement. The differences between the end values are small. Fig. 3.4 compares the outlet air temperatures between measurement and simulation. The maximum difference is about 0.3°C (0.5°F). The simulated profile follows the measurement closely. The data from Table 3.2 and Fig. 3.4 indicate good agreement between the measured and the simulated results. Factors such as the accuracy of the thermocouples (± 0.5°C (0.9°F)), the difference of boundary conditions between reality and simulation setup, the uncertainties in the exact slab concrete thickness

and evenness, the measured flow rate, the CHTC at the inlet and the outlet, and other minor factors, contribute to the discrepancy between the simulated and measured values (see Chen et al. (2010b).

Table 3.3 Thermal Energy Shares Based on Simulations [16°C (60.8°F) air at 200 L/s (424 CFM) for 6 hrs] kWh (MBTU)

Date	Average Slab Temperature	Recovered from Air	Stored in Slab	From Slab to Upper Space	From Slab to Soil	From Slab to Air	From Air to Soil
July 16th	19.3°C (66.7°F)	-3.24 (-11.1)	-2.94 (-10.0)	-0.97 (-3.3)	0.46 (1.6)	3.45 (11.8)	0.21 (0.7)
Aug. 10th	21.8°C (71.2°F)	-6.15 (-21.0)	-5.81 (-19.8)	-1.00 (-3.4)	0.50 (1.7)	6.32 (21.6)	0.17 (0.6)

3. VCS thermal performance

The thermal performance based on measurements will be presented first, followed by simulated performance. At the end of the cooling period, the temperature readings at location B2 (center of the VCS, Fig. A2.1-a) in the Y direction were 19.0, 18.4 and 18.3°C (66.2, 65.1, and 65.0°F) for TC-1, TC-2, and TC-5 (Fig. A2.1-b), respectively. Therefore, the difference between the bottom and top surfaces was 0.7°C (1.3°F). For locations at A2 and C2 (Fig. A2.1-a), the differences were 0.5 and 0.6°C (0.9 and 1.1°F) respectively. Fig. 3.5 shows the temperature profiles of the middle layer at those four locations during the cooling period. The temperature differentials increased from about 0.5 to 1.2°C (0.9 to 2.2°F) longitudinally (i.e. in Z direction, the temperature difference between B1 and B3) and from about 0.2 to 0.5°C (0.4 to 0.9°F) transversally (i.e. in X direction, the temperature difference

between A2 and C2). Note that the temperatures of these locations at the beginning of the plotted period were not close to each other. That is because the slab cooling began one hour prior to the period plotted. From Fig. 3.4, it can be seen that the difference between the average temperatures of the slab top and bottom surfaces was about 0.4°C (0.7°F) throughout the cooling period. These measurements indicate that the temperature distribution in the VCS is quite uniform – the maximum temperature difference was about 1.2°C (2.2°F) longitudinally over 7.6 m (25.0 ft) length, except the areas near the inlet and outlet manifolds.

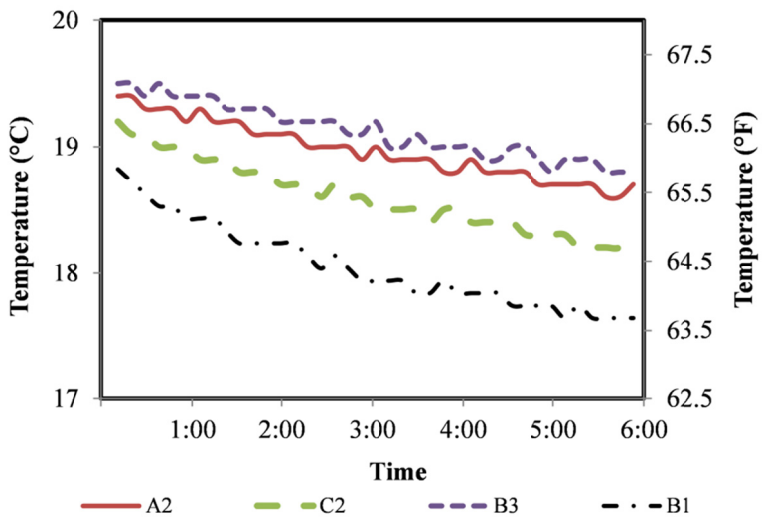

Fig. 3.5: Measured temperature profiles at different locations in the middle layer ("TC-2" in Fig. A2.1(b)) (July 16th)

At the end of the cooling period, the measured temperatures of the slab near the outlet were 18.8°C (65.8°F) at B3 (Fig. 3.5), and 18.7°C (65.7°F) at C3; while the outlet air temperature was 17.8°C (64.0°F) (Fig. 3.4). This temperature difference of about 1.0°C (1.8°F) indicates effective heat exchange between the warm slab and the cool air. Note that locations B3 and C3 are about 1.5 m (4.9 ft) and 1.2 m (3.9 ft) upstream from the outlet, respectively.

Numerical analysis of night time active slab cooling was carried out using the thermal model discussed earlier. Table 3.3 lists some key results from two sets of simulations: July 16th and August 10th of 2009. Their operating conditions are the same – 16°C (60.8°F) air at a flow rate of 200 L/s (424 CFM) for 6 hours, but the initial average slab and soil temperatures were different - 19.3 and 13.2°C (66.7 and 55.8°F) for July 16th, and 21.8 and 15.0°C (71.2 and 59.0°F) for August 10th, respectively. The simulated cooling power of air (i.e. heat flux removed from the slab) for July 16th was about 600 W (2.05 MBTU/hr or 0.17 Ton), while it reached a higher value of 1050 W (3.58 MBTU/hr or 0.30 Ton) for August 10th – a typical summer night in Montreal. In the simulation for August 10th, 6.15 kWh (21.0 MBTU) of heat was extracted by the cool air after 6 hours of slab cooling - 6.32 kWh (21.6 MBTU) of heat extracted from the slab and 0.17 kWh (0.6 MBTU) lost to the soil (the soil was cooler than the air). The amount of heat removed from the slab was 5.81 kWh (19.8 MBTU), which included 1.00 kWh (3.4 MBTU) of heat gained from the living space through the slab top surface, 0.50 kWh (1.7 MBTU) of heat lost to the soil, and 6.32 kWh (21.6 MBTU) of heat extracted by the air passed through its hollow channels.

Fig. 3.6 shows the contour plots of the slab top surface temperature distribution at the end of the simulations for August 10th. Small temperature gradients are also indicated here, matching those from field measurements. The fact that the slab is cooler at the inlet manifold than it is to the east of the manifold indicates that a considerable amount of heat exchange took place at the inlet manifold area. This is because the CHTC at the manifold area is about an order of magnitude higher than that in the air channel due to the former's higher turbulent flows. The cooler temperatures of the inlet area reveal the importance of proper distribution of air flow. Improper air path design will result in an uneven and inefficient distribution of stored thermal energy.

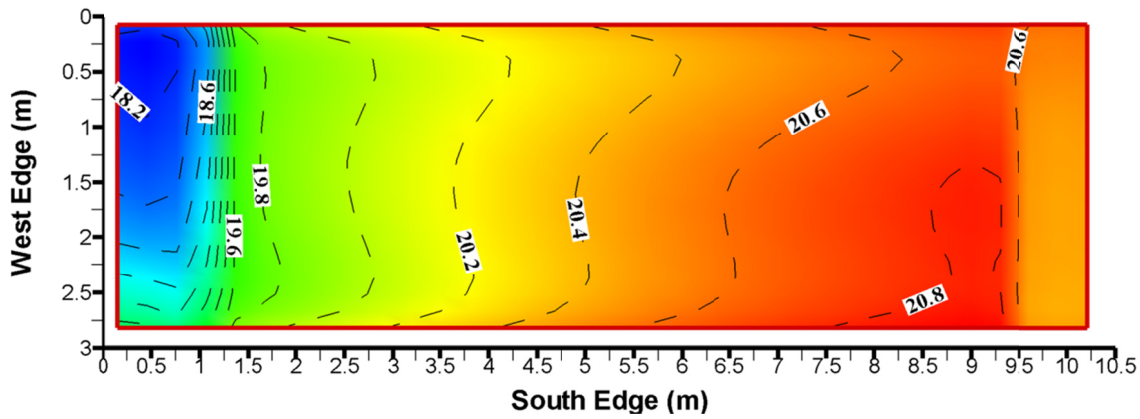

Fig. 3.6: Simulated VCS top surface temperature distributions at the end of the cooling period for August 10th

Fig. 3.7 shows the amount of coolness that will be stored in the slab, E_{store}, for August 10th initial conditions with different operating conditions. It is equivalent to the heat extracted from the slab by the channel air minus those transfer from the room air to the slab. Inlet air temperatures from 16 to 20°C (60.8 to 68°F) in 1.0°C (1.8°F) increments, cooling durations from 2 to 10 hours in 2-hour increments, and channel air velocities of 0.67, 1.01, 1.35 and 1.68 m/s (132, 199, 265, and 331 FPM) are combined and used as the operating conditions. There are totally 180 different operating conditions. The inlet air temperature is set constant in each simulation. Note that, an initial slab temperature of 21.8°C (71.2°F) (denoted as slab reference temperature $T_{ref.slab}$), constant soil temperature of 15.0°C (59.0°F), and constant $\Delta T_{clg.rm.slab}$ of 0.9°C (1.6°F) are used in all these simulations. The Reynolds numbers inside the channel for 0.67 and 1.68 m/s (132 and 330 FPM) air velocities are about 3685 and 9240, respectively.

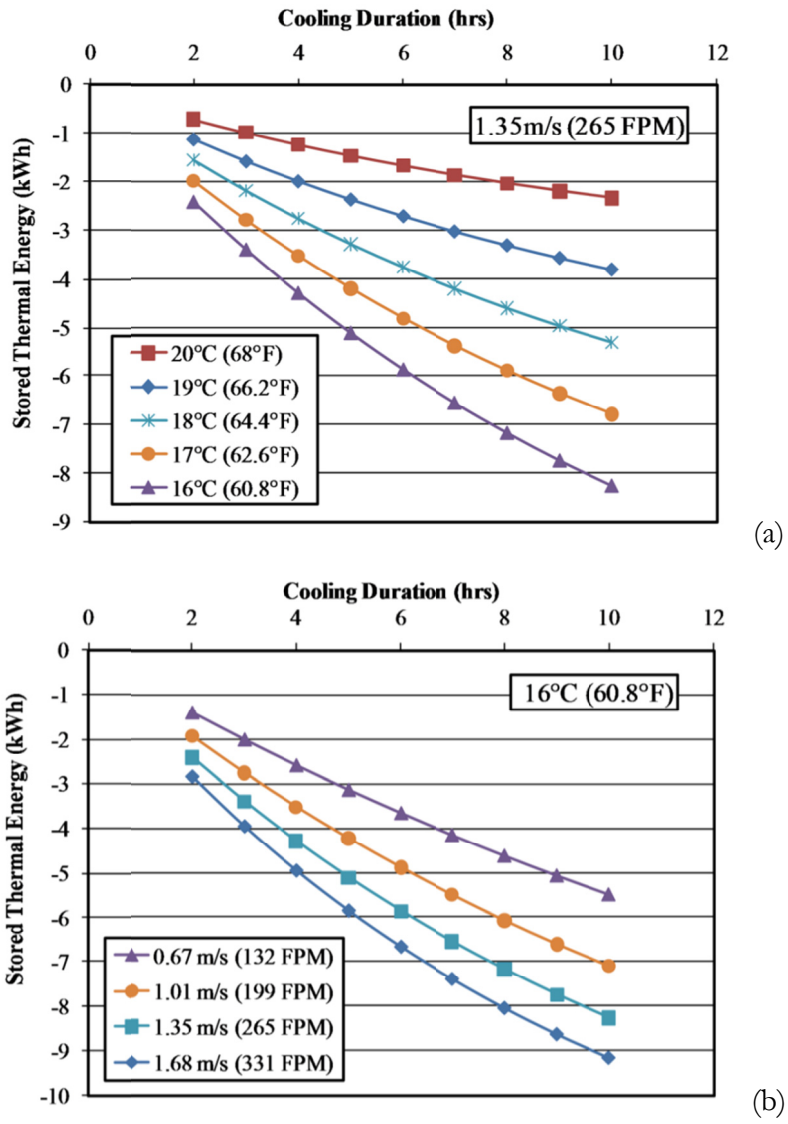

Fig. 3.7: Predicted thermal energy transferred from air to slab for August 10th initial conditions. (Initial slab and soil temperatures were 21.8 and 15.0°C (71.2 and 59.0°F), respectively. (a) 1.35 m/s (265 FPM) constant air velocity with different inlet air temperatures; (b) 16°C (60.8°F) constant inlet air temperature with different air velocities)

The measured pressure drop across the VCS is about 0.07 kPa (0.281 in. of water) for a flow rate of 200 L/s (424 CFM). The fan power consumption for this VCS is therefore about 28 W (0.038 hp), assuming a fan efficiency of 50%. The corresponding air velocity for a flow rate of 200 L/s (424 CFM) is of 1.35 m/s (265 FPM).

An approximately linear relationship is observed between the inlet air temperature and E_{store}, while exponential relationship exists between E_{store} and air velocity (i.e. flow rate) or the cooling duration. Eq. (3.4) is the fitted correlation with a maximum discrepancy of 8.6% of the corresponding simulation result[3]. The standard deviation of the discrepancies is 1.9%. This correlation could be further developed for better regression. Correlations similar to Eq. (3.4) for other types of TES systems with active charge can be developed using their corresponding thermal models.

$$E_{store} = (3.4 \cdot T_{inlet.air} - 74) \cdot \left(1 - \frac{1}{exp(0.85 \cdot V_{air})}\right) \cdot \left(1 - \frac{1}{exp(0.1 \cdot t)}\right) + 0.065 \qquad (3.4)$$

where E_{store} is negative in kWh, V_{air} is the air velocity inside the VCS channel in meter per second, $T_{inlet.air}$ is the constant inlet air temperature in Celcius, and t is time in hours.

4. Charge control and sizing methodology

In this subsection, a simple methodology for the charge control and sizing of the VCS TES system will be presented. The methodology makes use of the thermal comfort requirement and the observed thermal behavior of the VCS from long-term on-site measured data.

When a floor slab is used as cool storage, the top surface temperature of the slab will affect the thermal comfort of occupants. For example, for people with normal indoor footwear in office space, the floor temperature should not be lower than 19°C (66.2°F) (ASHRAE

3 Percentage discrepancy = (correlation value – simulation value) / simulation value

2004a). In residential and commercial/institutional buildings, the lower limit of the floor temperature, $T_{min.slab}$, will also be selected according to the occupants' preference. The standard-complied or occupant-preferred $T_{min.slab}$ and the initial slab temperature just before the active slab cooling, T_{slab}^{0} , define the maximum allowable amount of thermal energy, E_{allow}, that can be stored in the slab at current slab cooling operation (Eq. (3.5)). C_{slab} is the thermal capacity of the slab. T_{slab}^{0} is related to T_{rm}^{0} (initial room air temperature). When active slab cooling is desired, the amount of the coolness to be stored should equal to E_{allow} to achieve maximum storage.

$$E_{allow} = (T_{slab}^{0} - T_{min.slab}) \cdot C_{slab} \tag{3.5}$$

The observation of the thermal behavior of the VCS indicates that the slab temperature distribution is almost even. The changes of the $\Delta T_{clg.rm.slab}$ (temperature difference between room air and slab during active slab cooling operation) and the $\Delta T_{off.rm.slab}$ (temperature difference between room air and slab outside active slab cooling period) are slight, respectively. This observed thermal behavior of the VCS can be used to derive Eq. (3.6) from Eq. (3.5) for more convenient use. The average slab temperature can be estimated based on room air temperatures instead of being measured using sensors. Since slab temperature is usually $\Delta T_{clg.rm.slab}$ lower than the room air temperature during slab cooling operation, $T_{min.slab}$ can be replaced with $(T_{min.rm} - \Delta T_{clg.rm.slab})$. $T_{min.rm}$ is the minimum allowable room air temperature. It can be set by occupants but should comply with thermal comfort standards. Similarly, T_{slab}^{0} can be replaced with $(T_{rm}^{0} - \Delta T_{off.rm.slab})$. The values of $\Delta T_{clg.rm.slab}$ and $\Delta T_{off.rm.slab}$ can be obtained through on-site measurements.

$$E_{allow} = [(T_{rm}^{0} - \Delta T_{off.rm.slab}) - (T_{min.rm} - \Delta T_{clg.rm.slab})] \cdot C_{slab} \quad (3.6)$$

In buildings with energy-saving measures such as night time set-up (i.e. mechanical cooling is shut off, and the room air temperature is allowed to float up) and adaptive thermal comfort (ASHRAE 2009f), T_{rm}^{0} can be higher than $T_{sp.rm}$ (mechanical space cooling setpoint). It is also possible that T_{rm}^{0} is lower than $T_{sp.rm}$ in mild weather conditions.

In the preliminary design stage, optimal C_{slab} can be determined using Eq. (3.7), which is derived from Eq. (3.6) with T_{rm}^{0} replaced by $T_{sp.rm}$, and E_{allow} replaced by E_{max} (maximum storage of coolness). E_{max} is less than or equal to the maximum 24-hr cooling load of the building, which can be estimated through building thermal modeling under design weather conditions.

$$C_{slab} = \frac{E_{max}}{(T_{sp.rm} - \Delta T_{off.rm.slab}) - (T_{min.rm} - \Delta T_{clg.rm.slab})} \quad (3.7)$$

C_{slab} is the product of the thickness and the volumetric heat capacity (J/m^3/K (BTU/ft^3/°F)) of the slab. If larger slab thermal capacity C_{slab} is desired, it can be obtained by increasing the slab thickness. However, in commercial building applications, the slab thickness is normally determined by the structural need and the architectural plan (e.g. the storey height). Increasing the slab thickness for thermal storage purpose will occupy extra living space and increase the structural weight, which are important issues for high-rise buildings. Increasing the slab thickness will also increase the construction cost (materials and labour) and embodied energy cost. The final slab thickness may be smaller than desired due to architectural and structural requirements. Also note that general VCS design will, to a small degree, weaken the structural strength of the slab due to hollow voids and openings. Larger C_{slab} can also be achieved by using structural material with higher volumetric heat capacity;

though at the cost of adding weight. Adding phase-change materials (PCM) into the concrete composite is possible, but the chemical deterioration of PCM and the negative influence on the structural strength of the concrete composite remain challenges (Dincer 2002, Zhu et al. 2009b).

When E_{allow} is known from Eq. (3.5) or (3.6), by setting E_{store} equal to E_{allow}, Eq. (3.4) can be used to estimate the cooling duration t and V_{air} (i.e. flow rate) with corresponding $T_{inlet.air}$. Weather forecast data should be available so that the average outdoor air temperature can be used as $T_{inlet.air}$. Since fan power is proportional to the cube of flow rate, smaller V_{air} and longer t should be used if operating conditions allow. Based on the predicted $T_{inlet.air}$, a suitable V_{air} should be chosen along with a long t to meet the thermal energy storage requirement. Iterative calculations with Eq. (3.4) are needed since $T_{inlet.air}$, t, and V_{air} are interrelated. The maximum flow rate for fan capacity sizing can be determined using Eq. (3.4) with marginally favorable $T_{inlet.air}$ and by setting E_{store} equal to E_{max}. Sometimes, when E_{allow} is small, the cooling period may be shortened given minimum flow rate is reached. On the other hand, sometimes even with high flow rate and longest active cooling time possible (e.g. from 10 pm at night to 8 am of the next morning, depending on the outdoor air conditions), the largest possible E_{store} could still be less than E_{allow}. Note that E_{allow} will be constant if room air temperature is constant (i.e. mechanical space cooling is continuous; $T_{rm}^{0} = T_{sp.rm}$ in Eq. (3.6)). If the cooling duration is set constant, Eq. (3.4) can be further simplified, as can the control.

5. Discussion

The thermal behavior of the VCS under active slab cooling is affected by the varying room air temperature, initial slab temperature, inlet air temperature and flow rate, and cooling duration. Without a complex thermal model of the whole building and weather forecast data input, the prediction of the thermal behavior, potential thermal storage capacity, and optimal control strategy development are difficult. ASHRAE (2007b) reported that advanced optimal strategies often do not result in significant cost-savings benefits as compared to well-designed basic strategies that rely on simpler control routines. Furthermore, easy application of control is critical in promoting building-integrated thermal energy storage. In order to simplify the thermal modeling and hence develop a simple strategy for the control of the VCS in active slab cooling, the following two main approximations are adopted in the thermal model used in this section (paper):

- The varying room air temperature is replaced by the slab top surface temperature and the temperature difference between the room air and the slab top surface during the slab cooling operation, $\Delta T_{clg.rm.slab}$.
- The average temperature of inlet air is used throughout the cooling period.

Based on the simulation results from the simplified model, a correlation that has only three unknown variables, $T_{inlet.air}$, t, and V_{air} , is able to estimate E_{store} with acceptable accuracy. For the approximation of inlet air temperature being constant, results from simulations using constant and varying inlet air temperatures can be compared to quantify any potential discrepancy. However, since E_{store} is linear with constant inlet air temperature, it can be assumed that the discrepancy will not be significant. Using the average of the forecast air temperature as the constant value will lessen the error in the application of Eq. (3.4). The

observations of $\Delta T_{off.rm.slab}$, $\Delta T_{clg.rm.slab}$, and an even temperature distribution in the slab during and outside the slab cooling period simplify the estimation of the thermal energy allowed to be stored. On-site measured $T_{ref.slab}$, $\Delta T_{off.rm.slab}$, and $\Delta T_{clg.rm.slab}$ after the completion of construction will improve the accuracy of the correlation. The bottom boundary temperature of the slab considered in this section (paper) is almost constant during the cooling period; however in other cases, this temperature may vary during the period, such as the case in which a living space is underneath the slab. In this case, another constant ΔT between the room air underneath and the slab can be used. If there is a layer of insulation between them, the heat transfer can be ignored since the temperature difference between the slab and the room underneath will not be significant.

Eq. (3.4) is generated with a constant initial slab temperature, which is referred to as slab reference temperature, $T_{ref.slab}$. Meanwhile, the initial slab temperature T_{slab}^{0} will vary depending on the building space cooling strategies (e.g. setpoint set-up and chillers shutting down during unoccupied hours). The actual thermal energy that will be stored in the slab will differ from the E_{store} estimated by Eq. (3.4) if T_{slab}^{0} is different from $T_{ref.slab}$. This discrepancy can be reduced by using average initial slab temperatures as $T_{ref.slab}$, or creating a set of correlations for different values of $T_{ref.slab}$. Moreover, the discrepancy will be self-corrected by the slab due to the energy-storing nature of the slab (Shaw et al. 1994). For example, if T_{slab}^{0} is higher than $T_{ref.slab}$ before the active cooling operation, more coolness will be stored since the temperature difference between the actual slab temperature and the inlet air temperature is larger. If T_{slab}^{0} is lower than $T_{ref.slab}$, less coolness will be stored.

All the errors introduced by the assumptions and simplifications will be self-corrected by the slab to a certain extent because of the slab's high thermal capacity and energy-storing nature. The key step is to develop correlations (e.g. Eq. (3.4)) with suitable $T_{ref.slab}$, $\Delta T_{clg.rm.slab}$, and $\Delta T_{off.rm.slab}$. These three temperatures can be fine-tuned based on on-site measurements. Furthermore, since the slab temperature can be estimated using $\Delta T_{off.rm.slab}$ and room air temperature, detection of a problematic low room air temperature can be used to stop the cooling operation. If not enough coolness is stored by the end of the cooling period, the only drawback is that some potential energy saving will be lost. In any case, no thermal discomfort will occur. The greatest benefit of using this methodology for charge control is that frequent and complex thermal modeling can be avoided. The simplified thermal modeling will be needed only twice: firstly in the preliminary design stage to determine the optimal thermal capacity of the slab and the fan capacity, and secondly after building construction with fine-tuned parameters (e.g. $T_{ref.slab}$ and ΔT's).

In the design and operation of the active slab cooling, there are several other important considerations as follows:

- Active slab pre-cooling will not be needed if the weather condition of the following day does not create a cooling demand or allows free space cooling. Weather forecasts and finding the balance temperature are useful for control.
- If the outdoor air is not cool enough for efficient slab-cooling, chiller-assisted active slab cooling (i.e. cooling the inlet air using chillers) is viable, especially with low-cost, off-peak electrical energy (Braun 2003). Cost-related efficiency should also be considered.

- For buildings with multiple thermal zones, the slab temperatures can be different in different zones. The active slab cooling has to be controlled separately.
- Low floor surface temperature will cause low air temperatures at the ankle, and hence can cause thermal discomfort (ASHRAE 2004a). The lower limit of the surface temperature of the floor should comply with thermal comfort standard or occupant's choice.
- When the slabs are covered by indoor objects, such as furniture or carpets, the passive heat exchange (e.g. radiation and natural convection) between the room air and the slabs will be reduced. Active discharge can be used to make effective use of the VCS and other TES systems.
- Coolness from ground can be a thermal energy source for cooling the thermal storage system through certain kind of heat transfer fluid (e.g. air or water). Cost effectiveness has to be considered as well.

6. Conclusion

This section (paper) presented full-scale measurements and simulation results of the thermal performance of a building-integrated thermal energy storage (BITES) system – a ventilated concrete slab (VCS) – with active slab cooling using outdoor cool air in a near net-zero solar house. A methodology for sizing and control of VCS that can be used for active slab cooling was presented as well.

The long-term monitored data show that during the active slab cooling period, the room air temperature was about 0.9°C (1.6°F) ($\Delta T_{clg.rm.slab}$) higher than the average slab top surface temperature. This difference was about 0.5°C (0.9°F) ($\Delta T_{off.rm.slab}$) outside the cooling

period. These two important observations are used in the development of a simple thermal model, and in the estimation of the building's energy storage requirement. $\Delta T_{clg.rm.slab}$ and $\Delta T_{off.rm.slab}$ can be fine-tuned based on on-site measurements after construction completion. An on-site test under an early-summer night time outdoor condition was performed and the dynamic temperature distribution of the slab was monitored. The measured data are used to verify the thermal model for active slab cooling. The verification shows good agreement between the measured and simulated results. The simulation outputs are adequate for design and control purposes. The verified thermal model is then used to predict the thermal performance of the slab under different operating conditions (e.g. various air flow rates, temperatures of the inlet air and the soil underneath, and cooling durations) with a initial slab temperature of 21.8°C (71.2°F). The simulation for the typical operation summer condition (cool air at about 200 L/s (424 CFM) and 16°C (60.8°F) for 6 hours) shows that about 6.3 kWh (21.5 MBTU) (1.26 kWh/m^3 of concrete (4.3 MBTU/m^3)) of heat can be extracted by the cool air. Both on-site measurement and simulations show that the temperature distribution within a typical section of the slab is quite uniform.

Based on the simulation results, an approximately linear relationship is observed between the inlet air temperature and the coolness that will be stored in the slab (E_{store}), while exponential relationship exists between E_{store} and air velocity (i.e. flow rate) or the cooling duration. A correlation was developed to predict E_{store} under different operating conditions.

The lower limit of the slab surface and room air temperatures based on comfort requirements define the amount of heat that can be extracted from the slab. The use of the approximate temperature differences $\Delta T_{clg.rm.slab}$ and $\Delta T_{off.rm.slab}$ greatly simplifies the sizing of the BITES system and the estimation procedure of the daily energy storage

requirement to simple equations. The correlation facilitates the selection of required flow rate and duration period for the energy storage. The methodology of sizing and control presented in this section (paper) is applicable to other types of BITES systems in different kinds of buildings with appropriate modifications.

Section 3.2 Frequency domain and finite difference modeling of ventilated concrete slabs and comparison with field measurements: Part 1, modeling methodology

Based on a paper in press:

Chen, Y., A. Athienitis and K. Galal. 2013a. Frequency domain and finite difference modeling of ventilated concrete slabs and comparison with field measurements: Part 1, modeling methodology. *International Journal of Heat and Mass Transfer,* in press.

Section Abstract

This section (paper) is the first of two that focus on the thermal modeling of building-integrated thermal energy storage (BITES) systems using frequency response (FR) and lumped-parameter finite difference (LPFD) techniques. Structural/non-structural building fabric components, such as ventilated concrete slabs (VCS) can actively store and release thermal energy effectively by passing air through their embedded air channels. These building components can be described as ventilated BITES systems. To assist the thermal analysis and control of BITES systems, modeling techniques and guidelines for FR and LPFD models of VCS are presented in this two sections (papers). In this first part, modeling techniques for FR and LPFD approaches based on network theory are presented. A method for calculating the heat transfer between flowing air and ventilated components is developed for these two approaches. Discretization criteria for explicit LPFD models are discussed. For the FR approach, discrete Fourier series in complex frequency form are used to represent the boundary excitations. In the treatment of heat injection from the flowing air as internal

source in the VCS, network techniques such as Thévenin theorem, heat flow division, and Y-diakoptic transform are employed. The techniques presented in this section (paper) are applicable to other BITES with hydronic or electric charging/discharging systems. With the FR techniques, model-based control strategies based on transfer functions can be readily developed.

1. Introduction

Although active BITES systems potentially offer greater benefits over passive ones, realizing these benefits to an ideal extent requires cautious design and control (Hartman 1988, Winwood et al. 1997d). For design purposes, simple yet accurate models are needed to compare and evaluate the thermal response characteristics of different alternatives on relative bases. Detailed models require more detailed knowledge of geometry, which may not be known in the early design stages. Simplified models are also needed for whole building simulations over long simulation periods (e.g. monthly or yearly). For the development and deployment of control strategies, simple models such as those based on transfer functions are needed, especially for model-based predictive control (MPC) (Candanedo and Athienitis 2011). The weather forecast information and corresponding space heating/cooling load predicted from building models are needed as inputs for the control of BITES systems. Cooperman et al. (2010) showed that predictive control using weather forecast can result in substantial savings in both commercial and residential buildings.

Laplace transform has been traditionally used in deriving transfer functions for transient heat conduction in solids, especially for solid bounded by two parallel planes, such as wall and slab assemblies (Carslaw and Jaeger 1959, Kimura 1977). After Laplace transforming, time-series (discrete) response coefficients, such as thermal response factors (Stephenson and

Mitalas 1967), conduction transfer functions (CTF) (Stephenson and Mitalas 1971), and radiant time series (Spitler and Fisher 1999, Spitler et al. 1997), are derived with different methods and used in time domain modeling. Other than using Laplace transform formulation, CTF can also be obtained with state space formulation (Ceylan and Myers 1979, Seem et al. 1989). For assemblies with internal heat sources, Strand (1995) incorporated "source transfer functions" into CTF using either Laplace transform and state space formulations. The advantage of using time-series response coefficients is high computational efficiency for transient thermal simulations. A possible disadvantage is that it assumes a linear or linearized system. Besides time series coefficients, quasi-analytical algorithm was also developed to approximate the heat transfer among the assemblies, the heat transfer fluid, and room air (TRNSYS 2012).

Among other modeling approaches, finite difference (FD) models (Incropera and DeWitt 2002, Kreith and Bohn 2001) for active BITES systems have been widely used. The main advantages of FD approach are accurate treatment of non-linearization and easy formulation (e.g. heat transfer and control) (Incropera and DeWitt 2002). Detailed models reflecting the actual heat transfer process, such as 2- or 3-dimension spatial discretization, can provide more accurate results; however, they require more computational effort. Simpler lumped-parameter finite difference (LPFD) models with acceptable accuracy are needed for long-period simulations, especially for incorporation into whole building simulations and model-based control.

On the other hand, frequency response (FR) approach facilitates the integration of design and model-based control. FR approach can provide additional information, particularly for design optimization and comparison of design alternatives on relative basses and, without

tedious simulation (Athienitis et al. 1990). Furthermore, FR approach provides analytical solution and does not require spatial discretization. However, its main disadvantage is that it cannot directly model non-linear components. Another important application of FR approach is in the development of model-based control strategies for building HVAC systems (Athienitis et al. 1990, Candanedo and Athienitis 2011). FR models for ventilated BITES systems for design and model-based control purposes are thus presented in this section (paper).

FR approach is based on transfer functions derived from Laplace transform. Instead of inversing solutions back to time domain after Laplace transforming, FR approach generates solutions in the complex frequency domain by simply replacing s with $j \cdot \omega$ (Pipes 1957), where $j \cdot \omega$ is the imaginary angular frequency and $j = \sqrt{-1}$. When excitations are also represented in complex frequency form, the thermal responses of assemblies can be readily obtained in complex frequency domain. In the analysis of multi-layer assemblies (e.g. wall/floor/ceiling), the temperatures and heat flux at nodes of no interest do not need to be calculated. The magnitude and phase angle of admittance or impedance obtained from FR approach of an assembly provides substantial insight into its thermal behavior (Athienitis 1994, Athienitis et al. 1990, Balcomb and Jones 1983). These variables can be readily used for parametric analysis and design optimization. Athienitis (1994), Davies (1982, 1994), Athienitis et al. (1986), and Hittle (1981) conducted studies on the thermal behavior of building components and thermal zones using this approach.

Optimized RC (resistance and capacitance) network theory has been used to optimize the space-discretization of systems (Akander 2000). After obtaining the optimal discretization based on the frequency of the excitations of interest, thermal behavior is then obtained with

finite difference method in time domain (Akander 2000). Schmidt and Jóhannesson (2002) described a modeling method for active TES systems with heat transfer fluid flowing through. RC network technique was applied to optimize the space discretization. The study was later extended to quasi-two dimensional models (Schmidt and Jóhannesson 2004). Weber and Jóhannesson (Weber and Johannesson 2005) and Weber et al. (Weber et al. 2005) presented their studies on applying RC-network in modeling hydronic BITES systems.

The purpose of this section (paper) is to present network-based modeling methodologies for FR and explicit LPFD models of ventilated BITES systems. In the modeling of different active BITES systems (i.e. hydronic or ventilated, walls or slabs), even though they have different configurations (i.e. different heat transfer fluids with different fluid paths), the modeling concepts are universal and the techniques are similar. In this section (paper), FR and LPFD modeling concepts and techniques are presented using VCS systems for demonstration. The developed modeling methodologies are applicable to other active BITES systems. In the companion paper Part II (Section 3.3), the presented modeling techniques are applied to two types of VCS. The two approaches are compared, and modeling guidelines are withdrawn.

2. Modeling Methodology

This subsection describes the techniques adopted or developed in this study for FR and explicit LPFD modeling of VCS systems. One typical cross section of VCS is shown in Fig. 3.8-a. This cross section can represent either a slab on-grade or an intermediate floor. The insulation is optional for intermediate floors. It will be used if occupants would like to orientate the heat to one direction. The insulation layer can also represent the false ceiling and the air layer between the slab and the ceiling, from the point of heat transfer. Lumped-

parameter models of VCS and treatments of the effective capacitance around radial air channels were discussed by Barton et al. (2002) and Ren and Wright (1998). Chen et al. (2010b) studied experimentally and numerically the typical three dimensional temperature distribution in a VCS system. These studies showed that one-dimensional (normal to the room-side surface of the slab) thermal model can approximate the thermal behavior of the VCS well in cases of practical interest. Considerations in substituting two dimensional models with one-dimensional ones were further discussed by Strand (Strand 1995). An approximation approach in simplifying three dimensional heat transfer calculation is presented by Koschenz and Lehmann (TRNSYS 2012).

One-dimensional lumped-parameter modeling is adopted. The original cross section is transformed into an equivalent cross section (Fig. 3.8-b) by replacing the air channels with an imaginary layer without thickness (in this case at the bottom of the mass which has the same transformed cross sectional area as original). This transformation allows the heat transfer to be treated as one-dimensional. Fig. 3.8 also shows the thermal network of the VCS. Modeling results will be compared, in the companion paper Part II (Section 3.3), with field measurements from a solar demonstration house with a VCS system in the basement slab (Chen et al. 2010a). In the following subsections, formulations and calculations are developed to suit one-dimensional lumped-parameter modeling. The thermal characteristics of all material are assumed to be linear and time-invariant (e.g. conductivity and specific heat capacity do not depend on temperature or time).

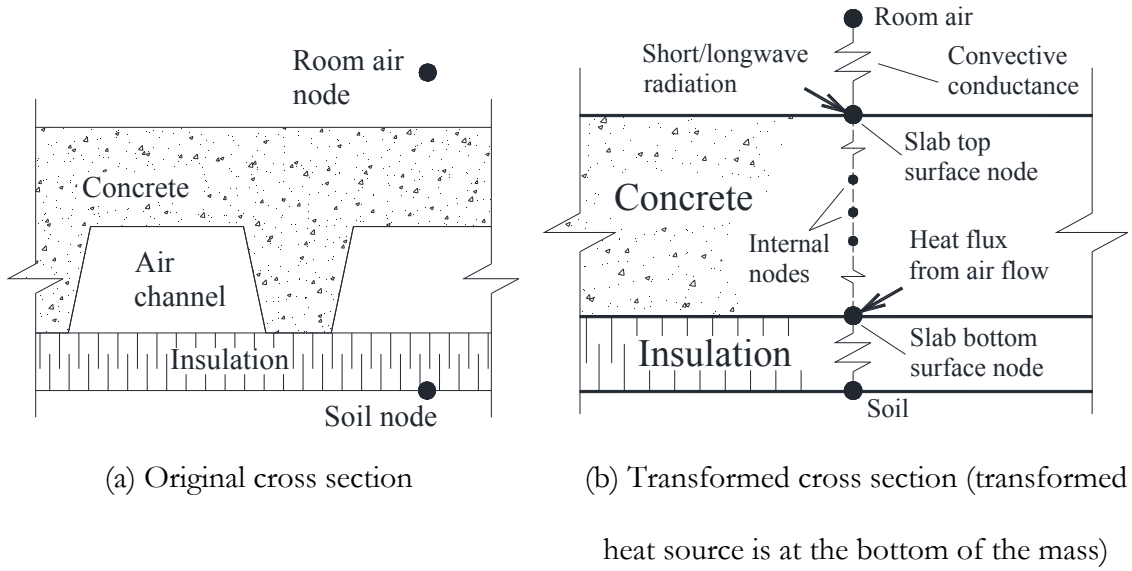

(a) Original cross section

(b) Transformed cross section (transformed heat source is at the bottom of the mass)

Fig. 3.8: Schematics of a VCS-b ("-b" indicates the air channels at the bottom of the concrete slab), its equivalent cross section, and one-dimensional thermal network after transformation (there is no need for "internal nodes" in FR thermal network)

2.1. Heat exchange between VCS and flowing air

In FR and LPFD models, heat transfer calculation is conducted on unit room-side surface area of the ventilated component. To calculate the average heat exchange per unit surface area between the flowing air and the slab, a representative (or mean) temperature of the flowing air, ${}_{mean_air}T$ is needed. When the thermal capacitance of the control volumes (CV's) surrounding the flowing air is much higher than that of air, the air channel surface temperature can be assumed to be uniform without causing significant errors (Ren and Wright 1998). Chen et al. (2010b) showed that the temperature gradient of a VCS-b along the air flow direction is not significant (less than 1°C). Ren and Wright (1998), Charron and Athienitis (2006), and Fraisse et al. (2006) presented methods for obtaining the local air

temperature along an air path, as well as the mean air temperature. Based on their work, a method applicable to FR and LPFD models is developed.

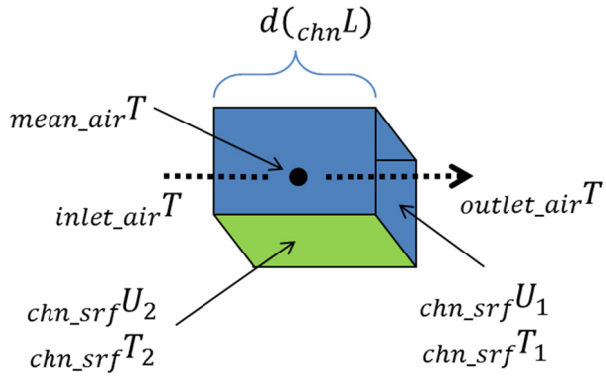

Fig. 3.9: A differential length of an air channel bounded by 2 surfaces ($B = 2$; one surface contains the top, front, and back surfaces; the other one is the bottom surface, which is in a different color).

Applying an energy balance to a differential length of the air channel being bounded by a number of B surfaces (Fig. 3.9), we obtain

$$d({}_{air}T) \cdot ({}_{air}Q \cdot {}_{air}\rho \cdot {}_{air}c_p) = \sum_{b=1}^{B} \left[d\left({}_{chn_{srf}}T_b - {}_{air}T\right) \cdot {}_{chn_srf}U_b \right] \cdot d({}_{chn}L) \tag{3.8}$$

where ${}_{air}Q$ is the volumetric air flow rate. ${}_{chn_srf}U_b$ is the conductance (convective and/or conductive) per meter channel length between the surface "b" and the air (unit: W/m/K). For example, Fig. 3.9 is used to exemplify the application of Eq. (3.8) to VCS-b shown in Fig. 3.9. ${}_{chn_srf}U_2$ in Fig. 3.9 represents the conductance between soil node and air flow. It combines the conductance of the insulation and the convective heat transfer coefficient (CHTC) between air flow and the insulation surface. The CHTC can be calculated using empirical equations (ASHRAE 2009d) or obtained by experiments.

Integrating over the total length of the air channel ${}_{ttl}L$, the outlet air temperature can be obtained with Eq. (3.9):

$$ {}_{outlet_air}T = {}_{eqv_chn}T + \left({}_{inlet_air}T - {}_{eqv_chn}T\right) \cdot exp\left(-{}_{hx}a \cdot {}_{ttl}L\right) \tag{3.9} $$

where ${}_{inlet_air}T$ is the air temperature at the inlet. ${}_{chn}T$ is the channel temperature weighted by the surfaces' respective heat transfer coefficients. When the air channel is bounded by only one surface, ${}_{chn}T = {}_{chn_srf}T$, where ${}_{chn_srf}T$ is the surface temperature of the air channel. In the case of being bounded by B number surfaces

$$ {}_{chn}T = \frac{\sum_{b=1}^{B}\left({}_{chn_srf}T_b \cdot {}_{chn_srf}U_b\right)}{\sum_{b=1}^{B}\left({}_{chn_srf}U_b\right)} $$

$$ {}_{hx}a = \sum_{b=1}^{B}\left({}_{chn_srf}U_b\right) \Big/ \left({}_{air}Q \cdot {}_{air}\rho \cdot {}_{air}c_p\right) $$

${}_{mean_air}T$ can be calculated using Eq. (3.10):

$$ {}_{mean_air}T = {}_{chn}T + \frac{\left({}_{inlet_air}T - {}_{chn}T\right) \cdot \left(1 - exp\left(-{}_{hx}a \cdot {}_{ttl}L\right)\right)}{{}_{hx}a \cdot {}_{ttl}L} \tag{3.10} $$

The total heat flow from the air to the channel can be calculated as follows:

$$ {}_{air_chn}P = \left({}_{mean_air}T - {}_{chn}T\right) \cdot \sum_{b=1}^{B} {}_{chn_srf}U_b \cdot {}_{ttl}L $$

${}_{air_chn}P$ calculated in this way is numerically equal to the heat loss/gain rate of the air flow (i.e. $\left({}_{inlet_air}T - {}_{outlet_air}T\right) \cdot \left({}_{air}Q \cdot {}_{air}\rho \cdot {}_{air}c_p\right)$), but slightly different from calculating it by another approach ${}_{air_chn}P = {}_{ttl}L \cdot \sum_{b=1}^{B}\left(\left({}_{mean_air}T - {}_{chn_srf}T_b\right) \cdot {}_{chn_srf}U_b\right)$. The

difference is within 3% in practical situations (e.g. expected inlet air temperature in the range 10 to 50°C, flow rates of 5-20 L/s per air channel, and boundary temperature of 10 to 30°C).

The analytical results obtained using Eq. (3.9) and (3.10) are compared with those from a finite difference model with fine mesh – the air channel is divided into significant small CV's along the air path to approach accurate results. Upwind differencing scheme (Patankar 1980) is used for modeling the heat transfer between the flowing air and the air channel surface. This comparison verifies the method adopted in this section (paper) for the calculation of heat flow from the flowing air to the slab. This method can be used for air channels with any path configuration, such as "U" (inlet and outlet on the same perimetric side of the slab) or "S" (inlet and outlet on the opposite sides after two or more turns) shapes. There may be several paths in one ventilated system. Furthermore, the air flow boundary can consist of more than one surfaces (e.g. insulation and concrete surfaces as shown in Fig. 3.8-a). This method can also be applied to hydronic BITES systems if the piping configuration results in a nearly uniform temperature across the BITES.

2.2. Frequency response approach

This subsection describes the techniques adopted or developed in this section (paper) for FR models. FR analysis is conducted in the complex frequency domain, typically with periodic excitations. Time domain equations have to be converted to frequency domain equations. These equations include heat transfer and excitation (e.g. boundary temperatures and heat flux, and internal heat sources) representation equations. These equations will be expressed in exponential complex frequency form as explained in later subsections or Appendix. Detailed information for the representation of excitations and calculation of transfer

functions in complex frequency domain is provided in Appendix. Some important points are given below:

- The analysis period, P, can be of any time span, from a few hours to one year, depending on study objectives (Athienitis et al. 1987).
- Simulation time step does not have a significant impact on the results, except in situations that there are changes/controls of excitations. For example, on/off control of auxiliary heating would be on multi-minute time interval instead on hourly interval. Hence, hourly time step is not appropriate.
- The equations for FR approach in this section (paper) are given for unit surface area.

2.2.1. Discrete frequency representation of excitations

In the time domain, time dependent excitations are generally given in two forms: continuous form (i.e. a function of time) and discrete form (i.e. sampled values, discrete values in forms of time series, such as in Eq. (A3.1) in Appendix). Time-series discrete values are most common in building thermal simulations. Values given in continuous form can also be converted to discrete form by sampling at desired time intervals. In the analysis for rough estimation, periodic excitations with simple profiles, such as diurnal outdoor temperature and solar incident on a surface on a clear day, can be represented approximately with simple sine- or cosine-wave function (Athienitis 1994). For more complicate excitation profiles, they can be approximated by the superposition of several simple profiles, using the idea from series expansions theorems such as Fourier series. In this section (paper), discrete Fourier series (DFS) in exponential complex frequency form are used to represent the boundary excitations, such as the surface temperature variation and heat flux from the air flow to the VCS.

2.2.2. Influence of number of harmonics

The desired number of harmonics in a DFS representation is determined by the profile of the excitation (mainly its frequency) and the desired accuracy of its representation in the frequency domain. Take the representation of a 24-hour external solar radiation profile for example, since its frequency is one (i.e. one cycle per 24 hours), one harmonic can be used; however, in order to better represent the sharp change at the sunrise and sunset moments, three harmonics are more desirable (Athienitis 1994). Another example, if an excitation with an irregular profile that has a shortest fluctuation time (e.g. the shortest time between two adjacent concave or convex points) of 3 hours, 8 harmonics should be used for a 24-hour simulation period (24/3=8), or 16 harmonics for a 48-hour period (48/3=16).

Furthermore, the Nyquist-Shannon sampling theorem shows that the excitation frequency or the highest frequency component must not be more than half the sampling frequency, to prevent aliasing (Franklin et al. 2006) (e.g. a different profile will appear). Since the highest frequency component in a DFS representation is determined by the number of harmonics, the number of harmonics shall not be more than half of the number of the sampled (discrete) data. For example, hourly value in a 48-hour period means 48 discrete values, and hence maximum of 24 harmonics are allowed.

2.2.3. Thermal response in complex frequency domain

In FR analysis, heat fluxes and temperatures on the two opposite surfaces of an assembly are the four variables of interest. If any two of the four variables are given, the total thermal responses (mean and oscillatory) of the other two variables can be readily obtained without discretizing the solid (also called two-port network method (Athienitis et al. 1985)). The two

given variables are considered as excitations, and can be represented with discrete Fourier series (DFS) in exponential complex frequency form as described in Appendix A1.

Eq. (3.11) from references (Carslaw and Jaeger 1959, Kimura 1977) shows the matrix expression for the oscillatory response at time t ($t = \Delta t \cdot i$, Δt is the time interval of data sampling). The oscillatory heat flux ${}^{n}_{0}\tilde{p}_{i,h}$ and temperature ${}^{n}_{0}\tilde{T}_{i,h}$ on surface $x = 0$ are due to excitations on surface $x = l$ of layer n (Fig. 3.10). ${}^{n}_{trs}[M]_h$ is the transmission matrix of layer n. See Appendix A4 for more explanation. In this study, surfaces 0 and l are the opposite outer surfaces of any layer, including the room air (air film layer) and soil nodes as shown in Fig. 3.8-b. It is important to note that the values in the excitation vectors are of various harmonics h, as in their DFS representations.

$$\begin{bmatrix} {}^{n}_{0}\tilde{T}_{i,h} \\ {}^{n}_{0}\tilde{p}_{i,h} \end{bmatrix} = {}^{n}_{trs}[M]_h \begin{bmatrix} {}^{n}_{l}\tilde{T}_{i,h} \\ {}^{n}_{l}\tilde{p}_{i,h} \end{bmatrix} \tag{3.11}$$

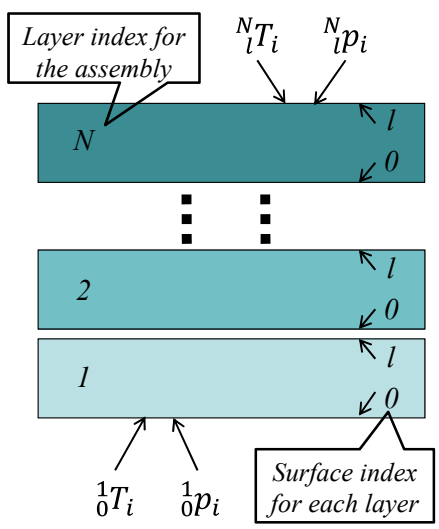

Fig. 3.10: Schematic of an assembly consisting of N layers, and the labeling of its excitations and its indices.

The overall transmission matrix for a N-layer assembly

$$ {}^{1\leftarrow N}_{trs}[M]_h = {}_{trs}^{1}[M]_h \cdot {}_{trs}^{2}[M]_h \cdot {}_{trs}^{3}[M]_h \ \ \dots \ \cdot {}_{trs}^{N}[M]_h \tag{3.12} $$

where left-hand-side superscript "$1 \leftarrow N$" indicates this transmission matrix is of the assembly containing layers from 1 to N (Fig. 3.10). As indicated by Eq. (3.11) and (3.12), the temperature and heat flux on surface l of layer N have to be the excitations for this formulation.

If the oscillatory temperatures on the two surfaces of one layer are given as excitations, Eq. (3.13) can be used to obtain the oscillatory heat fluxes. Matrix ${}_{adm}[M]_h$ is referred to as the admittance matrix. See Appendix A4 for more explanation.

$$ \begin{bmatrix} {}_{0}^{n}\tilde{p}_{i,h} \\ {}_{l}^{n}\tilde{p}_{i,h} \end{bmatrix} = {}_{adm}^{n}[M]_h \begin{bmatrix} {}_{0}^{n}\tilde{T}_{i,h} \\ {}_{l}^{n}\tilde{T}_{i,h} \end{bmatrix} \tag{3.13} $$

For any single layer, ${}_{trs}^{n}[M]_h$ and ${}_{adm}^{n}[M]_h$ can be derived from each other by mathematical manipulation (i.e. rearrangement of the variables). If the assembly of interest consists of more than one layers, the overall admittance matrix can only be obtained by rewriting the overall transmission matrix as follows, not by multiplying individual admittance matrices.

Let $\quad {}_{trs}[M]_h = \begin{bmatrix} t11_h & t12_h \\ t21_h & t22_h \end{bmatrix}$ and $\quad {}_{adm}[M]_h = \begin{bmatrix} a11_h & a12_h \\ a21_h & a22_h \end{bmatrix}$

then $\quad a11_h = t22_h/t12_h; a12_h = -1/t12_h; a21_h = 1/t12_h; a22_h = -t11_h/t12_h.$

For an assembly consisting of N layers of material, the matrix expression for calculating the oscillatory heat flux and temperature at surface 0 of layer 1 due to excitations on surface l of layer N is Eq. (3.14). If the oscillatory temperature excitations on two opposite surfaces are given, the oscillatory heat flow responses on these two surfaces can be obtained with Eq. (3.15). For other combinations of excitations, different matrices can be derived (Stephenson and Mitalas 1971).

$$\begin{bmatrix} {}^{1}_{0}\tilde{T}_{i,h} \\ {}^{1}_{0}\tilde{p}_{i,h} \end{bmatrix} = {}^{1\leftarrow N}_{trs}[M]_h \begin{bmatrix} {}^{N}_{l}\tilde{T}_{i,h} \\ {}^{N}_{l}\tilde{p}_{i,h} \end{bmatrix} \tag{3.14}$$

$$\begin{bmatrix} {}^{1}_{0}\tilde{p}_{i,h} \\ {}^{N}_{l}\tilde{p}_{i,h} \end{bmatrix} = {}^{1\leftarrow N}_{adm}[M]_h \begin{bmatrix} {}^{1}_{0}\tilde{T}_{i,h} \\ {}^{N}_{l}\tilde{T}_{i,h} \end{bmatrix} \tag{3.15}$$

2.2.4. Treatment of internal heat sources

To facilitate the FR analysis of a N-layer assembly (e.g. wall/floor/ceiling), heat flow sources that are not located at the two outermost nodes can be transformed to equivalent temperature potentials, and then added to the original temperatures of the two nodes (Fig. 3.11). Alternatively, the assembly (e.g. floor system) and the heat source can be split into two parts at the level of the heat source. These two approaches will be presented here. Examples of heat sources/sinks include heat flux from internal heat transfer fluids or from electric wires that are embedded in the active BITES components, and transmitted solar/long-wave radiation absorbed by the top surface of these components.

<u>Thévenin theorem for heat sources transformation</u>

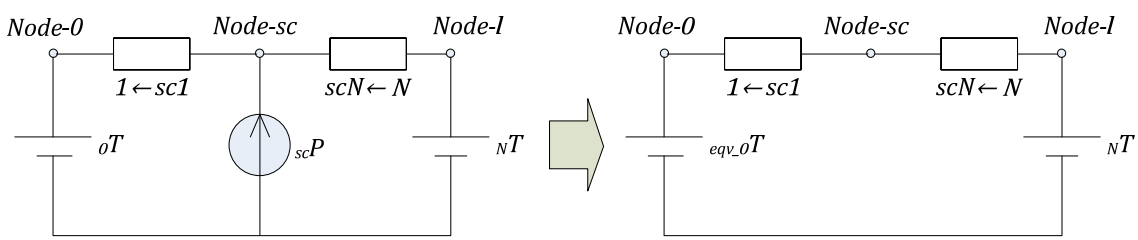

(a) Original thermal network (b) Transformed thermal network

Fig. 3.11: Transformation of thermal network (node 0 is the outermost node of assembly $1 \leftarrow sc1$, while node l is the outermost node of assembly $scN \leftarrow N$. Heat source node sc is in-between the two assemblies)

Heat flux can be transformed to equivalent temperature potential using Thévenin theorem from network theory (Bird 2007) as shown in Fig. 3.11. This transformation is similar to the process of obtaining the sol-air temperature (ASHRAE 2009e), which is commonly used in building thermal calculations. Eq. (3.16) can be used to calculate the oscillatory value of the potential due to heat flux at the source. See Eq. (3.12) for the definition of ${}^{1\leftarrow sc1}t12_h$. The mean potential can be obtained in a similar manner with normal resistances (e.g. r). If the assembly $1 \leftarrow sc1$ is purely resistive, ${}^{1\leftarrow sc1}t12_h$ equals to ${}^{1\leftarrow sc1}r$ with ${}^{1\leftarrow sc1}r$ being the thermal resistance of assembly $1 \leftarrow sc1$.

$$_{eqv_sc_0}^{\;\;1}\Delta\tilde{T}_{i,h} = {}^{1\leftarrow sc1}t12_h \cdot {}_{sc}\tilde{p}_{i,h} \tag{3.16}$$

where $1 \leftarrow sc1$ indicates the assembly consists of layers from 1 to $sc1$ (to the left of source node).

The total equivalent temperature at node 0 becomes

$$_{eqv_0}^{\;\;1}\tilde{T}_{i,h} = {}_{eqv_sc_0}^{\;\;1}\Delta\tilde{T}_{i,h} + {}_{0}^{1}\tilde{T}_{i,h}$$

<u>Heat flow division</u>

Instead of transforming the internal heat flow and transporting it to one of the outermost nodes, the heat flow can be divided into two portions, one for each node (e.g. nodes 0 and l in Fig. 3.11), using current division method (Bird 2007). Take the thermal network from Fig. 3.11 for demonstration. The oscillatory portion into node 0 will be

$$_{sc_0}^{\;\;1}\tilde{p}_{i,h} = -\frac{{}^{scN\leftarrow N}t12_h}{{}^{1\leftarrow N}t12_h} \cdot {}_{sc}\tilde{p}_{i,h} \tag{3.17}$$

where $scN \leftarrow N$ indicates the assembly consists of layers from scN (to the right of source node) to N. The negative sign indicates the heat flow direction.

Thévenin theorem transformation and heat flow division are actually equivalent to each other (i.e. the same amount of heat flux from the internal source to the outermost nodes). Their equivalence can be proved analytically. From Eq. (3.15), ${}_{sc_0}^{1}\tilde{p}_{i,h} = {}^{1\leftarrow N}a12_h \cdot {}_{eqv_sc_l}^{N}\Delta\tilde{T}_{i,h}$. Similar to Eq. (3.16), ${}_{eqv_sc_l}^{N}\Delta\tilde{T}_{i,h} = {}^{N\leftarrow scN}t12_h \cdot {}_{sc}\tilde{p}_{i,h}$, and ${}^{N\leftarrow scN}t12_h = {}^{scN\leftarrow N}t12_h$. Hence

$$ {}_{sc_0}^{1}\tilde{p}_{i,h} = {}^{1\leftarrow N}a12_h \cdot {}^{N\leftarrow scN}t12_h \cdot {}_{sc}\tilde{p}_{i,h} = {}^{1\leftarrow N}a12_h \cdot {}^{scN\leftarrow N}t12_h \cdot {}_{sc}\tilde{p}_{i,h} \qquad (3.18) $$

As presented previously, ${}^{1\leftarrow N}a12_h$ and $-1/{}^{1\leftarrow N}t12_h$ are numerically equal. Therefore, Eq. (3.17) and (3.18) result in the same values, and hence the equivalency of these two techniques is proved.

2.2.5. Y-diakoptic method

In ventilated BITES systems, the activation of the air flow (i.e. fan on/off) depends on the temperatures of the available inlet air and the system. Generally, the air flow will be activated if the temperature of the inlet air is certain degrees higher that of the BITES system and the BITES system needs to be conditioned. Furthermore, the heat exchange between the air flow and the system is affected by the temperature difference between the air flow and the air channel surface. Therefore, the temperature of the channel surface is desired for these two reasons – activation of air flow and calculation of heat transfer.

In order to obtain the temperature at the internal source level (i.e. air channel) in the FR approach, the VCS needs to be split into two parts at the source level and their transmission matrices need to be calculated. Furthermore, considering the heat flow can be divided into

two portions using heat flow division technique discussed previously, if the two parts of the VCS can be treated separately, splitting into two parts will facilitate the solution for complex thermal network, resulting from integrating the VCS model into a whole building model. The difficulty is that the capacitance of the floor assembly is common (i.e. linked) to its two outermost nodes that have time-varying temperatures. The split needs special treatment. Athienitis et al. (1985) used Y-diakoptic method (Y represents admittance) to represent a two-zone common wall with two self-admittances and one transfer-admittance. Then, the common wall is split into two parts - each original outermost node is connected to one equivalent self-admittance and an equivalent heat source.

Take the node 0 from Fig. 3.11 as one of the outermost nodes for demonstration. The equivalent self-admittance ${}_{eqv_slf}^{1\leftarrow sc1}Y_h$ of the assembly $1 \leftarrow sc1$ is obtained with Eq. (3.19). The equivalent heat source is the product of the equivalent transfer-admittance ${}_{eqv_trf}^{1\leftarrow sc1}Y_h$ (Eq. (3.20)) and the temperature difference between the two outermost nodes. See paper Part 2 (Section 3.3) for further demonstration.

$$ {}_{eqv_slf}^{1\leftarrow sc1}Y_h = {}^{1\leftarrow N}a11_h + {}^{1\leftarrow N}a12_h \tag{3.19} $$

$$ {}_{eqv_trf}^{1\leftarrow sc1}Y_h = {}^{1\leftarrow N}a12_h \tag{3.20} $$

2.2.6. Calculating the total response

The final discrete response to any excitation is the summation of the system's mean response and the responses to all the harmonics (i.e. oscillatory response), as given in Eq. (3.21). The calculation of the mean response is similar to that of the oscillatory responses, but using mean values of the excitations and steady-state conductance. If there is more than one

excitation, the total response will be the summation of individual responses to the respective excitations by superposition (based on the attributes of a linear time-invariant system).

$$\hat{R}(\hat{E}_i) = \bar{R}(\bar{E}) + \sum_{h=1}^{H} \left(\tilde{R}(\tilde{E}_{i,h})\right) \tag{3.21}$$

where $\bar{R}(\quad)$ represents the steady state response transfer function. $\tilde{R}(\quad)$ is the oscillatory response transfer functions, and it is from the transmission or admittance matrix in this section (paper).

Considering an example, if the excitations are the temperatures on two outermost surfaces – surface 0 of layer 1 and surface l of layer N of a N-layer assembly, the steady-state response of heat flow at surface 0 is ${}_0^1\bar{p} = ({}_0^1\bar{T} - {}_l^N\bar{T})/{}^{1\leftarrow N}r$ with ${}^{1\leftarrow N}r$ being the total thermal resistance of all layers. Oscillatory heat flow (i.e. response) at surface 0, ${}_0^1\tilde{p}_{i,h}$ can be obtained using Eq. (3.15). The final response can then be obtained using Eq. (3.21): ${}_0^1\hat{p}_i = {}_0^1\bar{p} + \sum_{h=1}^{H}\left({}_0^1\tilde{p}_{i,h}\right)$, and time domain (i.e. real value) heat flux is ${}_0^1p_i = Re\{{}_0^1\hat{p}_{i_i}\}$.

2.3. Explicit lumped-parameter finite difference approach

Techniques adopted in this study for the discretization and time step selections in explicit LPFD models are presented and discussed in this subsection.

2.3.1. Discretization

In the multi-layer discretization schemes to be studied for one-dimensional LPFD models, each layer of the concrete slab is represented by one CV. The optimal thickness of each CV has to be determined for desirable simulation accuracy. The thickness of the outermost CV can be made as the thinnest to take into account the relatively higher heat transfer on the top surface. Paper Part 2 (Section 3.3) discusses effects of different discretization schemes.

Dimensionless Biot number (ratio of the internal thermal resistance of a solid to the boundary layer thermal resistance) (Kreith and Bohn 2001) can be used to decide the thickness of CV's. Ideally, Biot number should be less than 0.1 in order to minimize the error introduced by assuming uniform temperature distribution inside one CV (Kreith and Bohn 2001). However in LPFD models, coarse discretizations will result in Biot numbers larger than 0.1. The recommendation for proper Biot number and its resulting errors for different types of VCS are presented in paper Part 2 (Section 3.3). Once the Biot number is chosen, the thickness of the edge CVs (e.g. slab top surface node in Fig. 3.8-b) can be determined as follow

$$_{edge_CV}Th = \frac{_{Biot}No \cdot {}_{cnc}k}{_{crt}h} \tag{3.22}$$

where $_{cnc}k$ is the conductivity of the concrete, $_{Biot}No$ is the Biot number of the CV, and $_{crt}h$ is the critical (i.e. largest) combined convective and radiative conductance on the concrete surface, either the room side or the air flow side.

When direct heat flux, $_{heat_flux}p$, on the boundary (e.g. solar radiation) is significant enough to be considered, converting radiative heat flux to equivalent temperature potential (e.g. sol-air temperature) is not correct here. The heat flux needs be converted into an equivalent CHTC using

$$_{eqv}h = {}_{heat_flux}p / {}_{cnv}\Delta T \tag{3.23}$$

and then superimposed on the CHTC, $_{cnv}h$. Hence, $_{crt}h = {}_{cnv}h + {}_{eqv}h$. $_{cnv}\Delta T$ is the air film temperature difference. This treatment will be exemplified in paper Part 2 (Section 3.3).

2.3.2. Time step

In explicit FD approach, Fourier number ($Fo = \alpha \cdot \Delta t / l^2$, the ratio of the heat conduction rate to the rate of thermal energy storage) needs to be less than 0.5 to stabilize the marching of the FD equations forward in time (Incropera and DeWitt 2002). Therefore in our case of one-dimensional heat transfer, the maximum allowable time step can be calculated as follow:

$$\Delta t < \frac{{}_{edge_CV}c}{{}_{node}u + {}_{crt}h} \tag{3.24}$$

where ${}_{edge_CV}c$ is the capacitance of the edge CV, and ${}_{node}u$ is the conductance between the edge capacitance node and the adjacent inner capacitance node.

One of the advantages of using LPFD models is their less critical time step requirement in explicit formulation, extending from less than five minutes for a 1-cm thick layer to more than an hour for a 5-cm layer in one-dimensional model. However, large time step may not be adequate to obtain a sufficiently accurate solution reflecting practical operating situations. Effects of time step selection are discussed in the companion paper Part 2 (Section 3.3).

3. Conclusion

Modeling techniques for frequency response (FR) and lumped-parameter finite difference (LPFD) approaches are presented in this section (paper) for active building-integrated thermal energy storage (BITES) systems. The methodology is applied to ventilated concrete slabs (VCS) system. The techniques are applicable to other ventilated, electric, and hydronic BITES systems.

Network modeling techniques, such as heat source transformation with Thévenin theorem, heat flow division, and Y-diakoptic method are presented as means to develop transfer

function models in frequency domain. Thévenin transformation and heat flow division are equivalent in the treatment of the heat flow from the flowing air. Y-diakoptic method can split the BITES system into two parts at the internal heat source level, and hence facilitates the formulation and calculation. Discrete Fourier series (DFS) representation in complex frequency form are used to represent the boundary excitations, such as the surface temperature variation, solar radiation and heat flux associated with flowing air. Since the heat transfer equations are also solved and represented in complex frequency domain, simple and efficient solutions can be readily obtained. Frequency domain results can be easily transformed back to the time domain. The criteria for choosing the number of harmonics have also been discussed. Furthermore, equations for one-dimensional discretization and time step selection are discussed, taking into account convective and radiative heat transfer on the boundaries. A method used in simplified models for calculating the heat transfer between flowing air and ventilated BITES systems is developed. Application of these techniques is presented in the second part of the study (Section 3.3).

Section 3.3 Frequency domain and finite difference modeling of ventilated concrete slabs and comparison with field measurements: Part 2, application

Based on a paper in-press:

Chen, Y., A. Athienitis and K. Galal. 2013b. Frequency domain and finite difference modeling of ventilated concrete slabs and comparison with field measurements: Part 2, application. International Journal of Heat and Mass Transfer, in press.

Section Abstract

This section (paper) is the second of two that present techniques and guidelines for frequency response (FR) and lumped-parameter finite difference (LPFD) approaches for the thermal modeling of building-integrated thermal energy storage (BITES) systems. To assist the thermal analysis and control of active BITES systems, development of FR and LPFD models are presented in this two-part study. Modeling methodology and techniques are presented in paper Part 1 (Section 3.2) using ventilated concrete slabs (VCS) for demonstration. In this part, the methodology is applied to two types of VCS. The modeling results from different FR and explicit LPFD models with different time steps and discretization schemes are presented. The results are compared to each other, and with field-measured data from a solar demonstration house with a VCS. Simulation results show that time step of half an hour for FR models results in less than 3% errors in thermal performance. For LPFD models, discretization with a Biot number smaller than 0.5 can reduce errors to about 5%.

1. Introduction

In Section 3.2 of this chapter, the model development for FR and explicit LPFD models of ventilated BITES systems are presented, using VCS systems for demonstration. In this part, the techniques are applied to two common types of VCS systems (Fig. 3.12). VCS-b systems have air channels at the bottom of the slab ("b" stands for "bottom") while VCS-c systems use their hollow cores as air channels ("c" stands for "center" or "core"). This cross section can represent either a slab-on-grade or an intermediate floor slab. The insulation layer can be replaced by a false ceiling and the air layer between the slab and the ceiling. Insulation is optional, but should be used if occupants would like to limit the heat to the opposite direction. The air flow in the channels does not interact directly with room air (i.e. a close-loop system). The FR and LPFD modeling results are compared with each other. The LPFD modeling results of the VCS-b system are also compared with field-measurement. The accuracies for corresponding choices of time step and discretization are quantified. The purpose of this part is to provide modeling guidelines for FR models and explicit LPFD approaches for ventilated BITES systems.

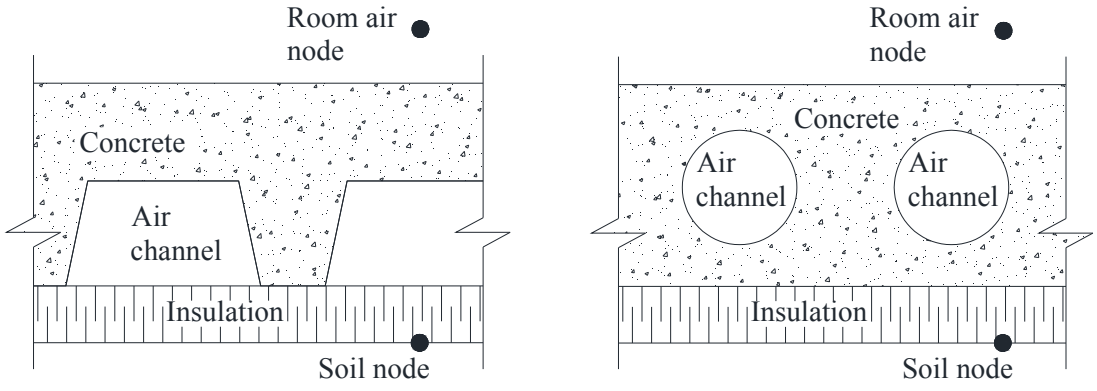

(a) VCS-b configuration (b) VCS-c configuration

Fig. 3.12: Schematics of two types of VCS

2. Model development

The cross sections of the two types of VCS systems (Fig. 3.12) are transformed into the two equivalent cross sections (Fig. 3.13) by replacing the space of the air channels with one equivalent air layer with no thickness. This transformation allows the heat transfer to be treated as one-dimensional. The transformed cross sections have the same cross sectional areas as the original ones. As discussed in paper Part 1 (Section 3.2), studies (2002, 2010b, 1998) showed that the modeling errors introduced by the transformation will be minimized by calculating the heat transfer rate between air flow and the slab with the original air channel geometry. Heat transfer is treated one-dimensional normal to the room-side surface of the slab. The thermal characteristics of all material are linear and time-invariant (e.g. conductivity and specific heat capacity are not dependant of temperature or time). The thermo-physical properties of concrete are taken as follows: 840 J/kg/K for specific heat; 2200 kg/m^3 for density; 1.7 W/m/K for conductivity. The conductance of the insulation is 0.5 W/m^2/K.

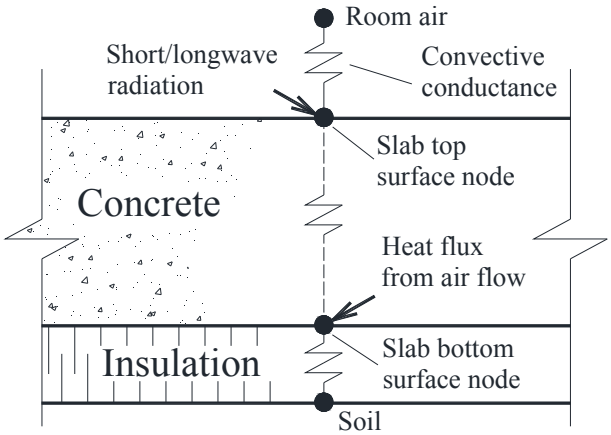

(a) Transformed VCS-b (transformed heat source at the bottom of the concrete)

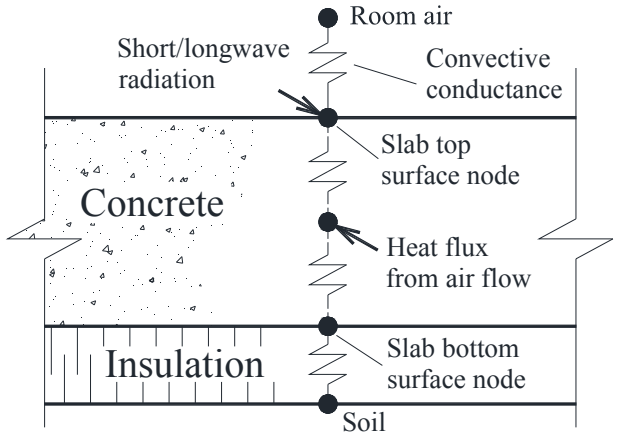

(b) Transformed VCS-c (transformed heat source inside the concrete)

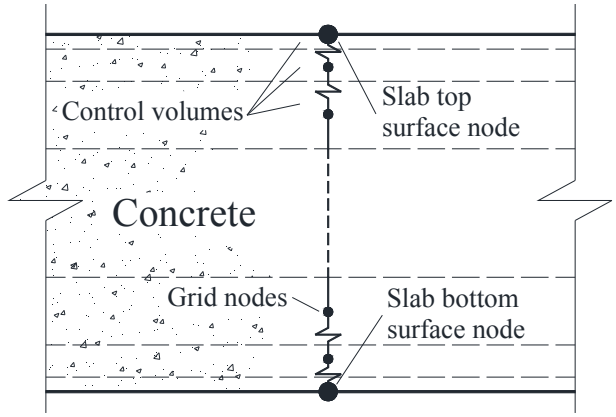

(c) Spatial discretization of concrete slab for LPFD models

Fig. 3.13: Equivalent cross sections, one-dimensional thermal networks and spatial discretization of the two kinds of VCS (Fig. 3.12) after transformation (there are no internal grid nodes for FR thermal networks)

2.1. LPDF model discretization

In the LPFD models, the multi-layer discretization schemes to be discussed have grids symmetric about the center plane of the slab. Each layer is one control volume (CV). The thickness of the outermost CV is chosen to be the thinnest taking into account the intensive heat transfer rate due to convection and radiation on the top surface. From the outer layer to

the inner layer, the thickness of the layer increases with a factor of two. For edge CVs, the capacitance nodes are chosen to be at the outer surfaces (Fig. 3.13-c). For other CVs, their capacitance nodes are at the centers of the CVs. Other discretization schemes may be adopted, such as even layer thickness. See subsection 4 "Discussion" for further discussion.

2.2. Excitation profiles

LPFD models can be subjected to periodic or non-periodic excitations, while the FR models are used under periodic excitations. However, FR models can accommodate non-periodic excitations as sub-components into periodic excitations. Since the simulation period can be as long as needed (Athienitis et al. 1987), a non-periodic excitation can be changed to a periodic excitation by adding extra simulation periods to the end and/or the beginning of the original non-periodic excitation, equalizing the beginning and the ending values of the new excitation. The non-periodic excitation becomes part of the new periodic excitation. By allowing a long enough stabilization (i.e. warm-up) period before the non-period of interest, accurate thermal responses under the non-periodic conditions can be obtained. Stabilization period is also needed for LPFD models. When the models are subject to periodic excitations, accurate initial conditions are not needed. The thermal response of the slabs can be obtained through iteration until convergence criteria are met as shown in the ending part of subsection 2.3.

Fig. 3.14 shows the periodic excitation profiles for the following studies of the LPFD and FR modeling. The room air temperature profile is pre-set as a function of solar radiation and exterior temperature. Soil temperature is set at 11°C. When available inlet air temperature is higher than that of slab and heat storage is desirable, fan will be activated. The air flow rate is 0.2 m^3/sec, and the corresponding convective heat transfer coefficient (CHTC) between the

core air and the concrete surfaces is 15 W/m^2/K (Chen et al. 2010b). There are two simulation periods for each configuration - one day (the first day from Fig. 3.14) and two days. Note that, different simulation period means different excitations profiles. In the one-day simulation period, since the excitation profiles are periodic, the previous day and the following day are the same sunny days as shown. This is different from a two-day simulation period. Studies on LPFD modeling under non-periodic conditions are conducted for VCS-b. The modeling results are compared with field-measured data from a full-scale experimental VCS shown in Fig. A2.1 in Appendix. The surface dimensions of the models are the same as the experimental VCS.

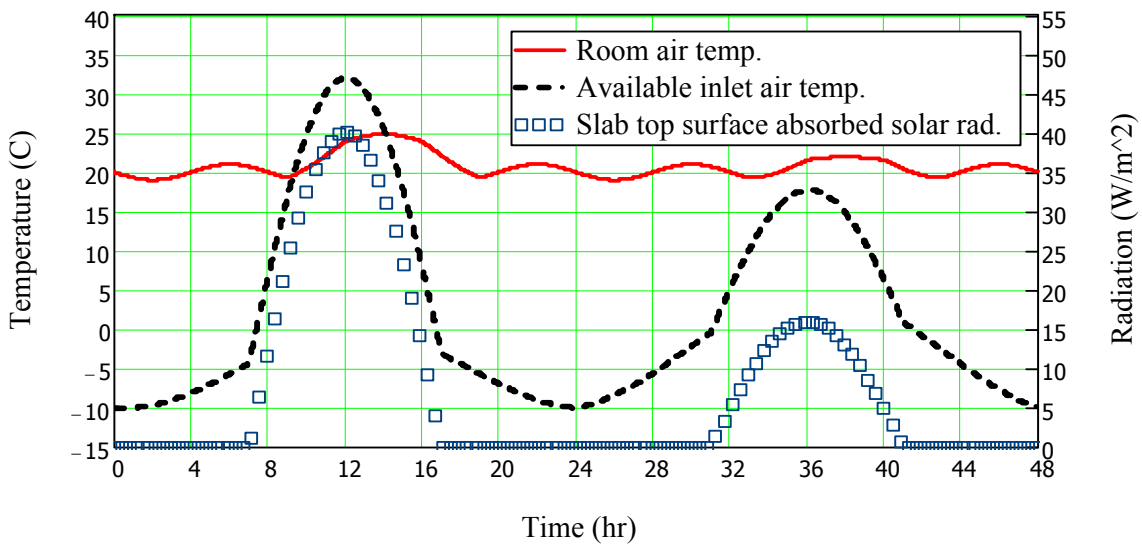

Fig. 3.14: Excitation profiles (a sunny day is followed by a cloudy day; room air temperature is controlled by a space heating system and optimized for passive solar heating)

2.3. Heat flow calculation in FR models

In FR models, the distribution of the heat flux to the two outermost nodes of an assembly (e.g. insulation, concrete, and the air film on the top) at any time step can be obtained easily. In this study, Thévenin theorem (Bird 2007) is used for "b" type VCS without splitting the

assembly. Heat flux is transformed to an equivalent temperature potential and added to the temperature of one of the outermost nodes (room air or soil). This is similar to the calculation of sol-air temperature (ASHRAE 2009e), but with frequency-domain transfer functions. See paper Part 1 (Section 3.2) for more information. Meanwhile, Y-diakoptic with heat flow division methods are used for the FR analysis on "c" type VCS. The assembly is divided into two parts at the level where the heat sources is located (Fig. 3.13-b). In the following paragraphs, procedure for calculating channel heat flow for VCS-c systems will be described. A similar procedure, with the parts of Y-diakoptic and heat flow division being replaced by Thévenin transformation, is applied to VCS-b systems. The simulation results from both types of VCS are shown in the following subsection.

In the complex discrete Fourier series (DFS) representation of any excitation/response, the time-series values of all time steps need to be known in advance. Since the activation of the air flow depends on channel temperature and the heat flow from the air will affect the channel temperature, the process for obtaining the heat flow from the channel air, has to be iterative. That is to say, simulations have to be repeated over the whole simulation period several times until the desired convergence criteria are met. See Subsection 4 "Discussion" for further discussion on alternative modeling method. The following paragraphs depict the process. The thermal network of a N-layer assembly (Fig. 3.11) is taken for demonstration. Node 0, representing the room air node, is the outermost node of sub-assembly $1 \leftarrow sc1$ consisting of the top portion concrete and the air film; while node l (soil) is the outermost node of sub-assembly $scN \leftarrow N$ (the bottom portion concrete and the insulation layer). Heat source node sc (heat flux from air channel inside the concrete slab) is in-between the two sub-assemblies.

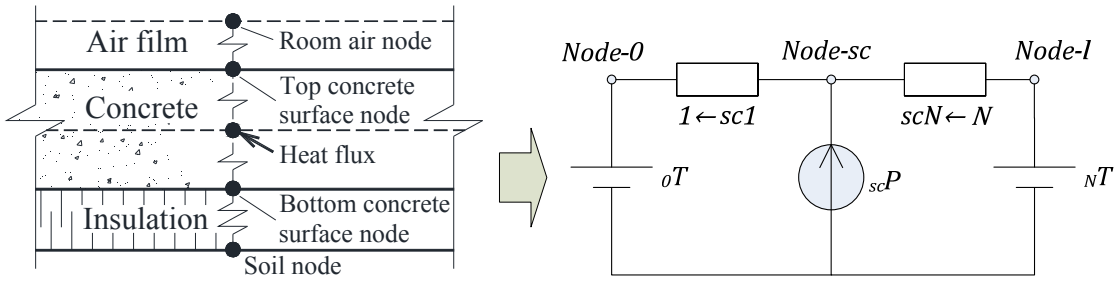

Fig. 3.15: Thermal network of a VCS-c system

With initial guessed values of the channel surface in all time intervals, the heat flow from source to the slab ${}_{sc}p_i$ in time domain (i.e. real value) can be calculated with Eq. (3.25). When there is no air flow, the heat flow is zero. See paper Part 1 (Section 3.2) for detailed information of the equations used below.

$$ {}_{sc}p_i = \left({}_{mean_air}T_i - {}_{chn}T_i\right) \cdot {}_{eqv}u \tag{3.25} $$

${}_{chn}T_i$ is the temperature of the air channel. ${}_{eqv}u$ is the equivalent conductance per square meter room-side slab surface area. For example, if a ventilated component has a 2 meters long air channel per unit room-side surface area (i.e. 2 m/m^2), and the ${}_{chn_srf}U$ is 10 W/m/K, then ${}_{eqv}u$ will be $10 \times 2 = 20$ W/m^2/K. ${}_{chn_srf}U$ is the conductance (convective and/or conductive) per meter channel length between the channel surface and the air flow. In this case, it is the convective conductance, varying with different air velocities. The CHTC between the core air and the concrete surfaces can be either calculated using empirical equations from literature or obtained from experiments.

After obtaining the initial ${}_{sc}p_i$ for the whole simulation period based on guessed channel temperature, it is represented in complex DFS. Then, the total oscillatory response of the heat flow into node 0 is calculated using Eq. (3.26).

$$ {}_{0}^{1}\tilde{p}_{i,h} = {}_{eqv_slf}^{1\leftarrow sc1}Y_h \cdot {}_{0}^{1}\tilde{T}_{i,h} + {}_{eqv_trf}^{1\leftarrow sc1}Y_h \cdot \left({}_{l}^{N}\tilde{T}_{i,h} - {}_{0}^{1}\tilde{T}_{i,h}\right) - {}_{sc_0}^{1}\tilde{p}_{i,h} \tag{3.26} $$

where ${}_{l}^{N}\tilde{T}_{i,h}$ represents equivalent oscillatory temperature of the outermost node l of assembly $1 \leftarrow N$. The "$-$" sign before ${}_{sc_0}^{1}\tilde{p}_{i,h}$ accounts for heat flow from source to node 0 being considered negative, and

$$ {}_{sc_0}^{1}\tilde{p}_{i,h} = \frac{{}^{scN\leftarrow N}t12_h}{{}^{1\leftarrow N}t12_h} \cdot {}_{sc}\tilde{p}_{i,h} \tag{3.27} $$

After that, the temperature of the outermost node can be calculated based on heat balance at that node. With the known heat flow and temperature of the outermost node, the channel surface temperature can then be updated using Eq. (3.28). Note that the order of layers in transmission matrix ${}_{trs}^{sc1\leftarrow 1}[M]_h$ is from 1 to $sc1$.

$$ {}_{chn}\tilde{T}_{i,h} = {}^{sc0\leftarrow 1}t11_h \cdot {}_{0}^{1}\tilde{T}_{i,h} + {}^{sc0\leftarrow 1}t12_h \cdot {}_{0}^{1}\tilde{p}_{i,h} \tag{3.28} $$

In the next iteration, Eq. (3.25) to (3.28) will be repeated. The updated heat flow from the channel air is represented again in complex DFS. The calculations of mean values of the variables of interest, such as the mean heat flux at node 0, ${}_{0}^{1}\bar{p}$, contributed from the mean temperature difference of two outermost nodes and from the mean heat flow from the source, are similar to Eq. (3.25) to (3.28). After the desired convergence criteria are met, the final heat flux (total response) into node 0 in complex frequency form is ${}_{0}^{1}\hat{p}_i = {}_{0}^{1}\bar{p} + \sum_{h=1}^{H}\left({}_{0}^{1}\tilde{p}_{i,h}\right)$.

3. Simulations and comparison results

In the LPFD approach, for VCS-b, two discretization schemes are applied and compared – the multi-layer dense scheme and 2-layer scheme. The number of layers in the multi-layer scheme depends on the thickness of the slab and the chosen value of the Biot number (0.05

is chosen). For VCS-c, 5- and 3-layer schemes are applied based on the study of the discretization schemes for VCS-b. The source-level node for VCS-c is located at the center of the air channel. However, the air channels do not have to be at the center of the cross section. In FR models, the treatment of the heat flow from the channel air uses Thévenin transformation for VCS-b, and Y-diakoptic with current division method for VCS-c.

3.1. Modeling VCS-b

Simulation results under periodic excitations for "b" type VCS are compared between LPFD models and FR models for different time steps, discretization schemes, and simulation periods. After that, the simulation results under non-periodic excitations for a 2-layer LPFD model are compared with field-measured data.

3.1.1. Periodic excitations

Simulation results from the numerical models with different discretization schemes, time steps, and simulation periods are tabulated in Table 3.4. With time step of 60 seconds, the simulation results from LPFD and FR models are extremely close to each other for different slab thickness. The differences in the cumulative values (e.g. heat from air to slab) are negligible; while the standard deviations of dynamic temperature differences are about 0.05 and 0.2°C for the slab bottom surface and the outlet air, respectively. Results from FR models are considered accurate since they are analytical solutions. Fig. 3.16 shows the simulated temperature and heat flux profiles for one of the LPFD simulation configurations in Table 3.4 (bold numbers). Roughly between hour 10 and 13, the air flow temperature, which is affected by the solar radiation and exterior temperature, is higher than that of the slab, and hence there is heat delivered from the air flow to the slab.

Table 3.4: Comparison of VCS-b models with excitation profiles and interior temperature from Fig. 3.14.

Slab thickness	**Simulation period**	**Time step**	**Heat from channel air flow to slab**		**Heat from slab top surface to room air**		**Layers in FD model**
			(kWh)		(kWh)		
		(sec)	FR	FD	FR	FD	
0.1 m	one day	60	3.92	3.91	10.14	10.15	6
		300	3.89	4.00	10.12	10.27	4
		600	3.90	4.07	10.13	10.38	2
		1800	4.05	3.90	10.25	10.39	
		3600	4.04	4.58	10.20	11.30	
	two day	60	4.09	4.05	12.22	12.18	6
		300	4.14	4.10	12.27	12.24	4
		600	4.14	4.17	12.26	12.33	2
		1800	4.17	3.99	12.28	12.21	
		3600	4.17	4.68	12.21	12.94	
0.15 m	one day	60	4.26	4.26	10.47	10.48	8
		600	4.21	4.27	10.42	10.58	4
			4.21	4.57	10.42	10.88	2
		1800	4.23	4.68	10.42	11.20	
		3600	4.27	4.88	10.41	11.73	
	two day	**60**	4.70	**4.68**	12.81	**12.79**	**8**
		600	4.78	4.83	12.87	12.97	4
			4.78	5.02	12.87	13.15	2
		1800	4.54	5.01	12.63	13.22	
		3600	4.57	5.23	12.59	13.52	
0.2 m	one day	60	4.31	4.28	10.50	10.48	8
		600	4.32	4.36	10.50	10.66	4
			4.32	4.62	10.50	10.91	2
		1800	4.20	4.70	10.37	11.22	
		3600	4.25	4.89	10.38	11.75	
	two day	60	4.97	4.92	13.05	13.01	8
		600	5.04	4.95	13.11	13.08	4
			5.04	5.45	13.11	13.56	2
		1800	5.04	5.26	13.10	13.47	
		3600	4.71	5.49	12.72	13.79	

Note:

(1) 10 harmonics are used in the FR models;

(2) For LPFD models with 60-second time step, the Biot number is set to be 0.05;

(3) One-day simulation uses the first day conditions of the two-day period illustrated in Fig. 3.14;

(4) Different simulation period means different excitations profiles. In the one-day simulation period, since the excitation profiles are periodic, every day is sunny. This is different from a two-day simulation period.

For FR models, time step of half an hour is sufficient to provide results with acceptable accuracy. The differences are less than 2% as compared to the simulations with 60-second time step. The main reason for the difference is the on/off durations of the air flow affected by the time step. This is also the reason for excluding one-hour time step. Note that 10 harmonics are used in the FR models.

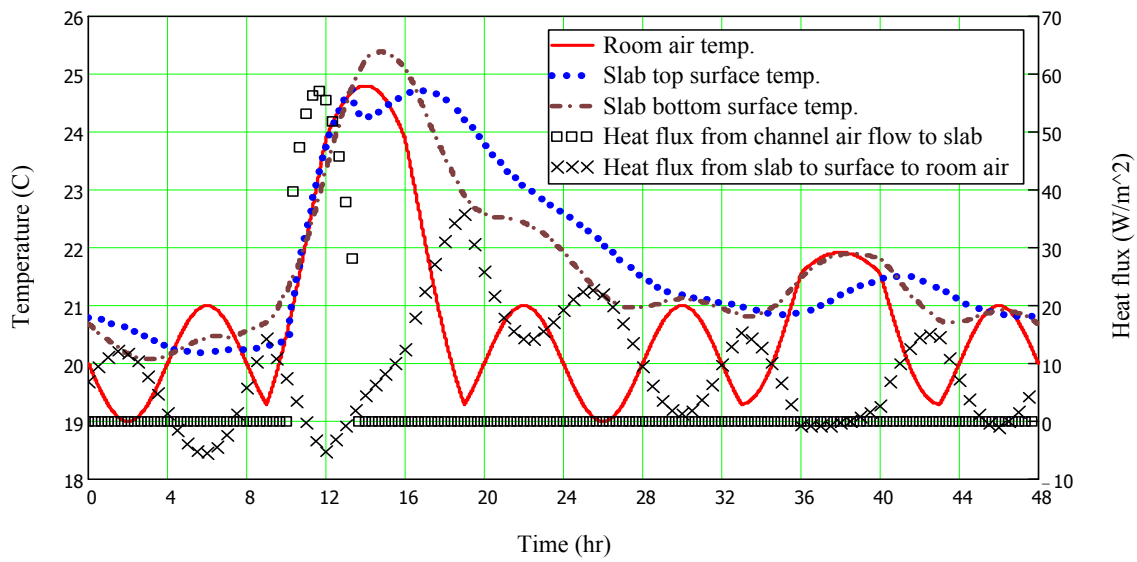

Fig. 3.16: Temperature and heat flux profiles for VCS-b in a two-day design period (Fig. 3.14) (8-layer LPFD model, time step of 60 seconds, and effective slab thickness of 0.15 m)

For LPFD models, comparison shows that time step is not as influential as spatial resolution of discretization on error introduction. Change of time step from 60 seconds to 10 minutes for multi-layer scheme, or from 10 minutes to half an hour for 2–layer scheme, does not introduce significant errors (less than 2%, respectively). Note that maximum time step is

limited by equation stability (Incropera and DeWitt 2002). Changing the layer numbers from 4 to 2 for 0.15-m and 0.2-m VCS-b introduces errors about 5 to 10%, comparing to the values from FR models with 60-second time step. The Biot number for 0.05-m thick grid (0.1-m slab split into two layers in this case) is 0.44 (${}_{Biot}No = {}_{edge_CV}Th \cdot {}_{crt}h/{}_{cnc}k$, ${}_{crt}h = 15$ W/m^2/K and ${}_{cnc}k = 1.7$ W/m/K); While, it is 0.66 for the 0.075-m grid. Hence, keeping Biot number below 0.5 and choosing maximum allowable time step accordingly, $\Delta t < {}_{edge_CV}c/({}_{node}u + {}_{crt}h)$, is sufficient to generate results with errors less than 5%.

Fig. 3.17 shows the simulated profiles from both LPFD and FR models for VCS-b. The simulation profiles are close to each other – the maximum temperature difference is about 0.6°C for the bottom surface of the slab. The closeness is also shown under dramatized excitations (i.e. the mean values and amplitudes of excitations are escalated to extreme values). The resemblance of simulation results suggests that the modeling techniques are correct, and the LPFD and FR models generate similar results.

The temperature discrepancy is mainly caused by the overshoots/undershoots of the DFS-represented profiles of the excitations. By increasing the number of harmonics, the magnitudes of overshoots and undershoots can be reduced; however, it will not have significant impact on the cumulative values. For example, the magnitude of the difference in the heat transferred from air to the slab (Table 3.4) over the simulation periods is of 0.01 kWh by changing of the number of harmonics from 6 to 20. 6 harmonics is the minimum acceptable number of harmonics considering the excitations (e.g. room air temperature, solar radiation) profiles.

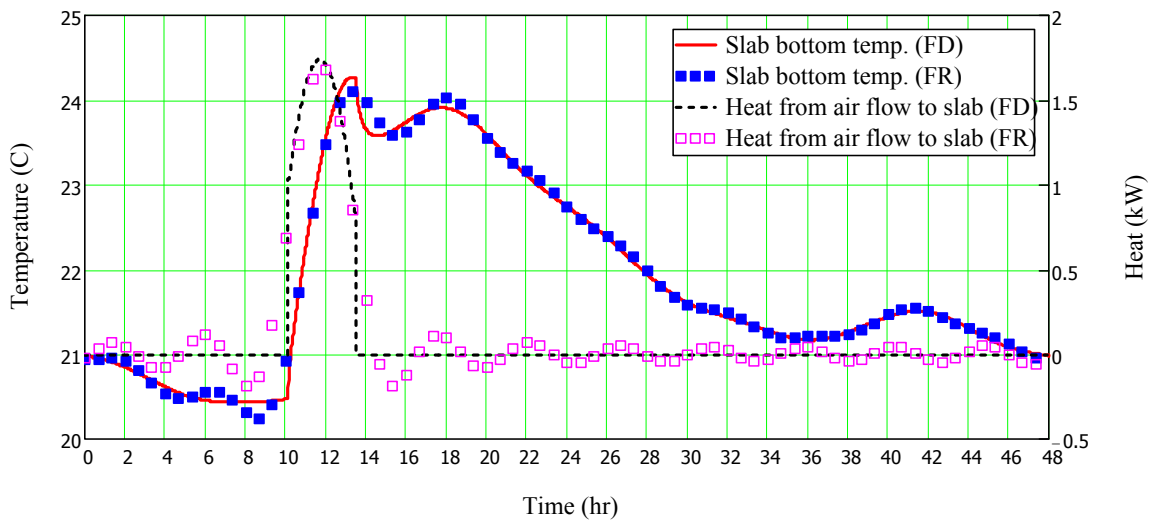

Fig. 3.17: 8-layer LPFD model vs. FR model for VCS-b (time step of 60 seconds, effective slab thickness of 0.2 m. Other information is in Table 3.4)

3.1.2. Non-periodic excitations

The LPFD model with a 2-layer discretization scheme is used to simulate the thermal behavior of a "b" type VCS, which is constructed and in use. The VCS slab is located at the basement of an energy-efficient solar house "ÉcoTerra", which has annual energy consumption about 10% of that of typical homes (Chen et al. 2010b, Doiron et al. 2011). The hot air is supplied from a building-integrated photovoltaic/thermal (BIPV/T) solar air collector (Chen et al. 2010a). The reason for choosing a 2-layer scheme is to superpose the positions of the capacitance nodes on the actual locations of the thermocouples (Fig. A2.1 in Appendix). The Biot number for the bottom layer of this 2-layer model is about 0.6, which is slightly larger than 0.5 suggested in previous subsection. The time step for the simulation is 180 seconds, which matches the measurement time interval.

A set of 24-hour data from a slab heating operation is compared with the simulation results from the LPFD model. The measured values are used as the initial values and the boundary

conditions. The heat transfer coefficients $_{chn_srf}u_b$ from the air to the slab and to the soil are calculated based on measured data (Chen et al. 2010a). Fig. 3.18 shows the measured excitation profiles. The curve "Flow rate on/off" in the figure is only an indicator of whether there is flow, not assigning to any y-axis.

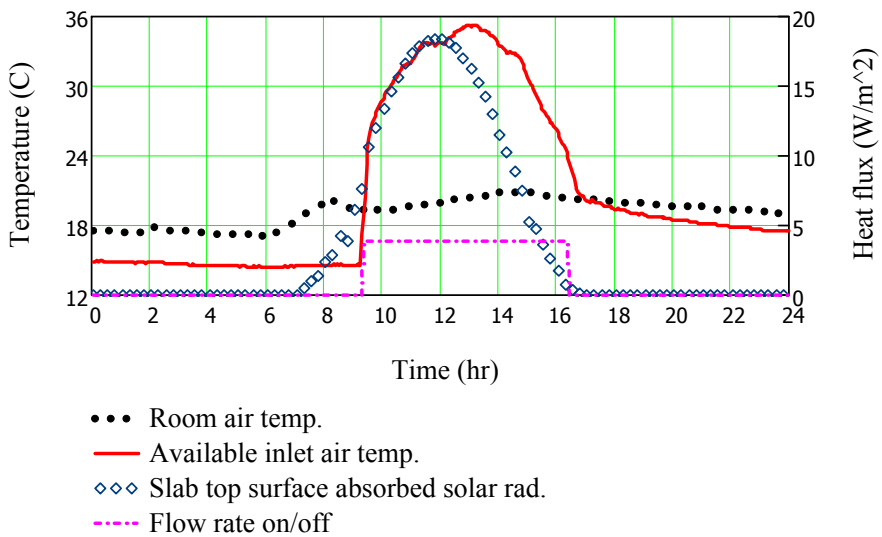

Fig. 3.18: Measured excitation profiles

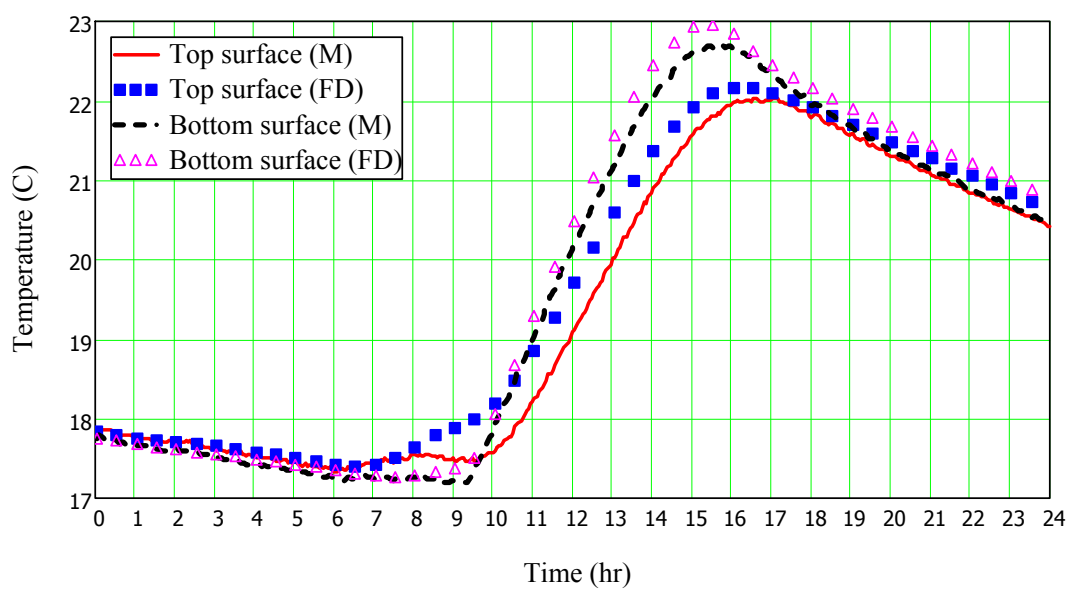

Fig. 3.19: Measured and simulated response profiles for VCS-b (2-layer LPFD model; time step of 180 seconds; equivalent slab thickness of 0.15 m)

Fig. 3.19 shows the measured and simulated thermal response of the slab. The shapes of simulated top and bottom surface temperature profiles are similar to the measurement, but with obvious discrepancy. The largest difference is at 9 am, where the simulated top surface temperature is about 0.6°C higher than that of the measurement. This discrepancy directly results in the following discrepancy during the slab heating operation (i.e. when air is flowing). There are several potential causes for this discrepancy. The first one is that the measured room air temperature (Fig. 3.18) does not reflect the exact value of the average temperature of the room air and the interior surfaces. The thermocouple for the room air is located 1.1 meters above the slab on an interior partition. From 6:30 am to 8:30 am, the forced-air space heating was on. The measurement could have been affected by the supply air temperature. Second cause may be that the thermocouples in the slab may be not located exactly at the top surface of the slab. It could be up to one or two centimeters lower than the top surface due to deficient workmanship during fresh concrete pouring. Other causes include the imperfect modeling of the boundary condition, such as the heat loss around the edge of the VCS and the CHTC between the slab top surface and the room air. See Subsection 4 "Discussion" for treatment of temperature-dependent natural CHTC. Nevertheless, the simulation result does not significantly differ from the measurement. The thermal energy changes in the slab between 10 am to 4 pm are 9.55 kWh by simulation, and 9.92 kWh based the average values of the measured slab temperatures. The difference percentage is 4% of the measured value.

FR analysis is not compared with the measurement because the excitation profiles are not periodic. However, the comparison between the FR and LPFD models in the previous subsection indicates that the FR models are capable of providing accurate results after

accommodating the non-periodic excitations into periodic excitations of longer periods, as discussed previously.

3.2. Modeling VCS-c

Y-diakoptic method and heat flow division are applied in the FR modeling of VCS-c systems. Based on the investigation from previous subsections, one can conclude that FR and LPFD models with time step up to half an hour can still provide satisfying results. Hence, thermal models for 'c' type VCS are created using time step of half an hour time. 3-layer discretization scheme (layer thickness of 0.05, 0.1, and 0.05 m from top to bottom) on the transformed cross section (Fig. 3.13-c) is used for the LPFD models. Simulations are first run under the excitations depicted in Fig. 3.14, and then the top surface radiation is increased to 4 times of the previous value to study the discretization criteria under high surface heat flux conditions.

Fig. 3.20 shows the comparison of the simulation results under the excitations shown in Fig. 3.14. Total heat flow from air to slab is 7.52 kWh for the FR model and 7.97 kWh for the LPFD model. The maximum temperature difference is 0.60°C at the source level of the slab, and 0.58°C for the outlet air. The temperature difference is mainly caused by the overshoots/undershoots of the DFS-represented profiles of the excitations as discussed earlier. These two models provide similar results. This indicates that the modeling techniques (i.e. Y-diakoptic method, heat flow division, and iteration procedure) of the FR model are successful and reliable.

Another study is conducted for surface exposed to high heat flux situations. This is to emulate the passive solar heating situation – the VCS-c is exposed to strong transmitted solar radiation, besides heat flow from channel air. Assumption of uniform solar radiation incident

on the floor is adopted in the models. In reality, normally only part of the top surface is exposed to direct solar radiation and the illuminated area will have a relatively high temperature. FR and LPFD models are not able to simulate local temperatures; however, the assumption of uniform incident is acceptable for overall estimation of space heating/cooling energy consumption (Athienitis and Chen 2000).

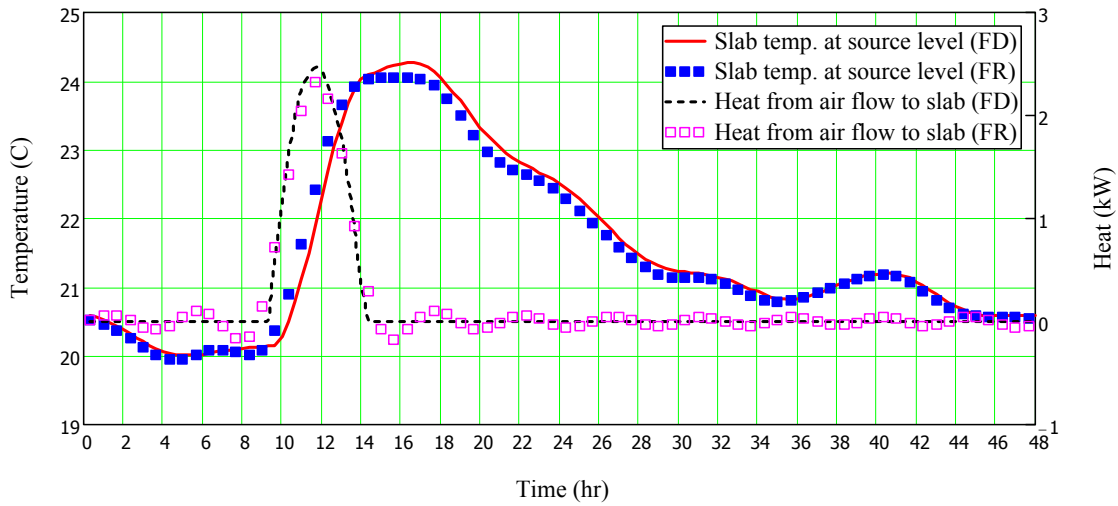

Fig. 3.20: 3-layer LPFD model vs. FR model for VCS-c (time step of half an hour, equivalent slab thickness of 0.2 m)

When the top surface absorbed solar radiation is increased to 4 times of the original values in Fig. 3.14, the total heat from air to slab is 5.20 kWh from the FR model. For LPFD models with 3-layer discretization scheme, it is 5.70 kWh with a time step of half an hour, and 5.55 kWh for a time step of 10 minutes. For half-an-hour time step, the maximum temperature difference is 0.57°C at the source level of the slab, and 0.56°C for the outlet air. The resulting profiles from FR and 3-layer LPFD simulations (Fig. 3.21) are close to each other as they were in the previous cases. When the discretization is changed to 5-layer scheme (layer thickness of 0.02, 0.04, and 0.08 m from top to center), the heat is 5.45 kWh for time step of 10 minutes (maximum time step is limited by equation stability).

To calculate the required ${}_{edge_CV}Th$, the radiative heat flux is converted into an equivalent ${}_{eqv}h$, and hence ${}_{crt}h = {}_{cnv}h + {}_{eqv}h$. In the case considered here, the slab surface on average is about 3°C higher than that of the room air during strong radiation period (comparing Fig. 3.14 and Fig. 3.21) (i.e. ${}_{cnv}\Delta T = 3$°C). Since the average surface radiation is about 100 W/m^2, ${}_{eqv}h$ is then about 35 W/m^2/K. Therefore ${}_{crt}h = {}_{eqv}h + {}_{cnv}h \cong 45$ W/m^2/K. With ${}_{Biot}No = 0.5$, which is suggested for VCS-b LPFD models, the required ${}_{edge_CV}Th$ is 0.02 m. This suggests that the 5-layer model is preferable.

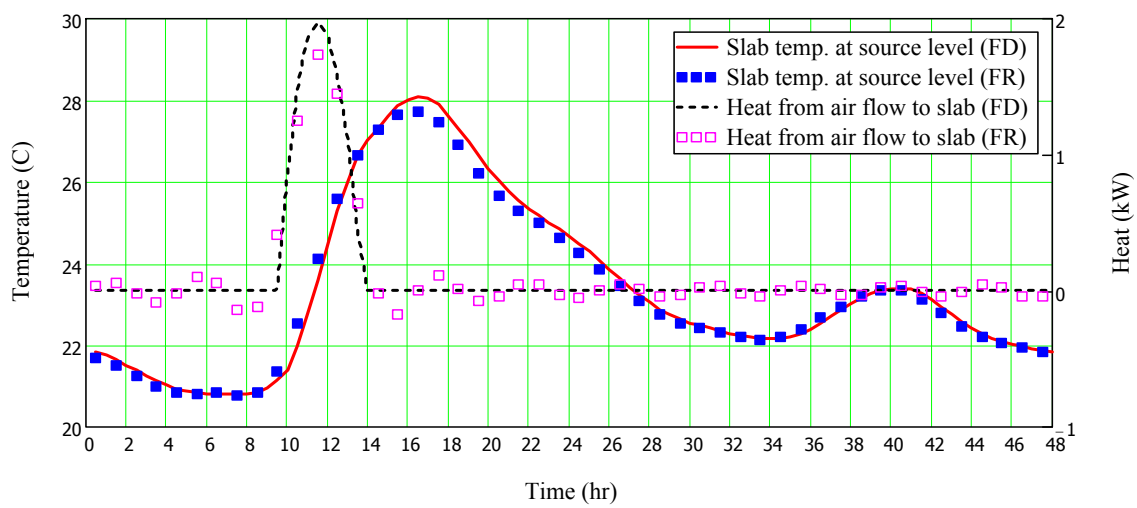

Fig. 3.21: FR model and 3-layer LPFD model for VCS-c under high absorbed solar radiation (time step of half an hour, equivalent slab thickness of 0.2 m)

4. Discussion

In the FR approach, the thermal characteristics of assemblies have to be constant in the calculation of the overall transmission or admittance matrices. Hence, the treatments of temperature-dependent (i.e. non-linear) or time-varying variables, such as the CHTC, require linearization. In the case of heat exchanges between the room air and the interior surfaces, the varying air movement and temperature difference between the room air and the surfaces

will affect the real time CHTC, ${}_{real_c}h_i$. To resolve this problem, a correctional heat flux $\Delta p_i = \left({}_{real_c}h_i - {}_{M}h\right) \cdot \left({}_{srf}T_i - {}_{air}T_i\right)$ can be added to the air node to compensate the error introduced by using constant CHTC, ${}_{M}h$, in the calculation of the transmission matrices, according to the substitution theorem (Athienitis et al. 1987). Similar technique can be used for other non-linear and time-varying situations.

The ideal Biot number (${}_{Biot}No$) suggested above is based on the discretization scheme adopted in this section (paper) – layer thickness increases inward. In cases that critical ${}_{crt}h$ is not on the slab outer surface but at the air channel surface, such as the slab is covered with carpet or wood flooring, the thinnest layer should be of the CV at the air channel surface. Since the suggested ideal Biot number (0.5) is not small (i.e. the thinnest CV is not so thin), evenly thick layers can be adopted for discretization. With a 0.5 Biot number, the thickness of the CV surrounding air channel will be smaller than that in the increasing-inward schemes. The potential error introduced can be expected to be smaller.

When temperature-controlled heat sources (heat source is always available if needed and its power output is dependent of the temperature variable, e.g. electric wire heating) are involved in thermal response analysis, the network formulation techniques by Athienitis et al. (1987) can be applied to obtain the thermal response of room components by solving systems of equations. In the case of air as the heat transfer fluid, the mean air temperature and the CHTC depend on flow rate and the air channel surface temperature, and hence does the heat flux from the air flow. Furthermore, the inlet air temperature may be a function the flow rate or other variables, such as air from a solar air collector (Chen et al. 2010a). Therefore the formulation techniques may not be suitable or readily implemented. However, alternatively the heat injection from air to the slab can be calculated through iteration.

The excitation profiles used for above simulations represent the practical operating conditions measured in full-scale studies such as in references (Chen et al. 2010a, Chen et al. 2010b). By comparing with on-site monitored data, the practicability of LPFD model is evaluated. By comparing the simulation results from LPFD and FR models, the reliability of FR models are also evaluated. These comparisons indicate that both LPFD and FR models are able to provide satisfactory results under practical operation conditions.

5. Conclusion

In previous paper Part 1 (Section 3.2), modeling techniques for frequency response (FR) approach and lumped-parameter finite difference (LPFD) approaches for building-integrated thermal energy storage (BITES) systems are presented. Ventilated concrete slab (VCS) systems are used in this part for demonstration of the methodology.

The modeling techniques are applied to two kinds of VCS – one has air channel at the bottom of the mass (VCS-b) while the other kind has hollow cores as air channel (VCS-c). The explicit LPFD and FR models generate almost identical outcomes under periodic conditions. Accuracies of different discretization configurations and choices of time step are quantified. Time step of half an hour for FR models typically results in less than 3% error in thermal performance. For LPFD models, discretization with Biot number smaller than 0.5 can reduce error to about 5%. Larger Biot number tends to overestimate the heat flow from air to slab over time. For practical slab thickness (0.1 to 0.2 m), simulation results from 2-layer VCS-b and 3-layer VCS-c models with time step of half an hour have errors less than 9%. LPFD simulation results under non-periodic conditions were presented for VCS-b and compared with field-measured data from a near net-zero energy solar house.

Chapter 4 Design of predictive control strategies for active BITES systems using frequency domain model

This chapter contains one ready-for-submit manuscript titled the same as the chapter.

Chapter Abstract

Active building-integrated thermal energy storage (BITES) systems, such as ventilated concrete slabs, can help exploit the benefits of thermal energy storage when properly operated. The desire of satisfying thermal comfort and utilization of cheap or renewable energy, together with BITES' slow thermal response, place challenges in the operation of BITES systems. With suitable temperature set-profiles and estimated corresponding thermal loads, frequency domain models of active BITES systems can provide predictive operation information for the systems. This section (paper) presents a frequency domain methodology for the control of active BITES systems. The modeling and calculation approaches for the active BITES configurations of closed-loop and open-loop to room interior are presented. Using frequency domain models for design optimization of active BITES systems will also be discussed.

1. Introduction

Even though active BITES systems have shown high potential for improving thermal and energy performance of buildings, challenges exist for their efficient operation (i.e. charge and/or discharge) and design due to the following key factors and requirements (See Chapter 1for more discussion):

(1) Active BITES systems have strong thermal coupling with their thermal zone;

(2) High thermal inertia of BITES systems and their thermal zones;

(3) Need to improve building energy performance through use of active BITES systems.

Controls of active BITES systems usually employ conventional feedback control strategies, often controlling surface temperature to operate the active BITES systems so as to satisfy thermal comfort requirement (ASHRAE 2011, Simmonds 1994, Turner and Tovey 2006). These control strategies do not systematically improve the building energy performance through the TES function of BITES systems. To take better advantage of the TES function, Athienitis and Chen (1993) and Athienitis (1997) proposed control strategies using time-varying (e.g. sinusoidal or ramp) set points for the room air temperature. Recently, model-based predictive (or anticipatory) control (MPC) has attracted significant attentions, especially with optimal control approaches (Candanedo and Athienitis 2010, Kummert et al. 2000, LeBreux et al. 2006, 2009). Transfer functions derived from physics-based and inverse thermal models (i.e. data-driven models) are often used (Armstrong et al. 2006a, Candanedo et al. 2011, Gwerder et al. 2008, LeBreux et al. 2006).

Suitable room temperature, among other factors, is critical in satisfying thermal comfort requirement. Its profile bounds the operations of the active BITES system, and hence bounds the energy performance. In this study, room temperature set-profile will be used as

input for the predictive control of active BITES systems. The objective is to satisfy the thermal comfort requirement on room temperature, as well as to enhance the building energy performance while reducing peak heating/cooling loads.

With frequency domain models, if the required temperature and heat flux on one surface of an assembly are known, the temperature and heat flux on the other side of the active BITES can be calculated analytically. Furthermore, active BITES systems can be ideally designed with the analysis of key frequency domain transfer functions. Thus, frequency domain models can integrate and facilitate the design and operation of active BITES systems.

In the frequency domain modeling, discrete complex variables and transfer functions are used. Time-series values (e.g. temperature readings in different time intervals) are represented with complex discrete Fourier series (DFS). See Appendix for more information. The main assumption made is linear or linearized systems. The thermal characteristics of all material are assumed to be linear and time-invariant (e.g. conductivity and specific heat capacity do not depend on temperature or time). Although individual processes such as convection and radiation exchanges are nonlinear, the temperature differentials involved are generally small, so their linear approximations are usually adequate. Suitable techniques can also be applied to improve accuracy.

2. Methodology

Buildings with much thermal storage (i.e. BITES) can store a considerable amount of heat or coolness for later use. Thus, for their efficient utilization, it is important to predict the upcoming heat gains/losses due to forecasted weather and occupancy/internal gains. Then, by using a desirable room temperature set-profile, the proper heat/cool injection rates for a BITES system and the associated heating/cooling into its zone can be predicted using

frequency domain transfer functions over a prediction horizon (Fig. 4.1), which is typically about a day. Here, the establishment of zone temperature set-profile follows a heuristic approach based on building physics - taking into account the need to reduce peak demand, use renewable energy and satisfy comfort. Future research can involve optimization techniques. In this subsection, the main concepts and techniques used in each part of Fig. 4.1 will be discussed and exemplified. This thesis focuses on predictive control strategies useful at the design stage and not their actual implementation.

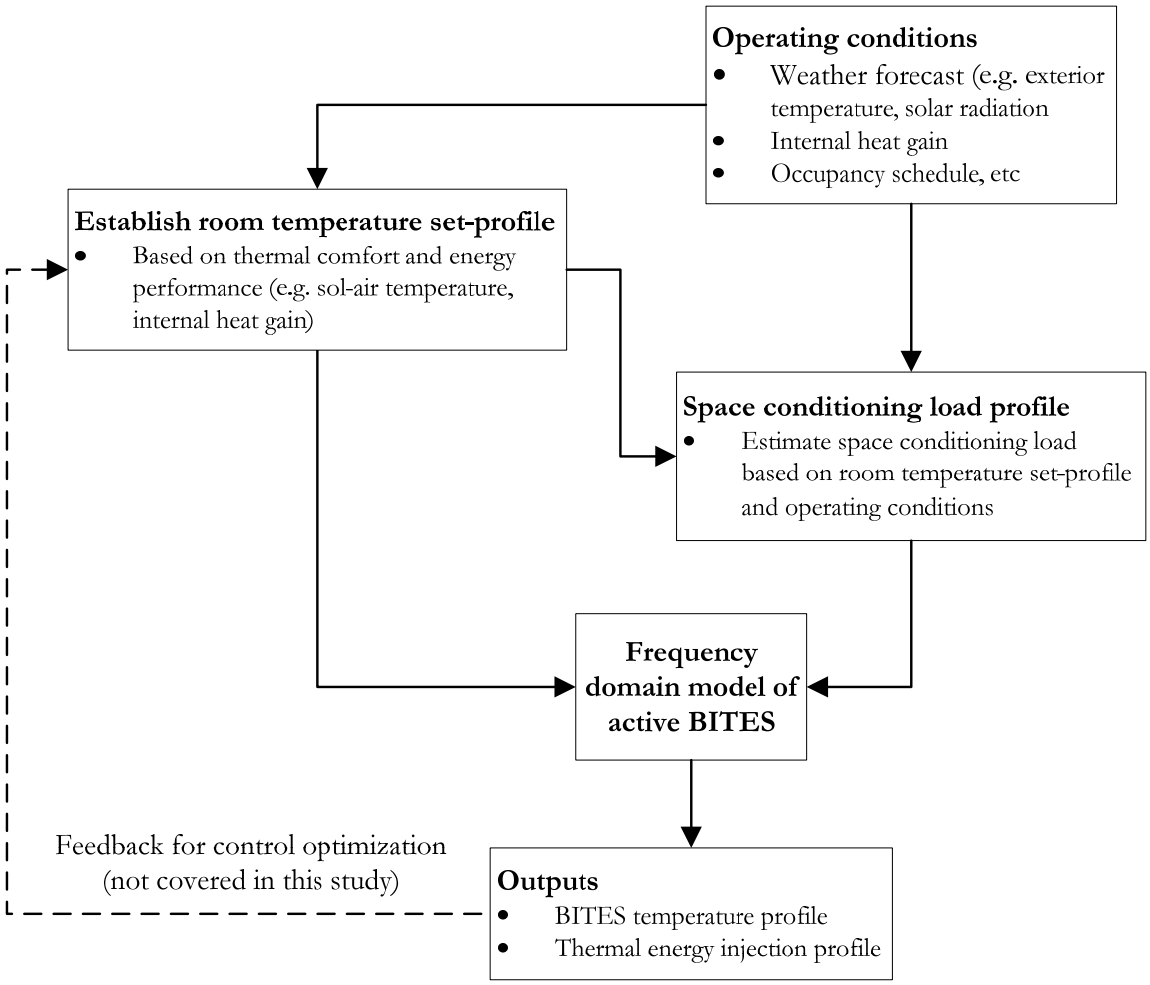

Fig. 4.1: Predictive control strategy flowchart

2.1. Room air temperature set-profile

In this methodology, a desirable room temperature set-profile (chosen based on heuristics) is used to obtain the operation of an active BITES system's charge/discharge. In addition to the consideration that the thermal behavior of the room and its BITES are strongly coupled, another main reason for adopting this approach is that appropriate room temperature is critical both to thermal comfort and overall energy performance of the building.

Thermal comfort factors related to room temperature are the operative temperature, interior surfaces' temperatures, and their fluctuation rates. Thermal comfort standards have suggested that for occupants wearing normal indoor footwear, the floor surface temperature should be within 19 to 27°C for less than 10% of occupants dissatisfied. The rate of operative temperature change should not be more than 1.1°C within 0.25 hours or 3.3°C within 4 hours according to ASHRAE (2004b). Since thermal comfort is subjective, building designers can initiate the temperature set point and throttling range according to standards, and allow occupants to adjust.

From the energy performance point of view, room temperature setting affects the space conditioning load and amount of thermal energy can be charged/discharged (i.e. pre-conditioning and buffering). For example, the temperature difference between the exterior and the interior defines the heat loss/gain of the interior due to infiltration and conduction through envelope, and ventilation. Under a free-floating room temperature condition, the thermal buffering effect of indoor mass may possibly balance its heat gain/loss. In passive solar heating during a cold sunny day, allowing the room temperature to rise will enable high storage of useful solar heat gain in the thermal zone (BITES system and other indoor mass). Hence, less space heating is needed for the following period; this is a simple but effective

predictive control strategy that needs weather prediction of about a day – something routinely available from Environment Canada.

In this methodology, room air temperature set-profile is established as a function of exterior temperature, solar radiation, and the thermal dynamics of the room. The room temperature follows the outdoor sol-air temperature with a first-order time lag (ASHRAE 2009c). The time lag is calculated as a function of the time constant of the room. This approach approximates the natural response of the room to its varying boundary conditions, and avoids sudden changes on the thermal output requirement of the active BITES systems. When sol-air temperature is ideal for building pre-heating/pre-cooling, the room air temperature will change faster. The temperature difference between the room and the exterior sol-air temperature (ASHRAE 2009e) is reduced within the allowable room temperature range in order to reduce space conditioning load.

A room air temperature set-profile during a space heating period (Fig. 4.2) is used here for brief demonstration. At first, a room temperature set-profile bound is constructed using 22.5°C as the set point with a throttling range of 5°C centered at the set point. In other words, the room temperature will not be lower than 20°C or higher than 25°C. Following the first-order time lag function, the rise of the room temperature (hour 9.5) lags behind the rise of the sol-air temperature (hour 7.5). The room temperature rises during sunny period to allow high storage of solar heat gain in the BITES and the rest of the room, and drop naturally after sunset to reduce the temperature difference between exterior and interior. With respect to thermal comfort, this temperature set-profile complies with upper and lower temperature limits and avoids rapid changes.

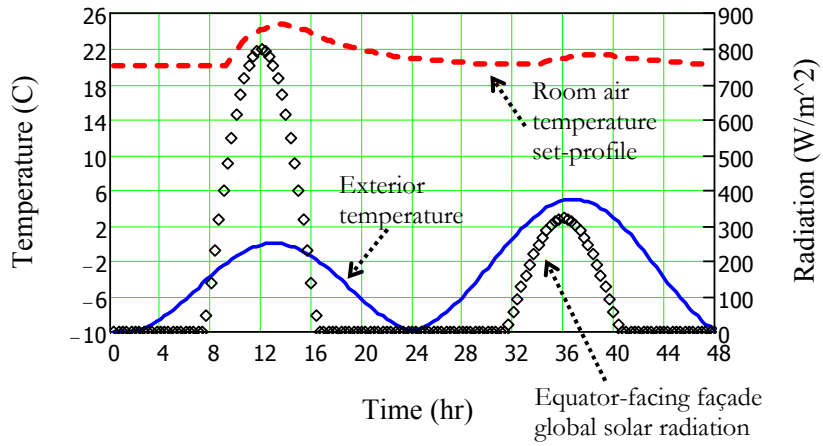

Fig. 4.2: Weather conditions and room air temperature set profile during a two-day space heating period (sunny day followed by cloudy day)

This preliminary approach enhances the thermal and energy performance of the room to a certain extent. It reduces space conditioning load and enhances charge/discharge at desirable time. Further optimization of temperature set-profile can be adopted. Occupancy schedule, internal heat gain, weather conditions, availability of ambient renewable energy, room thermal response, and utility energy fee structure can also be considered in establishing room temperature set-profiles. Using the outputs as feedback (dashed line in Fig. 4.1) for predictive control optimization and real time implementation is not covered in this thesis. Approaches for the optimization of room temperature profile need to be studied in future research.

2.2. Space conditioning load profile

After establishing the room air temperature set-profile, another measure is needed to estimate the space conditioning loads (i.e. the required thermal output from the BITES system). An explicit finite difference thermal model of the room is created to perform this estimation. Besides the forward approaches (or physical thermal models) such as the one

used here, data-driven (inverse) models, such as Black-Box (empirical) or Gray-Box types of models (ASHRAE 2009a), can also be used to estimate the space conditioning load (Armstrong et al. 2006a, b, ASHRAE 2009a, Braun et al. 2001). Data-driven models can be trained and further fine-tuned with filed-measured (i.e. online) data (Nassif et al. 2008). Self-tuning models may be more appropriate because of the various uncertainties of the built environment and occupant behavior.

The space conditioning load estimation uses a finite difference model. This finite difference thermal model is also used to help with the development and verification of the control methodology, as presented later. A 10.5m (length) x 3m x 3m room is used for demonstration. This room has five square meters of windows on the long façade facing the equator. An active BITES system is located on the floor of the room. Table 4.1 lists the key parameters of the room. The finite difference thermal model of the room will calculate the room's space conditioning loads based on the room air temperature set profiles.

The set profile of room air temperature for a winter period and the weather conditions are shown in Fig. 4.2. The required space conditioning (i.e. thermal output required from the active BITES system) is calculated with the finite difference room thermal model and shown in Fig. 4.3. The room air heat gain/loss is due to internal heat gain (e.g. appliance, human body), transmitted solar radiation, ventilation, infiltration, and conduction through envelope. The small spikes are due to cooking. Some key treatments in the calculation are as follows:

- The room air temperature set profile is represented with complex discrete Fourier series (DFS) (Fig. 4.3, 6 harmonics is used for DFS). Then, the DFS-represented values will be converted back to time domain and used to calculate the space conditioning loads;

- When calculating the space conditioning load, the active BITES floor including the solar radiation impinging is separated from the rest of the room;
- The required thermal output of the BITES including the release of its absorbed solar radiation is set equal to the room space conditioning load.

Table 4.1: Key parameters of the room thermal model

Parameters	Values	Note
Concrete slab thickness	0.3 meters	
Location of source layer in concrete	0.108 meters below the top concrete surface	Source layer in Fig. 4.4
Thermal insulation under concrete slab	0.5 $W/m^2/K$	
Total envelope thermal conductance	32 W/K	Ventilation and infiltration heat/gain is included
Room air temperature	Set point of 22.5°C, and throttling range of 5°C	
Effective thermal storage capacitance of room	50 times room air capacitance	Including indoor objects such as furniture
Thermo-physical properties of concrete	840 J/kg/K for specific heat; 2200 kg/m^3 for density; 1.7 W/m/K for conductivity	Constant
Thermo-physical properties of air	1300 $J/m^3/K$ for volumetric heat capacity	Constant
Soil node temperature	10°C	Constant

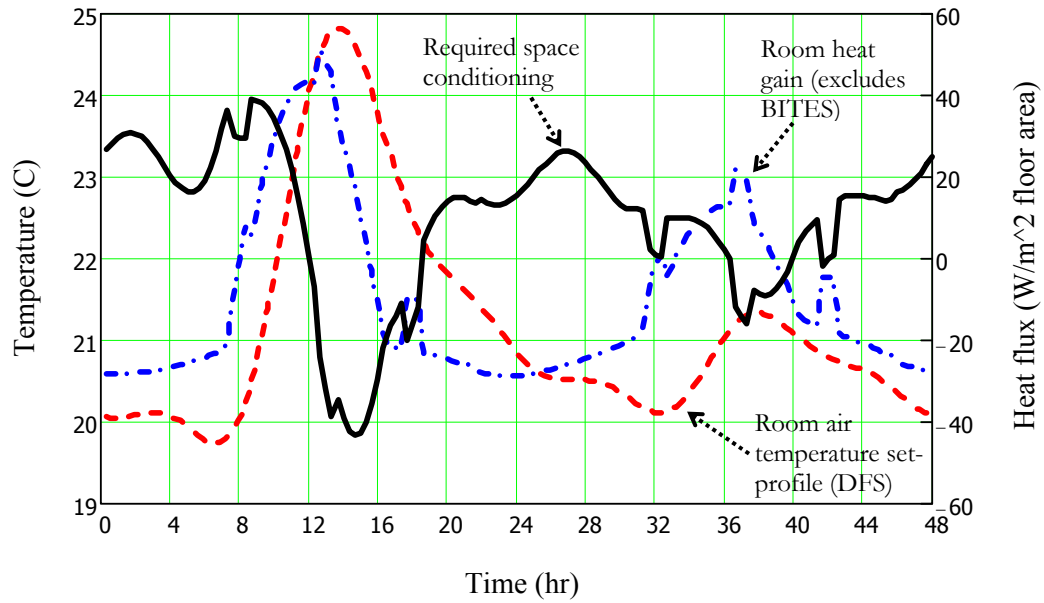

Fig. 4.3: DFS represented room air temperature set-profile and corresponding energy profiles

2.3. Source layer temperature and thermal energy injection rate

One-dimensional thermal model for active BITES systems (Section 3.2 and Section 3.3 in Chapter 3) is used in this study. The active BITES slab (Fig. 4.4) is used for demonstration. It can be represented with an assembly consisting of N layers of material (Fig. 4.5). Using discrete frequency response modeling, the oscillatory responses of heat flux ${}_{0}^{1}\tilde{p}_{i,h}$ and temperature ${}_{0}^{1}\tilde{T}_{i,h}$ at surface 0 of layer 1 due to excitations ${}_{l}^{N}\tilde{p}_{i,h}$ and ${}_{l}^{N}\tilde{T}_{i,h}$ on surface l of layer N can be calculated with Eq. (4.1) (Carslaw and Jaeger 1959, Kimura 1977). The right-hand side subscript i means the ith time interval, and h is the harmonic index. The mean responses can be obtained in a similar way with the transfer functions matrix ${}_{trs}^{1\leftarrow N}[M]_h$ replaced with a thermal resistance matrix. Then the total responses in frequency domain at surface 0 will be ${}_{0}^{1}\hat{T}_i = {}_{0}^{1}\bar{T} + \sum_{h=1}^{H}\left({}_{0}^{1}\tilde{T}_{i,h}\right)$, and ${}_{0}^{1}\hat{p}_i = {}_{0}^{1}\bar{p} + \sum_{h=1}^{H}\left({}_{0}^{1}\tilde{p}_{i,h}\right)$. Time domain values can then be obtained through ${}_{0}^{1}T_i = Re\left\{{}_{0}^{1}\hat{T}_i\right\}$ and ${}_{0}^{1}p_i = Re\{{}_{0}^{1}\hat{p}_i\}$, where $Re\{\quad\}$ takes

the real part value from the complex number. See Appendix for more information on discrete frequency response modeling.

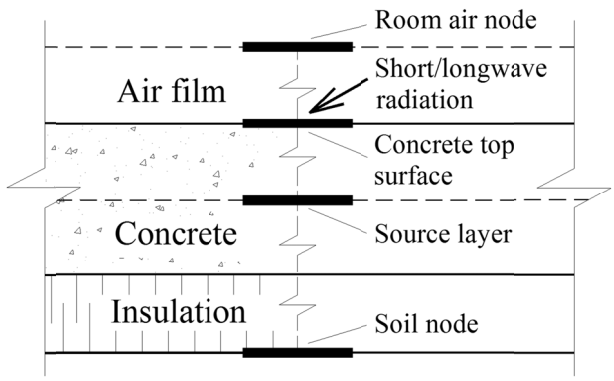

Fig. 4.4: Thermal network of an active BITES floor with its cross section transformed

$$\begin{bmatrix} {}^{1}_{0}\tilde{T}_{i,h} \\ {}^{1}_{0}\tilde{p}_{i,h} \end{bmatrix} = {}^{1\leftarrow N}_{trs}[M]_h \cdot \begin{bmatrix} {}^{N}_{l}\tilde{T}_{i,h} \\ {}^{N}_{l}\tilde{p}_{i,h} \end{bmatrix} \tag{4.1}$$

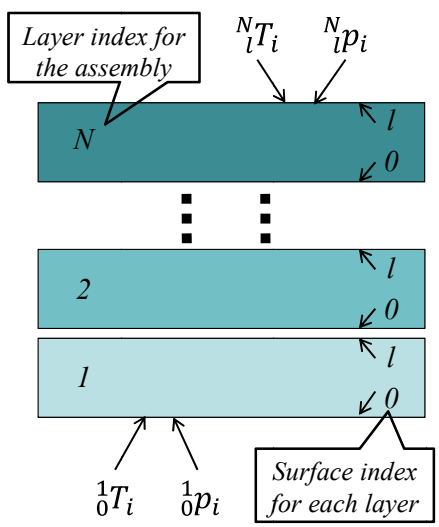

Fig. 4.5: Schematic of an N-layer assembly, and its excitations (same as Fig. 3.10)

Similarly, let room air node be at surface l of N layer, and excitations ${}_{rm}\tilde{T}_i$ and ${}_{CR.B}\tilde{p}_i$ be the room air temperature and the heat flux from the BITES exposed surface to the room air, respectively. Also, let BITES source layer (Fig. 4.4) be at surface 0 of layer 1, and surface 0

be adiabatic to its exterior boundary (e.g. the concrete underneath the source layer). The responses ${}_{sc}\tilde{T}_i$ and ${}_{sc}\tilde{p}_i$ at time interval i at source layer can be calculated with Eq. (4.2), given that ${}_{rm}\tilde{T}_i$ and ${}_{CR.B}\tilde{p}_i$ are known. In reality, source layer (i.e. surface 0 of layer 1) is not adiabatic to the exterior boundary of the assembly. Heat flux through BITES to the room air node will also include those from the heat sources and temperatures of the exterior boundary. A portion of source heat flux will also be distributed to the exterior boundary. Detailed calculations are presented in Subsection 3.

$$\begin{bmatrix} {}_{sc}\tilde{T}_{i,h} \\ {}_{sc}\tilde{p}_{i,h} \end{bmatrix} = {}^{sc\leftarrow rm}_{trs}[M]_h \begin{bmatrix} {}_{rm}\tilde{T}_{i,h} \\ {}_{CR.B}\tilde{p}_{i,h} \end{bmatrix} \tag{4.2}$$

Considering the energy balance at the room air node, ${}_{CR.B}p$ is the combined convective and radiative thermal output to the room from the room-side exposed surface of the BITES. It compensates the room air heat gain/loss, and hence maintains ${}_{rm}T$ at its set values. With an open-loop system (Fig. 1.8-b), the thermal output from the BITES includes an advective portion ${}_{A.B}p$, accounting for the air flow released directly to the room. The calculation for ${}_{A.B}p$ is shown later.

3. Applications

In this subsection, control methodology and detailed calculation approaches will be demonstrated on a closed-loop BITES floor system (Fig. 1.8-a) in the room described previously, and then on an open-loop system (Fig. 1.8-b) for the same floor. The profiles of the room air temperature and the required thermal output are shown in Fig. 4.3. The thermal model of the active BITES floor is shown in Fig. 4.4 (closed-loop or open-loop). The calculated thermal energy injection rates are verified with the explicit finite difference model

described previously. In the verifications, the room air temperature is not set, but calculated based on the thermal energy injection rate to the active BITES floor and thermal energy balance of the room. Results for space heating scenario and further treatment for thermal energy injection rates are presented below in detail, followed by the brief results for cooling scenario. In the following paragraphs and figures, "predicted" values are calculated using the methodology, while "simulated" values are from the verifications.

3.1. Closed-loop BITES systems

Fig. 4.6 shows the thermal network of the closed-loop BITES floor with its boundary conditions. In addition to the convective and radiative heat exchange with the room, the exposed surface of BITES receives solar radiation ${}_{slr}p$ transmitted through the windows.

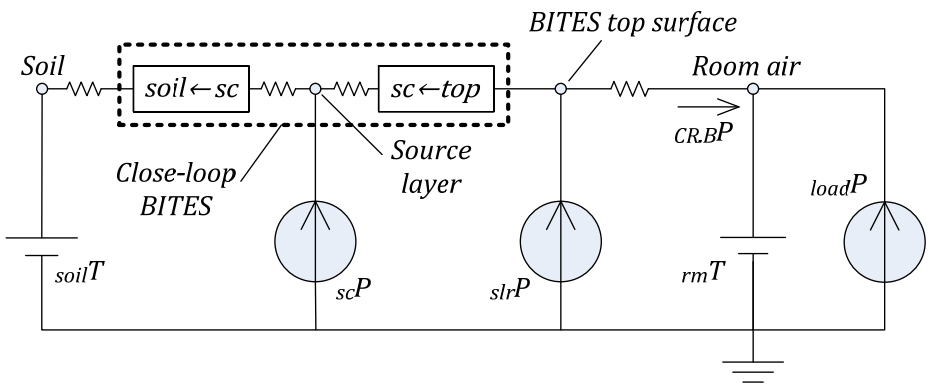

Fig. 4.6: Simplified thermal network of a room with a closed-loop BITES system sitting on soil (Fig. 4.4)

3.1.1. Formulation for closed-loop system

The convective heat transfer coefficient (CHTC) between the BITES exposed surface and the room air (i.e. air film in Fig. 4.4) is highly temperature-potential dependent – the heat transfer between these two nodes is not linear). Without proper treatment, the air film cannot be included in the assumed linearized system. Otherwise, significant errors may arise.

Considering the fact that instant thermal output from the exposed surface equals to the required thermal input to the room air node (i.e. no thermal capacitance between these two nodes), the thermal output ${}_{CR.B}p$ from the exposed surface and the surface temperature ${}_{top}T$ (instead of ${}_{rm}T$) can hence be used to calculate the source layer temperature ${}_{sc}T$ and the required thermal energy injection rates ${}_{sc}p$. Thus, the air film is not included in this sub-assembly. When the room air temperature ${}_{rm}T$ and the required thermal output from the top surface ${}_{CR.B}p$ are known, ${}_{top}T$ can be obtained by solving Eq. (4.3) and (4.4) simultaneously or by iterations to account for the change in the value of the film coefficient.

$$ {}_{top}T_i = {}_{CR.B}p_i / {}_{top}h_i + {}_{rm}T_i \tag{4.3} $$

$$ {}_{top}h_i = {}_{c.top}h_i + {}_{r.top}h = fn\left({}_{rm}T_i\,,\,{}_{top}T_i\right) + {}_{r.top}h_i \tag{4.4} $$

where $fn(a\,,b)$ means a function of a and b. ${}_{top}h$ is the combined convective and radiative heat transfer coefficient. An empirical formula Eq. (4.5) (ASHRAE 2009d) is used to determine the convective part ${}_{c.top}h$. A constant value of 4.5 W/m^2/K can be used for the radiative part ${}_{r.top}h$ under practical conditions (i.e. temperature difference between floor surface and the rest of room is less than 10°C) with negligible errors.

$$ \begin{aligned} {}_{c.top}h &= 2.42 \cdot \frac{|\Delta T|^{0.31}}{{}_{rm.c}L^{0.08}} \quad \text{when heating upward or cooling downward} \\ {}_{c.top}h &= 0.2 \cdot \frac{|\Delta T|^{0.25}}{{}_{rm.c}L^{0.25}} \quad \text{when heating downward or cooling upward} \end{aligned} \tag{4.5} $$

where ΔT is the temperature difference between the surface (${}_{top}T$ in this case) and the room air. ${}_{rm.c}L$ is the characteristic length of the room (4.7 meters in this case).

The combined convective and radiative thermal output ${}_{CR.B}p$ should equal to the space conditioning load. It is a combined output from different sources (e.g. a temperature potential across an assembly and heat flux absorbed on a surface) (Eq. (4.6)). Since the thermal system in question is linear, different attributions to ${}_{CR.B}p$ can be calculated separately. Then the required thermal energy injection rates ${}_{sc}p$ equal to the differences between the required ${}_{CR.B}p$ and the summed output from other sources. The following equations calculate the oscillatory responses of the variables in question. The mean responses and then the final values in the time domain are calculated in similar ways as discussed in Subsection 2.3. Subscript h for harmonic is omitted hereafter.

$$ {}_{CR.B}\tilde{p}_i = {}_{sc_top}\tilde{p}_i + {}_{slr}\tilde{p}_i + {}_{soil_top}\tilde{p}_i \tag{4.6} $$

where ${}_{slr}p$ is the transmitted solar radiation absorbed by the BITES top surface

The oscillatory part of the heat flux flowing to the floor top surface due to the temperature difference between the top surface and the soil, ${}_{soil_top}p$, can be calculated with Eq.(4.7).

$$ {}_{soil_top}\tilde{p}_i = {}_{soil}\tilde{T}_i \cdot {}^{soil \leftarrow top}a21 + {}_{top}\tilde{T}_i \cdot {}^{soil \leftarrow top}a22 \tag{4.7} $$

where $a22$ and $a21$ are from admittance matrix ${}_{adm}[M]$ of assembly $soil \leftarrow top$ (i.e. the concrete and the insulation layers in Fig. 4.4). See Appendix for more detail on admittance matrix.

The remaining portion of ${}_{CR.B}p$ due to thermal energy injection at source layer can be calculated according to Eq. (4.8):

$$ {}_{sc_top}\tilde{p}_i = {}_{CR.B}\tilde{p}_i - {}_{slr}\tilde{p}_i - {}_{soil_top}\tilde{p}_i \tag{4.8} $$

Hence, the required thermal energy injection rates can be obtained by reversing the heat flow division equation (Chapter 3):

$$ {}_{sc}\tilde{p}_i = {}_{sc_top}\tilde{p}_i \cdot \frac{{}^{soil\leftarrow top}t12}{{}^{soil\leftarrow sc}t12} \tag{4.9} $$

where $t22$ and $t21$ are from two different transmission matrices ${}_{trs}[M]$. See Appendix for more information on transmission matrices.

The mean response of the heat flow ${}_{sc}\bar{p}$ can be calculated similarly.

$$ {}_{soil_top}\bar{p} = \left({}_{soil}\bar{T} - {}_{top}\bar{T}\right) / {}^{soil\leftarrow top}r $$

and

$$ {}_{sc}\bar{p} = {}_{sc_top}\bar{p} \cdot \frac{{}^{soil\leftarrow top}r}{{}^{soil\leftarrow sc}r} $$

where ${}^{soil\leftarrow top}r$ is the thermal resistance between the soil and the top surface, and ${}^{soil\leftarrow sc}r$ is the thermal resistance between the soil and the source layer.

Finally, the required thermal energy injection rates at source layer in the time domain

$$ {}_{sc}p_i = {}_{sc}\bar{p} + Re\left\{\sum_{h=1}^{H} {}_{sc}\tilde{p}_{i,h}\right\} \tag{4.10} $$

After obtaining the required ${}_{sc}p$, the source layer temperature ${}_{sc}T$ is also needed in order to calculate the required inlet temperature of the fluids. This will be presented in Subsection 3.2. Even though Eq. (4.2) is not directly shown in the above equations, these equations are derived from Eq. (4.2) and the theory behind it (Chapter 3).

3.1.2. Preliminary results for space heating scenario

The thermal energy injection rates at the source layer predicted with the frequency domain model (Eq. (4.7) to (4.10)) are used in the finite difference thermal model to simulate the thermal responses of the room and its closed-loop BITES floor (Fig. 4.7 and Fig. 4.8). Both the temperatures of the room air and the floor top surface (Fig. 4.8) comply with thermal comfort requirement. As seen in Fig. 4.7, even though the thermal output does not precisely follow the required space conditioning, the resulting room air temperature closely matches the set-profile well. This is due to the high thermal storage mass of the room and the BITES. Using more harmonics for DFS representation will improve the matching; however, this is not necessary as the room temperature requirement is well satisfied.

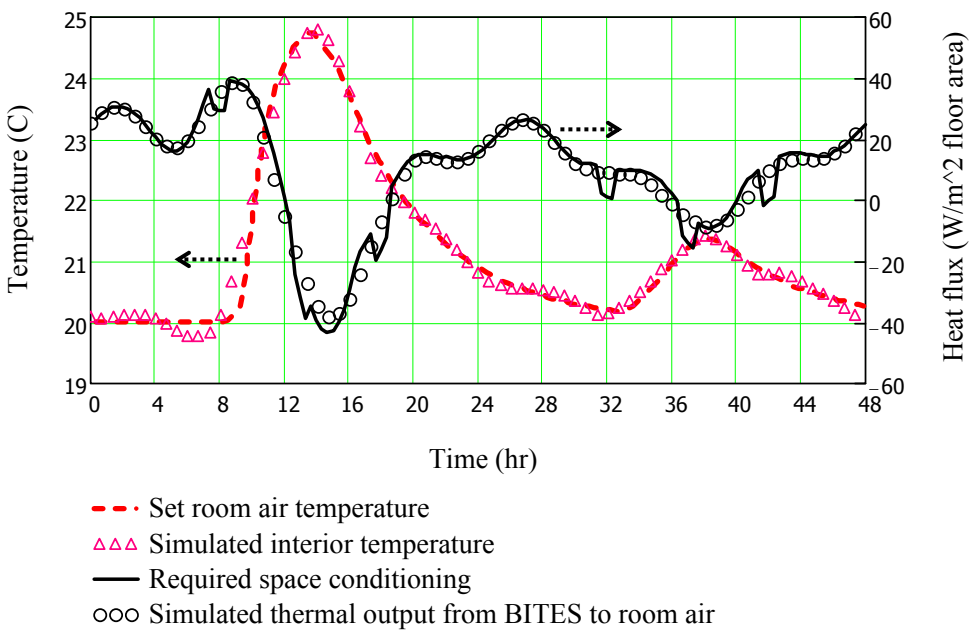

Fig. 4.7: Comparison of set and simulated room air temperatures and BITES thermal outputs (closed-loop)

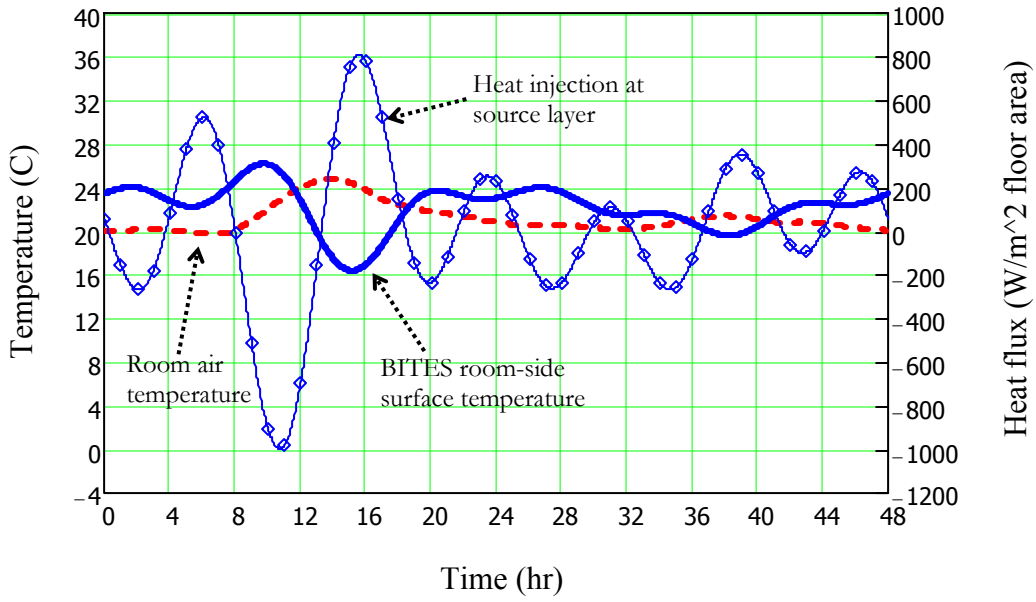

Fig. 4.8: Simulated thermal performance based on predicted thermal energy injection rates (closed-loop BITES)

3.1.3. Treatment on thermal energy injection rates

Looking at Fig. 4.8, thermal energy injection switches frequently between heating and cooling with large magnitudes. This is due to the precise control of the room air temperature; however, from an energy point of view, this is not desirable. Thermal energy is wasted and the cycling of mechanical systems supplying thermal energy is too frequent.

This problem can be avoided by taking the advantage of the high thermal storage mass of the active BITES system, and applying the principle of energy conservation law. Without changing the net amount of thermal energy injection (summation of numerical values, positive for heating) within a certain period, the BITES temperature will not change significantly from its original. Hence, the original thermal energy injection rate profile can be smoothed in a way that later injection does not counteract the previous one. A preliminary

formulation is provided here for the smoothing treatment – the original thermal energy injection rates are averaged with that of adjacent time intervals (Eq. (4.11)).

$$_{sc}p_i = \frac{_{sc}p_{i-1} + {_{sc}p_i} + {_{sc}p_{i+1}}}{3} \tag{4.11}$$

Under certain weather conditions, BITES thermal output is necessary to switch between cooling and heating in order to provide desired room temperature. Hence, the goal of the smoothing treatment is to avoid switching between cooling and heating more than once (double switching) within a period of 24 hours. A search action will be performed. Once double switching is detected within the first 24 hours, thermal energy injection rates at all time intervals within the whole modeling period (48 hours) will be smoothed using Eq. (4.11). This averaging process will be performed until double switching is eliminated within the search horizon (i.e. first 24 hours).

Fig. 4.9 shows the room's thermal response after smoothing the thermal energy injection rates using Eq. (4.11). The resulting room temperature profile generally follows the set-profile, being slightly lower than the set values during the first day. Even though the resulting room temperature profile does not match the set-profile closely, it serves the purpose – active BITES system is properly controlled and thermal comfort is provided. This deviation can be reduced by adjusting the heating set point or applying a scaling factor to the thermal energy injection rates. Scaling factor 1.2 is suitable for this case.

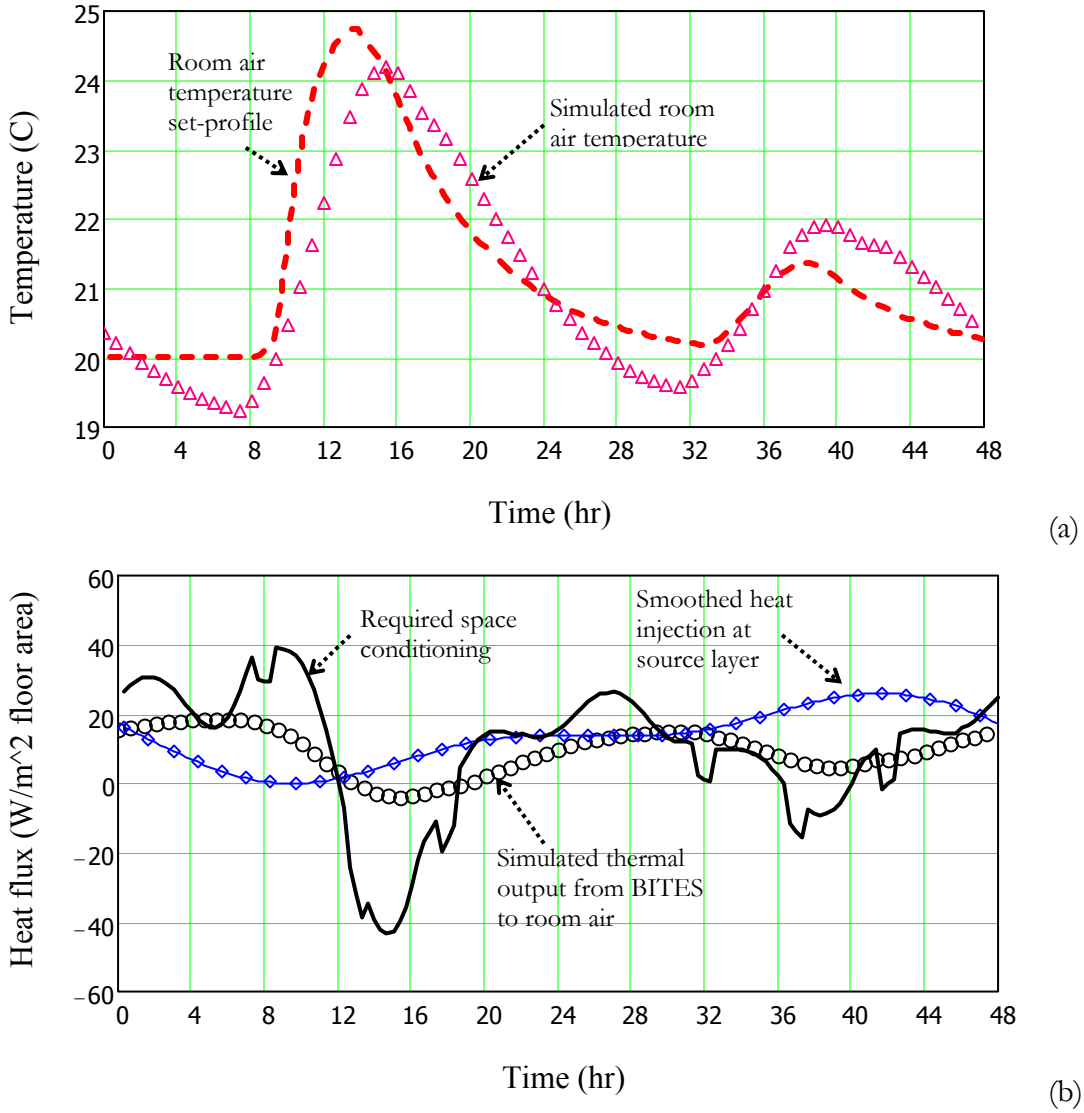

Fig. 4.9: Comparisons of (a) set and simulated room air temperatures and (b) BITES thermal output after smoothing thermal energy injection rates (closed-loop)

The thermal energy injection rate profile is sensitive to the room temperature set-profile. Fig. 4.10 shows the energy performance corresponding to a slightly different room air temperature set-profile – the rise of room temperature is set 2 hours later (i.e. the room air temperature set-profile is shifted 2 hours to the right). As compared to the thermal energy injection rate profile in Fig. 4.9, the profile in Fig. 4.10 has two times the highest power demand (i.e. thermal energy injection rate), about 50 W/m^2 around hour 40. However, it has

better utilization of ambient renewable energy (i.e. solar thermal energy during daytime). Both profiles have reduced or zero power demand during peak space heating hours (e.g. from hour 6 to hour 10). The comparison shows that room air temperature set-profiles are critical to the energy performance of active BITES systems and their buildings. The magnitudes and phase angle of transfer functions in frequency domain provides insights in improving the temperature set-profile. See Subsection "Discussion" for more information.

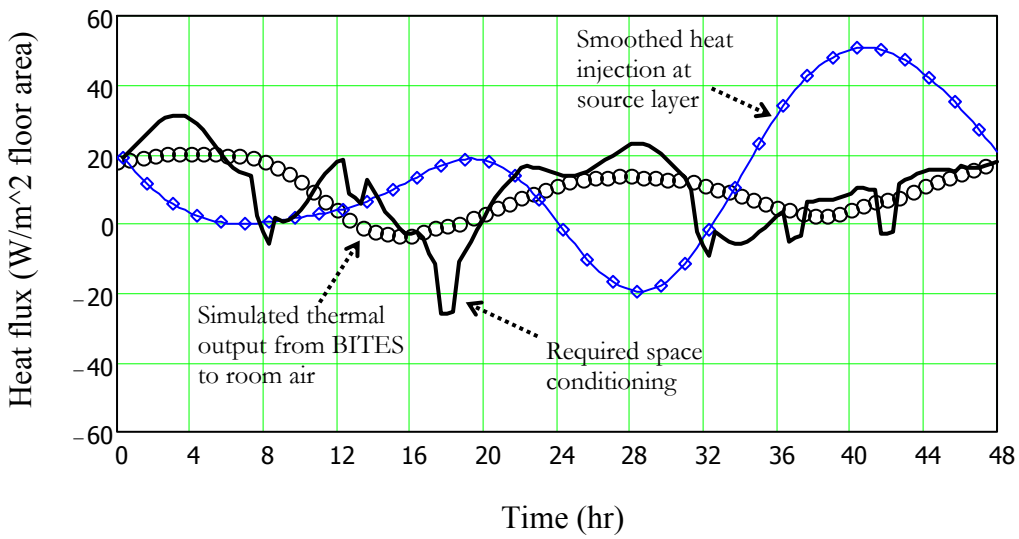

Fig. 4.10: Simulated room air temperatures and BITES thermal output after smoothing thermal energy injection rates with an altered room air temperature set-profile (closed-loop)

3.1.4. Space cooling scenario

Using the modeling and calculation approaches developed above, BITES predictive control for space cooling scenario is presented briefly here. The thermal responses for a cooling dominated period are plotted in Fig. 4.11. As seen, solar heat gain has significant influence on the cooling load – active BITES floor surface temperature has to be lower than 18°C in order to meet the room air temperature requirement during daytime. The low surface temperature requirement is partially because of the low CHTC resulted from cooling upward

conditions. The floor surface temperature needs to be significantly low in order to create large temperature potential, and hence exceeds the lower temperature comfort limit. Overall heat gain needs to be controlled in order to lower the cooling output requirement for the active BITES floor. On the other hand, open-loop systems can provide substantially higher thermal output without excessively cold or hot floor surface. In the following subsection, the methodology presented above will be extended and applied to open-loop systems.

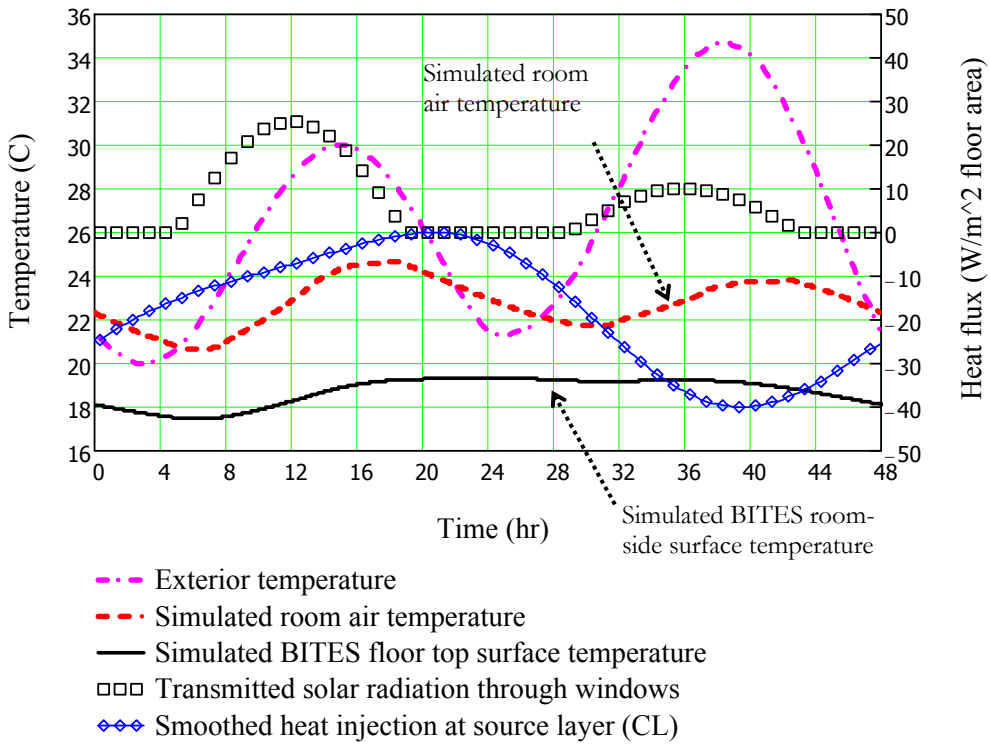

Fig. 4.11: Weather conditions and simulated room air and BITES temperatures based on smoothed thermal energy injection rates (closed-loop; smoothed injection; cooling dominated)

3.2. Open-loop BITES systems

In an open-loop system as shown in Fig. 1.8-b, the conditioned air will be supplied to the ventilated BITES systems first, and then released to the room. Hygienic measures for

avoiding air contamination risks have been discussed in Chapter 1 "Introduction". In addition to the convective and radiative thermal output from the exposed surface, there is an advective thermal output ${}_{A.B}p$ due to the released air (Fig. 4.12 and Fig. 4.13). Fig. 4.12 shows the thermal network and Fig. 4.13 shows the flows of heat and air of the open-loop BITES systems used here for demonstration. The space conditioning load ${}_{load}P$ (equals to required thermal output) includes the heat gain/loss due to ventilation.

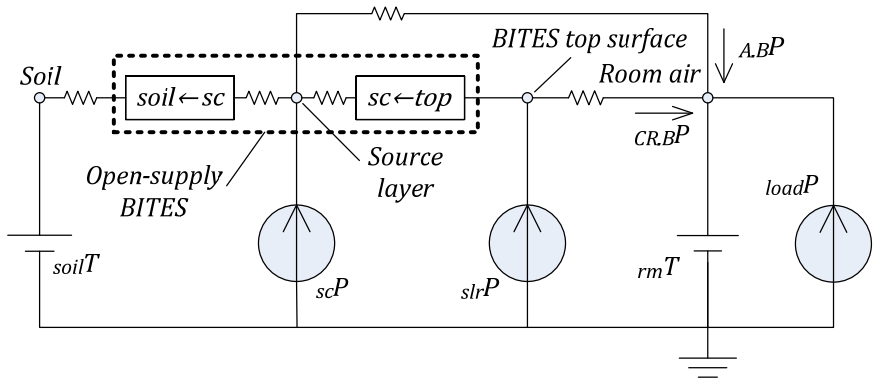

Fig. 4.12: Thermal network of an open-loop BITES system sitting on soil

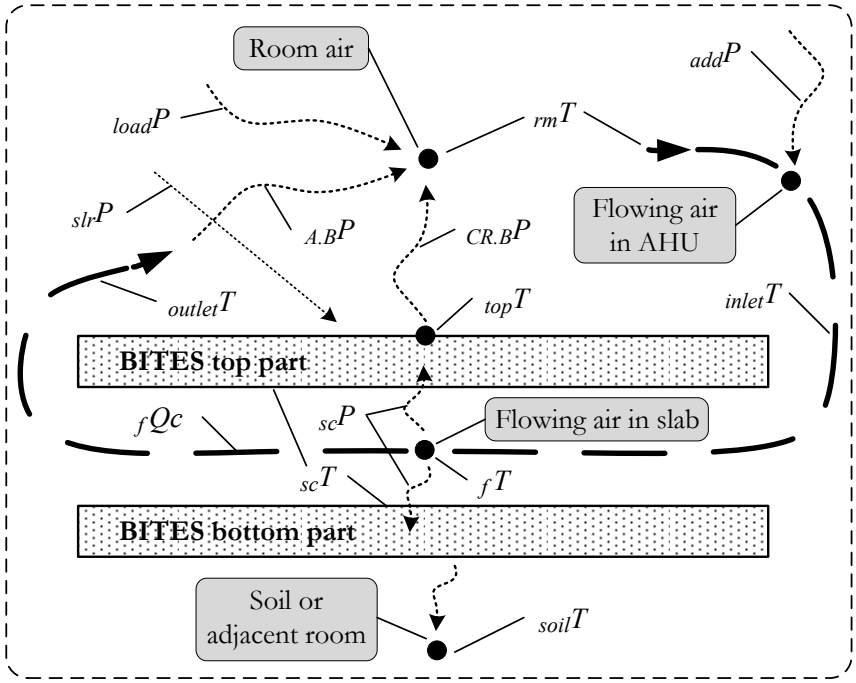

Fig. 4.13: Schematic of energy flows for the open-loop system shown in Fig. 1.8-b

3.2.1. Formulation for open-loop systems

The total thermal output ${}_{B}p$ of an open-loop system consists of a convective and radiative portion ${}_{CR.B}p$ and an advective portion ${}_{A.B}p$. For every different combination of flow rate and BITES inlet air temperature ${}_{inlet}T$, the apportionment and the resulting total thermal output ${}_{B}p$ will be different. A constant flow rate is chosen for clarity and practical purpose. In practice, multiple stages of flow rate can be used - high flow rates for high space conditioning load. Even with a constant flow rate, the inlet air temperature will still change with the varying thermal energy injection rate ${}_{add}p$ at the AHU (Fig. 1.8-b). An iterative formulation is needed to determine the required thermal energy injection. The following formulation calculates the ${}_{add}p$ per square meter floor area (W/m^2) that will meet the space conditioning load for a set-profile of room air temperature.

A two-layer iteration is adopted in this study. In the outer layer, the initial profile of thermal energy injection ${}_{add}p$ will be guessed. Using the guessed values, the inner iteration layer will begin with a guessed temperature profile of the source layer ${}_{sc}T$. With the guessed ${}_{add}p$ and the room air temperature set-profile, a converged ${}_{sc}T$ profile and the corresponding ${}_{A.B}p$ and ${}_{CR.B}p$ profiles will be obtained. Then the outer iteration layer will update the ${}_{add}p$ based the discrepancy between the current ${}_{B}p$ (i.e. ${}_{A.B}p + {}_{CR.B}p$) and the required thermal output ${}_{load}p$. The updated ${}_{add}p$ will then be sent back to the inner iteration layer to start a new iteration. In every iteration, variables' values at all time steps (i.e. profiles) have to be obtained in order to calculate their DFS representations, which are required for the frequency domain modeling. The two-layer iterations will continue until convergence criteria are met. Since 1200- to 1800-second time step and 6 harmonics can provide satisfactory

results (see more discussion in Subsection 4.2), this two-layer iteration approach will not be computationally intensive. Detailed formulation is as follows.

In starting each iteration, the inlet air temperature of the BITES slab, ${}_{inlet}T$, can be calculated with a guessed or updated ${}_{add}p$ using Eq. (4.12). Variable ${}_{rm}T$ should be the entering air temperature of the AHU coil (i.e. after mixing return air with fresh air) as shown in Fig. 1.8-b. However, since the ventilation heat lost/gain has been assigned to the space conditioning load ${}_{load}p$ (Fig. 4.13) to simplify the calculation without significant errors, the room air temperature can be used for ${}_{rm}T$ here.

$$ {}_{inlet}T_i = {}_{add}p_i \cdot {}_{B}Area/\left({}_{f}Qc \cdot {}_{path}N \right) + {}_{rm}T_i \tag{4.12} $$

where ${}_{B}Area$ is the room-side exposed surface area (i.e. floor area), equal to the floor area in this case. ${}_{f}Qc = {}_{f}Q \cdot {}_{f}\rho c$ with ${}_{f}Q$ being the volumetric flow rate of the heat transfer fluid (air in this case) in each air path, and ${}_{f}\rho c$ the volumetric heat capacity of the fluid. ${}_{inlet}T$ is the inlet temperature of the fluids. ${}_{path}N$ is the number of air paths. The air paths are assumed to have equal lengths and evenly share the total flow rate.

With current inlet air temperature ${}_{inlet}T$ and the guessed source layer temperature ${}_{sc}T$, the temporary heat exchange between the heat transfer fluid and the BITES system, ${}_{sc}p$, can be obtained. The calculation of ${}_{sc}p$ in a one-dimensional active BITES model (Subsection 2.3) was presented by Chen et al. (2013a) and is adopted here. ${}_{sc}p$ is for unit square meter of the BITES exposed surface area.

$$ {}_{sc}p_i = \left({}_{f}\bar{T}_i - {}_{sc}T_i \right) \cdot {}_{sc}U \cdot {}_{path}N / {}_{B}Area \tag{4.13} $$

where ${}_{f}\bar{T}_i$ is the mean temperature (not a DFS mean value) of the heat transfer fluid at ith time interval, and ${}_{sc}T$ is the source layer temperature. ${}_{sc}U$ is the total thermal conductance between each air path and the fluid. In this case, ${}_{sc}U = {}_{sc}h \cdot {}_{path}Area$ with ${}_{path}Area$ being the internal heat transfer surface area of each path, and ${}_{sc}h$ is CHTC between the path inner surface and the air flow. See Appendix for detailed calculation of ${}_{sc}h$. Eq. (4.12) and (4.13) can be applied for liquid heat transfer fluids as in hydronic BITES systems.

$$ {}_{f}\bar{T}_i = {}_{sc}T_i + \frac{\left({}_{inlet}T_i - {}_{sc}T_i\right) \cdot \left(1 - exp\left(-{}_{hx}c\right)\right)}{{}_{hx}c} $$

$$ {}_{hx}c = {}_{sc}U / {}_{f}Qc $$

With the temporary heat flux at the source layer ${}_{sc}p$, the source layer temperature ${}_{sc}T$ can be updated. The formulation from Chen et al.(2013b) (Section 3.3 in Chapter 3) is applied here. The general procedure is to obtain the combined convective and radiative thermal output ${}_{CR.B}p$ based on ${}_{sc}p$, and then update the source layer temperature ${}_{sc}T$ based on ${}_{CR.B}p$ and ${}_{rm}T$. The above calculated values in time domain will then be represented with complex DFS in frequency domain. The calculation of the oscillatory responses of the variables will be shown below. The mean responses are calculated in similar ways. The oscillatory part of ${}_{CR.B}p$ is calculated using Eq. (4.14), which is similar to Eq. (4.6). Harmonic subscript h is omitted for clarity.

$$ {}_{CR.B}\tilde{p}_i = {}_{soil_rm}\tilde{p}_i + {}_{slr_rm}\tilde{p}_i + {}_{sc_rm}\tilde{p}_i \tag{4.14} $$

where ${}_{slr_rm}p$ is the contribution from the solar radiation absorbed by the floor top surface. ${}_{sc_rm}p$ is from the heat flux injected by the heat transfer fluid. ${}_{soil_rm}p$ is the heat exchange between the soil and the room air, similar to Eq. (4.7):

$${}_{soil_rm}\tilde{p}_i = {}_{soil}\tilde{T}_i \cdot {}^{soil\leftarrow rm}a21 + {}_{rm}\tilde{T}_i \cdot {}^{soil\leftarrow rm}a22$$

where $a21$ and $a22$ are from admittance matrix ${}_{adm}[M]$ of assembly $soil \leftarrow rm$.

The assembly $soil \leftarrow rm$ includes the air film between floor top surface and room air node (Fig. 4.4). Since the outlet air from the open-loop BITES systems will create forced convection inside the room, Eq. (4.5) is not suitable for open-loop system applications. A constant value of 9 W/m^2/K is used for the combined heat transfer coefficient ${}_{top}h$ between the floor top surface and room air node. Formula with considerations of the direction and flow rate of the outlet air, heat flow direction, and outlets locations can be used in the future.

Using heat flow division technique

$${}_{sc_rm}\tilde{p}_i = {}_{sc}\tilde{p}_i \cdot \frac{{}^{soil\leftarrow sc}t12}{{}^{soil\leftarrow rm}t12}$$

and

$${}_{slr_rm}\tilde{p}_i = {}_{slr}\tilde{p}_i \cdot \frac{{}^{soil\leftarrow top}t12}{{}^{soil\leftarrow rm}t12} \tag{4.15}$$

where $t12$ are from different transmission matrices ${}_{trs}[M]$.

Note that the heat flow division for absorbed solar radiation neglects the advective connection between the room air node and the source layer. This treatment significantly simplifies the formulation without causing substantial error as shown later. Otherwise, the

"Δ" shape network between the room air, source layer, and the floor top surface (Fig. 4.12) have to be transformed into a "Y" shape network (Bird 2007). The transmission matrices for the whole BITES system will also have to be re-calculated.

The source layer temperature ${}_{sc}T$ can be updated now making used of the temporary ${}_{CR.B}p$.

$$ {}_{sc}\tilde{T}_i = {}_{rm}\tilde{T}_i \cdot {}^{sc\leftarrow rm}t11 + \left({}_{CR.B}\tilde{p}_i - {}_{slr_rm}\tilde{p}_i\right) \cdot {}^{sc\leftarrow rm}t12 \tag{4.16} $$

The mean response ${}_{sc}\bar{T}$ can be calculated as follows:

$$ {}_{sc}\bar{T} = {}_{rm}\bar{T} + \left({}_{CR.B}\bar{p} - {}_{slr_rm}\bar{p}\right) \cdot {}^{sc\leftarrow rm}r \tag{4.17} $$

Then

$$ {}_{sc}T_i = {}_{sc}\bar{T} + Re\left\{\sum_{h=1}^{H} {}_{sc}\tilde{T}_{i,h}\right\} \tag{4.18} $$

In the next inner layer iteration, Eq. (4.13) to (4.18) will be repeated. After the desired convergence criteria of the inner layer iteration are met, the updated total thermal output ${}_{B}p_i = {}_{A.B}p_i + {}_{CR.B}p_i$ will be sent to the outer layer iteration. ${}_{A.B}p_i = \left({}_{outlet}T_i - {}_{rm}T_i\right) \cdot {}_{f}Qc \cdot {}_{path}No/{}_{B}Area$, and ${}_{outlet}T_i = {}_{sc}T_i + \left({}_{inlet}T_i - {}_{sc}T_i\right) \cdot exp\left(-{}_{hx}c\right)$. ${}_{add}p_i$ will then be updated in the outer layer iteration (Eq. (4.19)) and sent back to the inner layer of iteration until convergence criteria of outer layer iteration are met.

$$ {}_{add}p_i = {}_{add}p_i + \left({}_{load}p_i - {}_{B}p_i\right) \tag{4.19} $$

3.2.2. Results

In selecting air flow rates, low values can reduce fan power consumption and avoid potential cold drafts. However, when space conditioning load is high, low flow rates will result in excessively high or low inlet air temperature. Efficiency attributed to low temperature

operation will be lost. Furthermore, if the inlet air temperature is excessively high or low, the temperature gradient along the air path will be significant. Consequently, one-dimensional model based on the assumption of uniform slab temperature may cause substantial errors. Total flow rate of 3 air changes per hour (ACH) for 3 air paths (total 78 L/s or 26 L/s per path) is used in the following calculations. The air paths are assumed to have equal lengths and evenly share the total flow rate.

The thermal energy injection rates at the AHU predicted with the frequency domain model is used in the finite difference thermal model to simulate the thermal responses of the room and its closed-loop BITE floor. Fig. 4.14 shows the simulation results before smoothing treatment. As seen, the above presented approach successfully calculates the thermal energy injection rates required to meet the space conditioning load.

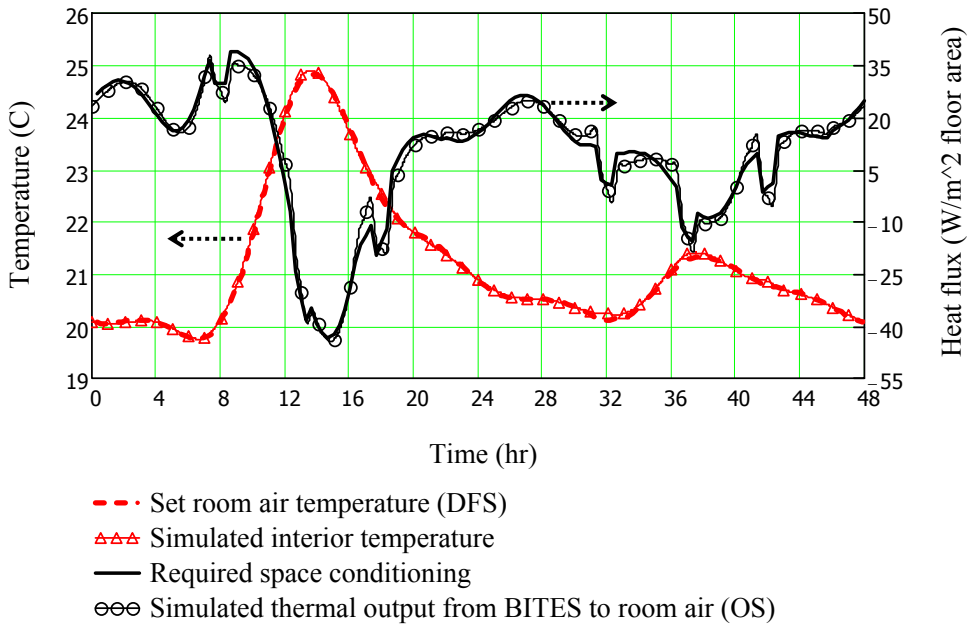

Fig. 4.14: Comparison of set and simulated room air temperatures and BITES thermal output (open-loop; flow rate of 3 ACH; heating dominated)

The smoothing treatment is then applied to the thermal energy injection rates ${}_{add}p$. Fig. 4.15 and Fig. 4.16 show the simulated thermal and energy performance of the room and its open-loop system after applying the treatment. As seen in Fig. 4.15, the combined convective and radiative output ${}_{CR.B}p$ is about 1.2 to 1.5 times the advective output ${}_{A.B}p$ during peak space conditioning load periods for the selected flow rate (3 ACH). This ratio is about 2.5 to 3 for total flow rate of 1.5 ACH (figure is not shown). The highest required inlet air temperature is about 31°C with a 3 ACH flow rate (Fig. 4.16); while with a 1.5 ACH flow rate, the highest temperature is about 40°C. However, similar to the discussion for the closed-loop system, the required thermal energy injection rates and hence the inlet air temperature are sensitive to the room air temperature set-profile. It can also be seen, while the thermal energy injection rate profile reduces on-peak heating demand, it does not make significant use of available solar thermal energy. The room air temperature set-profile can be improved by analyzing relevant frequency domain transfer functions (Chapter 5).

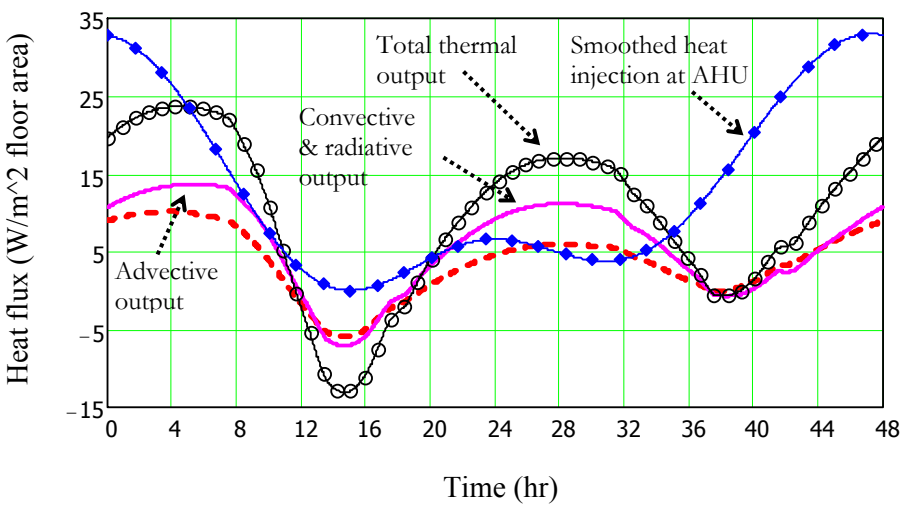

Fig. 4.15: Simulated thermal output based on predicted thermal energy injection rate at AHU (open-loop; smoothed injection; flow rate of 3 ACH; heating dominated)

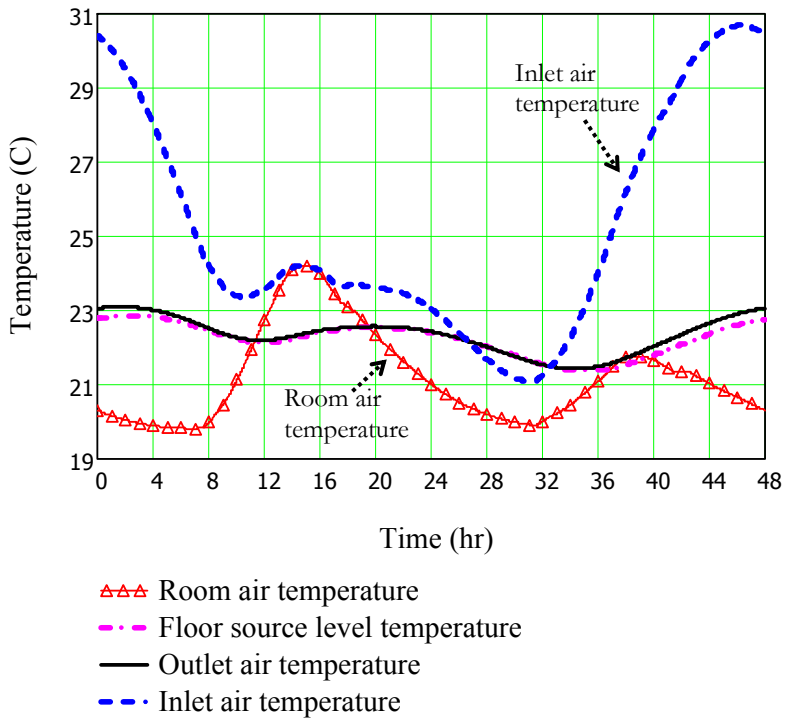

Fig. 4.16: Simulated thermal responses after injection smoothing (open-loop; flow rate of 3 ACH; heating dominated)

3.2.3. Simplified model for open-loop systems with low flow rates

As can be seen from Fig. 4.16, the outlet air temperature is close to that of the source layer. This typical thermal behavior of open-loop systems enables a simplified formulation without iterative calculation. By assuming the outlet air temperature ${}_{outlet}T$ equal to that of the concrete at source layer ${}_{sc}T$, the advective thermal conductance between room air and outlet air can be combined into the admittance for ${}_{sc_rm}p$, similar to the calculation of the total resistance of two electrical resistors in parallel.

Similar to the transmission matrix of a pure-resistive layer, the transmission matrix of the advective output ${}^{Qc}_{trs}[M] = \begin{bmatrix} 1 & {}_{Qc}r \\ 0 & 1 \end{bmatrix}$, where ${}_{Qc}r = {}_{B}Area/\left({}_{f}Qc \cdot {}_{path}N \right)$, the combined admittance matrix between the source layer and the room air equals to

$$ {}^{sc\leftarrow rm}_{adm.c}[M]_h = {}^{sc\leftarrow rm}_{adm}[M]_h + {}^{Qc}_{adm}[M] \tag{4.20} $$

Note that the combined transmission matrix ${}^{sc\leftarrow rm}_{trs.c}[M]_h$ between the source layer and the room air has to be obtained by mathematically transforming ${}^{sc\leftarrow rm}_{adm.c}[M]_h$ into ${}^{sc\leftarrow rm}_{trs.c}[M]_h$. Using ${}^{sc\leftarrow rm}_{trs.c}[M]_h = {}^{sc\leftarrow rm}_{trs}[M]_h + {}^{Qc}_{trs}[M]$ is not correct. See Appendix for the transformation between transmission and admittance matrices.

With known room air temperature and thermal output requirement, the temperature ${}_{sc}T$ and thermal energy injection rate at source layer ${}_{sc}p$ can be directly calculated. The formulation is similar to that for closed-loop systems, but with the additional air film. The aforementioned treatment on the solar radiation absorbed by the top surface in open-loop systems is applied here also. See explanation for Eq. (4.15). Some of the calculations are as follows.

$$ {}_{sc}\tilde{T}_i = {}_{rm}\tilde{T}_i \cdot {}^{sc\leftarrow rm}_{c}t11 + \left({}_{B}\tilde{p}_i - {}_{slr}\tilde{p}_i \cdot \frac{{}^{sc\leftarrow top}t12}{{}^{sc\leftarrow rm}t12} \right) \cdot {}^{sc\leftarrow rm}_{c}t12 \tag{4.21} $$

where ${}_{c}t12$ is from the combined transmission matrix ${}_{trs.c}[M]$. ${}_{B}p$ here is the total thermal output from the simplified formulation.

$$ {}_{sc}\bar{T} = {}_{rm}\bar{T} + \left({}_{B}\bar{p} - {}_{slr}\bar{p} \cdot \frac{{}^{sc\leftarrow top}r}{{}^{sc\leftarrow rm}r} \right) \cdot {}^{sc\leftarrow rm}_{c}r $$

where ${}^{sc\leftarrow rm}_{c}r = 1/\left({}_{Qc}r^{-1} + {}^{sc\leftarrow rm}r^{-1}\right)$, and ${}^{sc\leftarrow rm}r$ is the thermal resistance between the source layer and the room air through the solid floor.

Similar to Eq. (4.14), the contribution from the source layer thermal energy injection to the total thermal output of the open-loop BITES system

$$_{sc_rm}\tilde{p}_i = {}_{B}\tilde{p}_i - {}_{slr_rm}\tilde{p}_i - {}_{soil_rm}\tilde{p}_i \tag{4.22}$$

where $_{soil_rm}\tilde{p}_i = {}_{soil}\tilde{T}_i \cdot {}^{soil\leftarrow rm}_{c}a11 + {}_{rm}\tilde{T}_i \cdot {}^{soil\leftarrow rm}_{c}a12$, and $_{c}a12$ $_{c}a22$ are from the combined admittance matrices $_{adm.c}[M]$.

The oscillatory response of thermal energy injection

$$_{sc}\tilde{p}_i = {}_{sc_rm}\tilde{p}_i \cdot \frac{{}^{soil\leftarrow rm}_{c}t12}{{}^{soil\leftarrow sc}t12} \tag{4.23}$$

Similarly, the mean response can be obtained as follows.

$$_{sc}\bar{p} = {}_{sc_rm}\bar{p} \cdot \frac{{}^{soil\leftarrow rm}_{c}r}{{}^{soil\leftarrow sc}r} \tag{4.24}$$

The procedure for calculating the thermal energy injection at AHU is the same as previously demonstrated.

In general, smaller temperature difference between source layer and outlet air gives better results in using this simplified formulation. Table 4.2 and Fig. 4.17 give some sample simulation results. As can be seen, this simplified formulation gives better results under relatively high flow rate (higher channel CHTC) and long air path situations (more heat exchange area). In all the simulations, the maximum absolute temperature difference between source layer and outlet air takes place towards the end of the simulation period (i.e. after hour 40). This indicates that the simplified formulation is viable because operations focus on the first 24 hours and the prediction can be re-done hourly.

Fig. 4.17 plots the simulation results corresponding to the last row in Table 4.2. Comparing Fig. 4.17 with Fig. 4.16, the results are satisfactory and do not deviate significantly from that

of non-simplified formulation. Furthermore, even though this simplified model does not give highly accurate results, it provides important information for design.

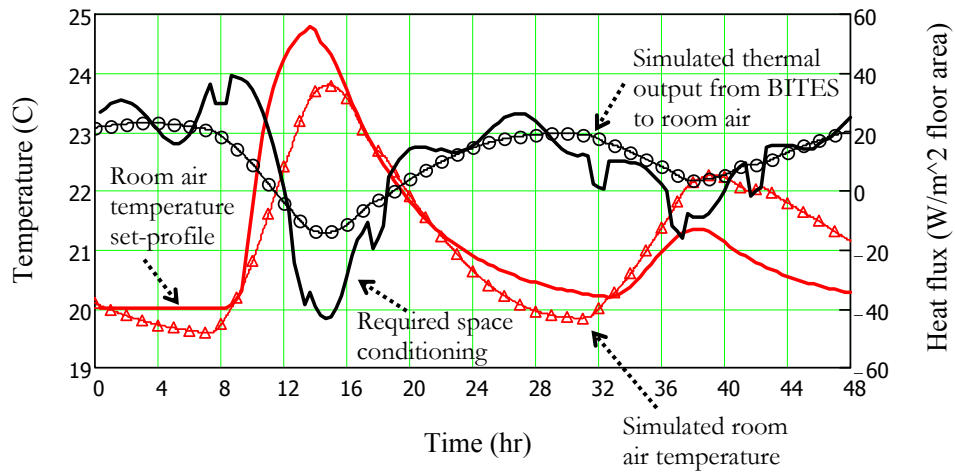

Fig. 4.17: Comparison of set and simulated room air temperatures and BITES thermal output (open-loop with simplified model; flow rate of 3 ACH (78 L/s or 26L/s per air path); smoothed injection; heating dominated)

Table 4.2: Sample results using simplified model (after source input smoothing treatment)

Flow rate per path [L/s]	Air velocity [m/s]	Channel length [m]	Maximum absolute temperature difference between source layer and outlet air [°C]	Corresponding absolute thermal output discrepancy [W/m^2]	Note
13	0.46	19.7	0.8	1.8	
18	0.62	26.3	0.4	0.8	
26	0.93	26.3	0.3	1.0	Fig. 4.17

Note: The corresponding absolute thermal output discrepancy is caused due to assuming the temperature of the outlet air equal to that of the source layer. The tabulated values correspond to the maximum absolute temperature difference.

4. Discussion

4.1. Comparing closed-loop and open-loop systems

Fig. 4.18 compares the thermal performance of the closed-loop and open-loop systems under a cooling-dominated period shown in Fig. 4.11. ACH of 3 is used for the open-loop system. As seen, the top floor surface of the open-loop systems is within the thermal comfort range for approximately the same room air temperature requirement. This suggests that open-loop systems are preferable under high space conditioning load conditions. Other advantages of open-loop systems include the following:

- Open-loop systems have faster responses to sudden demand changes because of their additional advective thermal output;
- Due to interior design or space function requirement, the floor surface may be fully/partially covered (e.g. carpet, furniture, false ceiling). This will affect the convective and radiative output of the BITES systems. Advective thermal output can alleviate this problem.

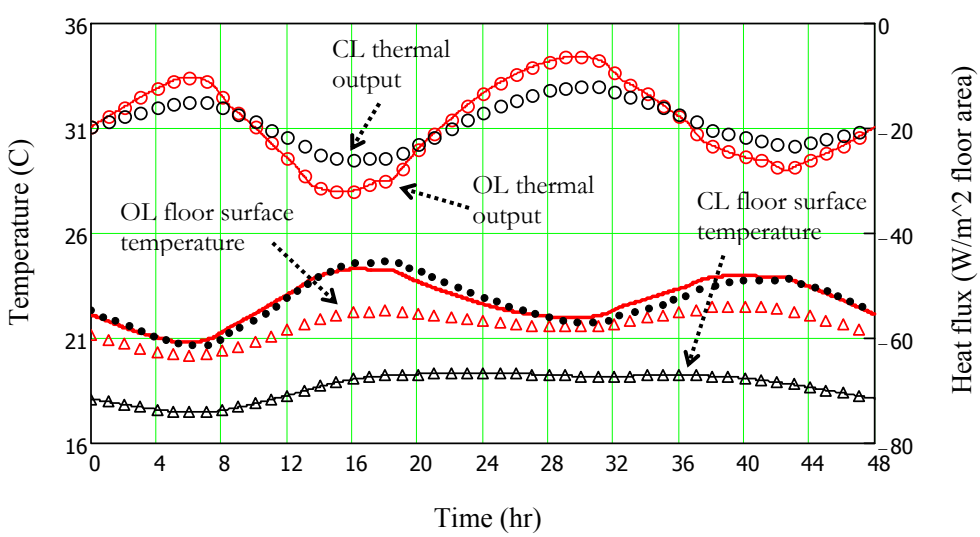

Room air temperature (OL)
Room air temperature (CL)

Fig. 4.18: Comparison of simulated thermal performance of a closed-loop (CL) and an open-loop (OL) systems (smoothed injection; cooling dominated)

4.2. Influence of time steps and harmonics

All frequency domain calculations performed above use 6 harmonics and 1200 seconds time step. As seen, they are satisfactory for study of predictive control strategies. Chen et al. (2013b) found that time step of 1800 seconds is sufficient for closed-loop systems. Open-loop systems are more sensitive on time step than closed-loop systems, mainly due to the simplifying treatment on the solar radiation absorbed on the floor surface and the advective thermal output to the room air. Using 12 harmonics generates better fitting results (e.g. room air and required thermal output); however, this is not necessary since the thermal output profile does not have to match closely to the required one due to the high thermal storage mass of the BITES system and the building which filter out the effects of the higher harmonics. Furthermore, the fluctuation frequency of the thermal energy injection will need to be lowered with the smoothing or other similar treatments. Hence, the number of harmonics for the frequency domain thermal modeling and DFS representations does not have to be large. These observations also indicate that thermal energy injection rate does not have to be highly precise. This facilitates the practical application of the design methodology developed here.

4.3. Using frequency domain transfer functions for design and operation

By comparing the peaks and lows in Fig. 4.7 and Fig. 4.8, we observe a time lag of about four hours between the thermal energy input at the source layer and its thermal output

through the active BITES system (e.g. hour 11 and hour 15 in Fig. 4.8). The time lag between the thermal output of the BITES system and the response of the room is about 5.5 hours (e.g. hour 8.5 and hour 14 in Fig. 4.7 or Fig. 4.8). Hence, the time lag between the thermal input of the BITES system and the response of the room is about nine to ten hours. These significant time lags are critical design factors to be considered. This need demonstrates the important application of frequency domain functions in design optimization.

With frequency domain transfer functions, systems' time lags can be readily obtained from the phase angles (or arguments) of the corresponding transfer functions. For example, the time lag between the thermal energy injection and its output through the closed-loop BITES system used in the above study is related to the phase angle of the heat flow division transfer function (e.g. Eq. (4.9)). As can be seen from Fig. 4.9, the principal frequency of the thermal energy injection rate is one cycle (i.e. 2π) per 24 hours (i.e. one harmonic). Since the phase angle for one harmonic is

$$Arg\left\{\frac{\left[{}^{soil\leftarrow sc}t12\right]_{h=1}}{\left[{}^{soil\leftarrow top}t12\right]_{h=1}}\right\} = -1.043\ radian$$

where $Arg\{\quad\}$ calculates the phase angle of a complex number

The time lag approximately equals to $-1.043\ radian \cdot (24\ hr/2\pi) = -3.985\ hr$. This value precisely reflects the value from observing the actual thermal response of the room (i.e. Fig. 4.7 and Fig. 4.8). In a similar way, dynamic responses (i.e. time lags and magnitudes) of other important design variables can be obtained by analyzing corresponding frequency domain transfer functions (Athienitis 1994). Hence the overall design optimization can be achieved on a relative basis.

The above discussion leads to a further thought for setting the room air temperature profile. Since the smoothing treatment will change the set profile of the room air temperature, the profile does not have to be set precisely. The profile can be defined by connecting several key points in the time-temperature coordinates with straight lines. The smoothing of thermal energy injection rates will result in similar temperature profiles to those presented above. These key points are critical in providing thermal comfort and improving energy performance. Their time coordinates can be located according to the time lags of the systems. See Chapter 5 for detailed application.

4.4. Deviations in thermal output and input

The exposed surfaces of BITES systems exchange heat radiatively with other interior surfaces and furniture, in addition to the convective heat exchange with room air. Hence, the temperature at the room air node in Eq. (4.2) should be an adjusted room air temperature weighted by the respective heat transfer coefficients between the interior objects and the BITES surfaces. In this study, room air temperature is assumed equal to the adjusted room air temperature, and used in Eq. (4.2) to calculate the required thermal energy injection rates for the BITES system. Since the room air temperature is normally different from that of the interior surfaces of envelope and other interior objects, therefore the thermal output of the BITES to the room ${}_{B}p$ (i.e. ${}_{CR.B}p + {}_{A.B}p$, or just ${}_{CR.B}p$) may be different from the actual need. This will result in a different room air temperature. However, this deviation will not be obvious to occupants due to the fact that the operative temperature will be largely defined by the exposed surface temperature of the BITES systems in a mainly radiant cooling/heating situation.

4.5. Non-periodic thermal excitations

Another technical issue is that the actual temperature of the room and the required thermal output of the active BITES system will deviate from the previously set/estimated values to a certain extent due to different causes. Also, they are also not periodically steady, which is different from the excitations used for frequency domain modeling. These two factors will result in errors in the prediction of thermal energy injection rates. Yet, if the profiles of the set room air temperature and the required thermal output in the modeling include a long enough period of data that precedes the current search horizon (i.e. the actual room air temperature and thermal output in the past), the errors from these two factors can be minimized. Preliminary study shows that two days is sufficient. This preceding period serves as the warm up or stabilization period in the frequency domain modeling. The actual preceding thermal output can be estimated with measured temperatures of the room air and interior surfaces, or by comparing the actual and set values of the room air temperature. With actual thermal response data, "online" data-driven models that can self-tune over time with continuously monitored (i.e. online) data will be an excellent choice for thermal load estimation.

5. Conclusion

In this chapter, a methodology for the design of predictive control strategies of active building-integrated thermal energy storage (BITES) systems using frequency domain modeling was presented. Frequency domain transfer functions are used to predict the required thermal energy injection rates based on the desired room air temperature set-profile and the corresponding space conditioning load. The objective of the methodology is to

satisfy the thermal comfort requirement for room temperature, as well as to enhance the building energy performance.

The applications of this methodology on two types of active BITES systems – closed-loop and open-loop to room interior – were demonstrated. The methodology is shown to be capable of predicting the required thermal energy injection rates based on room temperature set-profiles selected with heuristic criteria. General procedure is summarized as follows:

(1) Collect weather forecast information (solar radiation and exterior temperature) for about 1-2 days ahead;
(2) Establish the future room air temperature set-profile based on heuristic considerations, which are related to thermal comfort, energy savings and peak demand reduction/shifting. Then, precede it with historic room air temperature. Represent the merged profile with complex discrete Fourier series (DFS);
(3) Estimate the required future thermal output of active BITES systems based on the DFS represented future room air temperature, and then precede it with historic thermal output. Represent the merged profile with complex DFS;
(4) Use the DFS-represented room air temperature and thermal output to calculate the required thermal energy injection rates to the active BITES system;
(5) Apply smoothing treatment to the calculated thermal energy injection rates (in part to eliminate errors due to omission of higher harmonics);

It was shown that open-loop systems are preferable in high space conditioning load situations. A simplified model has been developed for open-loop systems.

Chapter 5 Design and operation methodology for active building-integrated thermal energy storage systems and applications using standard structural components

This chapter contains one ready-for-submit manuscript titled the same as the chapter.

Chapter Abstract

A methodology for integrating design and operation is developed using a frequency domain approach. Predictive control strategy in conjunction with optimizing dynamic response within the allowable comfort range is proposed to improve the energy performance of BITES systems in a whole building context. Using a heuristic room air temperature set-profile and the calculated corresponding space conditioning load profile as inputs, the thermal energy injection rates can be predicted over a desired prediction horizon. A bounding condition based design approach is presented. A simplified approach for integrating structural and thermal designs is demonstrated with focus on ventilated BITES systems using standard structural components and their variations.

1. Introduction

The two configurations of active BITES systems shown in Fig. 1.8 are the focus of this chapter. In closed-loop configurations (Fig. 1.8-a), the heat transfer fluids (e.g. air or water passing through the BITES) do not exchange heat directly with room air. The air flow in the open-loop configuration (OLS) handles BITES charge/discharge and ventilation.

Supplying primary space conditioning through active BITES systems are not suitable for two kinds of load conditions. The first kind is with large space conditioning loads, and the second one is thermally lightweight buildings with rapidly varying thermal load. Nevertheless, active BITES systems can still be used to facilitate space conditioning in these two situations. Reported studies showed that hydronic BITES floors have a cooling capacity of 40 to 60 W/m^2 and a heating capacity of 30 to 40 W/m^2, under operations compliant with thermal comfort standards (Hauser et al. 2000, Pfafferott and Kalz 2007). Open-loop systems can handle larger ranges of space conditioning load and fluctuation. Their potential thermal output capacity is about twice of that for closed-loop systems (Chapter 4). The second limiting condition is mainly due to the large thermal inertia of the BITES. The system's temperature cannot change rapidly enough to accommodate a sudden large change of space conditioning loads. To eliminate these two kinds of load conditions, the heat gain or loss needs to be controlled with a properly designed building envelope. For example, proper shading design is important for passive solar buildings. Internal heat gain needs to be controlled as well (e.g. small lighting power intensity). The effective thermal storage mass level should be medium to high in order to reduce the temperature fluctuation in case of large load fluctuations.

2. Scope

To efficiently implement the operation strategies (passive measures with possible fan assistance and pre-conditioning) exemplified in Fig. 1.9-c and Fig. 1.11, predictive control has to be implemented, and furthermore, the design and operation of the active BITES systems have to be well integrated. In the following subsections,

- A methodology will be developed for using frequency domain modeling to integrate the design and operation of active BITES systems. This iterative process includes the following key steps:
    - Analysis of dynamic response using frequency domain transfer functions
    - Predictive control design as functions of weather condition and dynamic response
    - Design optimization based on operation and bounding conditions
- Structural and thermal attributes-related design parameters of standard structural components and their applications as active BITES systems will be investigated.
- Key considerations for potential applications will be discussed.

3. Integrating design and operation

Frequency domain modeling offers a convenient approach for dynamic thermal response analysis of multi-layered building assemblies (e.g. wall/roof) and their thermal zones under periodically steady excitations (Athienitis 1994, Athienitis et al. 1990, Athienitis et al. 1986, Davies 1973, Hittle 1981, Johannesson 1981). A thermal-admittance-based technique is widely used in the UK to calculate room temperature swings and time lags between causes (e.g. sol-air temperature peak) and effects (peak of room temperature rise) (CIBSE 1988,

Davies 1994). The thermal admittance can be seen as a dynamic conductance of an assembly under sinusoidal inputs (over a period of a day).

Frequency domain transfer functions reveal the dynamic response, such as magnitude and phase angle, to temperatures and heat flows of a selected type of system with different configurations (e.g. thickness, material thermal properties) on relative bases. The phase angle reflects the time delay (or lag) between thermal energy input and output, while the magnitude indicates the output as a ratio of the input after the time delay. Detailed calculations of dynamic response are shown in a later subsection. By comparing the dynamic response, a suitable configuration with the desired thermal energy retaining time and releasing intensity can be selected conveniently.

Frequency domain thermal modeling for active BITES systems (Chen et al. 2013a, b) provides a viable approach to integrate design and predictive operations. With known room air temperature and the required thermal output of an active BITES system, the schedule and rate of the thermal energy input to the BITES can be obtained (Chapter 4). Hence, if the ideal charge time (i.e. off-peak period or sunny period in a winter day) is known, the conditioning and/or pre-conditioning of the active BITES system and its associated room can be scheduled at the ideal charge time period by setting the room air temperature accordingly. Take pre-heating for example: the peak room air temperature can be set at a known time delay after the peak sol-air temperature is reached. Detailed information is shown in Subsection 3.2.

A frequency domain model is used in this thesis to integrate the design and predictive control of active BITES systems. In this subsection, the thermal attributes of the active

BITES systems will be presented first. Then, the methodology for thermal-attributes-based predictive control will be presented. Finally, the integration procedure will be discussed.

3.1. Thermal attributes of active BITES

The thermal attributes of an active BITES system have to accommodate its operations. For example, for the purpose of storing renewable or off-peak purchased energy, BITES systems need to have large enough thermal energy storage capacity and fast enough charge/discharge capacity. There are four critical attributes (Fig. 5.1) influencing the operations and performance of active BITES systems. Among them, the thermal energy storage (TES) capacity, charge/discharge capacity, and interior thermal output capacity (i.e. thermal coupling) can be readily calculated based on the material and configurations of the active BITES system. Hence, they are grouped as apparent attributes. Meanwhile, dynamic response (phase angle and magnitude) needs frequency domain analysis as explained later.

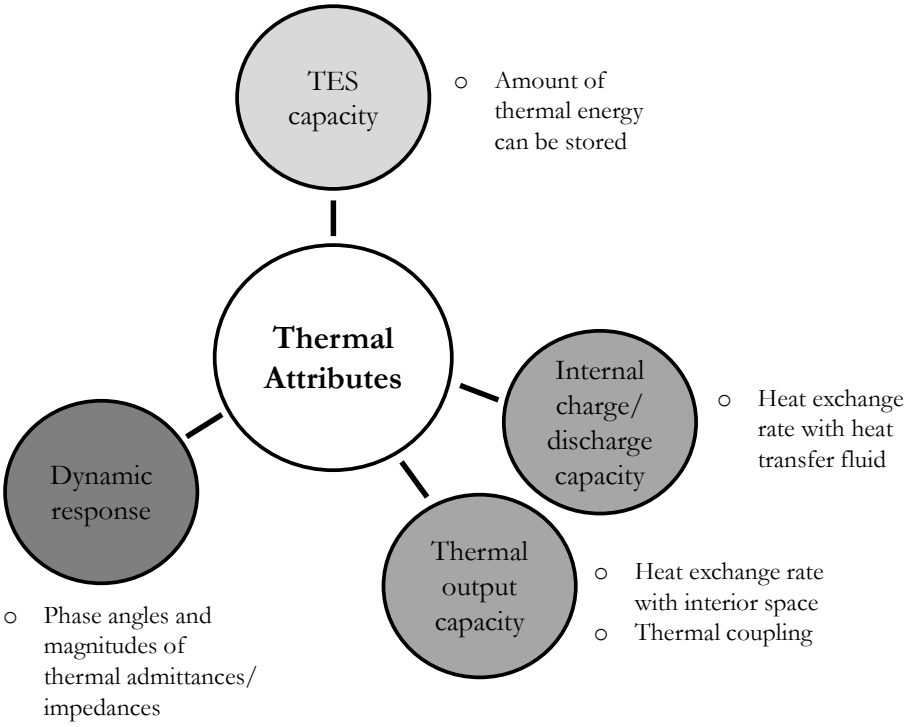

Fig. 5.1: Thermal attributes (TES: thermal energy storage)

3.1.1. Apparent attributes

The first apparent attribute, the TES storage capacity, defines the maximum possible amount of thermal energy that can be stored in the system within a given operation temperature range. The second attribute is the thermal output capacity (i.e. interior thermal coupling). It defines the maximum power of the space conditioning function of an active BITES system, under thermal comfort compliant operation temperatures of the room and itself. It is critical in satisfying the space conditioning load. Interior thermal coupling indicates the heat exchange rate between the room air and the BITES system. Thermal output capacity and interior thermal coupling will be used interchangeably in this study. The third apparent attribute is the charge/discharge capacity. It defines the amount of thermal energy that can be charged in a given period through heat transfer fluids. BITES charging can also be through interior thermal coupling. For example in sunny winter time, in addition to the warm charging/discharging fluids (e.g. air or water), the warm room air may also be heating up the BITES.

In a closed-loop system (Fig. 1.8-a), its charge/discharge rate is the heat exchange rate between the charging/discharging fluid and the BITES. Its thermal output capacity is the total radiative and convective heat exchange between the exposed BITES surface and the rest of the room. For an open-loop system (Fig. 1.8-b), the charge/discharge rate and the advective thermal output rate are commonly affected by the channel air flow rate. The thermal output capacity equals to the overall heat exchange on the exposed surface and the advection.

3.1.2. Dynamic response

Phase angle (i.e. phase shift or time lag) and magnitude of thermal admittances are the critical dynamic responses in the design and operation of active BITES systems. Dynamic response is independent of the room-side surface area of its active BITES system. A time lag is derived from the phase angle of a transfer function, let's say Y (Eq. (5.1)). The magnitude equals the absolute value of Y(i.e. $|Y|$). Fig. 5.2 shows the dynamic response (output wave) of a wall to a temperature excitation (input wave). Y is the wall's admittance transfer function in the frequency domain. ϕ is the phase angle (i.e. phase shift) of Y. $|Y|$ gives the magnitude of Y. As shown, the phase angle and magnitude of this wall define the output wave.

$$Time\ lag = Aug\{Y\}/\omega = \phi/\omega \tag{5.1}$$

where function $Aug\{Y\}$ calculates the argument (i.g. phase angle) of any complex number Y (i.e. transfer function or admittance in frequency domain). ω is the corresponding angular frequency. $\omega = 2\pi/86400\ sec$ for one cycle per day excitations.

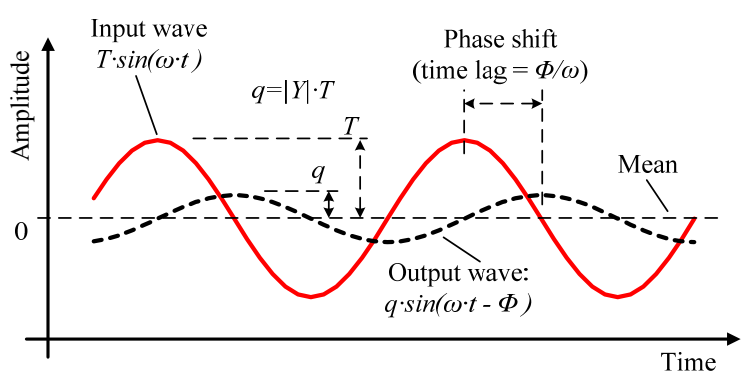

Fig. 5.2: Conceptual schematic of dynamic response (Athienitis and Santamouris 2000)

In this subsection, the analysis of the dynamic response of an open-loop BITES system and its zone (Fig. 5.3) will be presented. The dynamic responses of other types of BITES systems

(active or passive) can be obtained in a similar way. The original cross section of the active BITES system is transformed to fit one-dimensional heat transfer modeling (Fig. 5.3-a) required for frequency domain modeling (Chen et al. 2013a). The cross section can represent either a slab on-grade or an intermediate floor slab. The insulation is optional for intermediate floors, but not useful for structural purposes. It would be used if building designers would like to orient the heat to only one side of the slab. The insulation layer can also represent false ceilings and air cavity in the ceilings, from the view point of heat transfer.

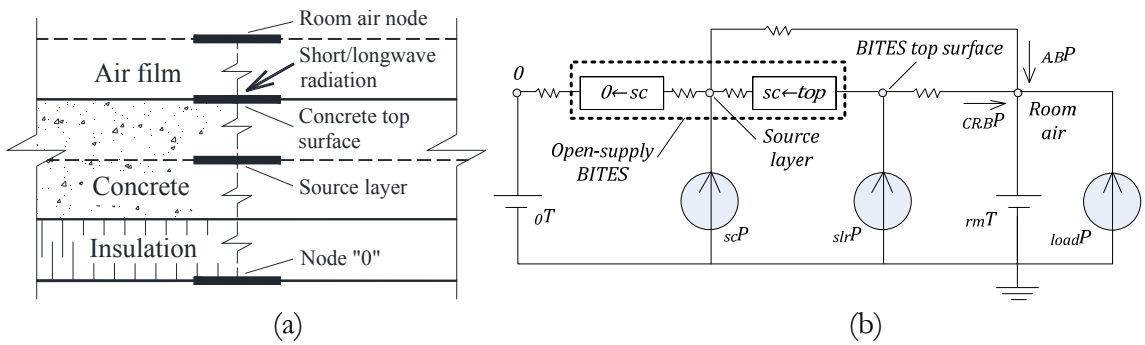

Fig. 5.3: (a) Transformed cross section and (b) thermal network of an open-loop BITES slab and its associated room

The total thermal output from the BITES system, ${}_{B}p$, drives the change of the room air temperature. It is critical to understand how the dynamic response of the BITES will affect this value. ${}_{B}p$ is normally a summation of three thermal potentials – temperature difference across the assembly, heat flux absorbed on the exposed surface, and the heat flux from the source layer (Fig. 5.3-b). Its oscillatory part can be calculated as follows.

$$ {}_{B}\tilde{p}_i = {}_{0_rm}\tilde{p}_i + {}_{slr_rm}\tilde{p}_i + {}_{sc_rm}\tilde{p}_i \tag{5.2} $$

where ${}_{0_rm}p$ is the heat exchange between the room air and the other side of the BITES (node "0" in this case). ${}_{slr_rm}p$ is the contribution from the solar radiation absorbed

by the exposed top surface. $_{sc_rm}p$ is from the heat flux injected by the core-conditioning fluid. It consists of the advective part due to the air flow released directly to the room and the combined convective and radiative part from the exposed surface of the BITES. For closed-loop systems, the advective part is zero (Chapter 4).

The analysis of the transfer functions related to each of the terms in Eq. (5.2) is presented in the following paragraphs, and the results are plotted in Fig. 5.4 for the BITES shown in Fig. 5.3-a. Fig. 5.4-a plots the time lag and magnitude of the self-admittance for different concrete thicknesses. Fig. 5.4-b to -d plot the values of transfer functions generated using the heat flow division method (Chen et al. 2013a). The effects of the thermal capacitance of the room air and the location of the source layer (Fig. 5.3-a) are included. The advection rate equals to two air changes per hour (ACH). See reference (Chen et al. 2013a) for more information on obtaining the transfer functions. The bottom insulation value is 0.5 W/m^2/K, and the combined convective and radiative heat transfer coefficient (i.e. film coefficient) between the top surface and the rest of the room is 9 W/m^2/K. See Chapter 4 for discussion on the film coefficient, and later paragraphs for a sensitivity analysis of the relevant parameters. The thermal properties of a BITES assembly also have significant influence on its dynamic response. Considering the practical application of this study mainly concerns concrete building fabric, the choice of storage mass only considers normal-weight concrete. The thermo-physical properties of the concrete used in this study are 840 J/kg/K for specific heat, 2200 kg/m^3 for density, and 1.7 W/m/K for thermal conductivity.

The dynamic response to excitations of one cycle per day (i.e. one harmonic) is the main parameter of interest for design and operation. This is because the variations of space conditioning load of buildings and the thermal energy input to active BITES systems are

primarily one cycle per day (Chapter 4). This is mainly due to the approximate 1-cycle-per-day characteristic of weather conditions (e.g. solar radiation and exterior air temperature fluctuation), the high thermal inertia of BITES assemblies, and the control approach used in this study. For excitations (i.e. temperature, heat flux) of more than one harmonic, the total response may be obtained by superposition of responses to different harmonics.

The influence of the wall on the room air temperature variation can be obtained by studying the self-admittance transfer function ${}^{0\leftarrow rm}a22$ in Eq. (5.3). The time lag equals to $Aug\{{}^{0\leftarrow rm}a22\}$ and the magnitude equals to $|{}^{0\leftarrow rm}a22|$. For a certain fluctuation of heat flux getting into the room, the larger the self-admittance, the smaller the room temperature fluctuation. Fig. 5.4-a shows that there is a maximum self-admittance and time lag regardless of the thickness of the assembly (Athienitis and Santamouris 2000). To minimize the room air temperature fluctuation (i.e. maximum storage) and to delay the response of the room temperature to its heat flux input to the utmost (i.e. long energy retaining time), a thickness of 0.2 meters is sufficient for the physical properties assumed. Analyzing ${}^{0\leftarrow rm}a21$ is not necessary since the node "0" temperature would be either similar to room temperature, or be much different (e.g. exterior). In the former case, the temperatures will have little influence on each other; while in the latter case, significant insulation will be normally adopted, and hence the influence of ${}_{0}T$ will be negligible.

$$ {}_{0_rm}\tilde{p}_i = {}_{0}\tilde{T}_i \cdot {}^{0\leftarrow rm}a21 + {}_{rm}\tilde{T}_i \cdot {}^{0\leftarrow rm}a22 \tag{5.3} $$

where $a21$ and $a22$ are from the admittance matrix ${}_{adm}[M]$ of assembly $0 \leftarrow rm$.

The dynamic response of the BITES to the heat flux (i.e. solar radiation, since interior long-wave radiation is combined with convection) absorbed on its room-side exposed surface,

${}_{slr}p$, can be found by analyzing the transfer function $\left({}^{0\leftarrow top}t12/{}^{0\leftarrow rm}t12\right)$ from Eq. (5.4). ${}^{0\leftarrow rm}t12$ takes into account the advective connection between the source level and the room air (Chapter 4).

The calculation results are plotted in Fig. 5.4-b. The thickness of 0.1 to 0.2 meter will give long time lag and small heat flux magnitude. For example, in a thermally heavy building with a 0.2-m thick BITES system, 1 W/m^2 of absorbed solar radiation will be released after 4.2 hours with an intensity of about 0.3 W/m^2. For an extremely light building, the time lag will be about 2.2 hours, and the magnitude will be about 0.4 W/m^2. Thermally lighter buildings have shorter time lags.

$$ {}_{slr_rm}\tilde{p}_i = {}_{slr}\tilde{p}_i \cdot \frac{{}^{0\leftarrow top}t12}{{}^{0\leftarrow rm}t12} \tag{5.4} $$

where ${}^{0\leftarrow rm}t12$ is from admittance matrix ${}_{adm}[M]$ of assembly $0 \leftarrow rm$, and ${}^{0\leftarrow top}t12$ is from assembly $0 \leftarrow top$ (Chapter 4).

The dynamic responses of the BITES to the heat injection in the source layer, ${}_{sc}p$, can be found by analyzing the transfer function $\left({}^{0\leftarrow sc}t12/{}^{0\leftarrow rm}t12\right)$ from Eq. (5.5). The influences on the dynamic responses of the BITES system – aside from the thickness of the concrete layer – also come from the location of the source layer. Fig. 5.4-c shows that the closer the source layer is to the bottom, the longer the time lag and slightly smaller the magnitude, regardless of the thickness and the building thermal storage mass (data are not plotted). The percentage of magnitude change is more significant for thick BITES systems and high advection flow rate.

Fig. 5.4-d plots the dynamic response for a source layer located 1/5 of the concrete layer thickness above the bottom surface of the concrete layer. Maximum time lags for different building mass level is shown. The difference in magnitude diminishes as the building thermal storage mass level increases. The dynamic response related to the source layer heat flux is the most important to active BITES systems since that heat flux is the main heat source.

$$_{sc_rm}\tilde{p}_i = {}_{sc}\tilde{p}_i \cdot \frac{{}^{0\leftarrow sc}t12}{{}^{0\leftarrow rm}t12} \tag{5.5}$$

where ${}^{0\leftarrow sc}t12$ is from admittance matrix ${}_{adm}[M]$ of assembly $0 \leftarrow sc$ (Chapter 4).

Further sensitivity analysis (Appendix A6) is conducted for the effects of relevant parameters on the dynamic response. The information from Fig. 5.4 and the sensitivity analysis gives insightful information and general guidelines for design and operation.

Generally, a larger time lag and smaller magnitude (i.e. thicker BITES) is preferable in practice for two main considerations. The first one is to enable a longer charging period within the off-peak period and hence to reduce the peak charging demand. The second consideration is to stagger in time the heat inputs to the room – passive solar heating and thermal output from active BITES systems. Therefore, more solar thermal energy can be stored in the BITES. Hence, a thickness of 0.2 m or larger is generally used for the purpose of providing enough TES capacity. Low conductive floor covering should be avoided in order to take advantage of the passive storage effect of the BITES systems.

Furthermore, a larger time lag and smaller magnitude (i.e. thicker BITES) is preferable in practice for two main considerations. The first one is to enable a longer charging period within the off-peak period and hence to reduce the peak charging demand. The second consideration is to stagger in time the heat inputs to the room. For example, staging the

passive solar heating and the thermal output from active BITES systems in a winter season will result in more solar thermal energy storage in the BITES.

The sensitivity analysis also shows that setting the bottom insulation (Fig. 5.3-a) value equal to the combined convective and radiative heat transfer coefficient (9 $W/m^2/K$) does not significantly affect the dynamic response for concrete thicknesses larger than 0.2 m. Changing the flow rate to less than 2 ACH will not alter the dynamic response significantly for equivalent concrete thickness of less than 0.3 m. Low flow rate should be used because it will save fan energy consumption and avoid thermal discomfort caused by draft. The variation of the top surface combined radiative and convective heat transfer coefficient have a considerable impact on the closed-loop systems (reduces the magnitudes by about 0.05 (half of original values) and increases the time lags by about 1 hour), but not significant on open-loop BITES systems with air flow rate of 2 ACH in thermally medium and heavy buildings (which are the suitable types of building for supplying primary space conditioning through active BITES system).

Therefore, a thickness of 0.2 to 0.3 m is a good value with which to initiate design, considering that the largest time lags and peak admittances are near that thickness range and it is not significantly sensitive to the above discussed design parameters. Further considering the fact that the dynamic response will deviate from the theoretical values in real practice, Fig. 5.4 alone will be sufficient for initial design and operation purposes for similar BITES assemblies. Fine tuning is necessary design and operation optimization.

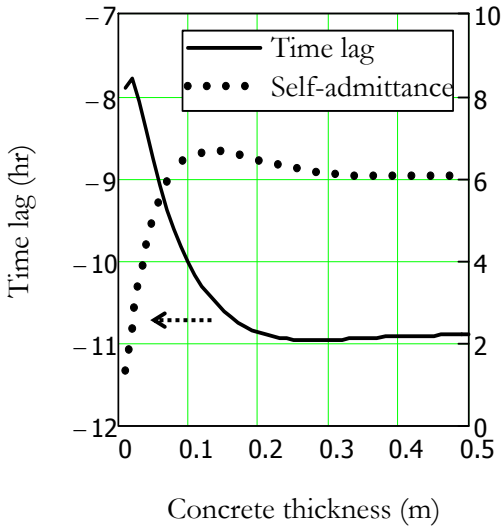

(a) Self-admittance; effect on room temperature

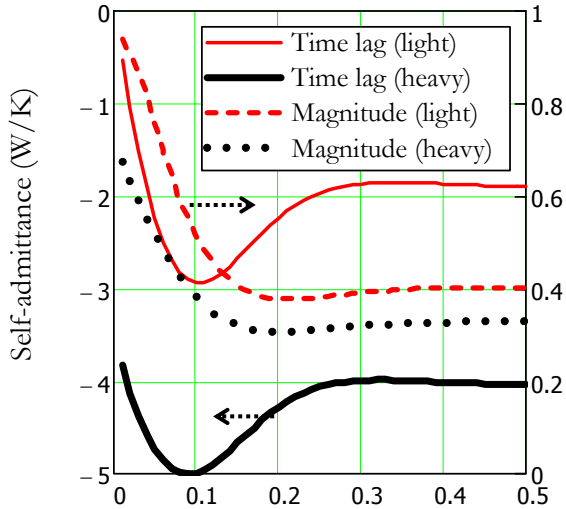

(b) Heat flow division for surface heat flux; buildings with different levels of thermal storage mass

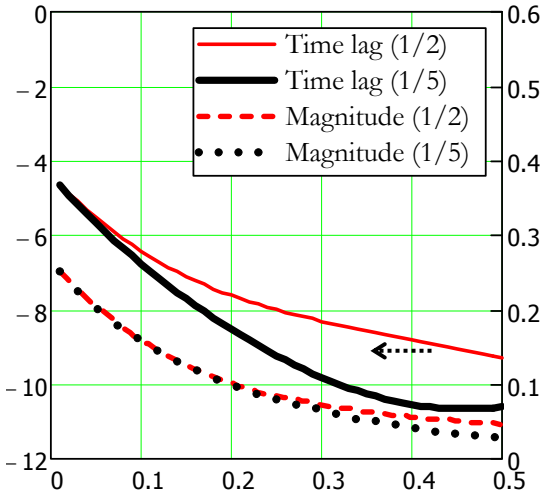

(c) Heat flow division for source heat flux; location of source for thermally heavy buildings

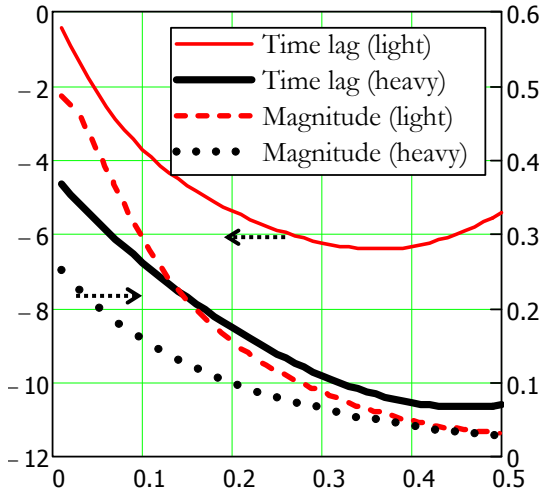

(d) Heat flow division for source heat flux; buildings with different levels of thermal storage mass; source layer at "1/5" level

Fig. 5.4: Dynamic response of an open-loop BITES slab and its associated room for 1 cycle per day excitations (left y-axis is time lag in hours; right y-axis is the magnitude of transfer functions (unit less); x-axis if equivalent concrete thickness in meters)

Notes for Fig. 5.4: equivalent concrete thickness equals to the net cross-section area divided by width; insulation is placed on the side opposite to room (Fig. 5.3); "light": thermally light buildings, thermal storage is insufficient; "heavy": thermally heavy buildings, effective thermal capacitance (including wall boards) is about 70 times that of enclosed air; "1/2": source layer (Fig. 5.3-a) is in the middle of the concrete layer; "1/5": source layer is 1/5 of the concrete layer thickness above the bottom surface of the concrete layer.

3.2. Design of predictive control strategies

As discussed earlier, the operations of the active BITES system should enable the utilization of off-peak and/or renewable energy at favorable periods. To accommodate the operations, a control methodology (Chapter 4) is adopted with slight modification – the weather forecast will be used to establish the room air temperature set-profile in association with the thermal dynamics of the active BITES system and its thermal zone (instead of the first-order time lag). The last two days of actual data (e.g. actual room air temperature and thermal output) before the prediction horizon should be incorporated into the excitations' profiles to "warm up" the thermal storage mass (see "Non-periodically steady thermal excitations" in Appendix for more information). Then, the room air temperature and required thermal output will be used as excitations (inputs) for the frequency domain model of the active BITES system to calculate the required thermal energy injection rate to the source layer of the BITES.

The establishment of a room air temperature set-profile for a space heating period (Fig. 5.5) is used here for a brief demonstration (see room configuration in Chapter 4). Note that for clarity, a warm-up period of data has not been incorporated into the excitation profiles. At first, 22.5°C is used as the set point with a throttling range of 5°C. In other words, the room temperature will not be lower than 20°C or higher than 25°C. One peak and one low

temperature pivot will be identified for each day. The temperature values (Y-axis) of these pivots is a function of outdoor peak and low sol-air temperature (ASHRAE 2009e). See Appendix for information of the function. The time difference (X-axis) between the peak room temperature and the peak sol-air temperature equals to the time lag (i.e. phase angle) of the whole system (i.e. BITES and the room). For example, the peak room air temperature for the first day (sunny and cold) is 25°C. In this demonstration, the construction is thermally medium heavy. The advection rate is 2 ACH. The source layer is located at the middle of the concrete slab, and the equivalent thickness of the slab is 0.3 m. Therefore, based on Fig. 5.4, the peak room temperature is set to occur 8 hours after the time when the peak sol-air temperature takes place, around hour 20. The preliminary room air temperature set-profile will be generated by connecting the adjacent pivots with straight lines. By setting the time difference in this way, the charging of the BITES and its associated room mass will start at the most favorable time (e.g. sunniest time for heating and coolest time for cooling). The design of the active BITES system allows the heat to be released in a small magnitude after the passive solar heating period. In this way, the maximum amount of the solar thermal energy is stored in the room and its BITES without space overheating. The time lags for control can be fine-tuned during commissioning since the effective room capacitance is not known beforehand.

In general, for a space heating scenario, the global solar radiation on equator-facing façades or solar thermal collector surfaces is recommended for the calculation of the sol-air temperature. For a space cooling scenario, the horizontal global solar radiation can be used, although for a building with large glazed facades (e.g. facing west), the facades may be used for an average sol-air temperature. To enable off-peak period charging even when ambient renewable energy is unavailable, a weighting factor (higher value for space heating, and lower

value for cooling) can be assigned to the off-peak period exterior temperature in the calculation of the sol-air temperature. Furthermore, a weighting factor for load matching (e.g. to consume electricity being generated from local photovoltaic panels) can also be applied. In this study, weighting factors are not applied. However, since favorable periods generally coincide with off-peak periods (e.g. sunny daytime during winter, and nighttime during summer), the adopted approach also enables utilization of off-peak purchased energy to a certain extent. Nonetheless, a systematic approach for the optimization of the room temperature set-profile that accounts for different parameters is worth further study.

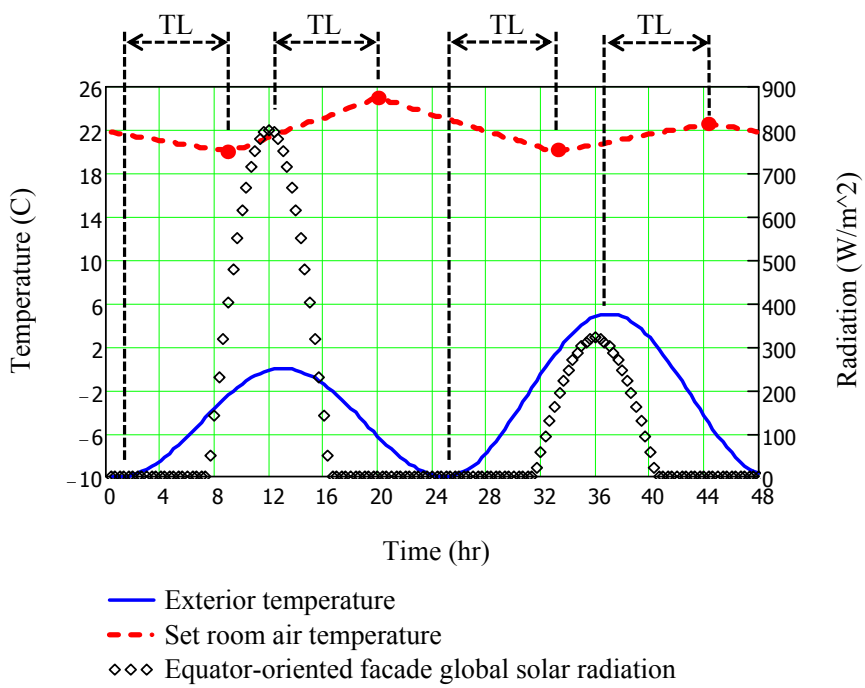

Fig. 5.5: Weather conditions and room air temperature set-profile during a two-day space heating period (Round dots: pivots, TL: time lag)

Even though the preliminary temperature set-profile shown in Fig. 5.5 seems abnormal, the final room air temperature turns up ideal (Fig. 5.6), with the calculation approach presented in Chapter 4. As shown in Fig. 5.6, the resultant room air temperature rises significantly during the sunny period of the first day to allow significant solar heat gain to be stored in the

BITES and the rest of the room. The room air temperature profile also reduces the space heating load after sunset by reducing the temperature difference between exterior and interior (letting the room temperature drop gradually). Peak power demands take place during the off-peak period (sunny daytime). Regarding thermal comfort, the temperature profile complies with temperature limits and avoids rapid changes.

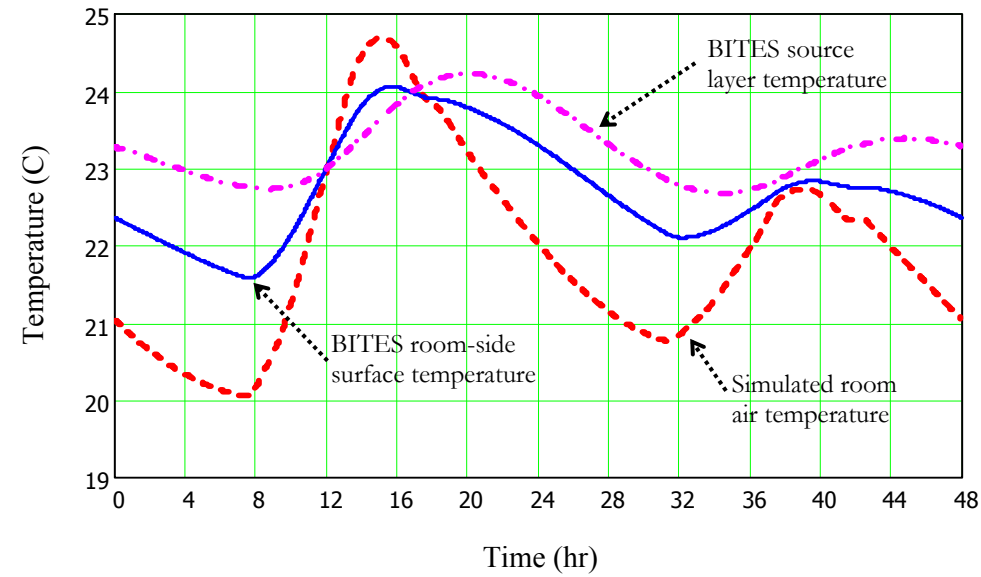

(a)

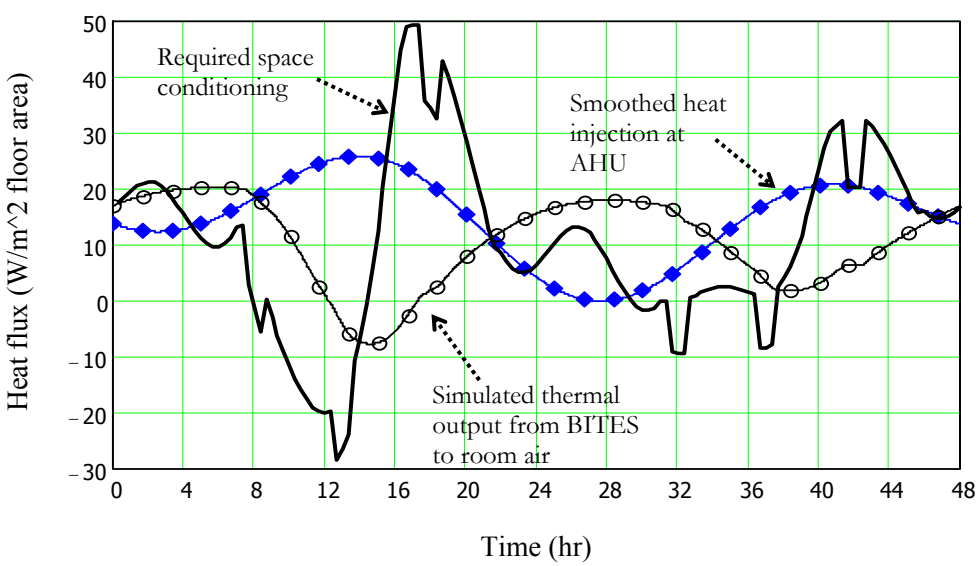

(b)

Fig. 5.6: Thermal energy injection rates at the air handling unit (AHU) and corresponding room air and BITES temperatures: (a) temperature profiles; (b) heat flux profiles (open-loop system)

The operation shown above requires proper parameter selection. In defining the key pivots for the room air temperature, the phase angles (i.e. time lag) are needed for scheduling the pivots. The phase angles are related to the concrete thickness, the location of the source layer, and the thermal output capacity of the active BITES system. The design provides desired charge/discharge and thermal output capacities with low temperature operation. In turn, the initial load profile helps determine the TES capacity and the thermal output capacity, which will be shown in the next subsection. Hence, the design and operation should be integrated, and there should be an iterative process in the integration. The design of the active BITES system has to suit the intended operation strategies.

3.3. Bounding conditions for design

The ideal performance of an active BITES system under bounding conditions (e.g. weather and internal heat gain), determines the required capacities (bounding performance) of its thermal attributes. The peak space conditioning load will take place under bounding conditions, and needs a matching thermal output capacity with low temperature operation. The TES capacity has to be large enough to store a matching amount of renewable or off-peak energy for the following extreme heat/cool period. Hence the charge/discharge needs to fulfill the TES requirement within a limited time by providing sufficient charging capacity. Fig. 5.6 shows that the energy performance of an active BITE system is related to dynamic room air temperature profile, weather condition, and its operation. The thermal attributes cannot be improved independently of these three parameters.

For a heating-dominated climate, a sunny cold day followed by an overcast mildly cold day would be an ideal bounding weather condition. The active BITES system will store as much energy as possible during the sunny period and then release the heat to its thermal zone to

sustain its comfort level until the next favorable charging time. A period consisting of two consecutive cold and overcast days may cause a larger space conditioning load. However, this is not practical for the control methodology – the active BITES system will not be fully charged during a cold and overcast period. It is similar in a cooling-dominated climate, where a relatively cool night followed by a hot day should be used as an ideal bounding weather condition.

Bounding conditions impose requirements on the dynamic response, but they are not as significant as those for apparent attributes. Under bounding conditions, room temperature set by the aforementioned control methodology defines the space conditioning load. The resulting bounding loads give good guidance on the design of the apparent attributes. The following paragraphs will present the calculation for proper thermal attributes. The profiles shown in Fig. 5.5 and Fig. 5.6 will be used for the demonstration.

3.3.1. TES capacity

The summation of thermal output and thermal energy injection rates during the unfavorable period defines the TES capacity, ${}_{TES}E$ (unit: kWh or J).

$$ {}_{TES}E \approx \int_0^t {}_BP(t)\,dt + \int_0^t {}_{sc}P(t)\,dt \approx \sum_1^{i=I} \left({}_BP_i + {}_{sc}P_i \right) \cdot \Delta t \qquad (5.6) $$

where ${}_BP$ is the total thermal output of the active BITES system, t is the time period, and I is the total of the time intervals, Δt, in the unfavourable period.

The TES capacity for unit square meter of exposed surface area (unit: J/m^2) can be calculated as follow:

$$_{TES}e = {}_{B}Th \cdot {}_{B}\Delta T \cdot {}_{B}\rho c \tag{5.7}$$

where ${}_{B}Th$ is the equivalent thickness of the thermal storage mass, ${}_{B}\rho c$ is the volumetric heat capacity of the mass, and ${}_{B}\Delta T$ is the operation temperature range of the BITES. For the total active BITES system,

$$_{TES}E = {}_{B}Area \cdot {}_{TES}e = {}_{B}Area \cdot {}_{B}Th \cdot {}_{B}\Delta T \cdot {}_{B}\rho c \tag{5.8}$$

With known volumetric heat capacity ${}_{B}\rho c$, initial thickness ${}_{B}Th$, and the operation temperature range ${}_{B}\Delta T$ from bounding conditions, the BITES area ${}_{B}Area$ can be determined. For the space heating scenario, the thermal output between the peak sol-air temperatures in the two days of the design period is used for Eq. (5.6). Hence, time period t equals 24 hours. The Literature shows that diurnal thermal energy storage is most important and effective (Balcomb 1983). This choice of time period is also applicable to the space cooling scenario.

For the profiles shown in Fig. 5.5 and Fig. 5.6, the total thermal output from the BITES to the room ($\int_0^t {}_{B}P(t)\, dt$ in Eq. (5.6)) between hour 12 to 36 is about 7.6 kWh (27.5x10^6 J), and the thermal energy injection ($\int_0^t {}_{sc}P(t)\, dt$) is 4.5 kWh (16.1x10^6 J). Also note that the slab was not charged to an ideal temperature (i.e. 25°C as the set upper limit of the room air temperature) during the sunny period. This is because there was excess solar gain, and hence some cooling is required from the slab. Ideally in practice, useful solar heat gain and free cooling should be controlled at a suitable level so that no excess heat or cool is admitted to the thermal zone. Under this condition, the space conditioning load (e.g. thermal output from BITES) will be (or set to) zero. Hence, the BITES will be fully charged, and less thermal energy injection will be required.

Let us take 12.1 kWh (7.6+4.5) as the required TES capacity, and ${}_{B}\rho c$ of normal weight concrete of 0.51 kWh/m^3/K (1.85x10^6 J/m^3/K). The temperature drop (i.e. operation temperature range) of the BITES after the sunny day is about 1.75°C (Fig. 5.6, source layer is about 0.5°C warmer). For design purposes and based on experiments, it is practical and sufficient to assume 0.5°C, or no significant temperature difference between the exposed surface and the source layer of the BITES. Let us take the operation temperature range (${}_{B}\Delta T$) of 2.25°C (extra 0.5°C for ideal operation). Therefore, the required area according to Eq. (5.8) is about 35.0 m^2. This is about 10% larger than the slab area used here (31.5 m^2) (Chapter 4).

3.3.2. Thermal output capacity

By satisfying the required thermal output under bounding conditions, the parameters related to thermal output capacity can be determined. For unit square meter of exposed surface area (unit: W/m^2/K),

$$ {}_{B}u = {}_{CR.B}u + {}_{A.B}u = {}_{top}h + {}_{f.t}Qc / {}_{B}Area \tag{5.9} $$

where ${}_{CR.B}u$ is the combined convective and radiative thermal output from the exposed surface, equal to a film coefficient ${}_{top}h$. ${}_{A.B}u$ is the advective output. It is zero for closed-loop systems. ${}_{B}Area$ is the top exposed surface area. ${}_{f.t}Qc = {}_{f.t}Q \cdot {}_{f}\rho c$ with ${}_{f.t}Q$ being the total volumetric flow rate of the heat transfer fluid (air in this case), and ${}_{f}\rho c$ the volumetric heat capacity of the fluid.

Hence, the thermal output capacity (unit: W) can be calculated as follows:

$$ {}_{B.max}P = {}_{rm_B.max}\Delta T \cdot {}_{B}Area \cdot {}_{B}u = {}_{rm_B.max}\Delta T \cdot \left({}_{B}Area \cdot {}_{top}h + {}_{f.t}Qc \right) \tag{5.10} $$

where ${}_{rm_B.max}\Delta T$ is the maximum temperature difference between the room air and the average BITES temperature.

The allowable maximum and minimum BITES temperature, ${}_{B.max}T$ and ${}_{B.min}T$, and maximum and minimum room air temperature, ${}_{B.max}T$ and ${}_{B.min}T$, should comply with thermal comfort standards and are subjective to occupants. To accommodate a larger range of occupant preferences, less extreme values can be chosen. For the space heating scenario, ${}_{rm_B.max}\Delta T = {}_{B.max}T - {}_{rm.min}T \approx 28 - 20 = 8$°C, and ${}_{rm_B.max}\Delta T = \left({}_{rm.max}T - {}_{B.min}T\right) \approx 25 - 20 = 6$°C for the space cooling scenario.

Once the maximum ${}_{f.t}Qc$ is determined, the exposed surface area of the BITES can be obtained. Similar to ${}_{rm_B.max}\Delta T$, ${}_{top}h$ is determined by heat transfer conditions, but approximate values can be used for design purposes. For a closed-loop system (i.e. ${}_{f.t}Qc = 0$), 6 and 8 W/m^2/K can be used for space cooling and heating, respectively. 9 W/m^2/K can be used for open-loop systems regardless of cooling or heating, since room air is being stirred by BITES outlet air. Hence, the combined radiative and convective thermal output capacity is about 64 to 72 W/m^2 for heating and 36 to 45 W/m^2 for cooling.

For the profiles shown in Fig. 5.5 and Fig. 5.6, the maximum thermal output (i.e. ${}_{B.max}P$ in Eq. (5.10)) is about 630 W (20 W/m^2 x 31.5 m^2 of floor area). If the maximum flow rate is 2 ACH (0.053 m^3/sec), ${}_{f.t}Qc$ will be about 69.0 W/K. The exposed surface area of the BITES should be about 1.1 m^2 according to Eq. (5.10). Without advection (i.e. closed-loop system), the area has to be about 9.8 m^2.

If the required thermal output for cooling is 630 W, the required BITES area will be 4.0 m^2 for open-loop configuration with 2 ACH, and 17.5 m^2 for closed-loop. Using the maximum temperature difference between the room air and average BITES temperature, ${}_{rm_B.max}\Delta T$, means relatively high temperature operation. To avoid this, a larger BITES surface area should be used.

3.3.3. Charge/discharge capacity

Knowing the operation during the bounding conditions and the required TES capacity, the needed charge/discharge capacity can be calculated. The charge/discharge capacity should be high enough to allow full charge of the BITES for a given period (e.g. sunny hour during a typical winter day). For unit square meter of room-side surface area (unit: $W/m^2/K$),

$$ {}_{sc}u = {}_{sc}h \cdot {}_{core}Area / {}_{B}Area = {}_{sc}h \cdot {}_{cs}Ratio \tag{5.11} $$

where ${}_{sc}h$ is the CHTC between the path inner surface and the air flow (e.g. source layer). ${}_{cs}Ratio$ is the area ratio of internal heat transfer surface to room-side surface. It is created in this study to quantify the charge/discharge capacity based on unit room-side surface area, since the calculation of other thermal attributes are also based on this parameter.

The thermal energy that can be stored should equal to the TES capacity. Hence, from Eq. (5.11),

$$ {}_{TES}E = {}_{sc_f}\Delta T \cdot {}_{sc}u \cdot {}_{B}Area \cdot {}_{charge}t = {}_{sc_f}\Delta T \cdot {}_{sc}h \cdot {}_{cs}Ratio \cdot {}_{B}Area \cdot {}_{charge}t \tag{5.12} $$

where ${}_{sc_f}\Delta T$ is the difference between source layer temperature and mean fluid temperature, and ${}_{charge}t$ is the charging time.

Charging time ${}_{charge}t$ can be assumed to be half of the annual shortest daytime. It is reasonable to assume there is no heat exchange between room air and BITES during charging time (i.e. the BITES temperature rises with that of the room air). Since the outlet air is close to the source layer temperature (around 23°C during charging period (Fig. 5.6)), and inlet air is less than 35°C for low temperature operation or using solar-heated air directly from solar thermal collectors (Chen et al. 2010a), ${}_{sc_f}\Delta T$ can be conservatively assumed to be about 6°C, half of the temperature difference between inlet air and source layer. Note that for closed-loop systems, ${}_{sc_f}\Delta T$ can be set constant; while for open-loop systems, ${}_{sc_f}\Delta T$ is affected by the required thermal output. With known flow rate (hence ${}_{sc}h$), the area ration of internal heat transfer surface to exposed surface, ${}_{cs}Ratio$, can be obtained. Once ${}_{B}Area$ is known from determining the ${}_{TES}E$ in Eq. (5.8), the air channel (i.e. core) surface can be obtained. Furthermore, the charging capacity has to satisfy the thermal output capacity. This is usually satisfied for open-loop systems. For closed-loop systems, the charging capacity can be achieved by increasing the fluid inlet temperature.

For the profiles shown in Fig. 5.5 and Fig. 5.6, the charging period is about 4 hours (daytime is about 9 hours). The ${}_{sc}h$ is about 5.1 W/m^2/K for 2 ACH flow rate (0.62 m/sec air velocity in the air channel) for the air channel used here. Using ${}_{B}Area$ of 35.0 m^2 from the previous calculation, the resultant ${}_{cs}Ratio$ is about 2.8. That means the required air channel surface is 2.8 m^2 per square meter of exposed surface area, or about 99.0 m^2 in total. As will be shown later, for standard hollow core structural components, ${}_{cs}Ratio$ of 2.8 is quite high. Further design improvement is needed.

3.4. Methodology implementation

As shown in the above calculations, Eq. (5.8) to (5.12), and in the analysis of the dynamic response, the BITES exposed area $_{B}Area$ and the thermal storage mass equivalent thickness play important roles. The TES capacity, charge/discharge capacity, and interior thermal coupling are commonly affected by the room-side area of the BITES. The equivalent thickness significantly influences the dynamic response and the TES capacity. Hence, designers can initiate the design with an initial BITES effective thickness (0.2 to 0.3 m for concrete as suggested previously) and one interior surface area (normally the floor or the ceiling). Using one entire interior surface is for practical construction and uniform room air temperature considerations. Normally, large thermal output also means large thermal energy needs to be stored. The area requirement for TES capacity and charge/discharge capacity is usually higher than that for thermal output, except in the case where buildings have high space conditioning spikes occasionally (e.g. conference room). In this case, the exposed surface area should be first determined through the required thermal output capacity (interior thermal coupling). Then the thickness can be determined by the required TES capacity. Sometimes, the requirement of the surface area has to consider the possibility that the room side surface of BITES maybe partially covered (e.g. carpet, acoustic panels). The largest impact due to covering is on the thermal output capacity and the dynamic response, especially for closed-loop systems.

If the initial surface area is not sufficient for the required peak thermal output or charging capacity (assuming maximum allowable flow rate have been reached), additional surface area can be added to increase the total exposed surface area. In the meantime, thickness can be adjusted if the desired dynamic response can be approximately maintained. This will slightly

change the suitable room air temperature set-profile and hence the space conditioning load. An iterative process is necessary. However, since the temperature will not change significantly, one iteration is expected to be sufficient.

In summary, the general procedure for integration of design and operation is as follows (Fig. 5.7):

(1) Identify bounding thermal load conditions (e.g. design weather conditions, internal heat gain);
(2) Decide on operation strategies that enhance (heuristically, based on thermal dynamics) thermal comfort and energy efficiency under the bounding conditions (e.g. allow room temperature to swing within comfort zone; pre-condition active system with ambient renewable energy or off-peak utility energy);
(3) Design active BITES (e.g. storage mass thickness and air flow rate) to provide suitable dynamic response for the operation strategies from Step (2) (Fig. 5.4);
(4) Control approach: operate active BITES based on room air temperature set-profile; generate temperature set-profile based on steps (2) and (3) under bounding conditions;
(5) Estimate the corresponding space conditioning load profile using numerical models of the thermal zone, excluding the BITES system;
(6) Select one or multiple available interior surfaces as the BITES room-side surface according to the maximum thermal output capacities of the different selected active BITES systems and the peak space conditioning load. Attention is needed for potentially covered area;

(7) Calculate the required thermal energy injection rates of the active BITES system, and the thermal output rates of the system (e.g. Fig. 5.6)

(8) Then:

   i. Check the inlet fluid flow rate and temperature, if they are within design values;

   ii. Check the sufficiency of the TES capacity;

   iii. Check the peak thermal output;

   iv. Calculate the required minimum area ratio of internal heat transfer surface to room-side surface (i.e. air channel surface area for ventilated systems and pipe perimetric area for hydronic systems).

(9) Adjust the active BITES design if needed and repeat the steps (3) to (8), which is the "Design optimization" in Fig. 5.7.

Steps (4) and (5) in this procedure are for the control approach presented in this thesis. This integration procedure can be applied to other control approaches, by replacing step (4) and (5) with counterparts.

The design of the building will also be influenced by the design and operation of BITES. For example, if the space conditioning load exceeds the thermal output capacity of the selected active BITES system, the envelope of the building (e.g. insulation level or shading device) should be improved or other types of active BITES systems should be chosen.

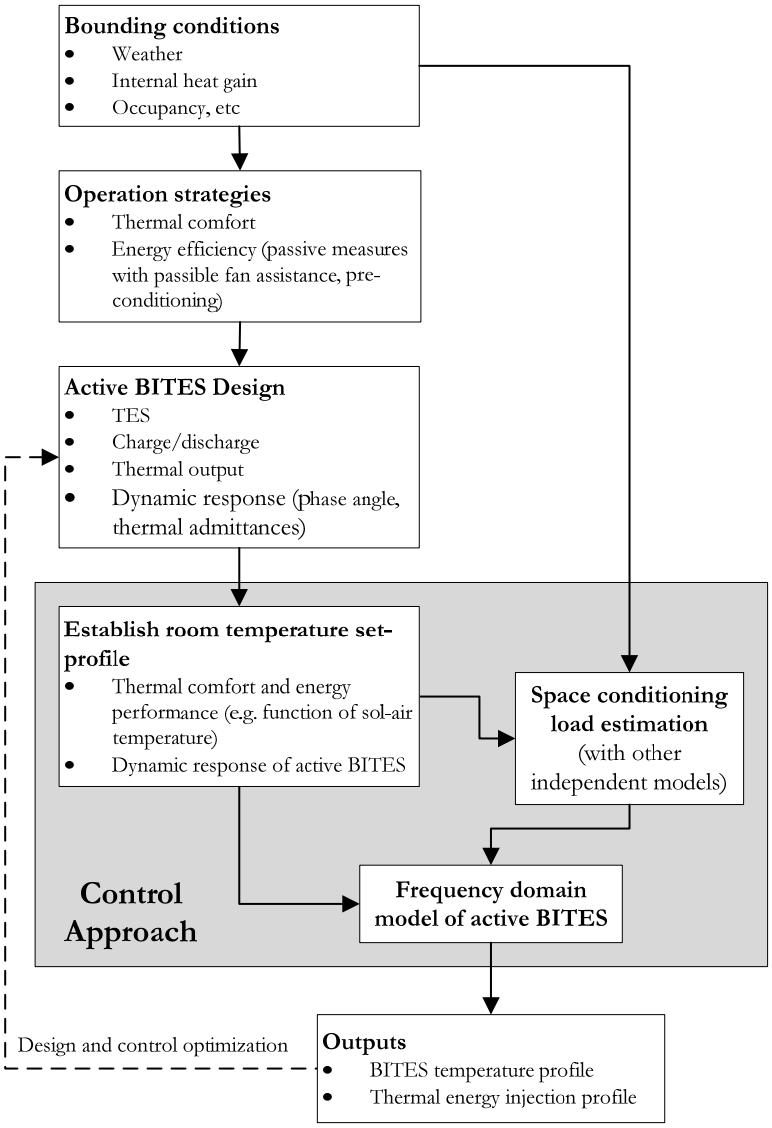

Fig. 5.7: Active BITES systems design procedure

4. Integrating structural and thermal functions

One of the major advantages of BITES systems is the combination of structural and thermal functions into one single system with reduced cost. Structural components with hollow cores, such as hollow core slabs and concrete masonry block walls, can become ventilated BITES systems by using the hollow cores as air channels with minor alterations. The alterations from conventional construction methods would mainly include connecting the hollow cores

inside the structural components and opening holes on the surface for air inlet and outlets (Fig. 5.8). To satisfy structural requirements and save effort on designing new structural components, the thermal attributes of standard structural components can be analyzed first.

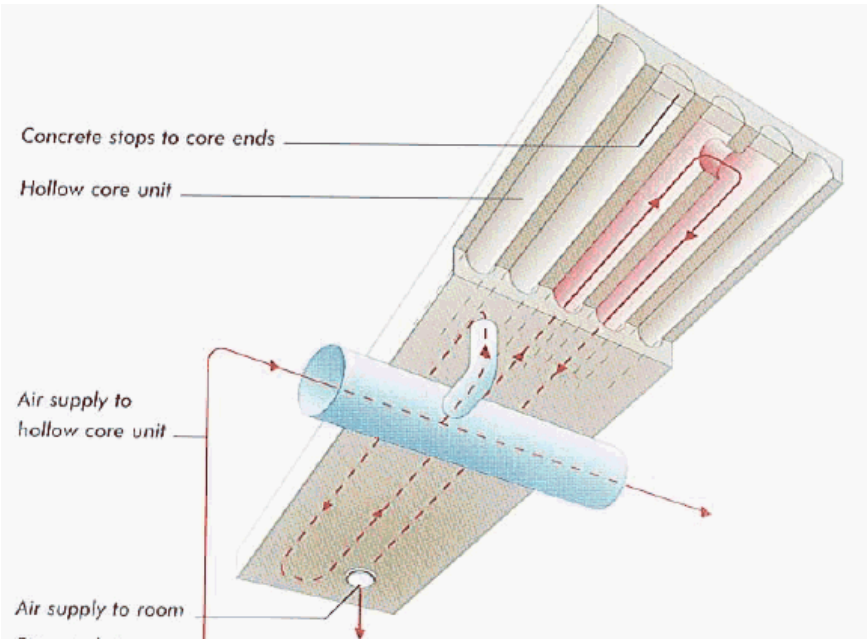

Fig. 5.8: A ventilated BITES system (source: PTY Ltd, www.hollowcore.com.au)

The idea of using structural components with hollow cores is mainly to save on cost by improving the use of material. This is because the material at the center of the cross section is not significant for the slab's structural functions, mainly flexural strength, yet it increases the self-weight of the structure and the building. For BITES functions, this hollow space can be used for air circulation to enable active charge and discharge of the BITES system and to engage more effective mass with increased heat transfer area. On the other hand, suitable amounts of thermal storage mass are needed for thermal energy storage. The hollow space has to be balanced for these two thermal functions as well as the structural function. For a given standard component, its cross section is designed for the structural function. Hence,

structural mass can be added (i.e. reducing hollow space), but not removed. Adding more mass will require a structurally stronger component, namely a larger panel depth.

Since the equivalent thickness and the area ratio of internal heat transfer surface to room-side surface ${}_{cs}Ratio$ are the two critical design parameters, the following study samples several typical slab depths and lists their equivalent thicknesses based on different ${}_{cs}Ratio$. For hollow core slabs/walls, their cross sections are different from each other, depending on the manufacturer. Cross sections with circular hollow cores are studied here since they have the maximum net cross section area for a given ${}_{cs}Ratio$, and hence more thermal storage mass. Furthermore, for a given ${}_{cs}Ratio$, the fewer the number of cores, the larger the hollow space (i.e. less thermal storage mass).

4.1. Precast hollow core slabs

Table 5.1 shows the cross section configurations of different standard hollow core slabs and their variations. 1220 mm (4 ft) is a common nominal panel width used in manufacturing, and is also used here. More mass is added to the standard cross sections by reducing the ${}_{cs}Ratio$ from the existing value to 1.0, and then reducing the number of cores. Keep in mind that the core diameter will affect the friction between the fluids and the pipe/channel surface, and consequently the fan/pump power for fluid transportation. In practice, 50 mm (2 inches) of topping is often added to slabs. In hydronic BITES systems, the tubes can be laid on top of the slab and embedded within the concrete topping.

Table 5.1: Thermal attributes related dimensions of standard hollow core slabs (CPCI 2010) and their variations

Slab depth	Net cross section area (1.22 m width)	Equivalent slab thickness	No. of cores	Core diameter	$_{cs}Ratio$
m (in.)	m^2 ($in.^2$)	m (in.)		m (in.)	
0.102 (4)	0.099 (154)	0.082 (3.2)	12	**0.051 (2.0)**	1.6
	0.109 (169)	0.090 (3.5)	8	0.049 (1.9)	1.0
0.152 (6)	0.121 (188)	0.100 (3.9)	8	**0.101 (4.0)**	2.1
	0.171 (265)	0.140 (5.5)	8	0.049 (1.9)	1.0
	0.156 (242)	0.128 (5.0)	4	0.097 (3.8)	1.0
0.203 (8)	0.138 (214)	0.113 (4.5)	6	**0.153 (6.0)**	2.4
	0.228 (353)	0.187 (7.3)	6	0.065 (2.5)	1.0
	0.208 (323)	0.171 (6.7)	3	0.129 (5.1)	1.0
0.254 (10)	0.167 (259)	0.137 (5.4)	5	**0.191 (7.5)**	2.5
	0.286 (443)	0.235 (9.2)	5	0.078 (3.1)	1.0
	0.270 (419)	0.222 (8.7)	3	0.129 (5.1)	1.0
0.305 (12)	0.186 (289)	0.153 (6.0)	4	**0.243 (9.6)**	2.5
	0.265 (411)	0.217 (8.6)	4	0.184 (7.3)	1.9
	0.342 (530)	0.281 (11.0)	4	0.097 (3.8)	1.0
	0.312 (484)	0.256 (10.1)	2	0.194 (7.6)	1.0

Note:

1. The values in the hatched area are for standard components;
2. Core diameters in bold are the maximum allowable values;
3. $_{cs}Ratio$ is based on one side of the slab;
4. 0.102 m thick slab is not common in practice;
5. Equivalent slab thickness equals to net cross section area per 1.22 m length divided by 1.22 m.

4.2. Concrete masonry block walls

A masonry concrete block unit (Fig. 5.9) has a standard actual length of 390 mm (15 5/8 in.), and a standard actual width of 190 mm (7 5/8 in.). In practice, a mortar joint of 10 mm is added between block units, and 10 to 20 mm of plastering is usually applied to the surface of a concrete masonry block wall. The minimum allowable web and face shell thickness and the net cross section area are defined by the structural strength requirement. On the other hand, masonry concrete blocks are often used as non-structural elements (i.e. partitions) due to their high fire rating and acoustic insulation characteristics. Table 5.2 shows the cross section configurations of different standard concrete masonry blocks and their variations.

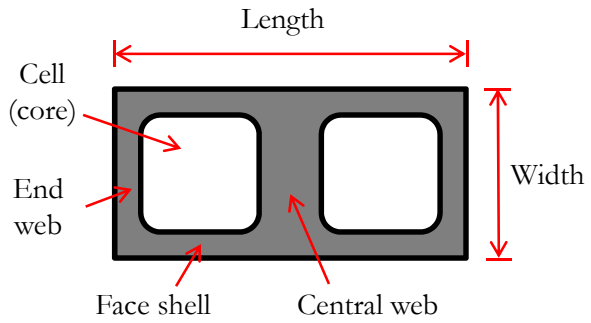

Fig. 5.9: A typical concrete masonry block

Fig. 5.10 proposes a connection configuration between parallel hollow cores (air channels). Webs of masonry units near the upper or lower ends of the wall are partially removed to create openings to connect the channels. Two channels (one in each separated course of units) can be created for a larger total opening area. Precast connecting blocks with web openings can be utilized to facilitate construction. Turning vanes smooth the air flow turning and hence reduce friction. Reinforcement is cut to avoid going through the air channels. Air channels between reinforcement and grouted cells can be connected without going through grout, and hence weakening the structural strength. For non-load bearing block walls, neither grout nor reinforcement is needed. Air channels can be connected freely.

Table 5.2: Thermal attribute related dimensions of standard concrete masonry blocks (CSA 2004, Drysdale 1999) and their variations

Nominal unit width	Face shell thickness	Equivalent web thickness	Equivalent wall thickness	$_{cs}Ratio$	Note
m (in.)	m (in.)	m/m (in./ft)	m (in.)		
0.152 (6)	0.025 (1.0)	0.188 (2.3)	0.070 (2.7)	2.5	Two normal cells
	0.029 (1.1)	0.549 (6.6)	0.106 (4.2)	1.7	Two smaller square cells
	0.025 (1.0)	0.582 (7.0)	0.106 (4.2)	1.2	One normal cell grouted
0.203 (8)	0.032 (1.3)	0.188 (2.3)	0.091 (3.6)	2.8	Two normal cells
	0.045 (1.8)	0.477 (5.7)	0.140 (5.5)	2.0	Two smaller square cells
	0.032 (1.3)	0.582 (7.0)	0.140 (5.5)	1.4	One normal cell grouted
0.254 (10)	0.035 (1.4)	0.209 (2.5)	0.111 (4.4)	3.3	Two normal cells
	0.064 (2.5)	0.398 (4.8)	0.177 (7.0)	2.3	Two smaller square cells
	0.035 (1.4)	0.592 (7.1)	0.177 (7.0)	1.6	One normal cell grouted
0.305 (12)	0.038 (1.5)	0.209 (2.5)	0.127 (5.0)	3.7	Two normal cells
	0.083 (3.3)	0.328 (3.9)	0.211 (8.3)	2.6	Two smaller square cells
	0.038 (1.5)	0.592 (7.1)	0.211 (8.3)	1.9	One normal cell grouted

Note:

1. The values in the hatched area are for minimum allowable thickness for face shell and webs;
2. In calculating the equivalent wall thickness, 0.025 m (3/8 in.) thickness of web is added to the equivalent web thickness per meter length;
3. $_{cs}Ratio$ is based on one side of the wall.
4. Two smaller square cell: splitting the void area of one standard cell into two cells (Fig. 5.11-a).

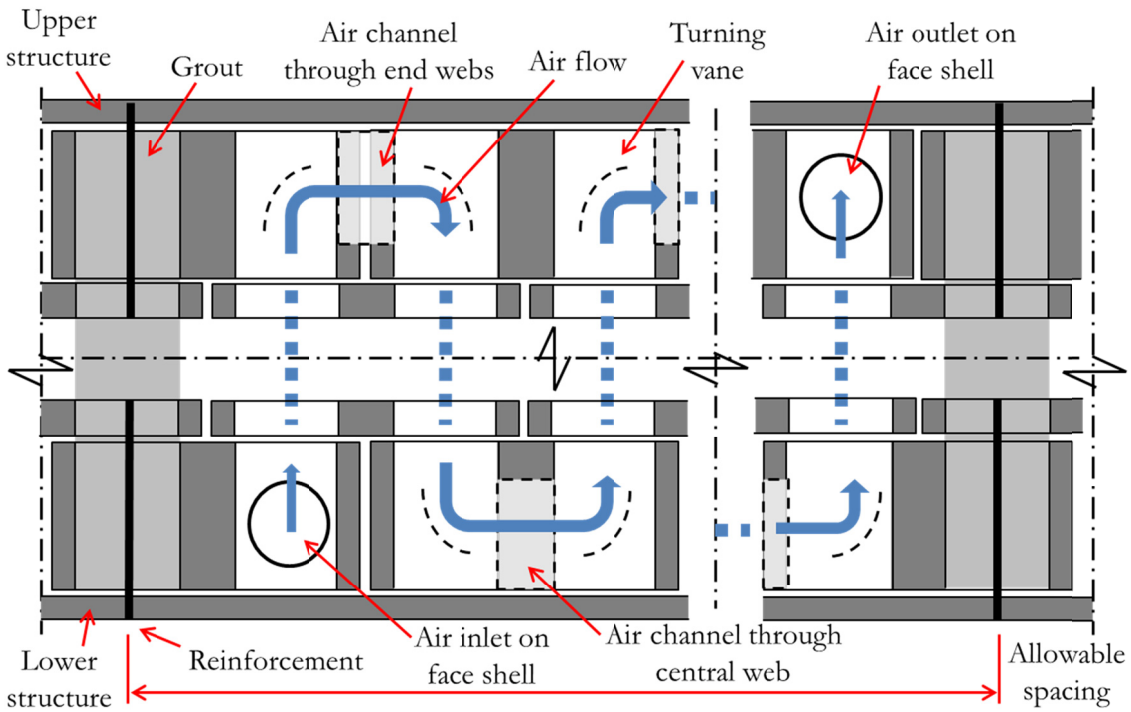

Fig. 5.10: Schematic of creating connection between hollow cores (air channels)

When equivalent wall thickness (i.e. net cross section area per meter length divided by one meter) larger than standard values is needed, three potential approaches can be adopted (Fig. 5.11). The void area can be reduced if smaller air channel cross section area does not result in significant friction loss for air flow. Thermal storage panels (e.g. PCM panels) can be adhered to the masonry block wall. Also, the face shell thickness can be increased.

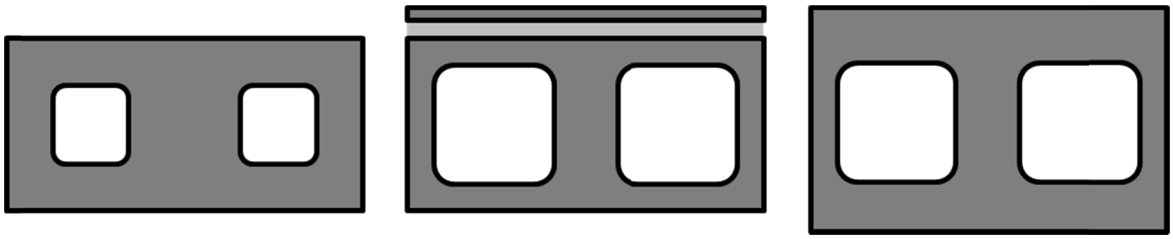

(a) (b) (c)

Fig. 5.11: Potential approach for increasing storage capacity: (a) reduce void space; (b) add thicker plastering or additional thermal storage panels; (c) increase face shell thickness

4.3. Effects of openings on structural strengths

For flexural strength of reinforced concrete slabs, since concrete is not essential in providing tensile strength, opening holes on the tension side of the components will not significantly affect its flexural strength. In some cases, holes are opened on the compression side. In these cases, the flexural strength may be affected, depending on the capacity of the remaining cross section. Note that brittle failure (compression side failure) is not permitted in concrete structure design. For horizontal components pin-supported at both ends, the maximum bending moment exists near the mid-span. For vertical structural components, the bending moment is approximately uniform along the height, if the supports are simply pin - connected.

In connecting the air channels within the walls and slabs, holes will be opened on the inner webs that are between the air channels and normal to the room-side surface. By doing this, the shear strength of the structural components will be weakened. For horizontal components (e.g. slabs), the largest shear load exists near their supports. For vertical components, the shear load is normally uniform along the height, but there is horizontal tensile stress near the lower end due to self-weight. Instead of one bigger hole, two smaller holes along the air channel can be opened. Hence the reduction to the shear capacity will be decreased.

4.4. Application and discussion

Using the aforementioned design procedure and the information provided, designers will be able to select a suitable cross section to meet the needs of the building in question. For the previous example, the TES capacity requires 35.0 m^2 of 0.3 m thick concrete, and the required ${}_{cs}Ratio$ is 2.8. Using the hollow core slabs listed in

Table 5.1 for reference, the equivalent concrete thickness of the slab with 0.305 m depth, ${}_{cs}Ratio$ of 1.9, and 0.05 m topping, will be only 0.267 m. Therefore, the thickness and ${}_{cs}Ratio$ are less than what is required. Hence, if this slab is used, a larger BITES area is needed to reduce the required ${}_{cs}Ratio$ value. The design procedure needs to be repeated. A conclusion can also be drawn – for ventilated BITES system, the slab thickness should be less than 0.3 m; otherwise, practical charge/discharge capacity (low temperature operation, low flow rate, and non-excessively large slab depth) will not be sufficient for the fully charging requirement. A properly designed envelope is required to reduce the space conditioning load of the space, and hence the apparent thermal attributes.

If the slab thickness is reduced and more area is added to the current area, a concrete masonry block wall can be used as an active BITES system. The air channels in these two parts (wall and the floor) can be connected with proper coordination of the spacing of air channels in both parts. Elbows can be used to facilitate the connection (Fig. 5.12). Ideally, the connection should be around the joining point (e.g. around the slab supporting beams) to avoid complicating the structure of the joints.

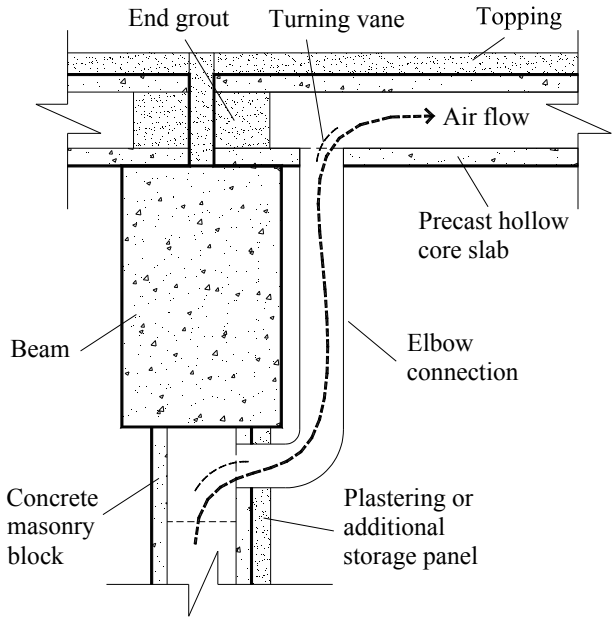

Fig. 5.12: Schematic of a connection between a hollow core slab and a masonry block wall

Fig. 5.13 shows a network of main design elements of active BITES systems that integrate structural and thermal functions. The dark grey elements, mainly related to the thermal function, are discussed in detail in this study. The light grey elements are studied briefly. As shown, the geometry and shape (or cross section) and material properties are the common elements that significantly influence structural and thermal functions. Although fluid mechanics-related technical issues and construction and operation costs are not included in this figure, it already shows that there are many elements to consider when designing such BITES systems. Using standard structural components can save significant effort in designing new models of active BITES systems that have a high level of integration of structural and thermal functions.

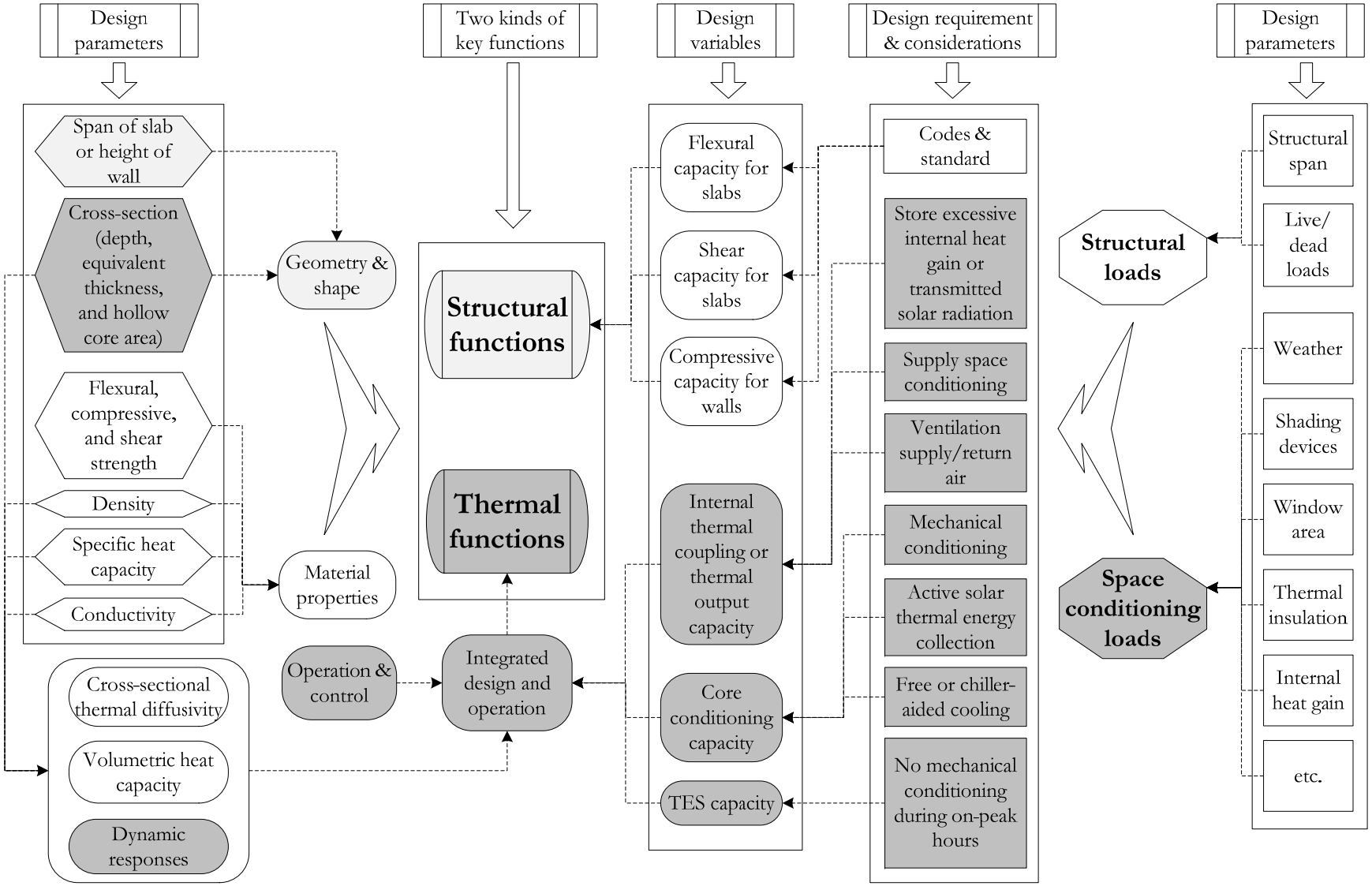

Fig. 5.13: Network of design elements for structural and thermal functions

5. Other application considerations

5.1. Thermal zoning

Different thermal zones have different space conditioning loads. Hence, the temperatures of their active BITES systems will be required to be different. In using precast hollow core slabs, the slabs should be laid out in a way that they do not span across different thermal zones. Within one thermal zone, the slab may be longer than the length of one room and hence span across different rooms. In this case, holes for air inlets and/or outlets may be required at the mid-span of the slabs. The air channel layout within the slab should be altered accordingly.

5.2. Occupant inputs for control

Occupants should be able to adjust the temperature set-point and the throttling range (i.e. upper and lower limits of the temperature range), especially in residential units. Furthermore, occupants should also be able to inform the control system of unusual thermal gains that the control system does not anticipate. During non-habitual events, such as gatherings, intensive internal heat gain will take place. Occupants should be able to and should input relevant information (e.g. number of people and schedule) in advance (e.g. hours) through the machine-user interface. Hence, operation (predictive control) will take corresponding action.

5.3. Broader integration

Reducing energy consumption is one of the goals for using active BITES systems. The energy consumption discussed above mainly concerns the thermal energy for space conditioning. In addition, operation energy, mainly for transporting the fluids, also contributes to the energy consumption. Fig. 1.8-b shows the potential application of an

open-loop BITES system in a large size building. In this example, the space conditioning energy is transported to the local AHU through water in pipes. The ventilation air flow rate does not depend on the space conditioning load. Local air re-circulation flow rate and supply water temperature in the AHU will be adjusted locally. For small buildings (e.g. houses) with open-loop systems, local AHUs are generally not adopted. The space conditioning and ventilation are both accomplished by the air. The flow rate will be adjusted according to the space conditioning load.

In the case where ventilation and space conditioning are accomplished by one ventilated BITES system, to reduce the transportation energy, it is ideal that the flow rate required for ventilation (around 0.2 ACH) can also satisfy the requirement for TES storage and space conditioning. Studying the previous example shows that this is possible. The room-side exposed surface area required for thermal output capacity is much less than that for TES capacity. If the area ratio of internal heat transfer surface to room-side surface $_{cs}Ratio$ cannot be satisfied with the floor surface, another interior surface can be used. Also, the building envelope can be improved to reduce the space conditioning load, and hence the TES requirement (capacity and charging/discharging rate). Furthermore, a local air re-circulation feature can be adopted to facilitate thermal storage and buffering – a short cut to avoid sending air back to the plant unnecessarily. The ideal ventilated BITES system should integrate the structural, thermal, and ventilation system together.

6. Conclusion

A design and operation methodology for active building-integrated thermal energy storage (BITES) systems was presented in this chapter. The influence of active BITES systems' thermal attributes (apparent capacities and dynamic response) on design and operation, and

the linkage between them through their thermal attributes are discussed in depth. An integrated design approach based on a previously proposed control methodology and bounding conditions was presented.

The ideal ventilated BITES system should integrate the structural, thermal, and ventilation systems together. To facility the integration of structural and thermal functions, the thermal attributes of standard structural components (precast hollow core slab and concrete masonry block wall) and their variations are studied. A configuration for using concrete masonry block walls as ventilated BITES systems was presented.

In the applications of ventilated BITES systems, a conclusion is drawn based on practical structural design and relationships between thermal functions/attributes. That is the equivalent slab thickness should not be more than 0.3 m; otherwise, thermal capacities will be mismatched – practical charge/discharge capacity will not be sufficient for fully charging/discharging requirements. Also based on dynamic response, 0.2 to 0.3 m equivalent thickness is a good value to use to initiate design. Energy efficient envelope design is required for successful applications of active BITE systems.

Chapter 6 Conclusion

Significantly reducing the purchased energy consumption and peak power demand of buildings can be realized through the reduction of space conditioning energy consumption and peak power demand, while maintaining or enhancing thermal comfort. Thermal storage is an important parameter in designing energy efficient and comfortable high performance buildings. Active BITES systems can store and release thermal energy in a controllable manner. Furthermore, they have strong thermal coupling with their thermal zones. Their charge/discharge systems (hydronic or air-based) heat/cool the building fabric (wall, floor or ceiling), which in turn heat/cool their zones through radiation and convection like large radiant heating/cooling panels integrated with storage mass. Open-loop configuration has advective thermal output in addition to the heat transfer from the BITES room surface. With properly design and operation of active BITES system, enhanced thermal comfort can be provided with energy saving operation and relatively flat power demand.

This thesis presented a methodology and guidelines for the modeling, design and operation of active BITES systems that facilitate primary space conditioning with low operating energy, relatively flat power demand, and enhanced thermal comfort. The three key factors considered by the methodology are as follows: sufficient thermal coupling between the BITES systems and their thermal zones, integration of design and operation, and integration of thermal and structural designs. The methodology and guidelines are general and applicable to different BITES systems and different buildings with different thermal and structural loads.

One important consideration in design and operation is sufficient thermal coupling between the BITES system and their thermal zones. This is critical to the space conditioning capacity of BITES systems. Ideas and solutions for improvement have also been presented. Furthermore, integration of different design aspects, such as building envelope or structure, are considered in an integrated manner during design process in order to achieve higher overall performance at reduced material use and cost.

Thermal modeling methodology, techniques, and guidelines were developed for active BITES systems to assist their design and operation analysis. Based on observations of long-term monitored data, a modeling approach was developed for using active BITES in space cooling applications. This approach decouples the BITES model from the building model, hence whole building simulation is not necessary for predicting the thermal behavior of the active BITES systems. Then an approach for developing simple regression models for BITES cooling operation was also presented.

Based on network theory, modeling techniques for explicit lumped-parameter finite difference approach in time domain and analytical approach in frequency domain are presented. Network modeling techniques, such as heat source transformation with Thévenin theorem, heat flow division, and Y-diakoptic method are presented as means to develop transfer function models in frequency domain. Y-diakoptic method can split the BITES system into two parts at the internal heat source level. Discrete Fourier series (DFS) representation in complex frequency form are used to represent the boundary excitations, such as the surface temperature variation, solar radiation and heat flux associated with flowing air. The criteria for choosing the number of harmonics were discussed. Furthermore, equations for one-dimensional discretization and time step selection are discussed, taking

into account convective and radiative heat transfer on the boundaries. A method with simplified models for calculating the heat transfer between charging/discharging fluids and BITES systems was also developed.

Ventilated concrete slab (VCS) systems are used to demonstrate the modeling methodology and techniques. Comparing with full-scale monitored data shows that time step of half an hour for frequency domain models typically results in less than 3% error in temperature and heat flux modeling. For explicit lumped-parameter finite difference models, discretization with Biot number smaller than 0.5 can reduce error to about 5%. Larger Biot number tends to overestimate the heat flow from air to slab over time. For practical slab thickness (0.1 to 0.2 m), models with time step of half an hour and with two or three discretization layers, have errors less than 9%.

Using the frequency domain modeling techniques presented above, a design methodology was developed for the predictive control of closed-loop and open-loop BITES systems. Using desired room air temperature and corresponding space conditioning load as inputs, the thermal energy injection rates can be predicted over a desired prediction horizon with the frequency domain models. The general procedure in this methodology is summarized. The typical thermal behavior and energy performance of closed-loop and open-loop BITES systems under practical operations has shown that open-loop systems are preferable in high space conditioning load situations. A preliminary method was provided for smoothing the over-fluctuating charge/discharge demand due to precise control. Relevant application consideration was discussed.

Since frequency domain modeling can provide insights for active BITES system design, a methodology for integrating design and operation is developed using frequency domain

approach. The proposed operation logic – passive measures with possible fan assistance, and then off-peak conditioning – improve the energy performance of buildings with active BITES by prioritizing the use of favorable energy (ambient renewable energy, off-peak purchased energy), reducing peak power demand, and providing thermal comfort at the same time. The dynamic responses of different active BITES systems were obtained from frequency domain modeling and were compared on a relative basis. They are used for the design of the active BITES system and selecting the suitable profile of room air temperatures, which are necessary for the realization of the proposed operation logic in the introduction chapter. A bounding condition based design approach is presented. The temperature and energy profiles of active BITES systems under bounding conditions and chosen operation strategies determine their required thermal attributes – thermal energy storage capacity, thermal coupling with interior (thermal output capacity), and charge/discharge capacity. An equivalent thickness of 0.2 to 0.3 m is typically suitable to initiate the iterative design process for ventilated concrete BITES systems (the peak admittance or smallest magnitude is for a thickness in that range). A practical approach for integration of structural and thermal designs is demonstrated with focus on ventilated BITES systems using standard structural components and their variations. For ventilated BITES systems, the equivalent concrete thickness should not be more than 0.3 m; otherwise, practical charge/discharge capacity will not be sufficient for full charge requirements. Furthermore, active BITES systems are not suitable as primary space conditioning systems for buildings with intensive space conditioning loads, or thermally light buildings with relatively large thermal load fluctuations. Proper building design (e.g. envelope and internal heat gain control) is required at extreme conditions.

Future studies

Chapter 4 provides a design methodology for predictive control. Using the outputs as feedback (dashed line in Fig. 4.1) for predictive control improvement and real time implementation is not covered in this thesis. The design uses off-line data for modeling, meaning that upcoming values of control inputs are not certain; however, this is not the case in practice – actual inputs (e.g. future weather conditions) and outputs (e.g. temperature of the BITES) will deviate from anticipation. The implementation of model predictive control is another important and challenging research topic.

Systematic approaches for improving the room temperature set-profile also need to be studied in future research. In this control methodology, room air temperature is set as a function of the exterior temperature, solar radiation, and the dynamic response of the active BITES systems and their associated rooms. This temperature setting approach enhances the room energy performance to a certain extent. Further improvement of temperature set-profile can consider enabling off-peak period charging even without ambient renewable energy being available, taking internal heat gain into consideration, load matching (e.g. to consume electrical being generated from local photovoltaic panels), and accounting utility fee structure. Approaches for the optimization of room temperature set-profile are worth studying in the future.

The initial mathematically generated control outputs from numerical models are not practical as pointed out in Chapter 4. A preliminary solution was provided to smooth the frequently cycling and self-counteracting outputs. Improvement in output treatment is suggested for future study. For example, pulse-width-modulation can be applied – step changing outputs can be generated based on initial outputs.

References

ACI committee 122. 2002. 122R-02: Guide to thermal properties of concrete and masonry systems. *In:* American Concrete Institute (ACI), ed. *Manual of Concrete Practice.* Detroit, Mich, US: American Concrete Institute.

Akander, J. 2000. *The ORC method: Effective modelling of thermal performance of multilayer building components.* Dr.Techn. C804980, Kungliga Tekniska Hogskolan (Sweden).

Akbari, H., D. Samano, A. Mertol, F. Bauman and R. Kammerud. 1986. The effect of variations in convection coefficients on thermal energy storage in buildings. I. Interior partition walls. *Energy and Buildings,* 9(3): 195-211.

Akbari, H., D. Samano, A. Mertol, F. Bauman and R. Kammerud. 1987. The effect of variations in convection coefficients on thermal energy storage in buildings. II. Exterior massive walls and simulations. *Energy and Buildings,* 10(1): 29-47.

Akbarzadeh, A., W. Charters and D. Lesslie. 1982. Thermocirculation characteristics of a Trombe wall passive test cell. *Solar Energy,* 28(6): 461-468.

Anderson, L. O., K. G. Bernander, E. Isfaelt and A. H. Rosenfeld. 1979. *Storage of heat and coolth in hollow-core concrete slabs. Swedish experience, and application to large, American-style buildings.*

Antonopoulos, K. A. and E. Koronaki. 1998. Apparent and effective thermal capacitance of buildings. *Energy,* 23(3): 183-192.

Antonopoulos, K. A. and E. Koronaki. 1999. Envelope and indoor thermal capacitance of buildings. *Applied Thermal Engineering,* 19(7): 743-756.

Armstrong, P. R., S. B. Leeb and L. K. Norford. 2006a. Control with building mass - Part I: Thermal response model. *ASHRAE Transactions,* 112(1): 449-461.

Armstrong, P. R., S. B. Leeb and L. K. Norford. 2006b. Control with building mass - Part II: Simulation. *ASHRAE Transactions,* 112(1): 462-473.

ASHRAE. 2004a. *Standard 55: Thermal environmental conditions for human occupancy,* Atlanta, GA, USA, American Society of Heating Refrigerating and Air-Conditioning Engineers (ASHRAE).

ASHRAE 2004b. Thermal Environmental Conditions for Human Occupancy. *ANSI/ASHRAE Standard 55,* .

ASHRAE. 2007a. Supervisory control strategies and optimization. *ASHRAE Handbook - HVAC Applications.* SI ed. Atlanta, GA, US: American Society of Heating Refrigerating and Air-Conditioning Engineers (ASHRAE).

ASHRAE. 2007b. Thermal Storage. *ASHRAE Handbook - HVAC Applications.* SI ed. Atlanta, GA, US: American Society of Heating Refrigerating and Air-Conditioning Engineers (ASHRAE).

ASHRAE. 2008. Panel heating and cooling. *ASHRAE Handbook - HVAC Systems and Equipment.* SI ed. Atlanta, GA, US: American Society of Heating Refrigerating and Air-Conditioning Engineers (ASHRAE).

ASHRAE. 2009a. Energy estimating and modeling methods. *ASHRAE Handbook - Fundamentals.* SI ed. Atlanta, GA, USA: American Society of Heating, Refrigerating, and Air-Conditioning Engineers (ASHRAE).

ASHRAE. 2009b. Fluid Flow. *ASHRAE Handbook - Fundamentals.* SI ed. Atlanta, GA, USA: American Society of Heating, Refrigerating, and Air-Conditioning Engineers (ASHRAE).

ASHRAE. 2009c. Fundamentals of Control. *ASHRAE Handbook - Fundamentals.* SI ed. Atlanta, GA, USA: American Society of Heating, Refrigerating, and Air-Conditioning Engineers (ASHRAE).

ASHRAE. 2009d. Heat transfer. *ASHRAE Handbook - Fundamentals.* SI ed. Atlanta, GA, USA: American Society of Heating, Refrigerating, and Air-Conditioning Engineers (ASHRAE).

ASHRAE. 2009e. Non-residential cooling and heating load calculations. *ASHRAE Handbook - Fundamentals.* SI ed. Atlanta, GA, USA: American Society of Heating, Refrigerating, and Air-Conditioning Engineers (ASHRAE).

ASHRAE. 2009f. Thermal comfort. *ASHRAE Handbook - Fundamentals.* SI ed. Atlanta, GA, USA: American Society of Heating, Refrigerating, and Air-Conditioning Engineers (ASHRAE).

ASHRAE. 2011. Radiant heating and cooling. *ASHRAE Handbook - HVAC Applications.* SI ed. Atlanta, GA, US: American Society of Heating Refrigerating and Air-Conditioning Engineers (ASHRAE).

Athienitis, A. K. 1994. *Building Thermal Analysis,* Boston, MA, USA, MathSoft Inc.

Athienitis, A. K. 1997. Investigation of thermal performance of a passive solar building with floor radiant heating. *Solar Energy,* 61(5): 337-345.

Athienitis, A. K., M. Chandrashekar and H. F. Sullivan. 1985. Modelling and analysis of thermal networks through subnetworks for multizone passive solar buildings. *Applied Mathematical Modelling,* 9(2): 109-16.

Athienitis, A. K. and T. Y. Chen. 1993. Experimental and theoretical investigation of floor heating with thermal storage. *ASHRAE Transactions,* 99(1): 1049-1057.

Athienitis, A. K. and Y. Chen. 2000. The effect of solar radiation on dynamic thermal performance of floor heating systems. *Solar Energy,* 69(3): 229-237.

Athienitis, A. K., C. Liu, D. Hawes, D. Banu and D. Feldman. 1997. Investigation of the thermal performance of a passive solar test-room with wall latent heat storage. *Building and Environment,* 32(5): 405-410.

Athienitis, A. K. and M. Santamouris. 2000. *Thermal Analysis and Design of Passive Solar Buildings,* London, EarthScan.

Athienitis, A. K. and M. Santamouris. 2002. *Thermal Analysis and Design of Passive Solar Buildings,* London, James & James.

Athienitis, A. K., M. Stylianou and J. Shou. 1990. A methodology for building thermal dynamics studies and control applications. *ASHRAE Transactions,* 96(2): 839-848.

Athienitis, A. K., H. F. Sullivan and K. G. T. Hollands. 1986. Analytical model, sensitivity analysis, and algorithm for temperature swings in direct gain rooms. *Solar Energy,* 36(4): 303-12.

Athienitis, A. K., H. F. Sullivan and K. G. T. Hollands. 1987. Discrete Fourier-Series Models for Building Auxiliary Energy Loads Based on Network Formulation Techniques. *Solar Energy,* 39(3): 203-210.

Balcomb (ed.), J. D. 1992. *Passive Solar Buildings,* Cambridge, MA, USA, MIT Press.

Balcomb, J. D. 1983. *Heat Storage and Distribution Inside Passive Buildings,* Los Alamos, NM, USA, Los Alamos National Laboratory.

Balcomb, J. D. and R. W. Jones. 1983. Passive solar design analysis. *In:* Los Alamos National Laboratory, ed. *Passive Solar Design Handbook.* Boulder, US: American Solar Energy Society.

Balcomb, J. D., R. W. Jones and Los Alamos National Laboratory. 1983. *Passive solar design handbook, volume 3 : passive solar design analysis,* Boulder, American Solar Energy Society.

Bansal, N. K. and Shail. 1999. Characteristic parameters of a hypocaust construction. *Building and Environment,* 34(3): 305-318.

Barton, P., C. B. Beggs and P. A. Sleigh. 2002. A theoretical study of the thermal performance of the TermoDeck hollow core slab system. *Applied Thermal Engineering,* 22(13): 1485-1499.

Baskin, E. 2005. Evaluation of hydronic forced-air and radiant slab heating and cooling systems. *ASHRAE Transactions,* 111(1): 525-534.

Bazilian, M. D., F. Leenders, B. G. C. Van der Ree and D. Prasad. 2001. Photovoltaic cogeneration in the built environment. *Solar Energy,* 71(1): 57-69.

Bilgen, E. 2001. Experimental study of massive wall systems with fins attached on the heated wall and with glazing. *Heat and Mass Transfer,* 38(1-2): 159-164.

Bilgen, E. and M. A. Richard. 2002. Horizontal concrete slabs as passive solar collectors. *Solar Energy,* 72(5): 405-413.

Bird, J. O. 2007. *Electrical circuit theory and technology,* Boston, US, Newnes.

Braham, G. D. 2000. Mechanical ventilation and fabric thermal storage. *Indoor and Built Environment,* 9(2): 102-110.

Braun, J. E. 2003. Load control using building thermal mass. *Journal of Solar Energy Engineering-Transactions of the ASME,* 125(3): 292-301.

Braun, J. E., K. W. Montgomery and N. Chaturvedi. 2001. Evaluating the performance of building thermal mass control strategies. *HVAC&R Research,* 7(4): 403-428.

Building Services 1993. It's quicker by tube. *Building Services.* London, UK.

Buzzoni, L., R. Dall'Olio and M. Spiga. 1998. Energy analysis of a passive solar system. *Revue Generale De Thermique,* 37(5): 411-416.

Candanedo, J. A., A. Allard and A. K. Athienitis. 2011. Predictive Control of Radiant Floor Heating and Transmitted Irradiance in a Room with High Solar Gains. *ASHRAE Transactions,* 117(2): 652-665.

Candanedo, J. A. and A. K. Athienitis. 2010. Investigation of anticipatory control strategies in a net-zero energy solar house. *ASHRAE Transactions,* 116(1): 246-259.

Candanedo, J. A. and A. K. Athienitis. 2011. Predictive control of radiant floor heating and solar-source heat pump operation in a solar house. *HVAC&R Research,* 17(3): 235-256.

Candanedo, L. M., A. K. Athienitis, J. A. Candanedo, W. O'Brien and Y. X. Chen. 2010. Transient and Steady State Models for Open-Loop Air-Based BIPV/T Systems. *ASHRAE Transactions,* 116(1): 600-612.

Carslaw, H. S. and J. C. Jaeger. 1959. *Conduction of heat in solids,* Oxford,, Clarendon Press.

Castellon, C., A. Castell, M. Medrano, I. Martorell and L. F. Cabeza. 2009. Experimental Study of PCM Inclusion in Different Building Envelopes. *Journal of Solar Energy Engineering-Transactions of the Asme,* 131(4): 6.

Ceylan, H. T. and G. E. Myers. 1979. Long-time solutions to heat-conduction transients with time-dependent inputs. *Journal of Heat Transfer,* 102: 115-120.

Charron, R. and A. K. Athienitis. 2006. Optimization of the performance of double-facades with integrated photovoltaic panels and motorized blinds. *Solar Energy,* 80(5): 482-491.

Chel, A., J. K. Nayak and G. Kaushik. 2008. Energy conservation in honey storage building using Trombe wall. *Energy and Buildings,* 40(9): 1643-1650.

Chen, W.-K. 1983. *Linear networks and systems,* Monterey, Ca, US, Brooks/Cole Engineering Division.

Chen, Y., A. Athienitis and K. Galal. 2013a. Frequency domain and finite difference modeling of ventilated concrete slabs and comparison with field measurements: Part 1, modeling methodology. *International Journal of Heat and Mass Transfer,* in press.

Chen, Y., A. Athienitis and K. Galal. 2013b. Frequency domain and finite difference modeling of ventilated concrete slabs and comparison with field measurements: Part 2, application. *International Journal of Heat and Mass Transfer,* in press.

Chen, Y., A. K. Athienitis and K. Galal. 2010a. Modeling, design and thermal performance of a BIPV/T system thermally coupled with a ventilated concrete slab in a low energy solar house: Part 1, BIPV/T system and house energy concept. *Solar Energy,* 84(11): 1892-1907.

Chen, Y., K. Galal and A. K. Athienitis. 2010b. Modeling, design and thermal performance of a BIPV/T system thermally coupled with a ventilated concrete slab in a low energy solar house: Part 2, ventilated concrete slab. *Solar Energy,* 84(11): 1908-1919.

Cheng, V., E. Ng and B. Givoni. 2005. Effect of envelope colour and thermal mass on indoor temperatures in hot humid climate. *Solar Energy,* 78(4): 528-534.

CIBSE. 1988. *CIBSE Guide , Volume A, Design Data,* London, The Chartered Institution of Building Services Engineers (CIBSE).

CMHC. 2006. *EQuilibrium™ Sustainable Housing Demonstration Initiative* [Online]. Canada Mortgage and Housing Corporation (CMHC). Available: http://www.cmhc-schl.gc.ca/en/inpr/su/eqho/ [Accessed July, 2011].

Cooperman, A., J. Dieckmann and J. Brodrick. 2010. Using Weather Data For Predictive Control. *Ashrae Journal,* 52(12): 130-132.

CPCI. 2010. *Design Manual for Precast and Prestressed Concrete,* Ottawa, ON, Canada, Canadian Precast Prestressed Concrete Institute (CPCI).

CSA. 2004. *Design of Masonry Structures,* CSA S304.1 2004, Canadian Standards Association (CSA).

Davies, M. G. 1973. The thermal admittance of layered walls. *Building Science,* 8(3): 207-220.

Davies, M. G. 1982. Transmission and storage characteristics of walls experiencing sinusoidal excitation. *Applied Energy,* 12(4): 269-316.

Davies, M. G. 1994. Thermal response of an enclosure to periodic excitation: the CIBSE approach. *Industrial and Engineering Chemistry Research,* 33(5): 217-235.

Demir, H., M. Mobedi and S. Ulku. 2008. A review on adsorption heat pump: Problems and solutions. *Renewable & Sustainable Energy Reviews,* 12(9): 2381-2403.

DETR 1998. Energy Consumption Guide 19 - Energy use in offices. UK Department of the Environment, Transport and the Regions (DETR)

Dincer, I. 2002. On thermal energy storage systems and applications in buildings. *Energy and Buildings,* 34(4): 377-388.

Dincer, I. and S. Dost. 1996. A perspective on thermal energy storage systems for solar energy applications. *International Journal of Energy Research,* 20(6): 547-557.

Doiron, M., W. O'Brien and A. Athienitis. 2011. Energy performance, comfort, and lessons learned from a near net zero energy solar house. *ASHRAE Transactions,* 117(2): 585-596.

Doran, D. 1992. *Construction materials reference book,* London ; Boston, Butterworth-Heinemann.

Drysdale, R. G. 1999. *Masonry structures : behavior and design,* Englewood Cliffs, N.J. :, Prentice Hall.
EEA 2008. Energy and Environment Report 2008. Europe Environment Agency (EEA) of European Union (EU).
EEA 2011. Energy Consumption and Efficiency. Europe Environment Agency (EEA) of European Union (EU).
EERE 2007. 2007 Buildings Energy Data Book. September 2007 ed.: Office of Energy Efficiency and Renewable Energy (EERE) in U.S. Department of Energy (DOE).
EERE 2011. 2010 Buildings Energy Data Book. March 2011 ed.: Office of Energy Efficiency and Renewable Energy (EERE) in U.S. Department of Energy (DOE).
Erell, E. 2007. Evaporative cooling. *In:* M. Santamouris, ed. *Advances in passive cooling.* London: James & James Science.
Fallahi, A., F. Haghighat and H. Elsadi. 2010. Energy performance assessment of double-skin facade with thermal mass. *Energy and Buildings,* 42(9): 1499-1509.
Fang, X. D. and Y. Z. Li. 2000. Numerical simulation and sensitivity analysis of lattice passive solar heating walls. *Solar Energy,* 69(1): 55-66.
Feustel, H. E. and C. Stetiu. 1995. Hydronic radiant cooling - preliminary assessment. *Energy and Buildings,* 22(3): 193-205.
Fort, K. 2000. Hypocaust and murocaust storage. *In:* O. C. Mørck and R. Hastings, eds. *Solar Air Systems: a Design Handbook.* London: James & James.
Fraisse, G., R. Boichot, J. L. Kouyoumji and B. Souyri. 2010. Night cooling with a Ventilated Internal Double Wall. *Energy and Buildings,* 42(3): 393-400.
Fraisse, G., K. Johannes, V. Trillat-Berdal and G. Achard. 2006. The use of a heavy internal wall with a ventilated air gap to store solar energy and improve summer comfort in timber frame houses. *Energy and Buildings,* 38(4): 293-302.
Fraisse, G., C. Menezo and K. Johannes. 2007. Energy performance of water hybrid PV/T collectors applied to combisystems of Direct Solar Floor type. *Solar Energy,* 81(11): 1426-1438.
Franklin, G. F., J. D. Powell and A. Emami-Naeini. 2006. *Feedback Control of Dynamic Systems,* Upper Saddle River, N.J., Pearson Prentice Hall.
Gan, G. H. 1998. A parametric study of Trombe walls for passive cooling of buildings. *Energy and Buildings,* 27(1): 37-43.
Gwerder, M., B. Lehmann, J. Toedtli, V. Dorer and F. Renggli. 2008. Control of thermally-activated building systems (TABS). *Applied Energy,* 85(7): 565-581.
Hadorn, J.-C. (ed.) 2005. *Thermal Energy Storage for Solar and Low Energy Buildings*: International Energy Agency (IEA) Solar Heating and Cooling Task 32 - Advanced storage concepts for solar and low energy buildings, IEA.
Hanibuchi, H. and S. Hokoi. Year. Basic study of radiative and convective heat exchange in a room with floor heating. *In:* Proceedings of the 1998 ASHRAE Winter Meeting. Part 1 (of 2), January 18, 1998 - January 21, 1998, 1998 San Francisco, CA, USA. ASHRAE, 1098-1105.
Hariri, A. S. and I. C. Ward. 1988. A review of thermal storage systems used in building applications. *Building and Environment,* 23(1): 1-10.
Hartman, T. B. 1988. Dynamic control: fundamentals and considerations. *ASHRAE Transactions,* 94(1): 599-609.
Hasnain, S. M. 1998a. Review on sustainable thermal energy storage technologies, part I: Heat storage materials and techniques. *Energy Conversion and Management,* 39(11): 1127-1138.

Hasnain, S. M. 1998b. Review on sustainable thermal energy storage technologies, part II: Cool thermal storage. *Energy Conversion and Management,* 39(11): 1139-1153.

Hauer, A., H. Mehling, P. Schossig, M. Yamaha, L. Cabeza, V. Martin and F. Setterwall 2004. Advanced Thermal Energy Storage through Phase Change Materials and Chemical Reactions - Feasibility Studies and Demonstration Projects. *IEA ANNEX 17 Final Report.* Internaltional Energy Agency (IEA).

Hauser, G., C. Kempkes and B. Olesen. 2000. Computer simulation of the performance of a hydronic heating/cooling system with embedded pipes. *ASHRAE Transactions,* 106(1): 702-712.

Henze, G. P., C. Felsmann, D. E. Kalz and S. Herkel. 2008. Primary energy and comfort performance of ventilation assisted thermo-active building systems in continental climates. *Energy and Buildings,* 40(2): 99-111.

Hittle, D. C. 1981. *Calculating Building Heating and Cooling Loads Using the Frequency Response of Multilayered Slabs.* Ph.D. 8127608, University of Illinois at Urbana-Champaign.

Howard, B. 1999. The CMU air-core passive hybrid heat storage system. *Proceedings of the Renewable and Advanced Energy Systems for the 21st Century, April*: 11-15.

Howard, B. D. 1986. Air core systems for passive and hybrid energy-conserving buildings. *ASHRAE Transactions,* 92(2): p 815-830.

Howard, B. D. and H. Fraker. 1990. Thermal energy storage in building interiors. *In:* B. Anderson, ed. *Solar Building Architecture.* Cambridge, MA, USA: MIT press.

IEA-SHC. 2008. *Towards Net Zero Energy Solar Buildings* [Online]. Solar Heating & Cooling Programme of International energy Agency (IEA-SHC). Available: http://www.iea-shc.org/task40/index.html [Accessed July, 2011].

Inard, C., A. Meslem and P. Depecker. 1998. Energy consumption and thermal comfort in dwelling-cells: A zonal-model approach. *Building and Environment,* 33(5): 279-291.

Incropera, F. P. and D. P. DeWitt. 2002. *Fundamentals of heat and mass transfer,* New York, J. Wiley.

Ji, J., J. Bin, Y. Huai, C. Tin-Tai, H. Wei and P. Gang. 2008. An experimental and mathematical study of efforts of a novel photovoltaic-Trombe wall on a test room. *International Journal of Energy Research,* 32(6): 531-542.

Ji, J., C. L. Luo, W. Sun, H. C. Yu, W. He and G. Pei. 2009. An improved approach for the application of Trombe wall system to building construction with selective thermo-insulation facades. *Chinese Science Bulletin,* 54(11): 1949-1956.

Ji, J., H. Yi, W. Lie and G. Pei. 2007a. PV-Trombe wall design for buildings in composite climates. *Journal of Solar Energy Engineering-Transactions of the Asme,* 129(4): 431-437.

Ji, J., H. Yi, G. Pei, B. Jiang and W. He. 2007b. Study of PV-Trombe wall assisted with DC fan. *Building and Environment,* 42(10): 3529-3539.

Johannesson, G. 1981. Active Heat Capacity, Models and Parameters for the Thermal Performance of Buildings. *Report TVBH-1003.* Lund, Sweden: Division of building technology, Lund Institute of Technology.

Karadag, R. and O. Akgobek. 2008. The prediction of convective heat transfer in floor-heating systems by artificial neural networks. *International Communications in Heat and Mass Transfer,* 35(3): 312-325.

Kato, Y. 2005. Chemical energy conversion technologies for efficient energy use. In proceedings of: NATO Advanced Study Institute on Thermal Energy Storage for Sustainable Energy Consumption. Turkey.

Kaushika, N. D. and S. K. Rao. 1983. Non-convective roof pond with movable insulation for passive solar space heating in cold climates. *Building and Environment,* 18(1-2): 9-17.

Kaushika, N. D., M. S. Sharma and S. Kaul. 1987. Honeycomb roof cover system for passive solar space heating. *Energy Conversion and Management,* 27(1): 99-102.

Kaushika, N. D., P. K. Sharma and R. P. Priya. 1992. Solar thermal analysis of honeycomb roof cover system for energy conservation in an air-conditioned building. *Energy and Buildings,* 18(1): 45-49.

Kimura, K.-I. 1977. Unsteady state heat conduction through walls and slabs. *In:* K.-I. Kimura, ed. *Scientific basis for air-conditioning.* London, UK: Applied Science Publishers Ltd.

Koschenz, M. and V. Dorer. 1999. Interaction of an air system with concrete core conditioning. *Energy and Buildings,* 30(2): 139-145.

Kreith, F. and M. Bohn. 2001. *Principles of heat transfer,* Australia ; Pacific Grove, Calif., Brooks/Cole Pub.

Kreyszig, E. 2006. *Advanced engineering mathematics,* Hoboken, NJ, John Wiley.

Kruger, E., E. G. Cruz and B. Givoni. 2010. Effectiveness of indirect evaporative cooling and thermal mass in a hot arid climate. *Building and Environment,* 45(6): 1422-1433.

Kummert, M., P. Andre and J. Nicolas. 2000. Optimal heating control in a passive solar commercial building. *Solar Energy,* 69(1-6): 103-116.

Kuznik, F. and J. Virgone. 2009. Experimental assessment of a phase change material for wall building use. *Applied Energy,* 86(10): 2038-2046.

Lakhal, E. K., E. Bilgen and P. Vasseur. 1995. Natural convection and conduction in masive wall solar collectors with honeycomb and without vents. *Journal of Solar Energy Engineering-Transactions of the ASME,* 117(3): 173-180.

LeBreux, M., M. Lacroix and G. Lachiver. 2006. Fuzzy and feedforward control of an hybrid thermal energy storage system. *Energy and Buildings,* 38(10): 1149-1155.

LeBreux, M., M. Lacroix and G. Lachiver. 2009. Control of a hybrid solar/electric thermal energy storage system. *International Journal of Thermal Sciences,* 48(3): 645-654.

Lehmann, B., V. Dorer, M. Gwerder, F. Renggli and J. Todtli. 2011. Thermally activated building systems (TABS): Energy efficiency as a function of control strategy, hydronic circuit topology and (cold) generation system. *Applied Energy,* 88(1): 180-191.

Lehmann, B., V. Dorer and M. Koschenz. 2007. Application range of thermally activated building systems tabs. *Energy and Buildings,* 39(5): 593-598.

Lehmann, B., R. Weber and J.-C. Hadorn. 2005. Thermal storage in building structures: thermally activated building systems (TABS). *In:* J.-C. Hadorn, ed. *Thermal Energy Storage for Solar and Low Energy Buildings - State of the Art.* International Energy Agency (IEA).

Letz, T. 2005. Storage in the building: Direct Solar Floor. *In:* J.-C. Hadorn, ed. *Thermal Energy Storage for Solar and Low Energy Buildings - State of the Art.* International Energy Agency (IEA).

Lin, K. P., Y. P. Zhang, X. Xu, H. F. Di, R. Yang and P. H. Qin. 2005. Experimental study of under-floor electric heating system with shape-stabilized PCM plates. *Energy and Buildings,* 37(3): 215-220.

Lindstrom, P. C., D. E. Fisher and C. O. Pedersen. 1998. Impact of surface characteristics on radiant panel output. *ASHRAE Transactions,* 104(1): 1079-1088.

Lucas, I. B., L. Hoese and D. Pontoriero. 2000. Experimental study of passive systems thermal performance. *Renewable Energy,* 19(1-2): 39-45.

Marmoret, L., P. Glouannec, O. Douzane, A. T. de Roodenbeke and M. Queneudec. 2000. Use of a cellular clayey concrete for a wall specially fitted with water pipes. *Energy and Buildings,* 31(1): 89-95.

Masruroh, N. A., B. Li and J. Klemes. 2006. Life cycle analysis of a solar thermal system with thermochemical storage process. *Renewable Energy,* 31(4): 537-548.

Morgan, S. and M. Krarti. 2007. Impact of electricity rate structures on energy cost savings of pre-cooling controls for office buildings. *Building and Environment,* 42(8): 2810-2818.

N'Tsoukpoe, K. E., H. Liu, N. Le Pierres and L. G. Luo. 2009. A review on long-term sorption solar energy storage. *Renewable & Sustainable Energy Reviews,* 13(9): 2385-2396.

Nagano, K., S. Takeda, T. Mochida, K. Shimakura and T. Nakamura. 2006. Study of a floor supply air conditioning system using granular phase change material to augment building mass thermal storage - Heat response in small scale experiments. *Energy and Buildings,* 38(5): 436-446.

Nassif, N., S. Moujaes and M. Zaheeruddin. 2008. Self-tuning dynamic models of HVAC system components. *Energy and Buildings,* 40(9): 1709-1720.

Nielsen, K., H. Gether and J. Gether 2003. Thermal Energy Storage-A State-of-the-Art. *Smart Energy-Efficient Building, Smartbuild.* Norwegian University of Science and Technology (NTNU) and SINTEF.

OEE 2011. Secondary Energy Use by End-Use. Office of Energy Efficiency (OEE) of Natural Resources Canada (NRCan).

Olesen, B. W., M. de Carli, M. Scarpa and M. Koschenz. 2006. Dynamic evaluation of the cooling capacity of thermo-active building systems. *ASHRAE Transactions 2006,* 112(1): 350-357.

Onmura, S., M. Matsumoto and S. Hokoi. 2001. Study on evaporative cooling effect of roof lawn gardens. *Energy and Buildings,* 33(7): 653-666.

Oswald, D. and K. K. N. Sedlbauer 1995. Analyse und Prognose der hygienischen Zustände und Wartungsnotwendigkeiten in Außenwänden mit offenen Luftkreisläufen bei hybriden Heizsystemen (Report GB 128/1995). Stuttgart, Germany: Fraunhofer Institut für Bauphysik.

Patankar, S. V. 1980. *Numerical heat transfer and fluid flow,* New York, USA, Hemisphere Pub. Corp.

Pearlmutter, D. and I. A. Meir. 1995. Assessing the climatic implications of lightweight housing in a peripheral arid region. *Building and Environment,* 30(3): 441-451.

Persaud, R. and D. Symons. 2006. Design and testing of a composite timber and concrete floor system. *Structural Engineer,* 84(4): 22-33.

Persson, M. L., A. Roos and M. Wall. 2006. Influence of window size on the energy balance of low energy houses. *Energy and Buildings,* 38(3): 181-188.

Pfafferott, J. and D. Kalz. 2007. Thermo-active building systems. *BINE Themeninfo* [Online], 2007. Available: http://www.recollective.ca/Resources_Files/Resources_11820081133301764/Thermoactive%20building%20systems%20guide2007.pdf [Accessed Sept. 2010].

Pfafferott, J. U., S. Herkel, D. E. Kalz and A. Zeuschner. 2007. Comparison of low-energy office buildings in summer using different thermal comfort criteria. *Energy and Buildings,* 39(7): 750-757.

Pipes, L. A. 1957. Matrix analysis of heat transfer problems. *Journal of the Franklin Institute,* 263(3): 195-206.

Ren, M. J. and J. A. Wright. 1998. A ventilated slab thermal storage system model. *Building and Environment,* 33(1): 43-52.

Santamouris, M., A. Sfakianaki and K. Pavlou. 2010. On the efficiency of night ventilation techniques applied to residential buildings. *Energy and Buildings,* 42(8): 1309-1313.

Schmidt, D. and G. Jóhannesson. 2002. Approach for modelling of hybrid heating and cooling components with optimised RC networks. *Nordic Journal of Building Physics,* 3.

Schmidt, D. and G. Jóhannesson. 2004. Optimised RC Networks Incorporated within Macro-Elements for Modelling Thermally Activated Building Constructions. *Nordic Journal of Building Physics,* 3.

Schuler, A., C. Roecker, J. Boudaden, P. Oelhafen and J. L. Scartezzini. 2005. Potential of quarterwave interference stacks for colored thermal solar collectors. *Solar Energy,* 79(2): 122-130.

Seem, J. E., S. A. Klein, W. A. Beckman and J. W. Mitchell. 1989. Comprehensive room transfer functions for efficient calculation of the transient heat transfer processes in buildings. *Transactions of ASME,* 111(2): 264-273.

Sharma, A., V. V. Tyagi, C. R. Chen and D. Buddhi. 2009. Review on thermal energy storage with phase change materials and applications. *Renewable & Sustainable Energy Reviews,* 13(2): 318-345.

Shaviv, E., A. Yezioro and I. G. Capeluto. 2001. Thermal mass and night ventilation as passive cooling design strategy. *Renewable Energy,* 24(3-4): 445-452.

Shaw, M. R., K. W. Treadaway and S. T. P. Willis. 1994. Effective use of building mass. *Renewable Energy,* 5(2): 1028-1038.

Shen, J. B., S. Lassue, L. Zalewski and D. Z. Huang. 2007. Numerical study on thermal behavior of classical or composite Trombe solar walls. *Energy and Buildings,* 39(8): 962-974.

Short, W. and C. F. Kutscher 1984. Analysis of an active charge/passive discharge solar space conditioning system. Golden, CO, USA: Solar Energy Research Institute.

Simmonds, P. 1994. Control strategies for combined heating and cooling radiant systems. *ASHRAE Transactions,* 100(1): 1031-1039.

Simmonds, P., S. Holst, S. Reuss and W. Gaw. 2000. Using radiant cooled floors to condition large spaces and maintain comfort conditions. *ASHRAE Transactions,* 106(1): 695-701.

Sodha, M. S., J. Kaur and R. L. Sawhney. 1992. Effect of storage on thermal performance of a building. *International Journal of Energy Research,* 16(8): 697-707.

Sodha, M. S., S. C. Kaushik and J. K. Nayak. 1981. Performance of Trombe walls and roof pond systems. *Applied Energy,* 8(3): 175-191.

Spitler, J. D. and D. E. Fisher. 1999. On the relationship between the radiant time series and transfer function methods for design cooling load calculations. *HVAC&R Research,* 5(2): 123-136.

Spitler, J. D., D. E. Fisher and C. O. Pedersen. 1997. Radiant time series cooling load calculation procedure. *ASHRAE Transactions,* 103(2): 503-515.

Stephenson, D. G. and G. Mitalas. 1967. Cooling load calculations by thermal response factor method. *ASHRAE Transactions,* 73(1): 1-7.

Stephenson, D. G. and G. P. Mitalas. 1971. Calculation of heat conduction transfer functions for multi-layer slabs. *ASHRAE Transactions,* 77(2): 117-126.

Strand, R. K. 1995. *Heat source transfer functions and their application to low temperature radiant heating systems.* Ph.D. 9543736, University of Illinois at Urbana-Champaign.

Sun, M. Q., X. Y. Mu, X. Y. Wang, Z. F. Hou and Z. Q. Li. 2008. Experimental studies on the indoor electrical floor heating system with carbon black mortar slabs. *Energy and Buildings,* 40(6): 1094-1100.

Team-Probe 1998. Probe 14: Elizabeth Fry building. *Building Services Journal.*

TRNSYS. 2012. Multizone Building (Type 56 - TRNBuild). *TRNSYS 17 Documention.* Transient Energy System Simulation Tool (TRNSYS).

Trombe, F., J. F. Robert, M. Cabanot and B. Sesolis. 1977. Concrete walls to collect and hold heat. *Solar Age,* 2(8): 13-19.

Turner, C. H. and N. K. Tovey. 2006. Case study on the energy performance of the Zuckerman Institute for Connective Environmental Research (ZICER) building. *ASHRAE Transactions,* 112(2): 320-329.

Tyagi, V. V. and D. Buddhi. 2007. PCM thermal storage in buildings: A state of art. *Renewable & Sustainable Energy Reviews,* 11(6): 1146-1166.

Wanphen, S. and K. Nagano. 2009. Experimental study of the performance of porous materials to moderate the roof surface temperature by its evaporative cooling effect. *Building and Environment,* 44(2): 338-351.

Weber, T. and G. Johannesson. 2005. An optimized RC-network for thermally activated building components. *Building and Environment,* 40(1): 1-14.

Weber, T., G. Johannesson, M. Koschenz, B. Lehmann and T. Baumgartner. 2005. Validation of a FEM-program (frequency-domain) and a simplified RC-model (time-domain) for thermally activated building component systems (TABS) using measurement data. *Energy and Buildings,* 37(7): 707-724.

Winwood, R., R. Benstead and R. Edwards. 1997a. Advanced fabric energy storage I: review. *Building Services Engineering Research and Technology,* 18: 1-6.

Winwood, R., R. Benstead and R. Edwards. 1997b. Advanced fabric energy storage II: computational fluid dynamics modelling. *Building Services Engineering Research & Technology,* 18: 7-16.

Winwood, R., R. Benstead and R. Edwards. 1997c. Advanced fabric energy storage III: theoretical analysis and whole-building simulation. *Building Services Engineering Research and Technology,* 18: 17-24.

Winwood, R., R. Benstead and R. Edwards. 1997d. Advanced fabric energy storage IV: experimental monitoring. *Building Services Engineering Research & Technology,* 18: 25-30.

Wongsuwan, W., S. Kumar, P. Neveu and F. Meunier. 2001. A review of chemical heat pump technology and applications. *Applied Thermal Engineering,* 21(15): 1489-1519.

Xu, X., S. Wang, J. Wang and F. Xiao. 2010. Active pipe-embedded structures in buildings for utilizing low-grade energy sources: A review. *Energy and Buildings,* 42(10): 1567-1581.

Yakubu, G. S. 1996. The reality of living in passive solar homes: A user-experience study. *Renewable Energy,* 8(1-4): 177-181.

Zalewski, L., M. Chantant, S. Lassue and B. Duthoit. 1997. Experimental thermal study of a solar wall of composite type. *Energy and Buildings,* 25(1): 7-18.

Zhai, X. Q., J. R. Yang and R. Z. Wang. 2009. Design and performance of the solar-powered floor heating system in a green building. *Renewable Energy,* 34(7): 1700-1708.

Zhang, Y. P., H. H. Ding, X. Wang, R. Yang and K. P. Lin. 2006a. Influence of additives on thermal conductivity of shape-stabilized phase change material. *Solar Energy Materials and Solar Cells,* 90(11): 1692-1702.

Zhang, Y. P., K. P. Lin, R. Yang, H. F. Di and Y. Jiang. 2006b. Preparation, thermal performance and application of shape-stabilized PCM in energy efficient buildings. *Energy and Buildings,* 38(10): 1262-1269.

Zhou, G., M. Krarti and G. P. Henze. 2005. Parametric analysis of active and passive building thermal storage utilization. *Journal of Solar Energy Engineering-Transactions of the Asme,* 127(1): 37-46.

Zhou, G. B., Y. P. Zhang, K. P. Lin and W. Xiao. 2008. Thermal analysis of a direct-gain room with shape-stabilized PCM plates. *Renewable Energy,* 33(6): 1228-1236.

Zhu, L., R. Hurt, D. Correia and R. Boehm. 2009a. Detailed energy saving performance analyses on thermal mass walls demonstrated in a zero energy house. *Energy and Buildings,* 41(3): 303-310.

Zhu, N., Z. J. Ma and S. W. Wang. 2009b. Dynamic characteristics and energy performance of buildings using phase change materials: A review. *Energy Conversion and Management,* 50(12): 3169-3181.

Zrikem, Z. and E. Bilgen. 1986. Theoretical study of a non-convective trombe wall collector with honeycomb structure. *Solar & Wind Technology,* 3(1): 33-44.

Zukowski, M. 2005. Heat transfer and pressure drop characteristics of the underfloor air distribution system. *Energy and Buildings,* 37(8): 890-896.

Appendices

A1. Literature review appendix

A1.1. Whole building

In this subsection, the BITES systems to be discussed are in their original forms (e.g. not ventilated or hydronic system) built for their original building functions (e.g. structure, envelope). Terms such as high-mass or heavyweight, medium mass/weight, and low-mass or lightweight are usually used as indicators for the thermal mass level of the building fabric.

In previous R&D activities on whole building thermal performance, the passive thermal responses of different construction types were investigated intensively (Balcomb (ed.) 1992, Cheng et al. 2005, Kruger et al. 2010, Pearlmutter and Meir 1995, Zhu et al. 2009a). These studies showed that thermal storage mass generally tampers the negative effects of internal /external heat gain and transmitted solar radiation on indoor thermal environment year around, by passively absorbing and releasing significant amount of thermal energy (i.e. heat sink). It helps in reducing indoor temperature swings. ACI committee 122 (2002) pointed out that concrete and masonry buildings that have large thermal capacity have lower annual heating and cooling loads than other similarly insulated buildings. Sodha et al. (1992) through simulations compared the thermal behaviours of the different TES systems, and pointed out that enlarging the surface area of the storage material is more effective in reducing the temperature swing than increasing their volume. However, in some cases like in desert areas, the excess heat stored in the thermal mass during the daytime may result in

undesired high indoor temperature at night time. Overall, it could be said that high-mass can significantly improve the thermal performance of buildings.

In using building's overall mass for TES, focuses of previous R&D activities were on passive solar designs and night time ventilation for pre-cooling. Daytime heat storage for night time heating applications, such as passive solar design, are mainly used in residential buildings, since non-resident buildings are generally not occupied at night. Night time pre-heating whole building using off-peak energy for daytime heating was rarely studied. One of the reasons is that good passive solar design can satisfy the heating need during a sunny day (Athienitis and Santamouris 2002, Balcomb (ed.) 1992). However, night-time pre-heating, which will increase total energy consumption, can be used to trade off energy cost, especially if a strong incentive time-of-use utility rate structure exists (Zhou et al. 2005). The general concepts and findings from night time pre-cooling can be applied to night time pre-heating.

Exposed concrete slabs/walls have been widely used as passive TES systems in passive solar heating designs. Concrete's relatively high solar absorptivity (0.6 (ASHRAE 2009d)) maximizes the absorptance of impinging solar energy. At the same time, concrete's high hemispherical emissivity (0.91 (ASHRAE 2009d)) enables efficient re-radiation of stored energy into occupied space (ACI committee 122 2002).

In passive solar design, some classic "rules-of-thumb" by E. Mazria and the diurnal heat capacity (DHC) method advanced by Los Alamos National Laboratory (LANL) Solar Group for the TES system design and analysis were described in Ref. (Balcomb 1983, Howard and Fraker 1990). Mazria provided heat storage guidelines for different generic passive solar systems. Homes designed with these rules performed fairly well; however, the application of these rules to multi-zone or internal-load-dominated commercial, industrial, or institutional

structures were not very satisfactory. Balcomb et al. (1983) suggested the diurnal concept for the storage capacity – the passive TES systems should be able to store solar gain during a sunny day without overheating the house. LANL's work showed that the optimal mass thickness of common construction materials can be determined by the analysis of a materials' DHC. A basic finding of the DHC method is that the density and the specific heat of the storage materials have a major effect upon optimal thickness and effective storage capacity. An optimal storage material would have relatively high density and specific heat, and reasonable, but not excess, thermal diffusivity. Thickness beyond optimal value has little added effect on diurnal heat storage. For example, the optimal thickness is about 10 cm for lower density masonry material and about 18 cm for high-density materials in direct gain zone (Athienitis and Santamouris 2002, Balcomb 1983). Howard and Fraker (1990) also discussed the optimal ratio of the storage layer area to the glazing area in direct gain applications. A 6-to-1 storage-to-glazing area ratio is considered to be most effective if the mass is well distributed in the direct gain space. In standard construction (no added mass, insulated light frame walls), the solar glazing area should be less than 8% of interior floor area.

In pre-cooling applications, many studies have been conducted on using night time cool outdoor air to pre-cool the building through night time ventilation. Zhou et al. (2005), through simulations, investigated and quantified the saving on energy cost by adopting night time temperature setback and pre-cooling in commercial buildings. The researchers pointed out buildings with heavier mass have larger saving potentials than light buildings. Braun (2003) carried out simulations, controlled laboratory testing, and field studies, and concluded that significant cost saving can be achieved by pre-cooling the building mass using mechanical cooling. Santamouris et al. (2010) analysed energy data from 214 Greek air

conditioned residential buildings using night ventilation techniques. The researchers found out that (1) the higher the cooling demand of the building, the higher the potential contribution of the night ventilation under specific boundary conditions; (2) the higher the flow rate, the more energy can be stored. Shaviv et al. (2001) simulated the influence of thermal inertia and night ventilation on the indoor temperature in summer in hot-humid climate of Israel. The researchers concluded that the maximum indoor temperature can be predicted using linear equations based on the outdoor temperature swing, the thermal inertia of the building, and night ventilation rates. The researchers also found out that night ventilation rate higher than 30 air changes per hour (ACH) is not necessary and heavier building is more beneficial in passive free cooling. Pre-cooling building's overall mass can significantly reduce the costs on energy consumption and peak power demand. These savings are sensitive to many factors, including utility fee structure, building thermal inertia, and control strategy (Braun 2003, Morgan and Krarti 2007).

In order to explore the TES potentials of the building fabric, many R&D activities were conducted on the TES performance of individual components, and of their alternative forms. These activities are presented in the following subsections.

A1.2. Trombe walls

Singling out the review on Trombe wall as a separated category is because intensive researches have been conducted on it. The classic Trombe wall is a passive solar thermal energy collecting, storing, and releasing system. It consists of a massive wall covered with its interior surface exposed to the room air and its other side covered by glazing (Trombe et al. 1977). The wall stores heat from the solar radiation transmitted through the exterior glazing. The cavity between the massive wall and the glazing can be ventilated by adding vents at the

upper and bottom parts of the massive wall (Trombe et al. 1977), or not ventilated (Balcomb and Jones 1983). When the cavity is not ventilated, the heat stored in the wall is released to room by natural convection and infrared radiation. When the cavity is ventilated, the stored heat is transferred to the room air mainly by the air circulating between the air cavity and room through the vents. The movement of the air inside the air cavity is due to buoyancy effect (also referred as thermo-circulation) (Akbarzadeh et al. 1982). A minor portion of collected heat will be transferred in the same mechanism as the un-vented type.

Several modifications have been applied to the classic Trombe wall type in order to improve its overall thermal performance. Zrikem and Bilgen (1986) proposed integrating horizontal fins on the exterior surface of massive wall to suppress the convective and infrared radiative heat lost from the wall to exterior: non-convective, honeycomb structured Trombe wall. Their parametric study showed that, with an optimal cavity aspect ratio, wall thickness and the fin thickness, the solar contribution can reach about 8% for a typical week of mix of sunny and overcast cold days (i.e. 8% of heat loss was reduced). Lakhal et al. (1995) through numerical study showed that the fin can effectively suppress the heat transfer in the cavity. An experimental study conducted by Bilgen (2001) showed that, under steady state conditions, 40 to 44% of the imposed heat flux dissipated from the interior surface of the massive wall to room air.

Zalewski et al. (1997) proposed a composite type of Trombe wall (Fig. A1.1) – an insulating panel was added behind the classic un-vented Trombe wall with a ventilated air cavity between this panel and the wall. The thermo-circulation in this air cavity brings the energy into the building by convection, and the insulating panel reduces undesirable heat loss when the wall is cooler than the room air. Measured data show that, in a sunny winter day, the

temperature increase of the air after flowing through the air cavity was 10°C, and the air flow rate was at 70 m^3/hr (20 L/s) - the heat output reached 233W for the 5.5 m^2 Trombe wall surface. The numerical study conducted by Shen et al. (2007) shows that the composite Trombe wall has better thermal performance than the vented classic Trombe walls - longer duration of supplying space heating and less heat loss through the wall from the room to exterior.

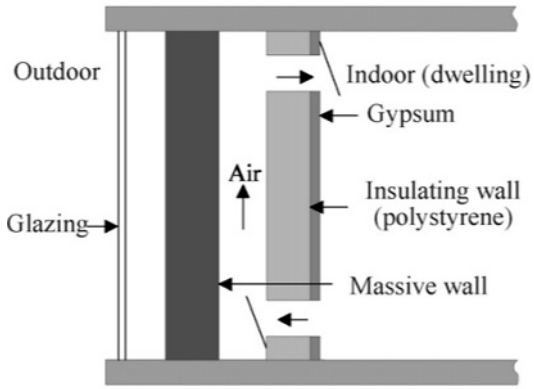

Fig. A1.1: Vertical cross section of the composite Trombe wall (Shen et al. 2007)

Another modified type of vented Trombe wall with additional function of facilitating summer natural ventilation was theoretically studied by Gan (1998). In addition to the top and bottom vents on the massive wall, a top vent and a bottom vent are added to the glazing (i.e. there are totally four vents on the Trombe wall system). A layer of insulation was applied on the interior side of the massive wall. The researcher stated that for mild climates, the interior surface of Trombe walls should be insulated. In the summer, the Trombe wall is used to facilitate ventilation. The study concluded that the ventilation rate in the air cavity can be enhanced by increasing the distance between the wall and the glazing, using double glazing, and insulating the interior side of the massive wall.

Chel et al. (2008) theoretically investigated the thermal performance a Trombe wall with 4 vents and the associated honey storage building. The analysis showed that a Trombe wall, which is located at 26°14' in India and facing southeast, can contribute to energy conservation in heating up to 220 kWh/yr per m^2 of wall. The payback time is short (~1 year), and hence, economically feasible. The investigation also showed that Trombe wall with four vents is able to save significantly more heating energy than other three alternatives – blackened wall, direct gain, and un-vented Trombe walls.

Fang and Li (2000) conducted numerical studies on the performance of lattice passive solar heating walls, which was a modified version of a Trombe wall – vents were distributed evenly all over the massive wall. The massive wall behaves somehow like a perforated solar collector. The researchers claimed that the lattice walls have significantly better thermal performance than classic Trombe walls.

A1.3. Roof type

Roof type BITES systems utilize the roof component of buildings – the roof slabs or the roof pond water plus the roof slabs. In space heating applications, the general mechanism is that solar thermal energy is absorbed by the BITES systems and stored as sensible heat in the roof. The stored heat is then distributed by convection and radiation to the room underneath. During off-sunshine hours, the systems are usually covered with insulation membranes on the exterior side to reduce heat loss. In cooling applications, the systems are covered in the same way during the day time to avoid solar thermal gain, and act as heat sinks to absorb the heat from the room. At night time, the cover is open and the system is cooled down by radiative heat exchange with the sky and convective heat transfer with the

cool night time air. Howard and Fraker (1990) illustrated the modes of operations in heating and cooling seasons.

Bilgen and Richard (2002) conducted experimental and theoretical studies on a horizontal concrete slab functioning as a passive solar thermal collector. The researchers reported that the ratio of the heat stored to the incident energy during the heating period decreased inverse-exponentially as a function of time. The same trend applied to the ratio of the heat released from the slab surface at various times to the heat released at the beginning of the cooling period. The major energy storage-restitution took place during the first three to four hours. Radiation made up about 60% of the heat loss while natural convection covered the rest. Slab thickness and surface radiative properties can be used to optimize the thermal performance, such as thermal storage efficiency. Simulation showed that by changing the slab thickness from 10 cm to 20 cm, the energy storage density was increased by 30% and the thermal efficiency was improved by 6%. Beyond 20 cm thickness, the amount of stored energy increased insignificantly.

Even though a roof pond is not an inherent part of the building fabric, it is an important part of the roof BITES systems. It significantly increases the effectiveness of the roof systems by introducing evaporative heat release and increasing the thermal capacity of the systems.

For heating applications using roof ponds, Kaushika et al. (1983) concluded through numerical simulations, that the space heating thermal performance of the non-convective roof pond with movable insulation was better than systems with transparent cover. Convective systems with movable insulation were not suitable for space heating in cold climates. The researchers also pointed out that water-soluble natural gums and polymers can

render a 10-30 cm layer of water sufficiently viscous to be non-convective. Kaushika et al. (1987, 1992), through simulations, investigated the solar thermal gain of a roof composed of a blackened concrete slab and an air-filled honeycomb cover on top of the slab. The researchers concluded that thicker concrete slab resulted in larger solar gain, and the thickness of the honeycomb cover between 10 and 15 cm was optimal.

Sodha et al. (1981) used transfer functions to study different configurations of roof ponds. They concluded that, for roof pond systems, a system comprised of water-concrete-insulation in ascending order of thickness in summer was desirable; the same combination with a descending order of thickness was most appropriate for hot climate winter. For a typical cold climate, a roof pond system with an ascending order of water-concrete-insulation layers was preferable. The case without water pond (i.e. with slab and insulation only) was not studied. Also, the researchers didn't clearly explain the treatment of top glazing in the simulations in the transfer functions.

In cooling applications with roof BITES systems, roof ponds are mostly adopted due to the fact that roof pond systems are able to provide indirect evaporative cooling (IEC) for buildings. Evaporative cooling accelerates the cooling process of the water, especially in arid climates. The water can be cooled close to the ambient wet bulb temperature (Erell 2007).

Kruger et al. (2010) investigated the thermal performance of a house with a roof-located IEC system in an arid area. The roof pond was equipped with a cover and has fans for forced ventilation (Fig. A1.2). The researchers concluded that during the summer, the IEC system created better comfort levels as compared to high-mass construction. However, that was partially because the night time cross ventilation in the high-mass building didn't function well. They suggested combining these two techniques to avoid over-cooling on a

cool summer night. This study responded to the concern of Pearlmutter and Meir (1995) regarding lightweight housing in an arid area.

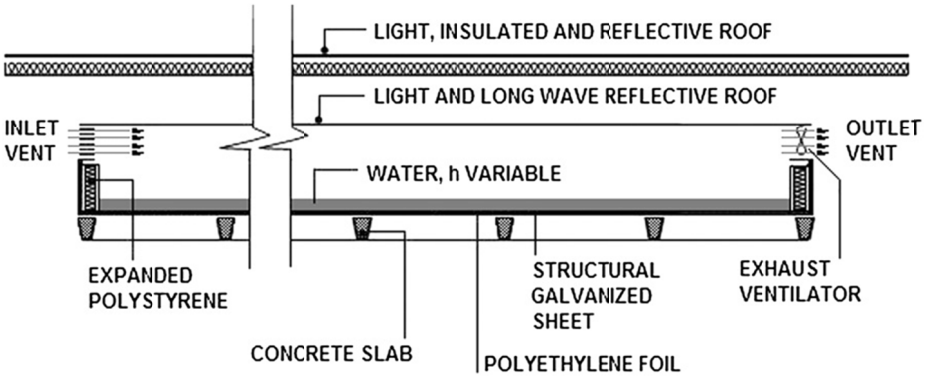

Fig. A1.2: Schematic of the evaporative cooling system (Kruger et al. 2010).

In the application of passive evaporative cooling, porous roofs are under research for their potential contribution. Some porous materials can passively absorb moisture from ambient humid air or store rainwater. The absorbed water evaporates later, and hence lowers the temperature of roof storage materials (e.g. porous material, roof structural mass, and soil in green roof applications). One of the experimental evaluations on passive evaporative cooling using porous material was conducted by Wanphen and Nagano (2009). They investigated the moisture absorption and evaporation capabilities of several non-porous and porous potential roofing materials. They found out that siliceous shale of both small and large particle diameter can lower the daily average surface temperature by up to 6.8 and 8.6°C, respectively. The better performance of large size particles could possibly be caused by the ventilation occurring within the material layers and high solar penetration through the large gaps between particles, which would release more latent heat when compared to materials of smaller particle sizes. Contribution from the passive evaporative cooling effect of a roof lawn garden was investigated experimentally and numerically by Onmura et al. (2001). The significant cooling effect was confirmed.

There are not many practical applications of BITES roofs due to its direct exposure to the exterior environment. There is an obvious drawback in using BITES roof systems to directly absorb solar thermal energy – during the heating season, the solar angle is low and hence limited solar radiation can be absorbed by near-horizontal roofs. Therefore, using roof systems for heating applications are seen as impractical for high-latitude regions. In theoretical studies of their energy and thermal performance, most of the research activities presented only the heat gain during sunny periods. The heat loss during non-sunny periods was not shown. Hence, the annual performance is not clear. In indirect evaporative cooling applications, the thermal resistance between the room air and the pond is required to be minimal to maximize the heat transfer rate. Insufficient thermal insulation for cold climates will result in excessive heat lost. Proper measures are needed to reduce the undesirable heat loss, such as the insulation cover proposed by Kruger et al. (2010).

A2. Additional figures

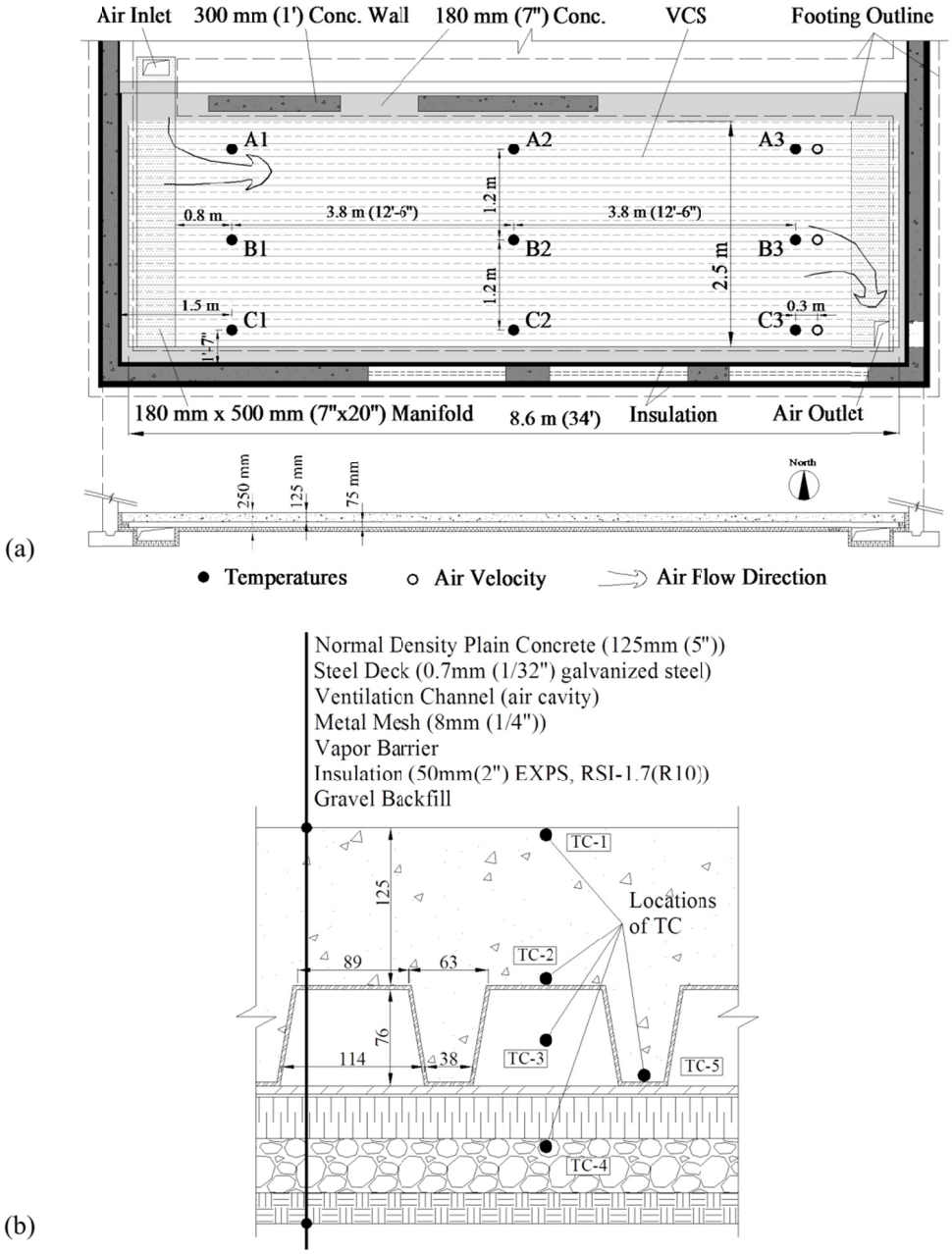

Fig. A2.1: Plan view, longitudinal cross section (a), and traversal cross section (b) of VCS with monitoring points indicated

A3. Discrete Fourier series (DFS) representation of excitations

Given a time series of discrete values, in Eq. (A3.1),

$$[A]_{\mathrm{I}} = [A_1\,, A_2\,, A_3\ \ldots\ A_i\ \ldots\ A_I] \tag{A3.1}$$

where $i = 1, 2 \ldots I$, is the time-series index, indicating the time (i.e. $t = \Delta t \cdot i$) at which the value is sampled. Δt is the time interval of data sampling. I indicates how many values are given.

The function of any excitation can be assumed to be even (i.e. symmetric about time origin) since only one period (i.e. cycle) is of interest. Its complex DFS representation can be approximated using Eq. (A3.2). See Chen (1983) and Kreyszig (2006) for more details on Fourier series and discrete Fourier series.

$$\hat{A}_i = \bar{A} + \tilde{A}_i \cong a_0 + 2\sum_{h=1}^{H}\left(a_h \cdot e^{jh\omega_f i\Delta t}\right) = a_0 + 2 \cdot \sum_{h=1}^{H}\left(a_h \cdot e^{jh\frac{2\pi}{I}i}\right) \tag{A3.2}$$

where accent "Λ" means DFS or complex frequency form, and $\omega_f = 2\pi/P$ is the fundamental angular frequency. P is the analysis period in seconds ($P = \Delta t \cdot I$). H is a positive integer indicating the number of harmonics are used in the approximation.

$$\bar{A} = a_0 = \frac{1}{I}\sum_{i=1}^{I}\left(A_i \cdot e^{-j0\frac{2\pi}{I}i}\right) = \frac{1}{I}\sum_{i=1}^{I} A_i$$

$$a_h \cong \frac{1}{I}\sum_{i=1}^{I}\left(A_i \cdot e^{-jh\omega_f i\Delta t}\right) = \frac{1}{I}\sum_{i=1}^{I}\left(A_i \cdot e^{-jh\frac{2\pi}{I}i}\right)$$

Coefficient a_0 is the mean of all the given time-domain values $[A]_{\mathrm{I}}$. Each a_h calculates the magnitude (also called modulus) of the $'h'$th harmonic, which has an angular frequency of $\omega_h = h \cdot \omega_f$. The summation term in Eq. (A3.2) gives the oscillation about the mean value. It is the superposition of all the harmonics of different frequencies. When h equals to zero, a_0 numerically equals to a_h. Eq. (A3.2) shows that when a time-series excitation is

represented with a DFS (e.g. $\hat{A}_i$ in Eq. (A3.2)), each value in the DFS consists of a mean value $\bar{A} = a_0$, and an oscillating value approximated by the summation of different harmonics, each being $\tilde{A}_{i,h} \cong 2 \cdot a_h \cdot e^{jh\frac{2\pi}{I}i}$. Accent "−" represents mean value or response, and "∼" the oscillatory value or response. To convert the complex values back to real values, $A_i \cong Re\{\hat{A}_i\}$, where $Re\{\quad\}$ takes the real part of the complex number.

A4. Thermal response in complex frequency domain

The matrix ${}_{trs}[M]_h$ is referred to as the transmission matrix (Stephenson and Mitalas 1971) (sometimes as cascade matrix). Pipes (1957) provided an approach for direct derivation of the transmission matrix based on the analogy between thermal and electrical circuits. The use of transmission matrix simplifies the calculation of the heat transfer in multi-layered assemblies (e.g. walls and slabs) - the overall transmission matrix simply equals to the product of the individual transmission matrix in the order corresponding to their locations in the assembly (Eq. (3.12)). The theory behind the direct multiplication is that the temperatures of the two adjacent surfaces in contact are the same, and the heat flux through them conserves (Carslaw and Jaeger 1959, Pipes 1957).

${}_{trs}^{n}[M]_h$ is the transmission matrix of layer n (Eq. (A4.1)). In this study, surfaces 0 and l are the opposite outer surfaces of any layer, such as the room air and the wall surface in an air film layer. It is important to note that the values in the excitation vectors are of various harmonics h, as in their DFS representations.

$$ {}_{trs}^{n}[M]_h = \begin{bmatrix} cosh({}^{n}l \cdot \gamma_h) & \dfrac{sinh({}^{n}l \cdot \gamma_h)}{{}^{n}k \cdot \gamma_h} \\ {}^{n}k \cdot \gamma_h \, sinh({}^{n}l \cdot \gamma_h) & cosh({}^{n}l \cdot \gamma_h) \end{bmatrix} \tag{A4.1} $$

where ${}^{n}l$ is the thickness of layer n, and ${}^{n}k$ is the thermal conductivity (W/m/K). $\gamma_h = \sqrt{j\omega_f h \,/\, {}^{n}\alpha}$, and ${}^{n}\alpha = {}^{n}k / {}^{n}\rho \cdot {}^{n}c$ is the thermal diffusivity (m^2/sec) of the material of layer n.

For a layer that can be considered as purely resistive/conductive (e.g. insulation, air film), the transmission matrix becomes ${}_{trs}[M]_h = \begin{bmatrix} 1 & r \\ 0 & 1 \end{bmatrix}$. r is the thermal resistance of the corresponding layer. For an exterior air film, $r = 1/_{cnv}h$, with ${}_{cnv}h$ being the exterior CHTC.

$$ {}_{adm}^{n}[M]_h = \begin{bmatrix} {}^{n}k \cdot \gamma_h \, coth({}^{n}l \cdot \gamma_h) & \dfrac{-\,{}^{n}k \cdot \gamma_h}{sinh({}^{n}l \cdot \gamma_h)} \\ \dfrac{{}^{n}k \cdot \gamma_h}{sinh({}^{n}l \cdot \gamma_h)} & -\,{}^{n}k \cdot \gamma_h \, coth({}^{n}l \cdot \gamma_h) \end{bmatrix} \tag{A4.2} $$

In admittance matrices (Eq. (A4.2)), elements $a11_h$ or $a22_h$ is referred to as the self-admittance that relates the heat flow response to the temperature excitation at the same surface. $a12_h$ or $a12_h$ is transfer-admittance that relates the heat flow response to the temperature excitation at the opposite surface (Athienitis and Santamouris 2000). In some literatures, self-admittance is simply referred to as admittance, and transfer-admittance as dynamic transmittance (Akander 2000, Davies 1973). Multiplying individual admittance matrices like that for transmission matrices is not correct.

Let ${}_{trs}[M]_h = \begin{bmatrix} t11_h & t12_h \\ t21_h & t22_h \end{bmatrix}$ and ${}_{adm}[M]_h = \begin{bmatrix} a11_h & a12_h \\ a21_h & a22_h \end{bmatrix}$

then the conversion between admittance and transmission matrix are as follows:

from transmission matrix to admittance transmission matrix:

$a11_h = t22_h / t12_h$ $\qquad$ $a12_h = -1/t12_h$

$a21_h = 1/t12_h$ $\qquad$ $a22_h = -t11_h/t12_h$.

from transmission matrix to admittance transmission matrix:

$t11_h = -a22_h/a21_h$ $\qquad$ $t12_h = 1/a21_h$;

$t21_h = a12_h - a22_h \cdot a11_h/a21_h$ $\qquad$ $t22_h = a11_h/a21_h$

Note the sign conventions in the transmission and admittance matrices vary in the literature. In this study, the formulation of admittance matrices defines that heat flux is positive if it flows in the direction pointing from surface 0 to surface l of the same layer.

A5. Frequency domain modeling

<u>Heat flow division</u>

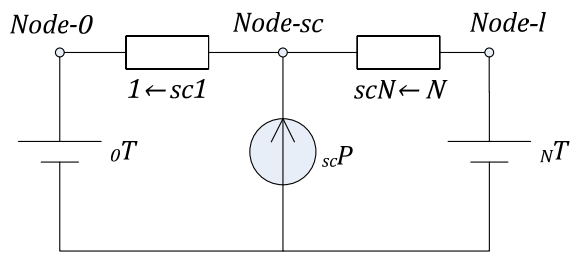

Fig. A5.1: Thermal network for heat flow division concept (node 0 is the outermost node of assembly $1 \leftarrow \mathrm{sc1}$, while node l is the outermost node of assembly $\mathrm{scN} \leftarrow \mathrm{N}$. Source node sc is in-between the two assemblies)

For the heat sources that are not located at the two outermost nodes, the heat flow can be divided into two portions, one for each node, using current division method (Bird 2007). Take the thermal network from Fig. A5.1 for demonstration. The oscillatory response from source heat ${}_{sc}\tilde{p}_{i,h}$ into node 0 will be

$$_{sc_0}^{1}\tilde{p}_{i,h} = \frac{^{scN\leftarrow N}t12_h}{^{1\leftarrow N}t12_h} \cdot {}_{sc}\tilde{p}_{i,h} \tag{A5.1}$$

where $scN \leftarrow N$ indicates the assembly consists of layers from scN (to the right of source node) to N.

<u>CHTC inside air channel</u>

Colburn's analogy Eq. (A5.2) (ASHRAE 2009d) is used to calculate the Nusselt number $_{Nu}No$ in the air channel with air flow.

$$_{Nu}No = \frac{f_{Darcy}}{8} \cdot {}_{Re}No \cdot {}_{Pr}No^{1/3} \tag{A5.2}$$

where f_{Darcy} is the Darcy-Weisbach friction factor (ASHRAE 2009b) (4 times the Fanning friction factor used in reference (ASHRAE 2009d)). $_{Pr}No$ is the Prandtl number of the fluid (0.71 for air).

$$f_{Darcy} = 8 \cdot \left[\left(\frac{8}{_{Re}No}\right)^{12} + \left(\frac{1}{A^{16} + B^{16}}\right)^{1.5}\right]^{1/12}$$

where $A = -2.457 \cdot ln\left[\left(7/_{Re}No\right)^{0.9} + \left(0.27 \cdot \varepsilon/\ _{h}D\right)\right]$ and $B = 37530/_{Re}No$. ε is the roughness of the channel surface (0.002 m is used here).

The Reynolds number can be calculated, $_{Re}No = {}_{h}D \cdot {}_{f}V/\ _{f}\nu$, where $_{h}D$ is the hydraulic diameter of the air channel, equal to the diameter of channel (0.19 m in this case). $_{f}V$ is the fluid velocity (m/s). $_{f}\nu$ is the fluid kinematic viscosity (constant value of 15.7E-6 m^2/s is used for air in this case). Then the CHTC $_{sc}h$ between the air channel and the air flow can be obtained, $_{sc}h = {}_{Nu}No \cdot {}_{air}k/\ _{h}D$, where $_{air}k$ is the thermal conductivity of air.

A6. Sensitivity analysis of dynamic response

Investigations have been conducted on the effects of insulation on the bottom side, different flow rates, and top surface coverings. With the insulation (Fig. 5.3-a) value set equal to the 9 $W/m^2/K$ (equals to the combined convective and radiative heat transfer coefficient, i.e. exposed surface), comparing the curves in both insulation conditions shows that changing the insulation value does not significantly affect the dynamic response for concrete thicknesses larger than 0.2 m.

Using the original settings but changing the flow rate will mainly affect the transfer function in Eq. (5.5) (i.e. dynamic responses plotted in Fig. 5.4–c and –d). A larger advection flow rate will shorten the time lags. With a 3 ACH flow rate, the largest thermal lag (about 9 hours) was found for an equivalent concrete thickness between 0.3 and 0.4 m (data are not plotted here).Changing the flow rate from 2 to 0.3 ACH (Fig. A6.1), which is the normal ventilation rate, the time lags become almost linear with the equivalent concrete thickness regardless of the building types and the source layer locations. The time lag is increased by 2 to 4 hours (i.e. larger absolute value) for concrete thickness larger than 0.4 m for thermally heavy buildings, comparing (d) in Fig. 5.4 and Fig. A6.1), but less than 0.5 hour for thickness less than 0.3 m. The magnitudes do not change significantly. Maximum time lags are not found within the thickness range of interest.

Another investigation uses the original settings, but changes the values of the top surface combined radiative and convective heat transfer coefficient) from 9 $W/m^2/K$ to 6 $W/m^2/K$ (for the case of supplying space cooling from the floor). For equivalent thickness of the concrete larger than 0.2 m, the magnitude of the self-admittance (Fig. 5.4-a) is reduced by 1.5, with time lag slightly increased (about 15 minutes). The time lag plotted in Fig. 5.4-b is

increased by about 1 hour for thermally heavy buildings, and 15 minutes for light buildings, while the magnitude is reduced by about 0.1 for both types of buildings. The curves in Fig. 5.4-c and –d for thermally medium and heavy buildings are not affected significantly.

Using the original settings, but changing the top surface combined radiative and convective heat transfer coefficient) from 9 W/m^2/K to 1 W/m^2/K, the effects of carpet/wood coverings are investigated. No significant thermal capacitance in the coverings is assumed. The magnitude of the self-admittance is reduced by 5 (becomes about 1 constantly). This means the buffering effect of the slab is insignificant. Similar effects for the transfer function from Eq. (5.4) (i.e. Fig. 5.4-b). For the curves in Fig. 5.4-c and -d, all the magnitudes are reduced to less than 0.05. The time lags are relatively flat for thermally heavy buildings with concrete thickness larger than 0.2 m, around 9 hours, regardless of the source layer location. It is around 4 hours for light buildings.

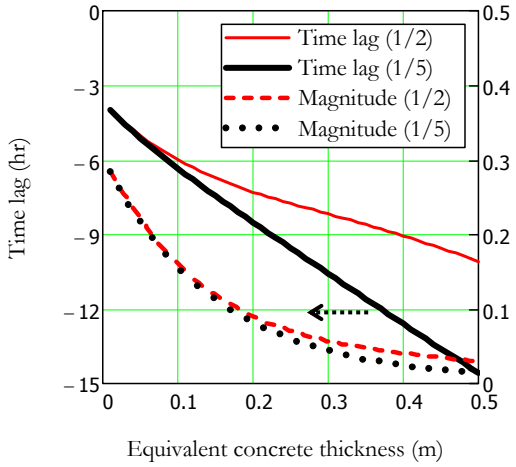

(c) Heat flow division for source heat flux; location of source for thermally heavy buildings

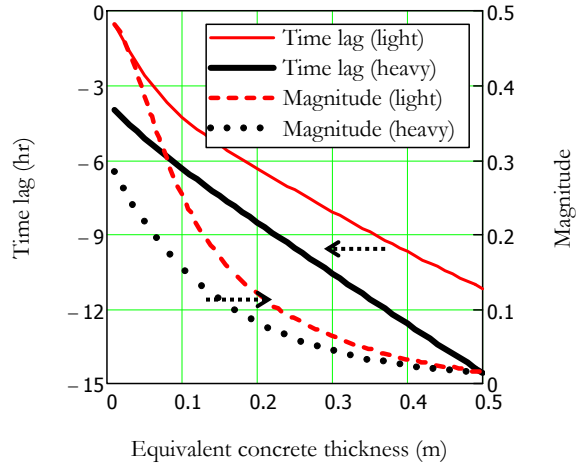

(d) Heat flow division for source heat flux; buildings with different levels of thermal mass; source layer at "1/5" level

Fig. A6.1: Dynamic response of an open-loop BITES slab and its associated room for 1 cycle per day excitations (flow rate of 0.3 ACH)

A7. Formula for setting room air temperature

The temperature value of the pivots is calculated based on the exterior sol-air temperature, but limited within the throttling range (Eq. (A7.1)).

$$_{pivot}T_i = {}_{sp}T + {}_{sp}\Delta T \cdot Limit\left[-1, \frac{{}_{sa}T_i - {}_1c}{{}_2c}, 1\right] \tag{A7.1}$$

where ${}_{sp}T$ is the room air temperature set point, and ${}_{sp}\Delta T$ is half the throttling range. ${}_{sa}T$ is the maximum or minimum exterior sol-air temperatures of one day. Function $Limit[a, x, b]$ takes a value from x, but limits it between a and b, inclusively. Coefficient ${}_1c$ is 23.3°C, and ${}_2c$ is 11.1°C in this case. Their values are obtained from simultaneously solving

$${}_{sp}\Delta T = \left({}_{sa.max}T - {}_1c\right)/\,{}_2c \qquad \text{and} \qquad -{}_{sp}\Delta T = \left({}_{sa.min}T - {}_1c\right)/\,{}_2c$$

where ${}_{sa.max}T$ of 56.7°C and ${}_{sa.min}T$ of -10°C are the annual exterior maximum and minimum sol-air temperatures, respectively.

A8. Non-periodically steady thermal excitations

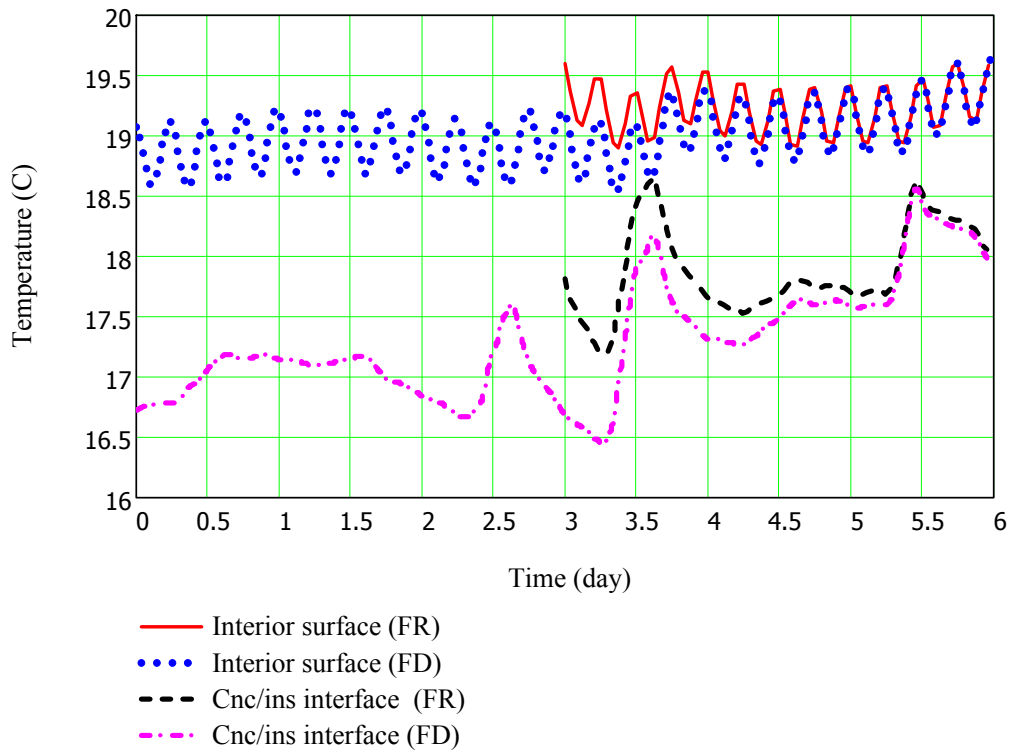

Fig. A8.1: Simulated temperatures of the wall assembly (FR: frequency response; FD: finite difference)

Excitations used for frequency domain modeling has to be steady periodic. Even the actual excitations are not steady periodic, their DFS representations will be. Deviation in values between the actual and model inputs will result in errors in the prediction of thermal energy injection rates. Yet, if the excitation profiles (i.e. room air temperature and required thermal output) include a long enough period of data that precedes the current period of interest (i.e. the actual room air temperature and thermal output in the past), the errors will diminish after the preceding period.

Fig. A8.1 compares temperatures of an insulated exterior concrete wall (Fig. A8.2) under two modeling approaches – explicit finite difference and frequency domain modeling (frequency

response). The boundary conditions are shown in Fig. A8.3. The explicit finite difference approach has a warm-up period of three days (day 1 to 3). Frequency domain modeling simulates the temperature response for the last three days (day 4 to 6). Temperatures from finite difference approach are considered accurate in this case since fine meshing is employed.

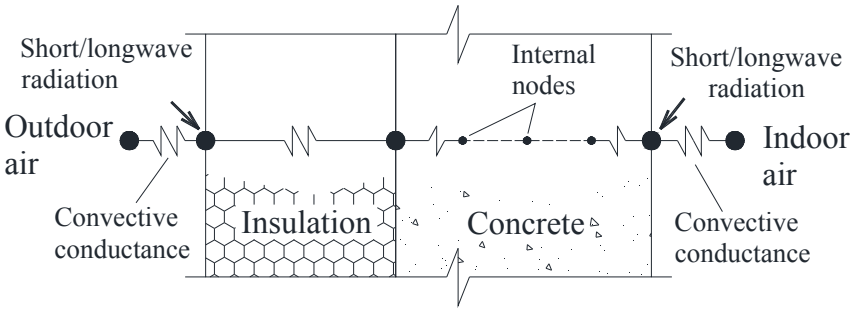

Fig. A8.2: Thermal network and schematic of a concrete wall with exterior insulation

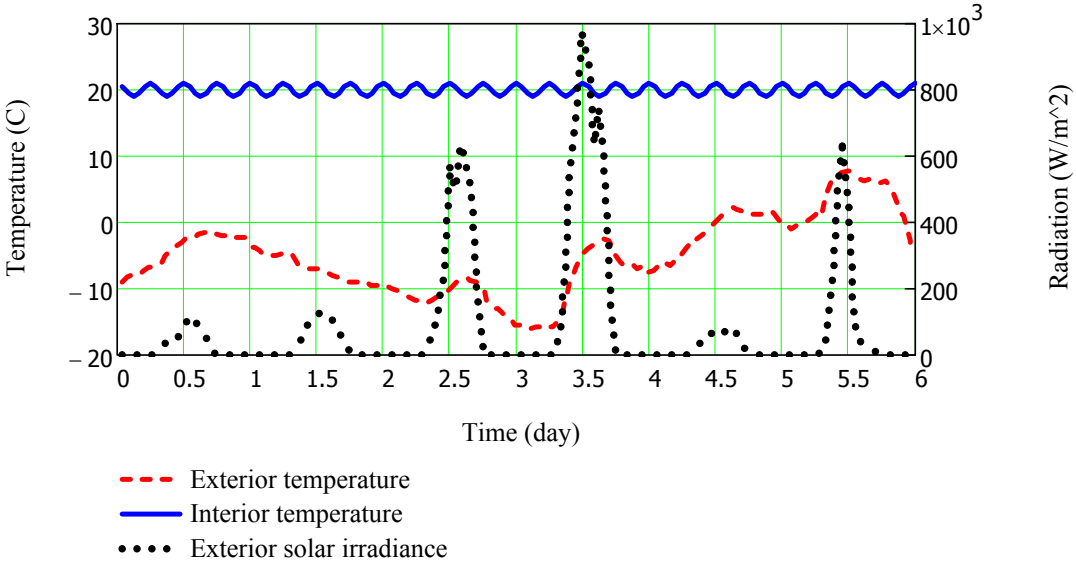

Fig. A8.3: Boundary conditions

The wall assembly (Fig. A8.2) consists of an insulation layer of 0.5 W/m^2/K and a concrete layer of 0.3 m. No heat source within the concrete. A dramatized non-periodicity of the

boundary condition is chosen – the temperature difference between the beginning and the end of the frequency domain simulation period is about 15°C (Day 3 and Day 6 in Fig. A8.3).

As seen in

Fig. A8.1, the temperature discrepancies between these two approaches diminish as the time marches forward. Two and a half days for temperatures of the concrete/insulation interface from two approaches to merge. However, the temperature discrepancy after two days is small (0.1°C), and the response of active BITES systems would be much faster with internal heat source (Fig. 1.8). Two days will be sufficient as warm-up period for typical active BITES thickness (0.2 to 0.3 m).

The preceding period serves as the warm-up or stabilization period in the frequency domain modeling. Actual data in the past should be incorporated into the excitation profiles. The actual room air temperature in the past can be measured. The actual thermal output from the BITES can be estimated with the measured temperatures of the room air and interior surfaces including the exposed surface of BITES, or by comparing the actual and set values of the room air temperature. Obtaining actual thermal output is another strong motive for adopting "online" data-driven models that can be self-tuned over time with continuously monitoring (i.e. online) data since the data is also needed for warming up models.

Nomenclature

Symbols

$\wedge$	DFS or complex frequency form
$-$	(overhead bar) mean value/response
$_$	(underscore) a_b means from a to b
$\sim$	oscillatory value/response
$\cong$	approximately equal to
Δ	difference or potential
$\leftarrow$	order of layers in an assembly. $1 \leftarrow N$ means the assembly contains layers from 1 to N, and the excitations are on surface l of layer N
[ ]	matrix or vector

Greek

α	diffusivity (m^2/sec), $\alpha = k/\rho \cdot c$
ρ	density (kg/m^3)
ρc	volumetric heat capacity ($J/m^3/K$)
ω	angular frequency (rad/sec), $\omega_f = 2\pi/P$ and $\omega_h = h \cdot \omega_f$
ϕ	phase angle of complex number

English

a	admittance matrix element, a numerical value, or coefficient
adm	admittance
A	advective/advection or a numerical value
$Area$	surface area
$Arg\{\ \}$	argument (phase angle) of the complex number
b	index of air channel bounding surface

B	total number of bounding surfaces, or BITES
c	coefficients, combined, convective, or capacitance
c/c_p	capacitance (J/kg/K)
chn	air channel
cnc	concrete
cnv	convective/convection
crt	critical
C	thermal capacitance (J/K)
CR	combined convection and radiation
d	mathematical symbol for differential
e	TES capacity per unit area (J/m^2) or exponential base
eqv	equivalent
E	energy (J) or excitations
f	fluids (air for open-loop system, and air or water for closed-loop system)
$R(\quad)$	response function
h	convective heat transfer coefficient (W/m^2/K) or harmonic index
hx	heat exchange
H	total number of harmonics
i	index of sampling order for time-series values
I	total number of sampled values
j	imaginary unit; $j = \sqrt{-1}$
k	thermal conductivity (W/m/K)
l	thickness of a layer (m), also used to indicated the surface at $x = l$
L	length (m)

$[M]$	matrix of transfer functions
n	layer index, layer n
N	total number of layers in one assembly
p	heat flux or power per unit area (W/m^2)
P	heat power (W) or period in seconds
Q	volumetric flow rate (m^2/sec)
r	thermal resistance per unit area (m^2·K/W)
rm	room or room air
$Re\{\ \}$	real part of the complex number
sc	source or source layer
slb	slab
slr	solar
t	time or duration (second/sec unless specified)
trs	transmission
ttl	total
Δt	simulation time step or sampling time interval (sec)
T	temperature (°C)
ΔT	temperature difference or potential (°C)
Th	thickness or equivalent thickness (m)
u	heat transfer coefficient per unit area (W/m2/K)
U	conductance (W/K)
x	distance to an outer surface of a layer (m)
Y	self-/transfer- Admittance, transfer function in frequency domain

Acronyms

ACH	air changes per hour (air flow rate in terms of how many times of room volume in one hour)
AHU	air handling unit
BITES	building-integrated thermal energy storage
CFM	cubic feet per minute
CHTC	convective heat transfer coefficient
CL	closed-loop BITES systems
CV/CVs	control volume(s)
DFS	discrete Fourier series
FD	finite difference
FPM	feet per minute
FR	frequency response
GSHP	ground source heat pump
LPFD	lumped-parameter finite difference
MPC	model-based predictive control
OL	open-loop BITES systems
PCM	phase-change materials
R&D	research and development
TES	thermal energy storage
VCS	ventilated concrete slab

Variables

${}_{hx}a$	heat exchange coefficient
${}_{c}a12$	the element at the first row and second column of the combined admittance matrix ${}_{adm.c}[M]$
${}^{soil\leftarrow rm}a21$	the element at the second row and first column of the admittance matrix ${}^{soil\leftarrow rm}_{adm}[M]$ of the assembly between soil and room air nodes

${}_{edge_CV}c$	capacitance per square meter of the edge control volume (J/m^2/K)
${}_{hx}c$	heat exchange coefficient ${}_{hx}c = {}_{sc}U / {}_{f}Qc$
C_{slab}	thermal capacity of the slab
E_{allow}	thermal energy that is allowed to be stored in the slab
E_{max}	maximum storage of thermal energy
E_{store}	thermal energy (coolness) that will be stored in the slab
f	fluid (air or water)
h_{cr}	combined convective and radiative heat transfer coefficient
${}_{sc}h$	CHTC between the path inner surface and the air flow
${}_{top}h$	combined heat transfer coefficient on BITES top surface
${}_{ttl}L$	length of one air channel
${}_{path}N$	mumber of air paths for the whole floor
${}_{Biot}No$	Biot number
${}_{Re}No$	Reynolds number
${}_{adm}^{1\leftarrow N}[M]_h$	admittance matrix of the hth harmonic for an assembly composed of layers 1 to N
${}_{trs}^{1\leftarrow N}[M]_h$	transmission matrix of the hth harmonic for an assembly composed of layers 1 to N
${}_{adm.c}[M]$	combined admittance matrix, for simplified open-loop system models
${}_{trs.c}[M]$	combined transmission matrix, for simplified open-loop system models
${}_{trs}^{scN\leftarrow N}[M]_h$	transmission matrix of the hth harmonic for an assembly composed of layers scN to N
${}_{0_rm}p$	heat exchange between the room air and the other side of the BITES (node "0" in this case)
${}_{A.B}p$	advective thermal output of BITES system

${}_{B}p$	thermal output of the BITES to the room (i.e. ${}_{CR.B}p + {}_{A.B}p$)
${}_{CR.B}p$	combined convective and radiative thermal output of BITES system
${}_{heat_flux}p$	heat flux on a surface, such as solar radiation (W/m^2)
${}_{sc}p_i$	heat flux from the heat source (W/m^2)
${}_{load}p$	space conditioning load or required thermal output from the BITES systems
${}_{sc}p$	source thermal energy injection rate
${}_{sc_rm}p$	heat flux injected by the core-conditioning fluid and then released to room
${}_{slr}p$	transmitted solar radiation absorbed by BITES top surface
${}_{slr_rm}p$	heat flux to room air from solar radiation absorbed by the floor surface
${}_{soil_top}p$	heat flux following to the floor top surface due to temperature difference between top surface and soil
${}_{add}p$	thermal energy injection rate at AHU for open-loop system per square meter floor surface area (W/m^2)
${}^{1}_{0}\bar{p}$	mean heat flow response on surface at $x = 0$ of layer 1
${}^{1}_{0}\tilde{p}_{i,h}$	oscillatory heat flow response on surface at $x = 0$ of layer 1 at time i and of the $'h'$th harmonic
${}_{sc_0}^{1}\tilde{p}_{i,h}$	oscillatory heat flow response on surface at $x = 0$ of layer 1 caused by internal source at time i and of the $'h'$th harmonic
${}_{chn}\tilde{p}_{i,h}$	oscillatory heat flow response on channel surface at time i and of the $'h'$th harmonic
${}^{1}_{0}\hat{p}_i$	DFS form of heat flow response on surface at $x = 0$ of layer 1 at time i
${}_{air_srf}P_b$	total heat flow from the air flow to surface b
${}_{f}Qc$	${}_{f}Qc = {}_{f}Q \cdot {}_{f}\rho c$
${}_{Qc}r$	convective resistance, ${}_{Qc}r = {}_{floor}Area/\left({}_{f}Qc \cdot {}_{path}N \right)$
${}_{soil\leftarrow top}r$	thermal resistance between soil and floor top surface

${}^{sc\leftarrow rm}_{c}r$	combined thermal resistance between source layer and room air
${}_{cs}Ratio$	area ratio of internal heat transfer surface to room-side surface
${}^{1\leftarrow N}t12_h$	the element at the 1st row and 2nd column of transmission matrix of assembly $1 \leftarrow N$ of the $'h'$th harmonic
${}^{sc\leftarrow rm}t11$	The element on the first row and first column of the transmission matrix ${}^{sc\leftarrow rm}_{trs}[M]$ of the assembly between source layer and room air node
$T_{inlet.air}$	temperature of the inlet air entering the slab
$T_{min.rm}$	minimum allowable room temperature
$T_{min.slab}$	minimum allowable slab temperature (i.e. the lowest slab temperature that slab cooling wants to achieve)
$T_{ref.slab}$	reference slab temperature, used as the initial slab temperature in the slab cooling simulation
T^0_{rm}	initial room air temperature
T^0_{slab}	initial slab temperature
$T_{sp.rm}$	mechanical space cooling setpoint
${}_{chn}T$	channel temperature weighted by the channel surfaces' respective heat transfer coefficients
${}_{chn_srf}T_i$	temperature of one channel bounding surface at time i, surface index b is omitted
${}_{f}T$	fluid temperature (air flow temperature in open-loop system)
${}_{inlet}T$	BITES system inlet fluid temperature
${}_{inlet_air}T$	inlet air flow temperature
${}_{mean_air}T$	mean air flow temperature
${}_{outlet}T$	BITES system outlet fluid temperature
${}_{rm}T$	room air temperature

${}_{sc}T$	floor source layer temperature
${}_{soil}T$	soil temperature
${}_{top}T$	BITES top surface temperature
${}_{l}^{n}\tilde{T}_{i,h}$	oscillatory temperature response on surface at $x = l$ of layer n at time i and of the $'h'$th harmonic
${}_{eqv_0}^{1}\tilde{T}_{i,h}$	equivalent oscillatory temperature response on surface at $x = 0$ of layer 1 at time i and of the $'h'$th harmonic
$\Delta T_{clg.rm.slab}$	temperature difference between room air and slab during active slab cooling operation
$\Delta T_{off.rm.slab}$	temperature difference between room air and slab outside active slab cooling period
${}_{cnv}\Delta T$	temperature difference during convective heat transfer
${}_{eqv_sc_0}^{1}\Delta\tilde{T}_{i,h}$	equivalent oscillatory temperature response potential on surface at $x = 0$ of layer 1 caused by internal source at time i and of the $'h'$th harmonic
${}_{edge_CV}Th$	thickness of edge control volume (m)
${}_{eqv}u$	equivalent conductance per square meter room-side surface area (W/m^2/K)
${}_{node}u$	conductance per square meter between two capacitance nodes (W/m^2/K)
${}_{chn_srf}U_b$	conductance per meter channel length of channel sub-surface b (W/m/K)
${}_{sc}U$	total heat transfer conductance between each air path and the fluids (W/K)
V_{air}	velocity of air inside the air channel of the slab
${}_{eqv_slf}^{1\leftarrow sc1}Y_h$	equivalent self-admittance of assembly $1 \leftarrow sc1$ of the $'h'$th harmonic
${}_{eqv_trf}^{1\leftarrow sc1}Y_h$	equivalent transfer-admittance of assembly $1 \leftarrow sc1$ of the $'h'$th harmonic

<u>The end</u>